FACULTY OF ENGINEERING AND ARCHITECTURE

Stability and feasibility of the complete hemodynamic and anesthetic regulatory problem - a multivariable predictive control study

Frederik Kussé
Student number: 01402284

Supervisor: Prof. dr. ir. Clara-Mihaela Ionescu
Counsellor: Dr. Dana Copot

Master's dissertation submitted in order to obtain the academic degree of
Master of Science in Electromechanical Engineering

Academic year 2018-2019

GHENT UNIVERSITY

FACULTY OF ENGINEERING AND ARCHITECTURE

Stability and feasibility of the complete hemodynamic and anesthetic regulatory problem - a multivariable predictive control study

Frederik Kussé
Student number: 01402284

Supervisor: Prof. dr. ir. Clara-Mihaela Ionescu
Counsellor: Dr. Dana Copot

Master's dissertation submitted in order to obtain the academic degree of
Master of Science in Electromechanical Engineering

Academic year 2018-2019

GHENT UNIVERSITY

Disclaimer - Dutch

De auteur geeft de toelating deze masterproef voor consultatie beschikbaar te stellen en delen van de masterproef te kopiëren voor persoonlijk gebruik. Elk ander gebruik valt onder de bepalingen van het auteursrecht, in het bijzonder met betrekking tot de verplichting de bron uitdrukkelijk te vermelden bij het aanhalen van resultaten uit deze masterproef.

Disclaimer - English

The author gives permission to make this master dissertation available for consultation and to copy parts of this master dissertation for personal use. In the case of any other use, the copyright terms have to be respected, in particular with regard to the obligation to state explicitly the source when quoting results from this master dissertation.

June 1, 2019

Preface

Dear reader,

Every year students in their second year of master's start the project which is feared most by all students: the legendary master's thesis. If you happen to encounter them during the year and ask how they are doing, they usually give a one-word answer: 'thesis'. It is a period of hard work, sleepless nights and a lot of coffee. I was however fortunate enough to work on a thesis subject I have a personal connection with in a research group that welcomed me with open arms and provided me with everything I needed to succeed. Yes, it was very hard work, but I would not have wanted it any other way.

First of all, I want to thank prof. dr. ir. Clara-Mihaela Ionescu for providing me with all the tools necessary to work on my thesis, for encouraging me to strive for more and for offering me several opportunities. I also want to thank my mentor, dr. ir. Dana Copot, for answering my many practical questions as well as providing me with useful feedback. Without her giving me the flexibility to work on my thesis outside of the office, I could not have combined my thesis with my work as a student representative. I want to thank the other master students in the research group for their support and wish them all the best in their future careers. Special thanks go out to the PhD students Jasper, Kevin, Maria and Mihaela for helping me navigate the complex world of anesthesia and for offering advice throughout the year.

Secondly, I want to thank my family and friends for supporting me during the last few years. I want to thank my twin sister, Nathalie, for being the best sister any brother can wish for and for keeping up with me even when I am tired or often absent. I am truly blessed that I have you as my sister. I also want to thank my parents for being the most supportive, kind and generally awesome parents in the world. You did not only provide me with emotional and practical support, but also gave me financial freedom so I could focus completely on my studies without having the worry about anything else. Thank you for always giving me good advice. However, as I am a stubborn Kussé, I probably have done just the opposite.

I want to thank my godmother for taking care of me and my sister after school when we were young, making sure we ate healthy and finished our homework. You taught us the importance of hard work, while being the greatest grandmother on the planet. I want to thank my godfather for encouraging me to explore new things and showing me that the world is bigger than just our country. I am forever grateful and consider myself extremely lucky to have you as my godfather. I also want to thank my friends for the many laughs and for making me realise that there is life outside of the thesis.

Finally, I want to thank you, the reader, for taking the time to read my work. Automated anesthesia is a very interesting topic with great potential, so I hope this thesis can inspire you to join the research effort and make it a reality!

Frederik Kussé
Ghent, June 2019

Abstract

The goal of any anesthesia is to obtain the required anesthetic level while minimizing side-effects coming from over- as well as underdosing. By taking advantage of accurate infusion devices and objective pain assessment, automated drug delivery increases the safety of the patient, cumulating in reduced recovery times and a minimization of the healthcare costs. The goal of this thesis is to build, analyse and control a benchmark model for the closed-loop control of the complete hemodynamic and anesthetic regulatory problem. Quasi-infinite Horizon Model Predictive Control is implemented, with special attention given to the stability of the scheme as well as the online feasibility. The performance of the designed controller is tested in simulation for varying parameter values of the patient model, taking into account surgical stimulus and the anticipatory reaction of the anesthesiologist.

Keywords: closed loop control, model predictive control, stability analysis, complete anesthesia system, patient safety

Stability and feasibility of the complete hemodynamic and anesthetic regulatory problem – a multivariable predictive control study

Frederik Kussé

Supervisor(s): Clara-Mihaela Ionescu, Dana Copot

***Abstract* – The goal of any anesthesia is to obtain the required anesthetic level while minimizing side-effects coming from over- as well as underdosing. By taking advantage of accurate infusion devices and objective pain assessment, automated drug delivery increases the safety of the patient, cumulating in reduced recovery times and a minimization of the healthcare costs. The goal of this thesis is to build, analyse and control a benchmark model for the closed-loop control of the complete hemodynamic and anesthetic regulatory problem. Quasi-infinite Horizon Model Predictive Control is implemented, with special attention given to the stability of the scheme as well as the online feasibility. The performance of the designed controller is tested in simulation for varying parameter values of the patient model, taking into account surgical stimulus and the anticipatory reaction of the anesthesiologist.**

***Keywords* – closed loop control, model predictive control, stability analysis, complete anesthesia system, patient safety**

I. Introduction

Studies into the pain evaluation by nurses and the pain assessment by patients lead to the conclusion that an objective automated drug delivery system would benefit the patient [1], [2], [3]. With closed-loop control of general anesthesia, human errors are avoided and more accurate drug administration can be achieved [4], [5]. Individualised protocols based on actual patient parameters can be used to match the drug administration profile to the stimulation intensity of each individual surgery [6], [7], [8], [9], [10]. Once developed, other applications of automated drug delivery include diabetes [11], cancer treatment [12], [13], immunodeficiency [14] and hormonal treatment [15].

General anesthesia itself comprises three main parts: hypnosis, analgesia and neuromuscular blockade (NMB). Hypnosis, measured by Bispectral Index (BIS), is the loss of consciousness of the patient, analgesia is the absence of perceived pain and neuromuscular blockade represents the induction of muscle paralysis [16]. Hypnosis and neuromuscular blockade are well understood, but analgesia still requires additional research [16]. These three components need to be controlled during three phases: induction, maintenance and recovery, each with different control objectives. The induction phase is a set-point following task, where a set-point needs to be reached while avoiding overshoots. In the maintenance phase, a fast disturbance rejection is required to sustain the desired sedation level. The recovery phase is left out of the control problem as the administration of drugs is simply stopped once the surgery has been completed [17]. To complete the patient model, the hemodynamic parameters cardiac output and mean arterial pressure are included. Propofol and Remifentanil are used to induce hypnosis and analgesia respectively due to their fast onset and recovery times as well as their suitability for control [9]. Atracurium is further selected for neuromuscular blockade, while Dopamine and Sodium Nitroprusside control the hemodynamics.

The purpose of this thesis is to build, analyse and control a benchmark model for the closed-loop control of general anesthesia (see Figure 1, taken from [18]). Model predictive control (MPC) is chosen to be used in this application as it mimics the real-life reaction of the anesthesiologist, therefore providing a way of control that can intuitively be understood by medical professionals [19], [20]. The designed controller is then tested in simulation for varying parameter values of the patient model, both between patients (interpatient variability) as well as gradually changing within a single patient (intrapatient variability). These simulations include the effect of a surgical stimulus as well as the anticipatory reaction of the anesthesiologist [20].

From an ethical point of view, it is essential that the stability of the controller is guaranteed during operation to ensure the well-being of the patient. Moreover, it is important to know when the controller could lose feasibility (i.e. the ability the find a possible solution) so the anesthesiologist can intervene in time. Hence, a stability and feasibility analysis of the designed controller is performed in this thesis. Hitherto, no stability analysis of an MPC scheme with a complete patient model is available in literature [21].

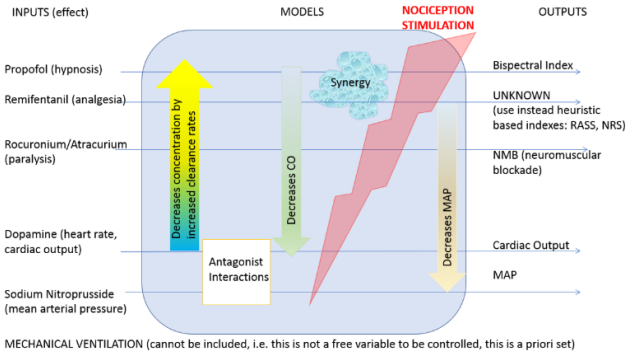

Figure 1: Full patient model general anesthesia

II. Models for the Control of Anesthesia

A. Anesthesia models

Each model for anesthesia should preserve the mass balance, as this implies that the link between physiological and mathematical parameters is maintained [22]. To model the pharmacokinetics (PK), the body is divided into three compartments: blood, muscles and fat. An additional effect-site compartment combined with a non-linear relationship is added to model the drug pharmacodynamics (PD). The complete PK-PD model can be found in Figure 2 [16].

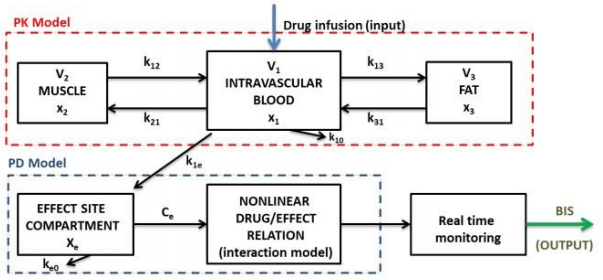

Figure 2: PK-PD model for anesthesia

The PK-PD models for Propofol and Remifentanil used in this thesis are the 4th order compartmental models proposed by Schnider [23] and Minto [24], see equation 1. The model for neuromuscular blockade is taken from Rocha [25], see equation 2.

$$\begin{aligned}\frac{dx_1(t)}{dt} &= -(k_{10}+k_{12}+k_{13})x_1(t) + k_{21}x_2(t) \\ &\quad + k_{31}x_3(t) + u(t) \\ \frac{dx_2(t)}{dt} &= k_{12}x_1(t) - k_{21}x_2(t) \\ \frac{dx_3(t)}{dt} &= k_{13}x_1(t) - k_{31}x_3(t) \\ \frac{dx_e(t)}{dt} &= -k_{e0}x_e(t) + k_{1e}x_1(t)\end{aligned} \tag{1}$$

$$C_{NMB} = \frac{k_1 k_2 k_3 \alpha^3}{(s+k_1\alpha)(s+k_2\alpha)(s+k_3\alpha)} \tag{2}$$

Both these models are then followed by a non-linear sigmoid function, the Hill-curve, of which the formulas can be found in equations 3 [26] and 4 [25], [21] respectively (P = Propofol, R = Remifentanil, A = Atracurium). Herein is γ [-] the Hill-coefficient of sigmoidicity, σ [-] a measure for the synergy between the two drugs, C_i [µg/ml] is the concentration of the drug i at time t and C_{50i} [µg/ml] is the concentration of drug i required to obtain 50% of the maximum effect. Note that there is a super-additive synergy between Propofol and Remifentanil [26].

$$Effect = 100\frac{(\frac{C_p}{C_{50P}} + \frac{C_R}{C_{50R}} + \sigma\frac{C_p}{C_{50P}}\frac{C_R}{C_{50R}})^\gamma}{1+(\frac{C_p}{C_{50P}} + \frac{C_R}{C_{50R}} + \sigma\frac{C_p}{C_{50P}}\frac{C_R}{C_{50R}})^\gamma} \tag{3}$$

$$Effect = 100\,\frac{{C_{50A}}^{\gamma_A}}{{C_{NMB}}^{\gamma_A} + {C_{50A}}^{\gamma_A}} + \frac{C_R}{3.4} \tag{4}$$

Finally, the model in equation 5 is used to link the effect-site concentration of Remifentanil to the Ramsay Agitation Sedation Score (RASS) [21].

$$RASS = \frac{1}{0.81\,C_R + 0.81}\frac{-2}{s+2} \tag{5}$$

B. Hemodynamic models

The antagonistic effects of Dopamine and Sodium Nitroprusside (SNP) on the cardiac output (CO) and mean arterial pressure (MAP) are modelled as in equation 6 [27]. The additional effect of the effect-site concentration of Remifentanil on the mean arterial pressure can be found in equation 7 [28].

$$\begin{bmatrix}\Delta CO \\ \Delta MAP\end{bmatrix} = \begin{bmatrix}\frac{K_{11}e^{-T_{11}s}}{1+\tau_{11}s} & \frac{K_{21}e^{-T_{21}s}}{1+\tau_{21}s} \\ \frac{K_{12}e^{-T_{12}s}}{1+\tau_{12}s} & \frac{K_{22}e^{-T_{22}s}}{1+\tau_{22}s}\end{bmatrix}\begin{bmatrix}\Delta Dopamine \\ \Delta SNP\end{bmatrix} \tag{6}$$

$$\begin{aligned}MAP &= \frac{-1}{0.81\,C_R + 0.81} \\ Effect &= 70\,\frac{MAP^{\gamma_{R,MAP}}}{MAP^{\gamma_{R,MAP}} + {C_{50R,MAP}}^{\gamma_{R,MAP}}}\end{aligned} \tag{7}$$

C. Approximation time delays

In the previous section, the hemodynamics are modelled as first order systems plus dead time. In practice, there is also some delay on the measurement of BIS [29], [9]. In the Laplace domain, both these delays are modelled as e^{-Ts}, with T being the time delay, which is nonlinear in s. Using Padé approximation, these nonlinear first order systems are transformed into linear systems of higher order [30]. This system has the same gain but a different phase angle for large frequencies. The higher the order, the better the approximation is, but also the higher the computational complexity is [30]. It is therefore chosen to use a 4th order approximation.

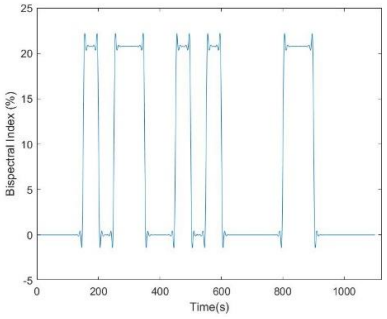

Figure 3: Nociception stimulation of patient model

D. Nociception stimulation and anesthesiologist in the loop

So far, no surgical stimulus has been modelled. Therefore, the stimulation profile from [20] is taken and then fed through the nociceptor pathway model from [21] (see equation 8). The end results can be seen in Figure 3. The signal is added as a disturbance to the output of the PK-PD model of Propofol and Remifentanil.

$$NOCI = 2\frac{(s^2 + 90s + 150^2)(s^2 + 26s + 165^2)(s^2 + 31s + 155^2)}{(s^2 + 66s + 149^2)(s^2 + 49s + 163^2)(s^2 + 31s + 155^2)} \quad (8)$$

As this disturbance can be anticipated by the anesthesiologist, this needs to be integrated into the closed-loop [20]. The signal to model this intervention is adapted from [20] for different values of γ (1 to 8) and can be found in Figure 4.

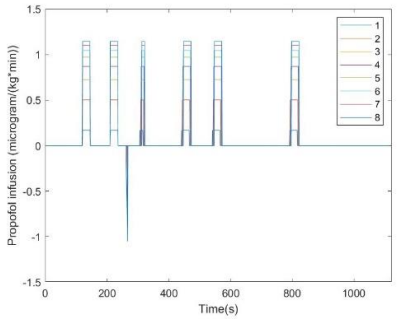

Figure 4: Anesthesiologist in the loop

III. ANESTHETIC REGULATORY PARADIGM

A. Dynamics of pharmacokinetic models

The bode plots for the PK models described in Section IIA can be plotted, while varying their respective parameters within the intervals described in [23], [24], [25]. An example of this can be found in Figure 5, where the age of male patients is varied in the PK model for Propofol. From these bode plots it is clear that these pharmacokinetic models are always stable (open-loop and closed-loop), independent of variations in their parameters. It is as Rocha claimed [25], these models are specifically built for control purposes.

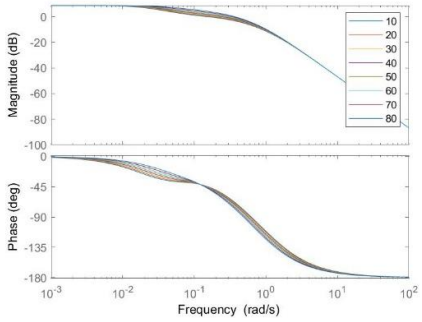

Figure 5: Bode plot PK model Propofol age variation

B. Dynamics of hemodynamic models

Within the intervals described in [27], the hemodynamic models are open-loop stable as they have no poles in the right half-plane. However, in contrast to the PK models, they can become unstable in closed-loop. An example of this can be seen in Figure 6 (gain variation of the transfer function modelling the influence of Dopamine on CO). Because of the unmodelled coupling between CO and MAP, there is a large variation in gain possible [31], resulting in unstable behavior for large gains.

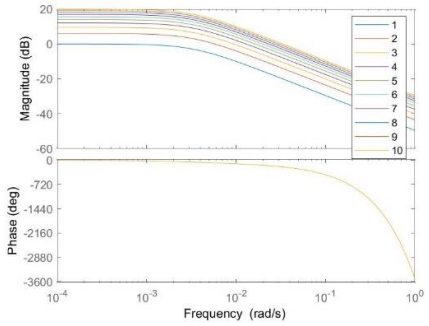

Figure 6: Gain variation influence Dopamine on CO

C. Hill-curve variation

In this thesis, inter- and intrapatient variability are simulated by changing γ. Therefore, the effect of γ on the Hill-curve is investigated (see Figure 7). For an effect level (100% means no effect, 0% maximum effect) above 50%, the effect-site concentration needed to reach a certain level is higher for larger γ and the reverse is true for levels below 50%.

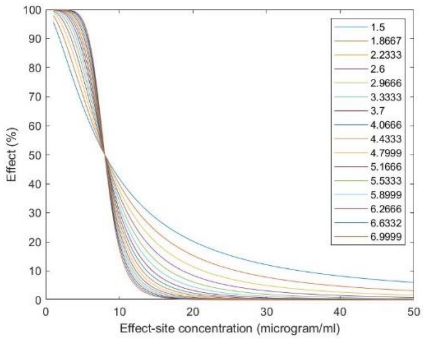

Figure 7: Hill-curve γ variation

D. Open-loop stability patient model for general anesthesia

It is assumed that the pharmacokinetic parameters are accurate and fixed so that the differences in individual responses are solely due to a variation of the (nonlinear) pharmacodynamic parameters [32]. Therefore, the dynamics of the patient model are linear and time-invariant. The non-linear transformation the outputs of these linear models undergo is irrelevant for the open-loop stability of the patient model. The open-loop stability of the patient model can be proven by looking at the open-loop poles (i.e. eigenvalues of the state matrix A) of the patient model. As all the models used are open-loop stable, it is no surprise that, when tested for the patient set in [32], all the eigenvalues have strictly negative real parts (i.e. all the poles in the left half-plane). Hence, the state matrix is Hurwitz and the entire system is asymptotically stable [33].

IV. MODEL PREDICTIVE CONTROL OF COMPLETE ANESTHETIC SYSTEM

A. Introduction to Quasi-infinite Horizon MPC (QIH – MPC)

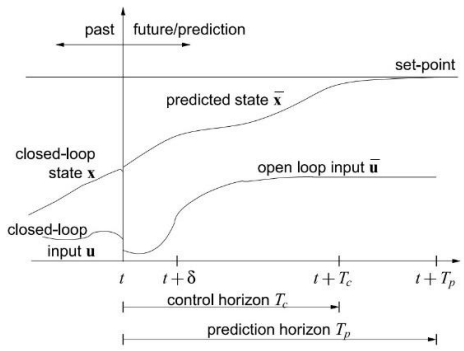

Figure 8: Basic scheme Model Predictive Control

The basic principle of MPC is shown in Figure 8, which is taken from [34]. At time t, the future states $\bar{x}$ until $t+T_p$ are predicted using the dynamic model of the system. Consequently, the optimal open-loop inputs $\bar{u}$ are calculated until $t+T_c$. These optimal inputs are found by iteratively minimizing a user-defined cost function. After these calculations, the open-loop input is implemented until $t+\delta$, with δ being the sampling time. By measuring the states at $t+\delta$, a new 'initial' state is obtained. It is at this point that the scheme is shifted from t to $t+\delta$ and the whole iteration starts again [34].

In basic MPC, the predicted states have to be exactly equal to the equilibrium point after the prediction horizon (terminal state equality constraint). Quasi-infinite Horizon MPC (QIH-MPC) loosens this constraint by only demanding that the states are within an invariant terminal region around the equilibrium point after the prediction horizon. As the terminal region is invariant, a local linear state feedback controller can be applied until the equilibrium point is reached exactly after an 'infinite' amount of time. The distance to the equilibrium point is penalized by a terminal penalty matrix included in the objective function, which is separate from the state and input weighting matrices also used in the objective function. It is important to note that the inputs are only calculated for a finite time (T_c), as the infinite 'tail' with the state feedback controller is never used in practice [35].

B. Stability, feasibility and robustness of QIH-MPC

Despite never being used, the terminal penalty matrix, the local linear feedback controller and terminal region are calculated and included in the objective function because their existence and inclusion allows for a Lyapunov-argument to prove the stability of the QIH-MPC scheme. Further details can be found in [35]. The following procedure for calculating these variables has been adapted from [35].

1. Calculate the Jacobian linearization (A,B) of the system at the equilibrium point
2. Check the stabilizability of the Jacobian linearization (for instance, with the Hautus-test for stabilizability [36]). The rest of the procedure is not applicable if the linearization is not stabilizable.
3. Find a linear state feedback matrix K such that A_K is Hurwitz

$$u = Kx \in U, \forall x \in X$$
$$A_K := A + BK \qquad (9)$$

4. Choose a value for κ (smaller than minus the largest eigenvalue of A_K) as well as positive semidefinite, real, symmetric weighting matrices Q and R. Solve the following Lyapunov equation to obtain the terminal penalty matrix P (with n being the number of states).

$$Q^* = Q + K^T R K \in \Re^{nxn}$$
$$\kappa < -\lambda_{max}(A_K), \kappa \in [0, \infty) \qquad (10)$$
$$(A_K + \kappa I)^T P + P (A_K + \kappa I) = -Q^*$$

5. Use the state feedback matrix K to find the largest $\alpha_1 \in (0, \infty)$ such that

$$\Omega_{\alpha_1} := \{x \in \Re^n | \, x^T P x \leq \alpha_1\}$$
$$Kx \in U, \forall x \in \Omega_{\alpha_1} \qquad (11)$$

6. Find the largest $\alpha \in (0, \alpha_1]$ such that

$$\dot{x} = f(x, Kx)$$
$$\phi(x) := f(x, Kx) - A_K x$$
$$L_\phi := sup\left\{\frac{\|\phi(x)\|}{\|x\|} \middle| \, x \in \Omega_\alpha, \; x \neq 0\right\} \qquad (12)$$
$$L_\phi \leq \frac{\kappa \lambda_{min}(P)}{\|P\|}$$

with Ω_α being an invariant terminal region, $sup(\cdot)$ the supremum and $\|\cdot\|$ the Frobenius norm

Once this procedure has successfully been completed and the results included in the controller, the stability of the QIH-MPC scheme is guaranteed if a feasible solution can be found at t=0. Feasibility thus requires that at each time step, a solution can be found such that the states are within Ω_α after the prediction horizon T_p. This also means robust stability is guaranteed, as long as the disturbances are small enough so that the states stay within the feasible region, i.e. the region were a feasible solution can be found.

C. Implementation of QIH-MPC

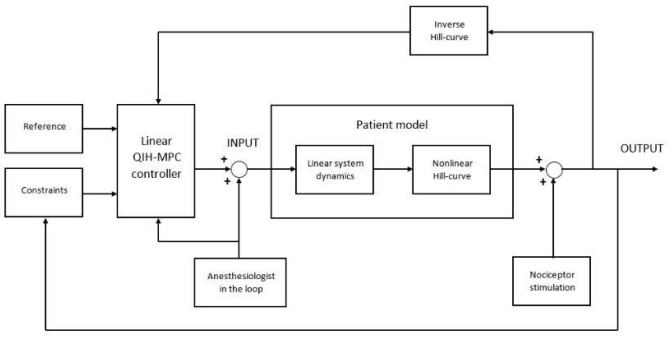

Figure 9: Implementation scheme closed-loop controller

Because of the inherent non-linearity of the Hill-curves used in the patient model (and therefore cost function and constraints), a nonlinear MPC scheme is required. Unfortunately, the optimization problem now potentially becomes non-convex. Hence, solvers which only find a single local optimum cannot be used anymore. As the convergence of non-convex problems is slow, a solver which could meet the above requirements within a reasonable CPU time (i.e. online feasible) was not found. Therefore, it was opted to apply inverse Hill-curves to the measured outputs of the system to estimate the effect-site concentrations. Doing so, the control problem that has to be solved by the linear MPC controller is now convex as the Hessian matrix of the linear quadratic objection function is positive semi-definite (i.e. the objective function is convex) [37]. As the constraints are linear, they do not affect the convexity of the control problem [38]. The constraints are also made adjustable to the current outputs to make sure feasibility is preserved. Additionally, the nociception stimulation and anesthesiologist in the loop are included in the closed-loop. The full implementation scheme of the closed-loop controller can be found in Figure 9.

V. Simulation Results and Discussion

A. *Interpatient variability*

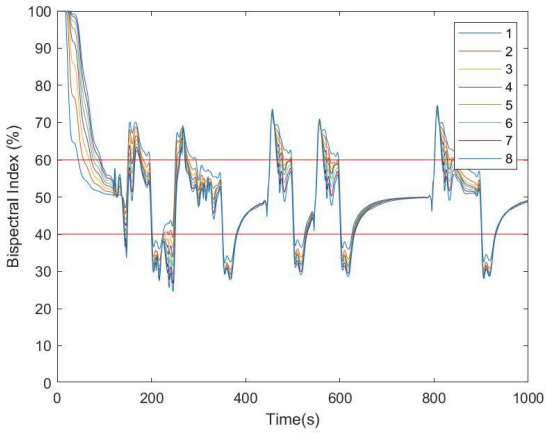

Figure 10: BIS output for interpatient variability - disturbed

The control performance for patients with different values for γ is investigated by varying γ between 1 and 8 (see Figure 10). It is assumed that the value of γ is exactly known and the closed-loop controller is adapted according to γ. Note: aside from BIS were all the setpoints for RASS, CO, MAP and NMB also reached (not shown).

During the induction phase, the setpoint for BIS (50%) is reached independently of the value of γ, but it takes longer for a larger value of γ. This can be explained by looking at Figure 7, for a BIS level above 50%, the require effect-site concentration to reach a certain level is higher. As the dynamics have not changed, it will take a longer time to reach this higher concentration.

Even when the surgical stimulus is applied and the intervention of the anesthesiologist is included, performs the controller as it should. Because the constraints are adapted online based on the current values of BIS and γ, is BIS primarily maintained within the 30%-70% range and quickly (approximately 25 seconds) returned to the preferred 40%-60% range.

It is further clear from Figure 10 that the BIS level after the administration of the bolus injection by the anesthesiologist is higher for patients with a lower sensitivity (i.e. lower γ). If the same surgical stimulus is then applied to all patients, patients with a lower sensitivity will generally have a higher resulting BIS-level. This means the anesthesiologist needs to take this into account while calculating the bolus injection.

B. *Intrapatient variability*

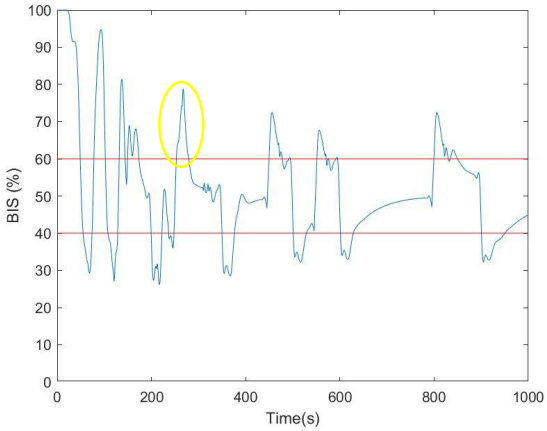

Figure 11: BIS output for intrapatient variability – disturbed

In contrast with the previous section will the value of γ of one patient now change from 1 to 8 during the simulation. This change is does not happen gradually, but in steps of 1. The steps are equally spaced, meaning each value of γ is valid for 1/8 of the simulation time. Once again, it is assumed that γ is exactly known at each time step and that the closed-loop controller is adapted accordingly.

It can be seen in Figure 11 that the performance of the controller is worse, but primarily during the induction phase. During the maintenance phase, the performance is very similar to the results in Figure 10. This illustrates the issue with changing γ during the induction phase as well as that it has to be made sure that the maintenance phase has certainly begun before any surgical stimulus is applied.

Additionally, it can be seen in Figure 11 that when a step occurs when the BIS level is far above or below 50%, there is a jump in the BIS level (for instance, see yellow ellipse in Figure 11). This is explained by looking at Figure 7. As the effect-site concentrations remain constant, changing γ results in a jump in the BIS level. The amplitude of this jump becomes larger for BIS levels far above and below 50%, reaches a maximum and becomes zero for 100% and 0%. This discussion demonstrates that the current level of BIS determines the effect a change in γ has.

C. *Stability analysis*

As the dynamics of the system are linear and time-invariant, is the Jacobian linearization (A,B) of the system exactly equal to the state and input matrix of the system. It was argued in Section IIID that the state matrix is Hurwitz. Hence, the system is asymptotically stable (and of course, stabilizable). Following the procedure described in IVB, a terminal penalty matrix, a local linear state feedback matrix and terminal region were obtained which fulfil all the requirements of the procedure. It is therefore concluded that the designed QIH-MPC controller is asymptotically stable within the feasible region.

VI. CONCLUSIONS AND SUGGESTIONS FOR FURTHER RESEARCH

The control performance of the designed Quasi-infinite Horizon MPC controller is generally as desired, even when considering inter- and intrapatient variability as well as nociceptor stimulation and interventions by the anesthesiologist. Moreover, it was shown that the controller is stable for a variety of patients and an objective way of checking stability for other patients has been presented. Further research is required to predict the size of the feasible region, to determine the robustness properties of the controller and to find a solver which can solve the non-convex optimization problem. Additionally, adaptive control needs to be implemented and the models in the patient model can also be improved to more accurately represent reality while maintaining their suitability for control.

REFERENCES

[1] R. Hamill-Ruth and M. Marohn, "Evaluation of Pain in the Critically Ill Patient, " *Critical Care Clinics*, vol. 15, no. 1, pp. 35-54, 1999.

[2] K. Puntillo, D. Stannard, C. Miaskowski, K. Kehrle and S. Gleeson, "Use of a Pain Assessment and Intervention Notation (P. A. I. N.) tool in critical Care Nursing Practice: Nurses' Evaluations, " *Heart and Long: the journal of critical care*, vol. 31, no. 4, pp. 303-314, 2002.

[3] N. Desbiens, A. Wu, S. Broste, N. Wenger, A. Connors, J. Lynn, Y. Yasui, R.S. Philips and W. Fulkerson, "Pain and Satisfaction with Pain control in seriously ill hospitalized Adults: findings from the SUPPORT research investigations. For the SUPPORT investigators. Study to understand Prognoses and Preferences for Outcomes and Risks of Treatment," *Critical Care Medicine*, vol. 24, no. 12, pp. 1956-1961, 1996.

[4] M. Neckebroek, T. De Smet and M. Struys, "Automated drug delivery in anesthesia," *Curr Anesthesiol Rep*, vol. 3, pp. 18-26, 2013.

[5] T. Schnider, C. Minto, S. Shafer, P. Gampus, C. Andresen, D. Goodale and E. Youngs, "The influence of age on Propofol pharmacodynamics," *Anesthesiology*, vol. 90, pp. 1502-1516, 1999.

[6] D. Copot, R. De Keyser and C. Ionescu, "Drug Interaction Between Propofol and Remifentanil in Individualised Drug Delivery Systems," *9th IFAC Symposium on Biological and Medical Systems*. The International Federation of Automatic Control, Berlin, Germany, Aug,31 – Sept 2, 2015.

[7] G. Dumont, "Feedback control for clinicians," *Journal of Clinical Monitoring and Computing*, vol. 23, pp. 435-454, 2014.

[8] A. Absalom, R. De Keyser and M. Struys, "Closed loop anesthesia: are we getting close to finding the holy grail?" *Anesthesia and Analgesia*, vol. 112, pp. 516-518, 2011.

[9] C. Ionescu, J.T. Machado, R. De Keyser, J. Decruyenaere and M.M.R.F. Struys, "Nonlinear dynamics of the patient's response to drug effect during general anesthesia," *Communications in Nonlinear Science and Numerical Simulation*, vol. 20, no. 3, pp. 914-926, 2015.

[10] C. Rocha, T. Mendonca and M. Silva, "Individualizing propofol dosage: a multivariate linear model approach," *Journal of Clinical Monitoring and Computing*, vol. 28, no. 6, pp. 525-536, 2014.

[11] L. Kovacs, "Linear parameter varying (LPV) based robust control of type-I diabetes for real patient data," *Knowledge based Systems*, vol. 122, pp. 199-213, 2017.

[12] D. Drexler, L. Kovacs, J. Sapi, I. Harmati and Z. Benyo, "Model-based analysis and synthesis of tumor growth under angiogenic inhibition: a case study," *IFAC Proceedings*, vol. 44, no. 1, pp. 3753-3759, 2011.

[13] B. Kiss, J. Sapi and L. Kovacs, "Imaging method for model-based control of tumor diseases," *Proceedings of the IEEE 11th International Symposium on Intelligent Systems and Informatics (SISY)*, pp. 271-275, 2013.

[14] J. K. Popovic, D. Spasic, J. Tovic, J. Kolarovic, R. Malti, I.M. Mitic, S. Pilipovic and T. Atanackovic, "Fractional model for pharmacokinetics of high dose methotrexate in children with acute lymphoblastic leukaemia," *Commun Nonlinear Sci Nummer Simulat*, vol. 22, pp. 451-471, 2015.

[15] A. Churilov, A. Medvedev and A. Shepeljavyi, "Mathematical model of nonbasal testosterone regulation in the male by pulse modulated feedback," *Automatica*, vol. 45, pp. 78-85, 2009.

[16] D. Copot and C. Ionescu, "Drug delivery system for general anesthesia: where are we?" *Proceedings of the IEEE International Conference on Systems, Man, and Cybernetics (SMC)*, pp. 2452-2457, 2014.

[17] F. Padula, C. Ionescu, N. Latronico, M. Paltenghi, A. Visoli and G. Vivacqua, "Optimized PID control of depth of hypnosis in anesthesia," *Computer Methods and Programs in Biomedicine*, vol. 144, pp. 21-35, 2017.

[18] D. Copot, F. Kussé, Ma. Ghita, Mi. Ghita, M. Neckebroek and A. Maxim, "Distributed model predictive control for hypnosis-hemodynamic maintenance during anesthesia," *15th IEEE International Conference on Control & Automation*, 16-19 July, Edinburgh, Scotland, accepted for publication.

[19] X. Jin, C. Kim and G. Dumont, "A semi-adaptive control approach to closed-loop medication infusion," *Int J Adapt Control and Signal Proce*, vol. 31, pp. 240-354, 2017.

[20] C. Ionescu, D. Copot and R. De Keyser, "Anesthesiologist in the loop and predictive algorithm to maintain hypnosis while mimicking surgical disturbance," *IFAC World Congress*, Toulouse, France, July 2017, pp. 15080-15085, 2017.

[21] C.M. Ionescu, D. Copot, M. Neckebroek and C.I. Muresan, "Anesthesia regulation: Towards Completing the picture," *2018 IEEE International Conference on Automation, Quality and Testing, Robotics (AQTR)*, Cluj-Napoca, 2018, pp. 1-6.

[22] D. Copot, A. Chevalier, C.M. Ionescu and R. De Keyser, "A two-compartment fractional derivative model for Propofol diffusion in anesthesia, "2013 IEEE International Conference on Control Applications (CCA), Hyderabad, 2013, pp. 264-269.

[23] C.F. Minto, T.W. Schnider, T.D. Egan, E. Youngs, H.J.M. Lemmens, P. L. Gambus, V. Billard, J.F. Hoke, K.H.P. More, D.J Hermann, K.T. Muir, J.W. Mandema and S.L. Shafer, "Influence of Age and Gender on the Pharmacokinetics and Pharmacodynamics of Remifentanil: I. Model Development," *Anesthesiology*, vol. 86, no. 1, pp. 10-23, 1997.

[24] C.F. Minto, M. White, N. Morton and G.N. Kenny, "Pharmacokinetics and pharmacodynamics of remifentanil, II model application," *Anesthesiology*, vol. 86, pp. 24-33, 1997.

[25] C. Rocha, T. Mendonça and M.E Silva, "Modelling neuromuscular blockade: a stochastic approach based on clinical data," in *Mathematical and Computer Modelling of Dynamical Systems*, vol. 19, no. 6, pp. 540-556, 2013.

[26] C.M. Ionescu, I. Nascu and R. De Keyser, in *J Clin Monit Comput*, vol. 28, pp. 537-546, 2014. https://doi.org/10.1007/s10877-013-9535-5

[27] C.C. Palerm and B.W. Bequette, "Hemodynamic control using direct model reference adaptive control – experimental results," *European Journal of Control*, vol. 11, no. 6, pp. 558-571, 2005.

[28] J.F. Standing, G.B. Hammer, W.J. Sam and D.R. Drover, "Pharmacokinetic-pharmacodynamic modelling of the hypotensive effect of Remifentanil in infants undergoing cranioplasty," *Pediatric Anesthesia*, vol. 20, no. 1, pp. 7-18, 2010.

[29] M.M. Struys, M.J. Coppens, N. De Neve, E.P. Mortier, A.G. Doufas, J.F. Van Bocxlaer and S.L. Shafer, "Influence of administration rate on propofol plasma-effect site equilibration," *Anesthesiology*, vol. 107, pp. 386-396, 2007.

[30] A.M. Kirit and S. Rajaguru, "Adopting pade approximation for first order plus dead time models for blending process," *International Journal of Engineering Technology*, vol. 7, pp. 2800-2805, 2018.

[31] C. Yu, R. J. Roy, H. Kaufman and B.W. Bequette, "Multiple-model adaptive predictive control of mean arterial pressure and cardiac output," *IEEE Transactions on Biomedical Engineering*, vol. 39, no. 8, pp. 765-778, 1992.

[32] M.M. Struys, T. De Smet, S. Greenwald, A.R. Absalom, S. Bingé and E.P. Mortier, "Performance evaluation of two published closed-loop control systems using bispectral index monitoring: a simulation study," *Anesthesiology*, vol. 100, no. 3, pp. 640-647, 2004.

[33] S.H. Lehnighk, "On the Hurwitz Matrix," *Zeitschrift für Angewandte Mathematic und Physik*, vol. 21, no. 3, pp. 498-500, 1970.

[34] R. Findeisen and F. Allgöwer, "An introduction to nonlinear model predictive control," *21st Benelux Meeting on Systems and Control*, 2002, pp. 1-23.

[35] H. Chen and F. Allgöwer, "A quasi-infinite horizon nonlinear model predictive control scheme with guaranteed stability," *Automatica*, vol. 34, no. 10, pp. 1205-1218, 1998.

[36] J.B. Rawlings and D.Q. Mayne, *Model predictive control: theory and design*, Madison, Wisconsin: Nob Hill Pub. 2009.

[37] G.V. Reklaitis, A. Ravindran and K.M. Ragsdell, *Engineering optimization: Methods and applications*, New York: Wiley, 1983.

[38] S.J. Wright, "Efficient convex optimization for linear MPC," in *Handbook of Model Predictive Control*, Birkhäuser, Cham, pp. 287-303, 2019.

Contents

List of Tables

List of Figures

List of Abbreviations

BIS bispectral index

CO cardiac output

CPU central processing unit

EEG electroencephalogram

MAP mean arterial pressure

MPC model predictive control

NMB neuromuscular blockade

NMPC nonlinear model predictive control

PD pharmacodynamic

PID control proportional-integral-derivative control

PK pharmacokinetic

QIH-MPC Quasi-infinite Horizon Model Predictive Control

RASS Ramsay Agitation Sedation Score

SNP Sodium Nitroprusside

Chapter 1

Introduction

1.1 Problem Statement

The goal of any anesthesia is to obtain the required anesthetic level while minimizing side-effects coming from over- as well as underdosing. As mentioned in [1], the outcomes of the studies [2], [3], [4] into the pain evaluation by nurses and the pain assessment by patients, lead to the conclusion that an objective automated drug delivery system benefits the patient. Especially considering the danger of significant physiologic consequences in case of inadequate pain treatment [5]. With a closed-loop control of general anesthesia, the safety of the patient is increased [6], [7] as human errors are avoided and a lower amount of drugs is injected. Moreover, by taking advantage of accurate infusion devices, novel monitoring techniques and drug synergies, under- and over-dosing are even further reduced [8]. If the delivery system would be enhanced with adaptive control, individualised protocols based on actual patient parameters could be provided. This is clearly the preferred option when compared to population based generic model parameters [8]. When tuned properly, an automatic controller could match the drug administration profile to the stimulation intensity of each individual surgery [9], [10], [11], [12]. This cumulates in reduced recovery times and in the end, a minimization of the healthcare costs [13]. Other possible benefits include the reduction of the workload of the anesthesiologist, who could focus on supervising in the procedure as well as on critical issues to the safety of the patient [8], [14]. Once demystified, other applications of automated drug delivery include for instance diabetes [15], cancer treatment [16], [17], immunodeficiency [18] and hormonal treatment [19].

1.2 State of the Art

As stated in [13], general anesthesia comprises three main parts: *hypnosis*, *analgesia* and *neuromuscular blockade*. Hypnosis is the loss of consciousness of the patient, which is commonly measured with a bispectral index (BIS) signal derived from an electroencephalogram (EEG) [20]. Analgesia on the other hand is the absence of perceived pain. Currently, it is quantified by a Ramsay Agitation Sedation Score (RASS) by indirect signs such as lacrimation, sweating and heart rate variability. One should note that heart rate is not a viable indicator during heart surgery or when additional drugs are taken to alter the patient's heart rate [21]. The lack of a direct and objective measurement of pain perception remains one of the main bottlenecks on the road to a control scheme for general anesthesia [21]. The recent availability of a nociceptor pathway model provides however a powerful tool for further research [21]. Finally, neuromuscular blockade (NMB) represents the induction of muscle paralysis during surgery as muscle movement is unwanted during surgical procedures. As an electromyography measures the activation of muscles, this is used to quantify the level of NMB [22]. From these three components, hypnosis and neuromuscular blockade are well understood, with contributions from various authors [23], [24], [25], [26], [27]. Analgesia however still requires further research.

When designing an automated controller for this task, one needs to realise that anesthesia consists of three phases (induction phase, maintenance phase and recovery phase), each with different control objectives. The induction phase is a set-point following task, where a target needs to be reached as fast as possible while avoiding dangerous overshoots. In contrast, during the maintenance phase it is important to have fast disturbance rejection to sustain the desired sedation level. The recovery phase finally does not pose a control problem as the administration of all the drugs is stopped after the surgery has been completed [14]. Administration of analgesic drugs to a conscious patient is not discussed in this thesis. The presence of two very different control tasks means that a single tuned controller might not be sufficient to provide adequate safety and comfort. In case of two controllers, a switching mechanism needs to be designed and implemented to ensure a smooth transition [14]. The ideal controller for general anesthesia is therefore one that quickly reaches the target without initial overshoot during the induction phase and is able to sustain the desired target level during the maintenance phase [28]. Possible control strategies for this application include PID control [24], adaptive PID control [29], adaptive polynomial control [30], [31], Bayesian filtering [32], [33] and predictive control [28], [34], [35]. More intricate optimal and nonlinear robust control strategies are not being applied due to their high complexity [22].

In [14], the performance of an optimally tuned PID controller is compared to the results in [28] and [36], where predictive control strategies were implemented. In all three papers, the same set of patients has been used, allowing a fair comparison between the simulations. It is observed in [14] that the derivative action of the PID controller is necessary to outperform the MPC controller. The PID controller namely combines a faster induction phase with a very similar maximum overshoot and a satisfactory disturbance rejection performance. The author of that paper therefore concludes that any control strategy for anesthesia should be compared in performance to optimally tuned PID controllers. However, predictive control schemes (together with online adaptation) have the advantage that they mimic the real-life anticipatory reaction of the anesthesiologist, therefore providing an intuitive way of control [37], [38].

In order to implement *model predictive control* (MPC) and deal with the different control objectives during separate phases of anesthesia, a patient model is required. Although a patient model based on neural network modelling would indeed be a step towards reality, a control law which can provide an analytical solution is currently still preferred to maintain constraints and guarantee patient safety by ensuring stability [21]. Hence, it is vital that any designed control scheme has been subject to a stability analysis. At present, no literature can be found that examines the stability of a MPC scheme with a complete patient model [21].

1.3 Objectives of the thesis

The first goal of this thesis is to create a benchmark model for the closed-loop control of the complete hemodynamic and anesthetic regulatory problem. This means that the three parts of anesthesia (hypnosis, analgesia, neuromuscular blockade) will be included as well as two hemodynamic parameters (cardiac output, mean arterial pressure). Additionally, the real-life synergy between the hypnotic and analgesic drug will be included in the patient model.

The second goal is to analyse this patient model in open-loop, taking into account the variation between several patients (interpatient variability). This will be done by looking up in literature the intervals as well as the nominal values of the parameters of the separate models used to build the patient model.

The third goal is to control the model in closed-loop using model predictive control. When implementing model predictive control, special attention will be given to the stability of the scheme as well as the online feasibility. The designed controller then needs to be tested in simulation. The performance of the controller for both inter- and intrapatient (gradual change within the same patient) variability also needs to be investigated. Finally, the real-life case where there is nociception stimulation and the anesthesiologist is part of the control loop has to be simulated.

1.4 Outline of each chapter

In Chapter 2, all the models required for the patient model are presented and discussed, including the intervals and adaptation schemes for the parameters in these models. In a separate section, nociceptor stimulation and the anticipatory intervention by the anesthesiologist are discussed. Further, in Chapter 3 the complete patient model is analysed and open-loop stability is checked. For these simulations, the parameters of the models are varied within the intervals described in Chapter 2. The actual implementation of model predictive control (MPC) is discussed in Chapter 4, whereby the chapter begins with an explanation of the working principle of MPC. Then, the choice for Quasi-infinite Horizon MPC (QIH-MPC) is argued and its working principle explained. Further, the chapter includes a discussion on the stability, feasibility and robustness of the QIH-MPC scheme. The chapter concludes with the actual implementation in MATLAB and Simulink. The results of the simulations are discussed in Chapter 5. These include the choice of the prediction horizon, the effect of the delay of BIS measurement, the performance for the nominal model, the effect of nociception stimulation and the anesthesiologist in the loop as well as the performance of the controller in the case of inter- and intrapatient variability. Finally, Chapter 6 provides concluding remarks as well as suggestions for further research.

Chapter 2

Models for the control of anesthesia

2.1 Introduction to general anesthesia

Propofol (a hypnotic drug) and Remifentanil (an opioid drug) are commonly used to respectively induce *hypnosis* and *analgesia*, but their usage is also contested [39]. In this thesis, they will be the selected drugs due to their fast onset and recovery times as well as their suitability for control [11]. These hypnotic and opioid drugs also have side-effects on the heart rate, respiratory rate, mean arterial pressure, etc. [21] These side-effects are partly negated by the infusion of Dopamine and Sodium Nitroprusside. The disadvantage of infusing Dopamine is that it increases the cardiac output, thereby clearing Propofol faster from the body. This results in an increase in BIS levels [40]. Currently, however, no model for this effect is available [21], so it will not be included in the patient model. The respiratory rate is not relevant in this study as patients are generally mechanically ventilated during general anesthesia, so a fixed respiratory rate is assumed. The full patient model can be seen in Figure 2.1 (taken from [41]). Cardiac Output (CO) is the amount of blood pumped by the heart each minute [42] and can be measured by both invasive (for instance, requiring a catheter) as well as non-invasive techniques (for instance, using ultrasound) [43]. Mean Arterial Pressure (MAP) is the average arterial blood pressure and can be calculated using the measured systolic (highest) and diastolic (lowest) blood pressure [44]. When creating the model, time delays also need to be considered as they threaten the stability of the closed loop [11], [22], [45], [46].

General anesthesia can be subdivided into three subsequent phases: induction phase, maintenance phase and recovery phase. These three phases also distinguish themselves in their specific nature for control. The induction phase is a set-point following task, where the setpoint needs to be achieved as fast as possible while avoiding overshoot. The maintenance phase is the phase where external disturbances related to surgical stimulation are rejected. During the recovery phase, the administration of the drug is stopped so the patient can recover consciousness. One should note that there are now two different control tasks: set-point following and load disturbance rejection, which is challenging in terms of control [47].

2.2 Models for control of depth of anesthesia

2.2.1 Compartmental models

When creating a model for anesthesia, it is important that the mass balance holds, as this implies that the link between physiological and mathematical parameters is maintained [48]. To model the pharmacokinetics (PK), the body is divided into three compartments: blood, muscles and fat whereby the last two compartments respectively represent the drug exchange with well and poorly diffused body tissues [13]. An additional effect-site compartment combined with a non-linear relationship is added to model the drug pharmacodynamics (PD). This non-linear relationship is often a sigmoid function [49], more specifically a Hill-curve according to formula 2.1. In this formula is E [%] the (predicted) effect of the drug, C [$\mu g/ml$] the concentration of the drug at time t, EC_{50} [$\mu g/ml$] the concentration needed to obtain 50% of the maximum effect E_{max}[%] and γ [-] the Hill-coefficient of sigmoidicity [13].

$$E = \frac{E_{max}.C^{\gamma}}{EC_{50}^{\gamma} + C^{\gamma}} \tag{2.1}$$

The PK-PD models for Propofol and Remifentanil that will be used throughout this thesis are the 4th order compartmental models proposed by Schnider [50] and Minto [51], [52] respectively. The complete PK-PD model can be seen in Figure 2.2 (taken from [22]).

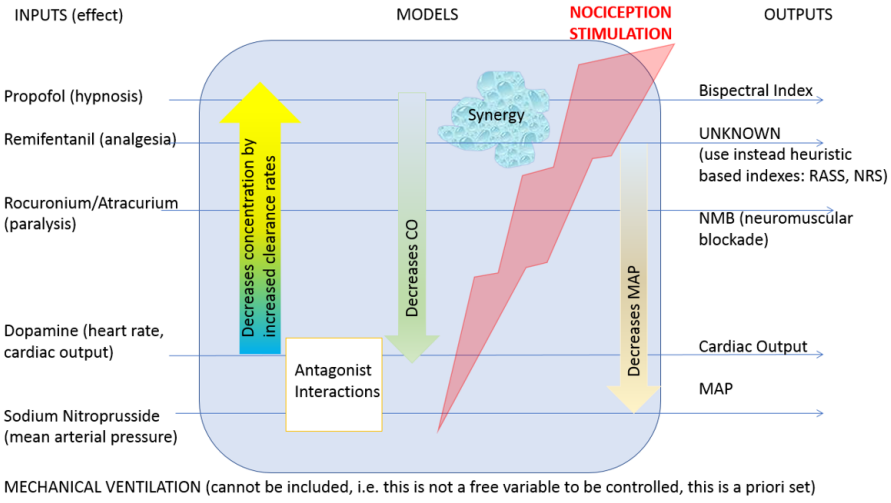

Figure 2.1: Patient model general anesthesia

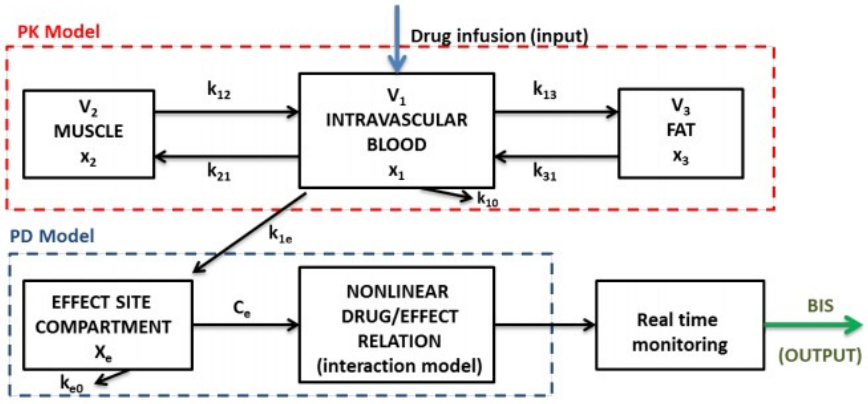

Figure 2.2: PK-PD Model with BIS as output

Deriving the equations from Figure 2.2, the model of equation 2.2 is obtained.

$$\begin{aligned}
\frac{dx_1(t)}{dt} &= -(k_{10}+k_{12}+k_{13})x_1(t) + k_{21}x_2(t) + k_{31}x_3(t) + u(t) \\
\frac{dx_2(t)}{dt} &= k_{12}x_1(t) - k_{21}x_2(t) \\
\frac{dx_3(t)}{dt} &= k_{13}x_1(t) - k_{31}x_3(t) \\
\frac{dx_e(t)}{dt} &= -k_{e0}x_e(t) + k_{1e}x_1(t)
\end{aligned} \tag{2.2}$$

In matrix form:

$$\begin{bmatrix} \frac{dx_1(t)}{dt} \\ \frac{dx_2(t)}{dt} \\ \frac{dx_3(t)}{dt} \\ \frac{dx_e(t)}{dt} \end{bmatrix} = \begin{bmatrix} -(k_{10}+k_{12}+k_{13}) & k_{21} & k_{31} & 0 \\ k_{12} & -k_{21} & 0 & 0 \\ k_{13} & 0 & -k_{31} & 0 \\ k_{1e} & 0 & 0 & -k_{e0} \end{bmatrix} \begin{bmatrix} x_1 \\ x_2 \\ x_3 \\ x_e \end{bmatrix} + \begin{bmatrix} 1 \\ 0 \\ 0 \\ 0 \end{bmatrix} u(t) \tag{2.3}$$

The transfer function is then according to the formula G(s) = C$(sI - A)^{-1}$B + D, with the following matrices:

$$\begin{aligned}
A &= \begin{bmatrix} -(k_{10}+k_{12}+k_{13}) & k_{21} & k_{31} & 0 \\ k_{12} & -k_{21} & 0 & 0 \\ k_{13} & 0 & -k_{31} & 0 \\ k_{1e} & 0 & 0 & -k_{e0} \end{bmatrix} \\
B &= \begin{bmatrix} 1 \\ 0 \\ 0 \\ 0 \end{bmatrix} \\
C &= \begin{bmatrix} 0 & 0 & 0 & 1 \end{bmatrix} \\
D &= 0
\end{aligned} \tag{2.4}$$

In this thesis it is assumed that the pharmacokinetic parameters (height, weight, age, gender) are accurate so that the differences in individual responses are solely due to the variation of the pharmacodynamic parameters. This simplification is also assumed in [33] and it is important to note if adaptive control is to be implemented. However, diseases or inaccurate measurement of the pharmacokinetic parameters impair a correct identification of the constants in the models employed [7], [50], [53], [54], [55]. These model uncertainties result in a loss of control performance. Furthermore, Rocha acknowledges that it is difficult to accurately estimate the parameters of the pharmacokinetic models as the concentration patterns are a mixture of declining exponential functions. This has led to models that are either specifically built from a control point of view or just to fit available data sets with parameters that have no physiological meaning [56].

The biggest challenges for control however are that a Hill-curve is non-linear and that the curve is subject to intra- and inter-patient variability. This variability is exemplified in Table 2.1 for the model that describes the effect of Propofol on the BIS-signal. These values are used in multiple papers in literature, for instance [28], [33], [36], [57]. Despite the challenges, the Hill-curve is nonetheless used as it is able to predict the maximum drug effect, which is a key characteristic describing biological phenomena, and because of its flexibility to fit measured data, due to the shape parameter γ. That being said, there is a lot of room for improvement [13].

Id	Age	H [cm]	W [kg]	Gender	C_{e50}	γ	E_0	E_{max}
1	40	163	54	F	6.33	2.24	98.8	94.1
2	36	163	50	F	6.76	4.29	98.6	86.00
3	28	164	52	F	8.44	4.10	91.2	80.70
4	50	163	83	F	6.44	2.18	95.9	102.00
5	28	164	60	M	4.93	2.46	94.7	85.30
6	43	163	59	F	12.00	2.42	90.2	147.00
7	37	187	75	M	8.02	2.10	92.0	104.00
8	38	174	80	F	6.56	4.12	95.5	76.40
9	41	170	70	F	6.15	6.89	89.2	63.80
10	37	167	58	F	13.70	1.65	83.1	151.00
11	42	179	78	M	4.82	1.85	91.8	77.90
12	34	172	58	F	4.95	1.84	96.2	90.80
13	38	169	65	F	7.42	3.00	93.1	96.58

Table 2.1: Parameter variability Hill-curve Propofol to BIS

If tools from fractional calculus were employed, the problem of the non-linearity of the Hill curve could be avoided, resulting in a linear system (when represented on a log-log plot). Hence, linear control strategies could be employed [58], [59]. This makes particular sense as drug assimilation, transport and clearance are dominated by diffusion, a process well-described by fractional calculus [58], [60]. Super-diffusion (faster process, more uptake) and sub-diffusion (slower process, less uptake) can respectively be modelled by making the order n of the derivatives greater or lower than one, with n a real number. As the alteration of the variable n can incorporate many effects, it captures well interpatient variability [48]. Moreover, the derivatives of non-integer positive order permit the inclusion of the so-called "memory-effect" [61], allowing the modelling of non-homogeneous mixed compartments [62]. A possible function for the modelling of these fractional dynamics is for instance formula 2.5. In this equation, $C_e(t)$ is the effect-site concentration versus time and BIS(t) the value of BIS versus time [58].

$$\frac{C_e(t)}{BIS(t)} = k.t^n \tag{2.5}$$

The problem with such a scheme is that the online identification and adaptation of the parameters k and n is challenging as a linear sampling time does not preserve linearity in this case as the model is only linear on a log-log plot. To remedy this problem, a logarithmic sample time has been proposed [63]. This however impairs the integration of the fractional order model into a closed loop control system. Further research needs to go into investigating whether a logarithmic sampling rate can successfully be applied to the closed loop control of depth of anesthesia [58]. Due to the complexity of tuning a controller for a fractional order model and the issues concerning the adaptation to interpatient variability, fractional order models are not further discussed in this thesis.

From the discussion above it is clear that intra- and interpatient variability of the PK-PD model poses a real challenge, demonstrating the importance of adaptive control strategies to ensure the best performance possible. Furthermore, the real-life varying time delay [13] is a big threat to the stability of the system. As compensating time delay is a struggle in control engineering, it is assumed in this thesis that all the time delays are fixed.

2.2.2 Synergies

There is a super-additive effect when using Remifentanil in combination with Propofol [22], reducing the Propofol concentration for loss of consciousness by 25% [8] and hence minimising the risk of over-dosages [64]. The Hill-curve now becomes a surface, that is modelled according to equation 2.6, with for example shape factor $\gamma = 8$, $\sigma = 8.2$ (measure for the synergy between the two drugs) and the maximum effect $E_{max} = 100$. The result of this model can be found in Figure 2.3.

$$BIS = Emax.\frac{(U_{prop} + U_{remi} + \sigma.U_{prop}.U_{remi})^{\gamma}}{1 + (U_{prop} + U_{remi} + \sigma.U_{prop}.U_{remi})^{\gamma}} \tag{2.6}$$

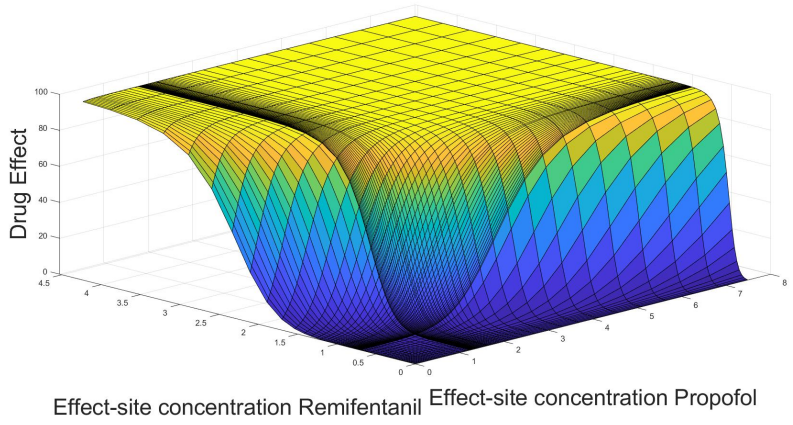

Figure 2.3: BIS interaction surface Propofol and Remifentanil

The issue is that this synergetic relation not only differs between different patients (i.e. interpatient variability), but also changes within the same patient (i.e. intrapatient variability) [22]. This means that an identification scheme is required. Knowledge about the actual synergetic relation can then be exploited by control engineers to improve the performance of individualised drug dosing strategies [22]. However, the identification is difficult as the surface is nonlinear and constraints imposed for the safety of the patient mean the global solution cannot be used if it is not feasible [11].

Remifentanil also influences the cardiac output, the mean arterial pressure and neuromuscular blockade. These interactions are currently modelled as simple linear addition (see discussion below). Dopamine and Sodium Nitroprusside both have an effect on the cardiac output as well as the mean arterial pressure, but their synergy is once again modelled in an additive way. In the present patient model, there is no reducing effect of Dopamine on the effect-site concentration of Propofol.

2.2.3 Parameter nociceptor transfer function

With the nociceptor pathway model (equation 2.7), a link is established between surgical stimulation and how it is perceived by the patient [21].

$$NOCI = K.\frac{(s^2 + z_1 s + z_2)(s^2 + z_3 s + z_4)(s^2 + z_5 s + z_6)}{(s^2 + p_1 s + p_2)(s^2 + p_3 s + p_4)(s^2 + p_5 s + p_6)} \tag{2.7}$$

zeros	$z_1 = 0.6 * 150$	$z_2 = 150^2$	$z_3 = 0.16 * 165$	$z_4 = 165^2$	$z_5 = 0.2 * 155$	$z_6 = 155^2$
poles	$p_1 = 0.44 * 149$	$p_2 = 149^2$	$p_3 = 0.3 * 163$	$p_4 = 163^2$	$p_5 = 0.2 * 155$	$p_6 = 155^2$
K	2					

Table 2.2: Parameter values nociceptor pathway model

The values in Table 2.2 were taken from [21], where it is explicitly stated that "the values of the model are by no means fixed or precise, they are approximations to fit clinical observations and measured data (where available)". Furthermore, in [65] the fitting of the transfer function model to the frequency response complex impedance data is discussed: "the fitting was obtained using nonlinear least squares identification with the MATLAB-command *lsqnonlin*, with steepest gradient descent, in an iterative manner. Iteration was performed as to avoid local minimum and the number of iterations between the identified results varied between #2-#4 in all data. The iteration was stopped when the model parameters changed less than 5%." This means the intervals from literature were determined using a least-squares method on a specific data set. Hence, they are strictly speaking not representative for a specific patient. They will however be used nonetheless.

2.2.4 PK parameters of Propofol and Remifentanil

In [20], the following model was used:

$$\begin{aligned} PK(s) &= \frac{(s+k_{21})(s+k_{31})}{V_1(s+\pi)(s+\alpha)(s+\beta)} \\ \pi+\alpha+\beta &= k_{10}+k_{12}+k_{13}+k_{21}+k_{31} \\ \pi\alpha+\pi\beta+\alpha\beta &= k_{10}(k_{21}+k_{31})+k_{31}(k_{12}+k_{21})+k_{13}k_{21} \\ \pi\alpha\beta &= k_{10}k_{21}k_{31} \end{aligned} \tag{2.8}$$

The values for the variables in this model can be found in Table 2.3 (according to [50] and [51] respectively).

Study	V_1 (l) (l/kg)	Poles			Zeros	
		π (s^{-1})	α (s^{-1})	β (s^{-1})	k_{21} (s^{-1})	k_{31} (s^{-1})
Propofol						
Adult, 30 years, 50kg, 1.70m	21.5	16.0e-3	14.0e-4	4.95e-5	3.3e-3	5.8e-5
Adult, 30 years, 70kg, 1.70m	30.1	16.5e-3	15.0e-4	4.9e-5	3.3e-3	5.8e-5
Adult, 30 years, 110kg, 1.70m	47.3	20.0e-3	19.0e-4	5.3e-5	3.3e-3	5.8e-5
Elderly, 70 years, 70kg, 1.70m	30.1	12.3e-3	20.0e-4	4.9e-5	3.3e-3	5.8e-5
Remifentanil						
Adult, 30 years, 50kg, 1.70m	4.5	20.6e-3	2.0e-3	2.6e-4	4.1e-3	2.7e-4
Adult, 30 years, 70kg, 1.70m	5.3	18.2e-3	1.8e-3	2.6e-4	3.7e-3	2.7e-4
Adult, 30 years, 110kg, 1.70m	6.2	16.3e-3	1.7e-3	2.6e-4	3.3e-3	2.7e-4
Elderly, 80 years, 70kg, 1.70m	4.1	12.0e-3	1.4e-3	0.9e-4	2.2e-3	0.9e-4

Table 2.3: Propofol and Remifentanil PK parameter sets

However, there are in literature formulas available to calculate the constants required for the model in equation 2.2 as well as the intervals. From [51], both the following formulas for Remifentanil as well as the intervals are obtained, see Table 2.4.

$$
\begin{aligned}
V_1 &= 5.1 - 0.0201(age - 40) + 0.072(lbm - 55)\ [l] \\
V_2 &= 9.82 - 0.0811(age - 40) + 0.108(lbm - 55)\ [l] \\
V_3 &= 5.42\ [l] \\
C_{l1} &= 2.6 + 0.0162(age - 40) + 0.0191(lbm - 55)\ [l.min^{-1}] \\
C_{l2} &= 2.05 - 0.0301(age - 40)\ [l.min^{-1}] \\
C_{l3} &= 0.076 - 0.00113(age - 40)\ [l.min^{-1}] \\
k_{10} &= \frac{C_{l1}}{V_1}\ [min^{-1}] \\
k_{12} &= \frac{C_{l2}}{V_1}\ [min^{-1}] \\
k_{13} &= \frac{C_{l3}}{V_1}\ [min^{-1}] \\
k_{21} &= \frac{C_{l2}}{V_2}\ [min^{-1}] \\
k_{31} &= \frac{C_{l3}}{V_3}\ [min^{-1}] \\
k_{e0} &= 0.595 - 0.007(age - 40)\ [min^{-1}]
\end{aligned}
\tag{2.9}
$$

From [50], the same is done for Propofol, see also Table 2.5.

$$
\begin{aligned}
V_1 &= 4.27\ [l] \\
V_2 &= 18.9 - 0.391(age - 53)\ [l] \\
V_3 &= 2.38\ [l] \\
C_{l1} &= 1.89 + 0.0456(weight - 77) - 0.0681(lbm - 59) \\
&\quad + 0.0264(height - 177)\ [l.min^{-1}] \\
C_{l2} &= 1.29 - 0.024(age - 53)\ [l.min^{-1}] \\
C_{l3} &= 0.836\ [l.min^{-1}] \\
k_{10} &= \frac{C_{l1}}{V_1}\ [min^{-1}] \\
k_{12} &= \frac{C_{l2}}{V_1}\ [min^{-1}] \\
k_{13} &= \frac{C_{l3}}{V_1}\ [min^{-1}] \\
k_{21} &= \frac{C_{l2}}{V_2}\ [min^{-1}] \\
k_{31} &= \frac{C_{l3}}{V_3}\ [min^{-1}] \\
k_{e0} &= k_{1e} = 0.456\ [min^{-1}]
\end{aligned}
\tag{2.10}
$$

The lean body masses (lbm) for men and women respectively, are calculated according to equation 2.11 [66].

$$
\begin{aligned}
Male:\ LBM &= 1.1 * weight - 128 * (weight/height)^2 \\
Female:\ LBM &= 1.07 * weight - 148 * (weight/height)^2
\end{aligned}
\tag{2.11}
$$

Parameter	No covariates		Weight Proportional		LBM Proportional	
	Value	% CV	Value	% CV	Value	% CV
Estimated parameters						
Volumes	(l)		$(l.kg^{-1})$		$(l.kg^{-1})$	
Central	4.98	37	0.0668	29	0.0894	27
Rapid peripheral	9.01	39	0.124	39	0.165	37
Slow peripheral	6.54	63	0.0655	65	0.0871	65
Clearances	$(l.min^{-1})$		$(l.kg^{-1}.min^{-1})$		$(l.kg^{-1}.min^{-1})$	
Metabolic	2.46	23	0.034	23	0.0454	21
Rapid peripheral	1.69	52	0.0242	57	0.0323	55
Slow peripheral	0.065	56	0.000893	67	0.00119	66
Derived parameters						
Volumes	(l)		$(l.kg^{-1})$		$(l.kg^{-1})$	
Steady state	20.53		0.263		0.3415	
Fractional coefficients (unitless)						
A	0.897		0.896		0.895	
B	0.103		0.103		0.104	
C	0.00056		0.00078		0.00078	
Exponents (min^{-1})						
α	0.932		0.975		0.975	
β	0.102		0.105		0.105	
γ	0.0097		0.0133		0.0133	
Rate constants (min^{-1})						
k_{10}	0.494		0.509		0.508	
k_{12}	0.339		0.362		0.361	
k_{13}	0.013		0.013		0.013	
k_{21}	0.188		0.195		0.196	
k_{31}	0.010		0.014		0.014	
Half-lives (min)						
α	0.74		0.71		0.71	
β	6.78		6.62		6.60	
γ	71.7		52.3		52.2	

Table 2.4: Intervals Pharmacokinetic Parameters Remifentanil

Parameter	Value	% CV
Volumes (l)		
Central	θ_1	4.04
Rapid peripheral	θ_2+θ_7.(age-53)	< 1
Slow peripheral	θ_3	14.35
Clearances ($l.min^{-1}$)		
Metabolic	θ_4 + ((weight - 77).θ_8) + ((lbm - 59). θ_9) + ((height - 177).$\theta_1$0)	10.05
Rapid peripheral	θ_5 + θ_{11}.(age - 53)	< 1
Slow peripheral	θ_6	11.79
Parameter estimates	Value	standard error
θ_1	4.27	0.278
θ_2	18.9	2.330
θ_3	238	34.900
θ_4	1.89	0.059
θ_5	1.29	0.112
θ_6	0.836	0.044
θ_7	-0.391	0.070
θ_8	0.0456	0.009
θ_9	-0.0681	0.017
θ_{10}	0.0264	0.009
θ_{11}	-0.024	0.005

Table 2.5: Intervals Pharmacokinetic Parameters Propofol

2.2.5 PD models of Propofol and Remifentanil

The separate Hill-curve for Propofol is modelled as in equation 2.12, with $C_{50P} = 2.2$, $\gamma_p = 2$, $E_0 = 100$ and $E_max = 100$ [20], [67]. The same thing is done for Remifentanil in equation 2.13, with $C_{50R} = 13.7$, $\gamma_R = 2.4$, $E_0 = 100$ and $E_max = 100$ [20], [67]. These separate Hill-curves are included for reference, but will not be used in this thesis.

$$Effect\ Propofol = E_0 - E_{max} \cdot \frac{Ce_P^{\gamma_P}}{Ce_P^{\gamma_P} + C_{50P}^{\gamma_P}} \tag{2.12}$$

$$Effect\ Remifentanil = E_0 - E_{max} \cdot \frac{Ce_R^{\gamma_R}}{Ce_R^{\gamma_R} + C_{50R}^{\gamma_R}} \tag{2.13}$$

2.2.6 Parameters of the hemodynamic system

The antagonistic effects of Dopamine and Sodium Nitroprusside on the Cardiac Output and Mean Arterial Pressure are modelled as in equation 2.14. This equations consists of first order plus dead time models gij(s) with i being the drug having an effect on hemodynamic parameter j.

$$\begin{bmatrix} CO \\ MAP \end{bmatrix} = \begin{bmatrix} \frac{K_{11}.e^{-T_{11}s}}{1+\tau_{11}s} & \frac{K_{21}.e^{-T_{21}s}}{1+\tau_{21}s} \\ \frac{K_{12}.e^{-T_{12}s}}{1+\tau_{12}s} & \frac{K_{22}.e^{-T_{22}s}}{1+\tau_{22}s} \end{bmatrix} \begin{bmatrix} Dopamine \\ Sodium\ Nitroprusside \end{bmatrix} \tag{2.14}$$

The interval values of the parameters for the hemodynamic system come from [42], see Table 2.6.

Parameter	Typical	Range	Units
K_{11}	5	1-12	ml/μg
τ_{11}	300	70-600	s
T_{11}	60	15-60	s
K_{12}	3	0-9	mmHg.kg.min/μg
τ_{12}	40	30-60	s
T_{12}	60	15-60	s
K_{21}	12	-15-25	ml/μg
τ_{21}	150	70-600	s
T_{21}	50	15-60	s
K_{22}	-15	-50-(-1)	mmHg.kg.min/μg
τ_{22}	40	30-60	s
T_{22}	50	15-60	s

Table 2.6: Intervals parameters hemodynamic system

2.2.7 Parameter values of the synergistic relation

To describe the response surface for the interaction of Propofol and Remifentanil, the parameters from [68] are used. This paper also contains the statistical information of these parameters, see Table 2.7.

Parameter	TCI Predicted Drug Concentration		Bayesian Predicted Drug Concentration	
	Typical Value (%SE)	%CV	Typical Value (%SE)	%CV
$C_{50,remifentanil,hypnosis}$, ng/ml	19.0 (9)	(-)	19.3 (<1)	52
$C_{50,propofol,hypnosis}$, μg/ml	2.16 (19)	37	1.6 (<1)	45
Steepness	7.94 (33)	(-)	5.25 (<1)	(-)
Interaction, hypnosis	2.13 (16)	(-)	2.55 (<1)	2
Objective function	82.7		83.8	

Table 2.7: Intervals parameters synergistic relation

Note: %SE is the standard error of the estimated parameter and CV is the standard deviation (log domain). (-) means the variability was not distinguishable from 0.

2.2.8 Parameter values of the NMB model

In the used NMB model (equation 2.15) from [56], k_1, k_2, k_3 and C_{50} are assumed to be known process parameters. Only α and γ are modelled to be unknown patient-dependent parameters. A parameter identification procedure for Atracurium is adapted from [56], where Table 2.8 contains the initial values that represent the mean values for the population. The procedure is as follows:

$$\begin{aligned} NMB &= \frac{k1.k2.k3.\alpha^3}{(s+k1.\alpha)(s+k2.\alpha)(s+k3.\alpha)} \\ Effect &= Emax.\frac{C_{50N}^{\gamma_N}}{NMB^{\gamma_N}+C_{50N}^{\gamma_N}} \end{aligned} \tag{2.15}$$

k1	k2	k3	C_{50N}	α	γ
1	4	10	3.2425	0.0374	2.667

Table 2.8: Parameters NMB model

1. Set initial values for the parameters as the mean values for the population ($\alpha_0 = 0.0374$, $\gamma_0 = 2.6677$)
2. Based on equations 2.16 and 2.17, compute r(t) for those initial values of (α,γ) and the dosage u(t) given to the patient.

$$\begin{aligned} \dot{x}_1(t) &= -k_3\alpha x_1(t) + k_3\alpha u(t) \\ \dot{x}_2(t) &= k_2\alpha x_1(t) - k_2\alpha x_2(t) \\ \dot{x}_3(t) &= k_1\alpha x_2(t) - k_1\alpha x_3(t) \end{aligned} \tag{2.16}$$

$$r(t) = \frac{100}{1+(\frac{x_3(t)}{C_{50}})^{\gamma}} \tag{2.17}$$

3. Obtain
$$(\alpha, \beta) = \underset{\alpha,\beta \in \Re}{arg\ min}(\frac{d_1}{10} + \frac{d_2}{2} + \frac{d_3}{5}) \tag{2.18}$$
by minimizing the loss function Q = $\frac{d_1}{2} + \frac{d_2}{2} + \frac{d_3}{5}$ with r(t) computed from equations 2.16 and 2.17, subject to the restrictions $0 < \alpha \leq 0.1$ and $0 < \gamma \leq 10$.

4. If (α, β) satisfy inequalities 2.19, these are the individual parameters. Otherwise, proceed to step 5.

5. Minimize the maximum of $(\frac{d_1}{10}, \frac{d_2}{2}, \frac{d_3}{5})$ using (α, β) from step 4 as the initialising value
$$\begin{aligned} d_1 &\leq 10\ for\ phase\ 1 \\ d_2 &\leq 2\ for\ phase\ 2 \\ d_3 &\leq 5\ for\ phase\ 3 \end{aligned} \tag{2.19}$$
where the major effect of α is in phase 1 and the major effect of γ is in phase 3. Phase 2 is an intermediate region.

In [69], the k_i (i=1,2,3) values are determined by minimising the normalised error for a given database. C_{50} was kept constant during this study as in [70] was shown that the variability of this parameter does not strongly affect the identification.

2.2.9 Parameters of the Remifentanil effect on RASS

The Ramsay Agitation-Sedation Score (RASS) is a function that scales from -5 to 4 and is a measure for the sedation of the patient [71]. The influence of Remifentanil on this score is modelled as in equation 2.20, with k1 = k0 = 0.81 [72].
$$RASS = \frac{1}{k1.CeR + k0}.\frac{-2}{s+2} \tag{2.20}$$

2.2.10 Parameters of the Remifentanil effect on MAP PK/PD model

$$\begin{aligned} MAP &= \frac{-1}{k1.CeR + k0} \\ Effect &= Emaxr.\frac{MAP^{\gamma_{rMAP}}}{MAP^{\gamma_{rMAP}} + C_{50rMAP}^{\gamma_{rMAP}}} \end{aligned} \tag{2.21}$$

The parameter values for the model in 2.21 come from [73], see also Table 2.9. In [73], the mean baseline MAP (Emaxr) is assumed to be 70. This paper also gives intervals for this parameter which can be found in Table 2.10. As in [73] and [21], a constant value of 15 for CeR is assumed.

Parameter	Fixed effect	$\%SE$
Clearance (l.min^{-1}.70kg^{-1})	2.99	5.1
V_1 (l.70kg^{-1})	6.35	7.8
Q (l.min^{-1}.70kg^{-})	3.76	16.8
V_2 (l.70kg^{-1})	9.88	5.4
k_{e0} (min^{-1})	0.81	23.6
E_0 (mmHg)	69.7	4.9
EC_{50} (ng.ml^{-1})	17.1	7.8
γ	4.56	17.6
Pharmacokinetic additive error (ng.ml^{-1})	4.73	8.7
Pharmacodynamic additive error (mmHg)	4.47	5.5

Table 2.9: Intervals parameters Remifentanil on MAP

	Value
Sex (M/F)	5/2
Age (year)	0.743 (0.3-1.0)
Weight (kg)	7.59 (6.6-9.6)
Height (cm)	65.2 (47-82)
Mean arterial blood pressure (mmHg)	71.7 (60-87)

Table 2.10: Intervals Emaxr

Note: the values in Table 2.10 are either of the form mean (range) or mean ± standard deviation.

2.2.11 Parameters of the Remifentanil effect on NMB model

The effect of Remifentanil on neuromuscular blockade is calculated according to equation 2.22. This effect is simply added to the effect of Atracurium on neuromuscular blockade [21].

$$EMG = \frac{CeR}{3.4} \tag{2.22}$$

2.3 Approximation of first order plus dead time

Both the hemodynamic models (Section 2.2.6) and the measurement of BIS (Section 5.2) are modelled to be subject to time delays. In the Laplace domain, this dead time is modelled as exp(-Ts), with T being the time delay in seconds, which is nonlinear in s. Using Padé approximation, this nonlinear first order system is transformed into a linear system of higher order [74]. This system has the same gain, but a different phase angle for large frequencies. Assume for example a system with only dead time. This system can then be transformed by Padé approximation into a higher order system of which the order can be chosen.

In Figure 2.4, the phase plot of the original system (red dotted line) is compared to the phase plots of the Padé approximations of increasing order (from 1st to 10th). The higher the order of the approximation, the higher the frequency is at which the approximated transfer function cannot follow anymore (i.e. the phase shift increases faster for the exponential than for the approximated function). Clearly, the higher the order the better the approximation is but also the higher the computational complexity is [74]. A compromise needs to be made and it is therefore chosen to use a 4th order approximation in this thesis.

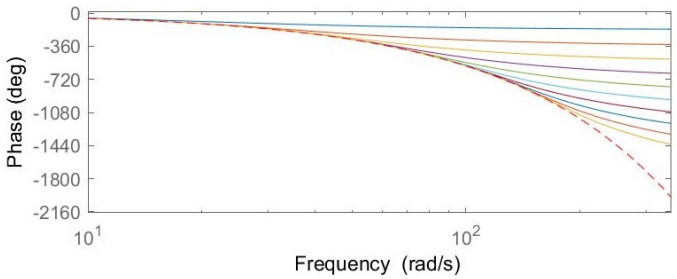

Figure 2.4: Comparison phase plot real delay with Padé approximation from 1st to 10th order

2.4 Nociceptor stimulation and anesthesiologist in the loop

So far, no surgical stimulus has been modelled to represent the stimulation during operation. The stimulation profile used in this thesis is taken from [38]. This input signal is filtered by a zero-phase digital Butterworth filter and subsequently passed through the nociceptor transfer function (equation 2.7). The result which will be used throughout this thesis can be found in Figure 2.5. As this disturbance can be anticipated by the anesthesiologist, the anesthesiologist might decide to intervene by administrating an additional bolus of Propofol. Consequently, this intervention needs to be integrated into the closed-loop [38]. The signal to model this intervention is adapted from [38] for different values of γ and can be found in Figure 2.6. This figure is constructed under the assumption that the anesthesiologist will adapt the bolus injection to the sensitivity of the patient.

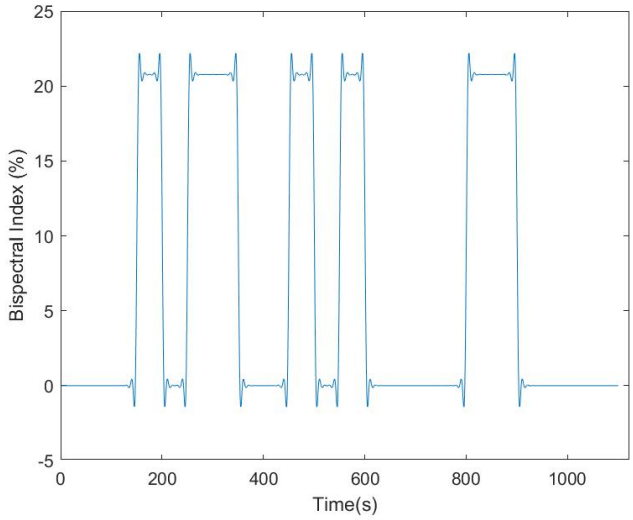

Figure 2.5: Nociceptor stimulation of patient model

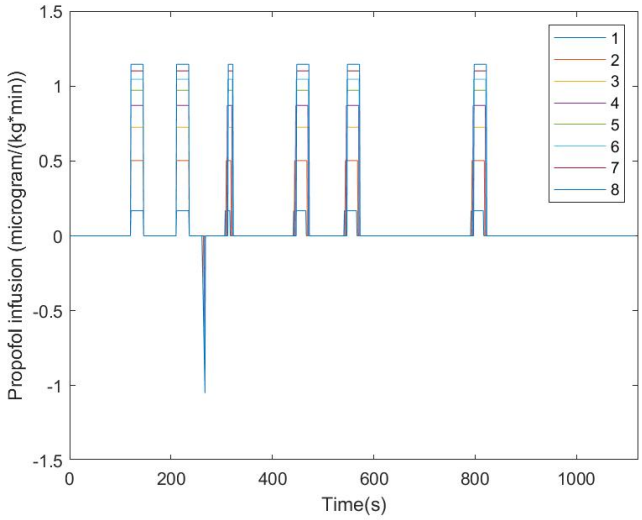

Figure 2.6: Anesthesiologist in the loop for γ = 1,2,3,4,5,6,7,8

Chapter 3

Anesthetic regulatory paradigm

3.1 Dynamics of the pharmacokinetic models

In Figures 3.1 to 3.6, the bode plots of the pharmacokinetic models for Propofol and Remifentanil are given. In each plot, one of the parameters of the model (i.e. age, height, weight) is varied within the intervals from Section 2.2.4. The parameter which is varied is always mentioned in the caption of the plot. This is done for male and female patients as the calculation of lean body mass is different for both. The phase margins of these bode plots can be found in Appendix B.1.1. From the bode plots it is however already clear that these pharmacokinetic models are always stable, independent of the variation of the parameters (within the defined intervals). The same is true for the bode plot of the pharmacokinetic model for neuromuscular blockade (see Figure 3.7). It is as Rocha claimed [56], these models are indeed specifically built for control purposes.

In Figures 3.1 and 3.4, it can be seen that there is one frequency at which all bode plots cross, independent of the age of the patient. This originates from the fact that, fundamentally, these two steady-state models are low-pass filters with 2 zeros and 4 poles. It is therefore claimed that the intersection of the bode plots is caused by the fact that the variation in age only affects the damping factor of the filter and not the natural frequency. The other parameters (i.e. height and weight) appear to affect both the damping factor and natural frequency.

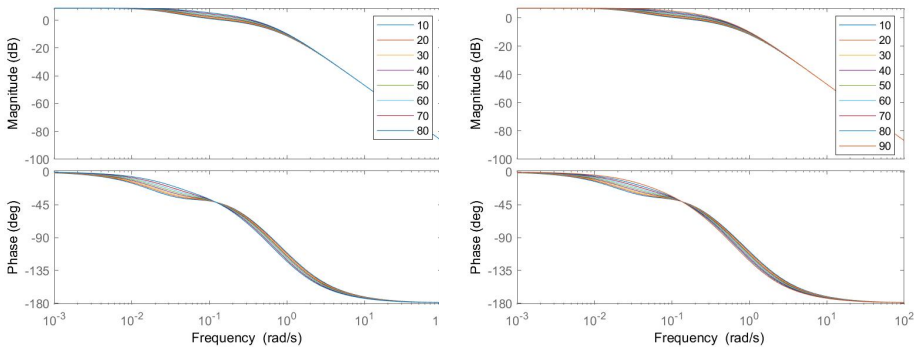

(a) Bode plot Propofol Male Age (years) (b) Bode plot Propofol Female Age (years)

Figure 3.1: Propofol SS PK model Age (years)

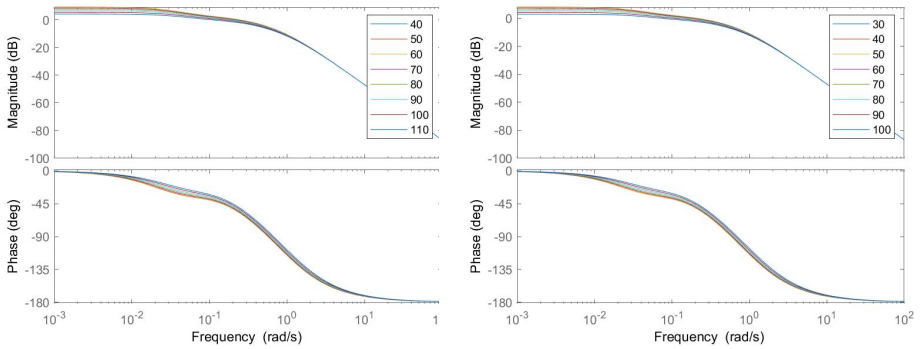

(a) Bode plot Propofol Male Weight (kg) (b) Bode plot Propofol Female Weight (kg)

Figure 3.2: Propofol SS PK model Weight (kg)

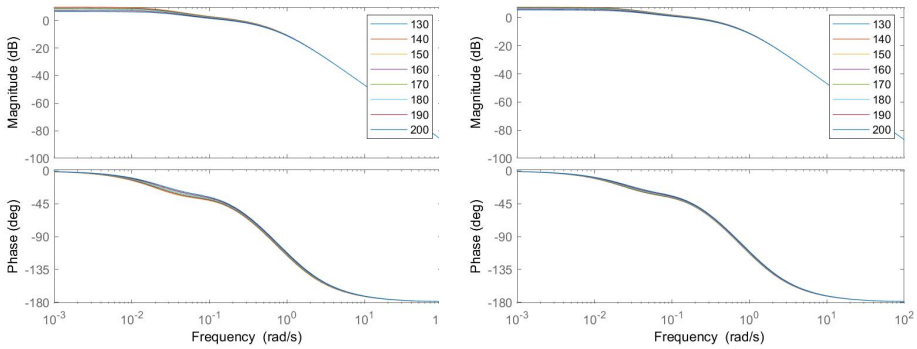

(a) Bode plot Propofol Male Height (cm) (b) Bode plot Propofol Female Height (cm)

Figure 3.3: Propofol SS PK model Height (cm)

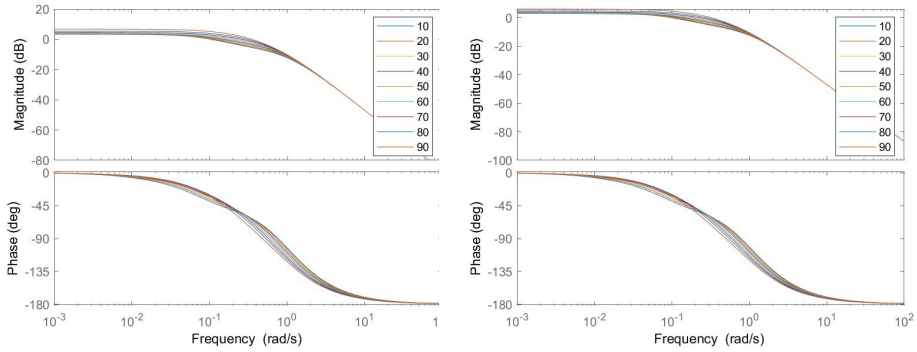

(a) Bode plot Remifentanil Male Age (years) (b) Bode plot Remifentanil Female Age (years)

Figure 3.4: Remifentanil SS PK model Age (years)

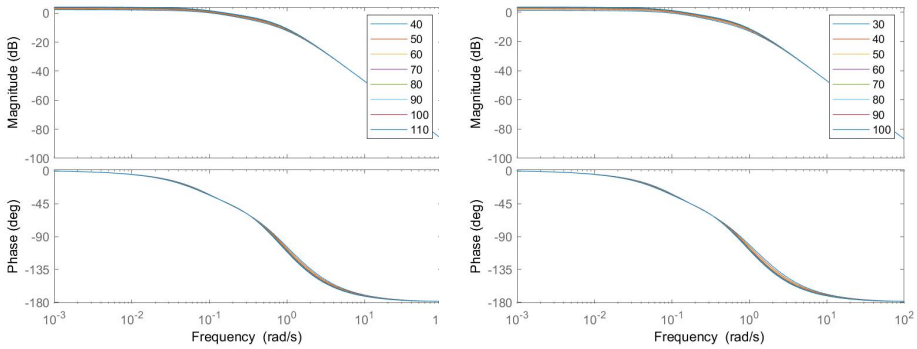

(a) Bode plot Remifentanil Male Weight (kg)

(b) Bode plot Remifentanil Female Weight (kg)

Figure 3.5: Remifentanil SS PK model Weight (kg)

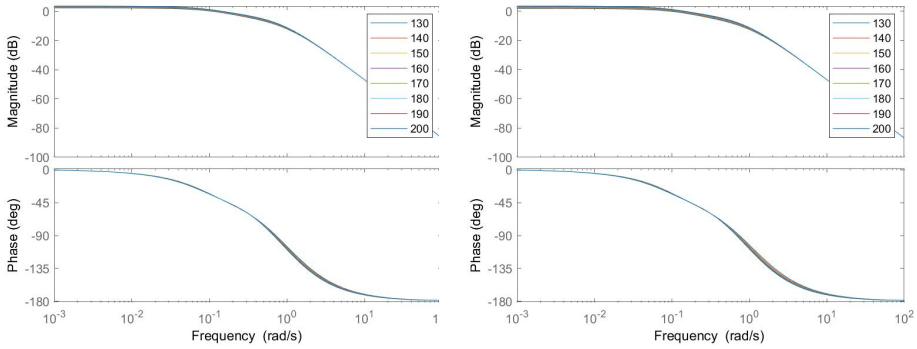

(a) Bode plot Remifentanil Male Height (cm)

(b) Bode plot Remifentanil Female Height (cm)

Figure 3.6: Remifentanil SS PK model Height (cm)

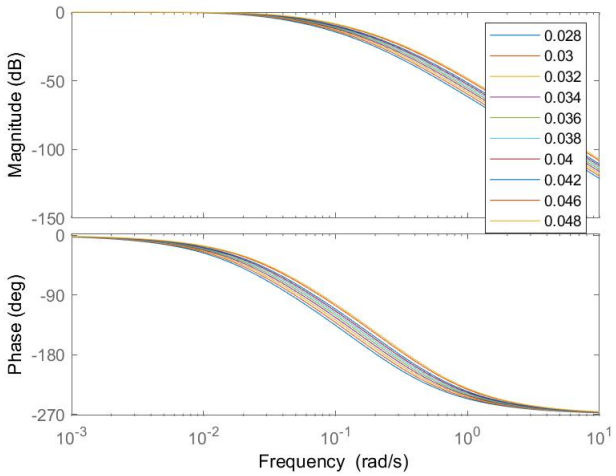

Figure 3.7: NMB SS PK model alpha (-)

3.2 Dynamics of hemodynamic models

The bode plots and the gain/phase margins of the four hemodynamic models (g11, g12, g21, g22) of Section 2.2.6 are shown in Figures 3.8 to 3.17. These figures have been constructed by varying the individual parameters within the intervals from [42]. Kij (i=1,2, j=1,2) represents the gain of the model, i.e. the sensitivity of the patient to the drug. Figures 3.8a, 3.11a, 3.14a and 3.17a demonstrate that this variation is very large (in dB). This is explained by Yu [75] by the fact that there is an unmodelled coupling between CO and MAP. This manifests itself in large parameter value changes, especially gain. As the hemodynamic models are first order plus dead time, varying τij (i=1,2, j=1,2) corresponds with a shift of the corner frequency and varying Tij (i=1,2, j=1,2) changes the time delay. This can be seen in Figures 3.9a, 3.12a, 3.15a, 3.18a and 3.10a, 3.10a, 3.10a, 3.10a respectively. Note that for the intervals described in Table 2.6, the hemodynamics models are open-loop stable as they only have poles in the left half-plane. The difference with the pharmacokinetic models is that the hemodynamic models can become unstable in closed-loop for certain values within the parameter intervals. This can be due to all three parameters (K, τ and T).

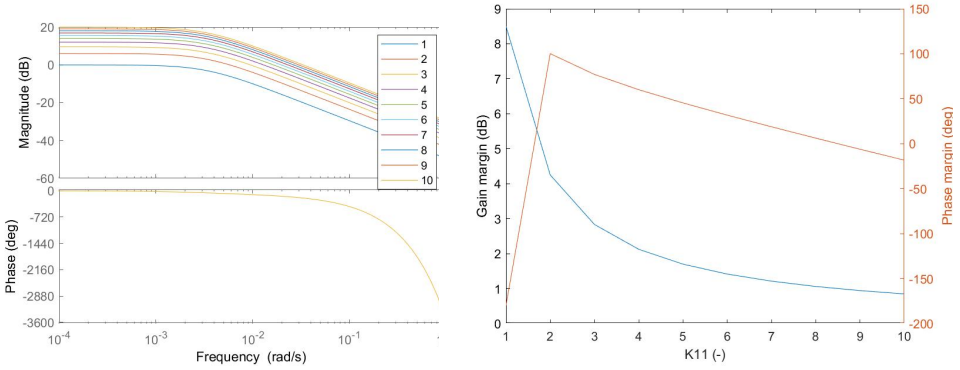

(a) Bode plot g11 K11 (b) Gain and phase margin g11 K11

Figure 3.8: Bode plot g11 K11 variation

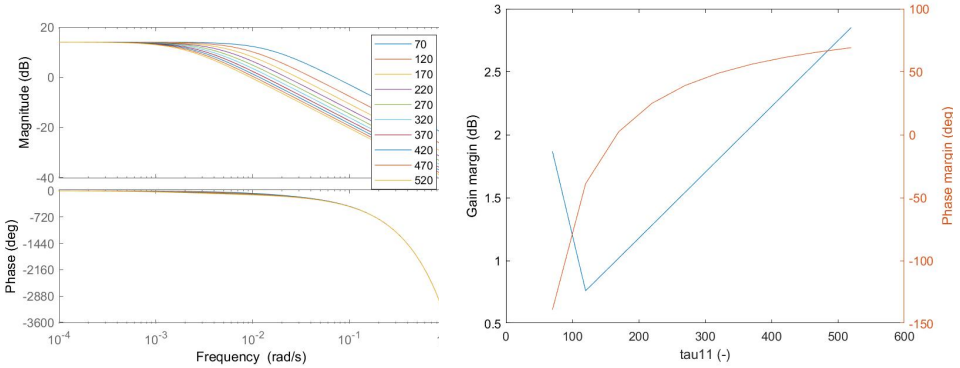

(a) Bode plot g11 τ11 (b) Gain and phase margin g11 τ11

Figure 3.9: Bode plot g11 τ11 variation

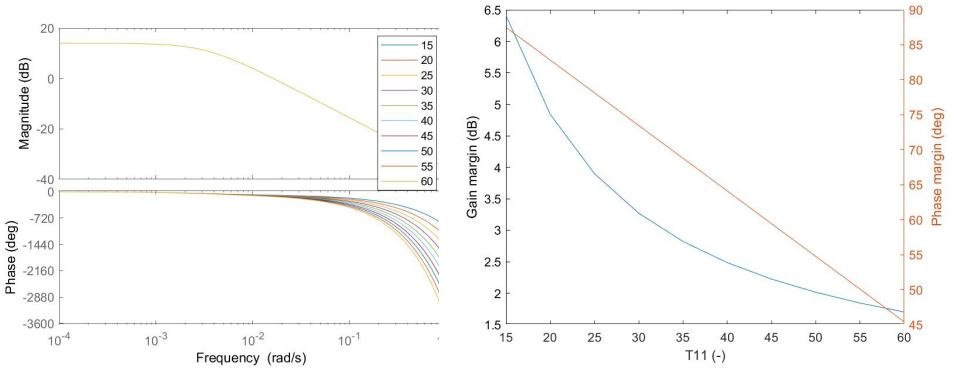

(a) Bode plot g11 T11 (b) Gain and phase margin g11 T11

Figure 3.10: Bode plot g11 T11 variation

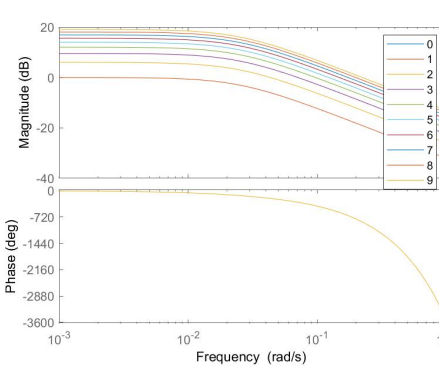

(a) Bode plot g12 K12

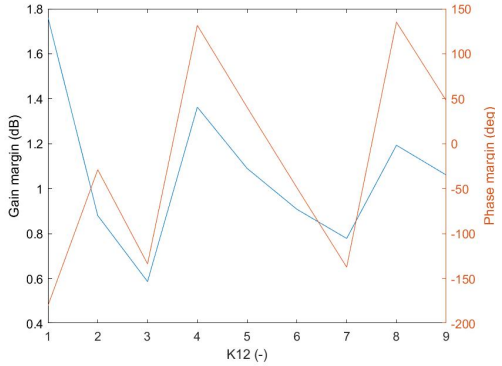

(b) Gain and phase margin g12 K12

Figure 3.11: Bode plot g12 K12 variation

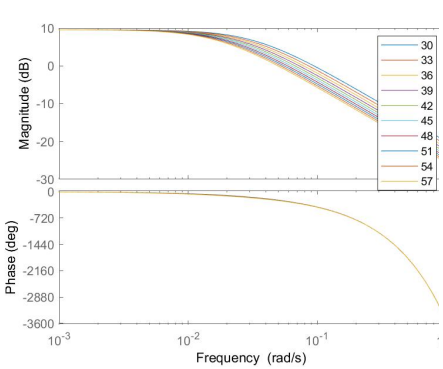

(a) Bode plot g12 τ12

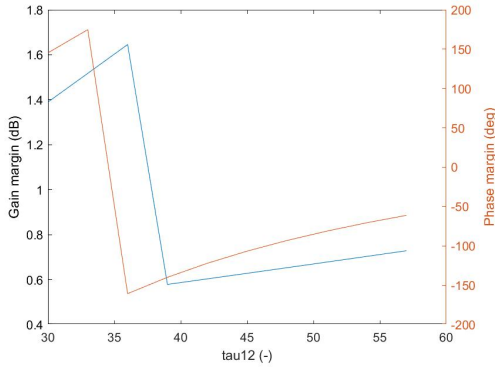

(b) Gain and phase margin g12 τ12

Figure 3.12: Bode plot g12 τ12 variation

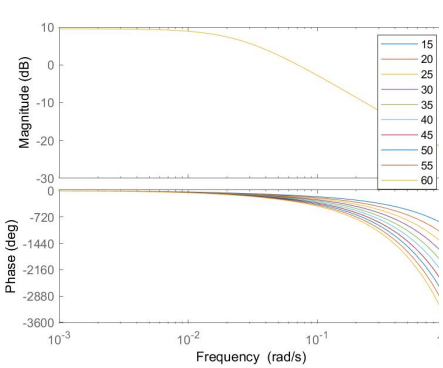

(a) Bode plot g12 T12

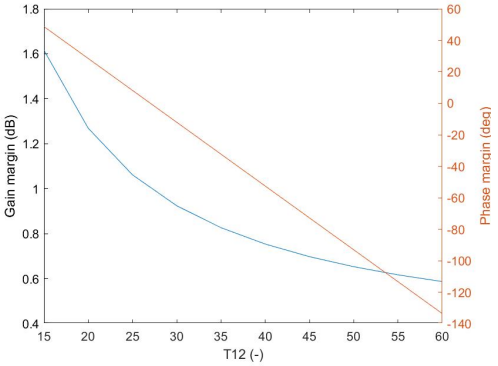

(b) Gain and phase margin g12 T12

Figure 3.13: Bode plot g12 T12 variation

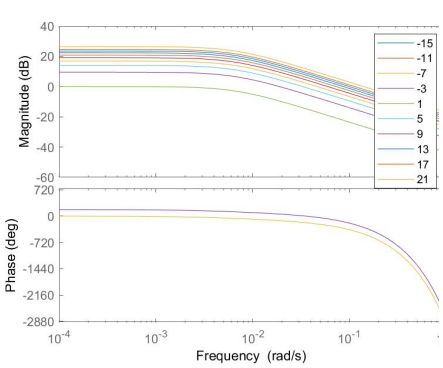

(a) Bode plot g21 K21

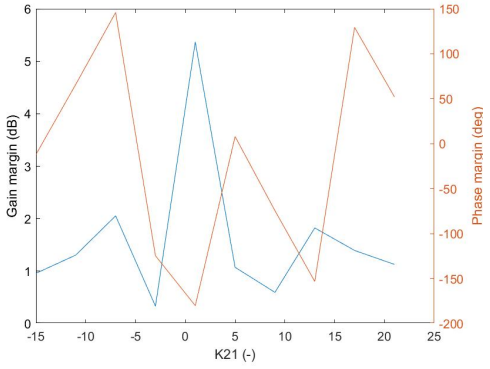

(b) Gain and phase margin g21 K21

Figure 3.14: Bode plot g21 K21 variation

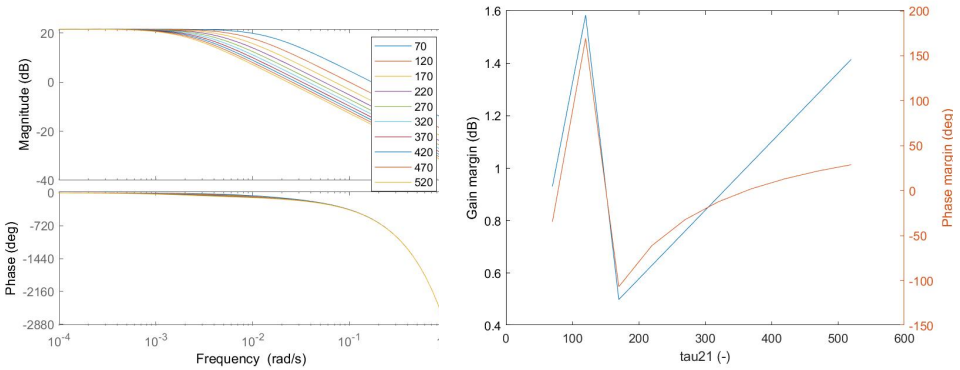

(a) Bode plot g21 τ21 (b) Gain and phase margin g21 τ21

Figure 3.15: Bode plot g21 τ21 variation

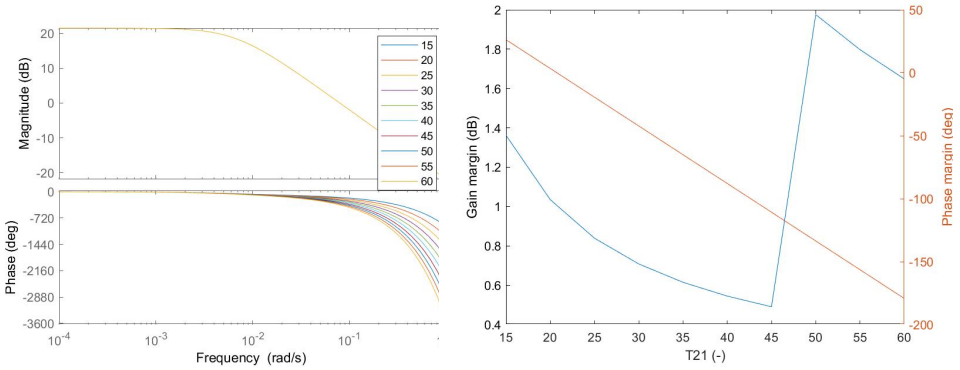

(a) Bode plot g21 T21 (b) Gain and phase margin g21 T21

Figure 3.16: Bode plot g21 T21 variation

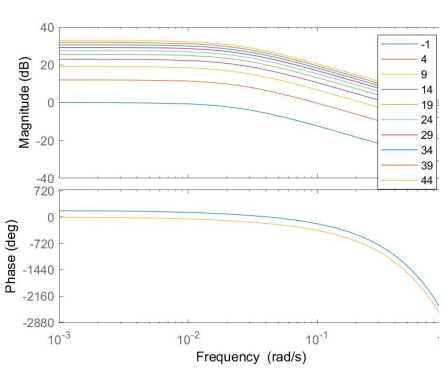

(a) Bode plot g22 K22

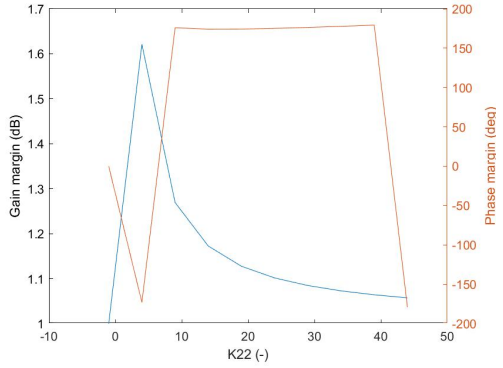

(b) Gain and phase margin g22 K22

Figure 3.17: Bode plot g22 K22 variation

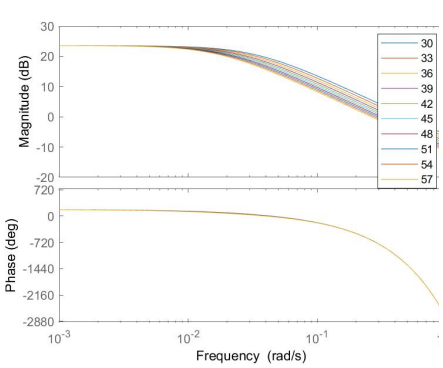

(a) Bode plot g22 τ22

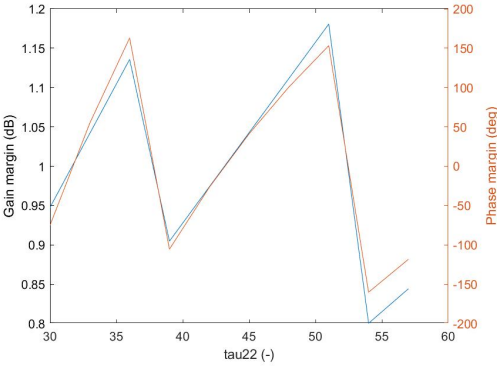

(b) Gain and phase margin g22 τ22

Figure 3.18: Bode plot g22 τ22 variation

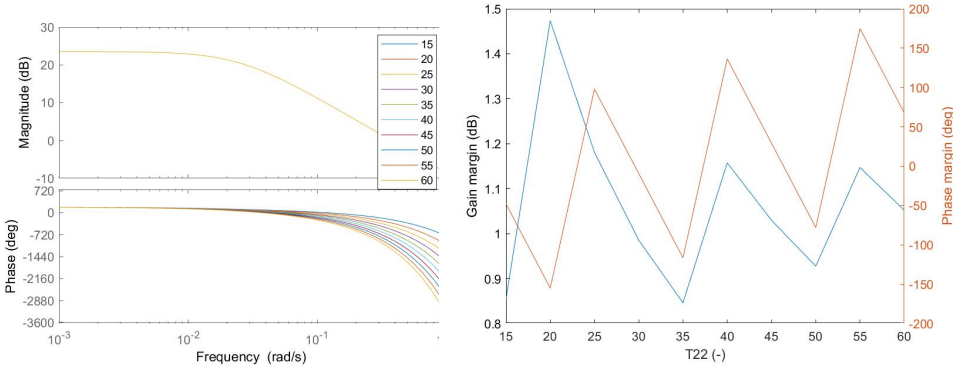

(a) Bode plot g22 T22

(b) Gain and phase margin g22 T22

Figure 3.19: Bode plot g22 T22 variation

3.3 Open-loop stability patient model for general anesthesia

The dynamics of the patient model are linear and time-invariant. The outputs of these dynamics then undergo a non-linear transformation (Hill-curve) to form the outputs of the patient model. For the open-loop stability, however, is this non-linear transformation irrelevant. Therefore, open-loop stability of the patient model can be proven by looking at the open-loop poles (i.e. eigenvalues of the state matrix A) of the patient model.

In Tables 3.1 and 3.2, each column represents the real part of the eigenvalues of the state matrix of one patient from Table 2.1. As all eigenvalues have strictly negative real parts, the state matrix A is Hurwitz. Hence, the system is asymptotically stable [76].

1	2	3	4	5	6	7
-1.079	-1.09	-1.139	-1.175	-1.101	-1.079	-1.136
-0.2136	-0.2136	-0.2136	-0.2136	-0.2136	-0.2136	-0.2136
-0.2136	-0.2136	-0.2136	-0.2136	-0.2136	-0.2136	-0.2136
-0.03165	-0.0301	-0.02864	-0.04109	-0.02661	-0.03331	-0.03291
-0.456	-0.456	-0.456	-0.456	-0.456	-0.456	-0.456
-0.294	-0.294	-0.294	-0.294	-0.294	-0.294	-0.294
-0.294	-0.294	-0.294	-0.294	-0.294	-0.294	-0.294
-0.2672	-0.2687	-0.274	-0.2749	-0.2706	-0.2669	-0.2729
-1.208	-1.242	-1.225	-1.073	-1.112	-1.172	-0.9645
-0.595	-0.623	-0.679	-0.525	-0.679	-0.574	-0.616
-0.2136	-0.2136	-0.2136	-0.2136	-0.2136	-0.2136	-0.2136
-0.2136	-0.2136	-0.2136	-0.2136	-0.2136	-0.2136	-0.2136
-0.294	-0.294	-0.01578	-0.294	-0.294	-0.294	-0.294
-0.294	-0.294	-0.1101	-0.294	-0.294	-0.294	-0.294
-0.1191	-0.0143	-0.294	-0.1149	-0.1044	-0.1188	-0.1005
-0.01355	-0.1179	-0.294	-0.01164	-0.01583	-0.01298	-0.01419
-0.004509	-0.004509	-0.004509	-0.004509	-0.004509	-0.004509	-0.004509
-0.004509	-0.004509	-0.004509	-0.004509	-0.004509	-0.004509	-0.004509
-0.02882	-0.02882	-0.02882	-0.02882	-0.02882	-0.02882	-0.02882
-0.02882	-0.02882	-0.02882	-0.02882	-0.02882	-0.02882	-0.02882
-0.003333	-0.003333	-0.003333	-0.003333	-0.003333	-0.003333	-0.003333
-0.004509	-0.004509	-0.004509	-0.004509	-0.004509	-0.004509	-0.004509
-0.004509	-0.004509	-0.004509	-0.004509	-0.004509	-0.004509	-0.004509
-0.02882	-0.02882	-0.02882	-0.02882	-0.02882	-0.02882	-0.02882
-0.02882	-0.02882	-0.02882	-0.02882	-0.02882	-0.02882	-0.02882
-0.025	-0.025	-0.025	-0.025	-0.025	-0.025	-0.025
-0.005411	-0.005411	-0.005411	-0.005411	-0.005411	-0.005411	-0.005411
-0.005411	-0.005411	-0.005411	-0.005411	-0.005411	-0.005411	-0.005411
-0.03459	-0.03459	-0.03459	-0.03459	-0.03459	-0.03459	-0.03459
-0.03459	-0.03459	-0.03459	-0.03459	-0.03459	-0.03459	-0.03459
-0.006667	-0.006667	-0.006667	-0.006667	-0.006667	-0.006667	-0.006667
-0.005411	-0.005411	-0.005411	-0.005411	-0.005411	-0.005411	-0.005411
-0.005411	-0.005411	-0.005411	-0.005411	-0.005411	-0.005411	-0.005411
-0.03459	-0.03459	-0.03459	-0.03459	-0.03459	-0.03459	-0.03459
-0.03459	-0.03459	-0.03459	-0.03459	-0.03459	-0.03459	-0.03459
-0.025	-0.025	-0.025	-0.025	-0.025	-0.025	-0.025
-0.374	-0.374	-0.374	-0.374	-0.374	-0.374	-0.374
-0.1496	-0.1496	-0.1496	-0.1496	-0.1496	-0.1496	-0.1496
-0.0374	-0.0374	-0.0374	-0.0374	-0.0374	-0.0374	-0.0374

Table 3.1: Real part eigenvalues state matrix A - part 1

8	9	10	11	12	13
-1.215	-1.146	-1.116	-1.101	-1.145	-1.139
-0.2136	-0.2136	-0.2136	-0.2136	-0.2136	-0.2136
-0.2136	-0.2136	-0.2136	-0.2136	-0.2136	-0.2136
-0.03661	-0.03534	-0.03196	-0.03382	-0.03182	-0.03354
-0.456	-0.456	-0.456	-0.456	-0.456	-0.456
-0.294	-0.294	-0.294	-0.294	-0.294	-0.294
-0.294	-0.294	-0.294	-0.294	-0.294	-0.294
-0.2792	-0.2734	-0.2711	-0.2691	-0.274	-0.2731
-1.039	-1.089	-1.168	-0.962	-1.155	-1.119
-0.609	-0.588	-0.616	-0.581	-0.637	-0.609
-0.2136	-0.2136	-0.2136	-0.2136	-0.2136	-0.2136
-0.2136	-0.2136	-0.2136	-0.2136	-0.2136	-0.2136
-0.294	-0.294	-0.294	-0.294	-0.294	-0.294
-0.294	-0.294	-0.294	-0.294	-0.294	-0.294
-0.1063	-0.1116	-0.1142	-0.1025	-0.1112	-0.1118
-0.01397	-0.01338	-0.01413	-0.01322	-0.0147	-0.01395
-0.004509	-0.004509	-0.004509	-0.004509	-0.004509	-0.004509
-0.004509	-0.004509	-0.004509	-0.004509	-0.004509	-0.004509
-0.02882	-0.02882	-0.02882	-0.02882	-0.02882	-0.02882
-0.02882	-0.02882	-0.02882	-0.02882	-0.02882	-0.02882
-0.003333	-0.003333	-0.003333	-0.003333	-0.003333	-0.003333
-0.004509	-0.004509	-0.004509	-0.004509	-0.004509	-0.004509
-0.004509	-0.004509	-0.004509	-0.004509	-0.004509	-0.004509
-0.02882	-0.02882	-0.02882	-0.02882	-0.02882	-0.02882
-0.02882	-0.02882	-0.02882	-0.02882	-0.02882	-0.02882
-0.025	-0.025	-0.025	-0.025	-0.025	-0.025
-0.005411	-0.005411	-0.005411	-0.005411	-0.005411	-0.005411
-0.005411	-0.005411	-0.005411	-0.005411	-0.005411	-0.005411
-0.03459	-0.03459	-0.03459	-0.03459	-0.03459	-0.03459
-0.03459	-0.03459	-0.03459	-0.03459	-0.03459	-0.03459
-0.006667	-0.006667	-0.006667	-0.006667	-0.006667	-0.006667
-0.005411	-0.005411	-0.005411	-0.005411	-0.005411	-0.005411
-0.005411	-0.005411	-0.005411	-0.005411	-0.005411	-0.005411
-0.03459	-0.03459	-0.03459	-0.03459	-0.03459	-0.03459
-0.03459	-0.03459	-0.03459	-0.03459	-0.03459	-0.03459
-0.025	-0.025	-0.025	-0.025	-0.025	-0.025
-0.374	-0.374	-0.374	-0.374	-0.374	-0.374
-0.1496	-0.1496	-0.1496	-0.1496	-0.1496	-0.1496
-0.0374	-0.0374	-0.0374	-0.0374	-0.0374	-0.0374

Table 3.2: Real part eigenvalues state matrix A - part 2

3.4 Hill-curve variation

In this section, the effect of changing parameters on the Hill-curve is studied. Intuitively, a larger C_{50} value corresponds with a shift to higher effect-site concentrations for the same level of BIS (see Figure 3.20). The effect of changing γ is shown in Figure 3.21. The resulting Hill-curves are steeper for larger values of γ. For a BIS level above 50%, the effect-site concentration needed to reach a certain BIS level is higher for larger γ and the reverse is true for BIS levels below 50%.

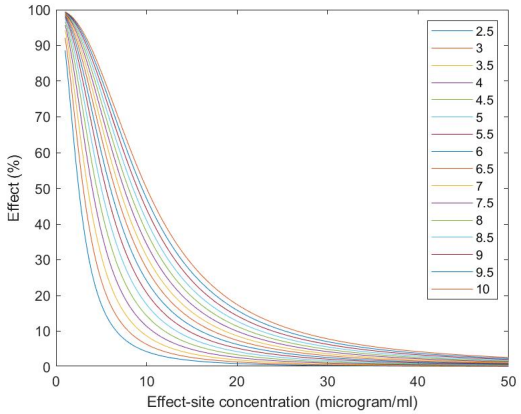

Figure 3.20: Hill-curve C_{50} (μg/ml) variation

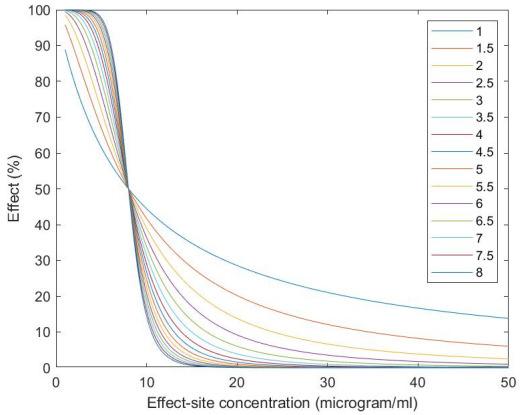

Figure 3.21: Hill-curve γ (-) variation

Chapter 4

Model Predictive Control of complete hemodynamic and anesthetic system

4.1 Quasi-Infinite Horizon (Nonlinear) Model Predictive Control (QIH-MPC)

4.1.1 Introduction to MPC

As stated by Rawlings and Mayne [77], Model Predictive Control (MPC) is based on optimal control. When implementing optimal control in open loop, one tries to find off-line the optimal input sequence that would make sure the equilibrium point is reached (taking into account constraints) while minimizing the control effort (when required). This is then used as an input to the system. However, model mismatches and disturbances cause the control performance to deteriorate, resulting in an inability to properly maintain the equilibrium point and possibly even instability (if the open-loop system is unstable). Closed-loop optimal control on the other hand is able to deal with open-loop instability, disturbances and model mismatches. However, in real-life applications, a closed solution is hard if not impossible to find [78].

To remedy the problems with both open-loop and closed-loop optimal control, model predictive control was conceived. At each time step, it solves an open-loop optimal control problem, but with the measured states as the new initial states. It can therefore be best described as *repeated open-loop optimal control in feedback fashion* [77], [78].

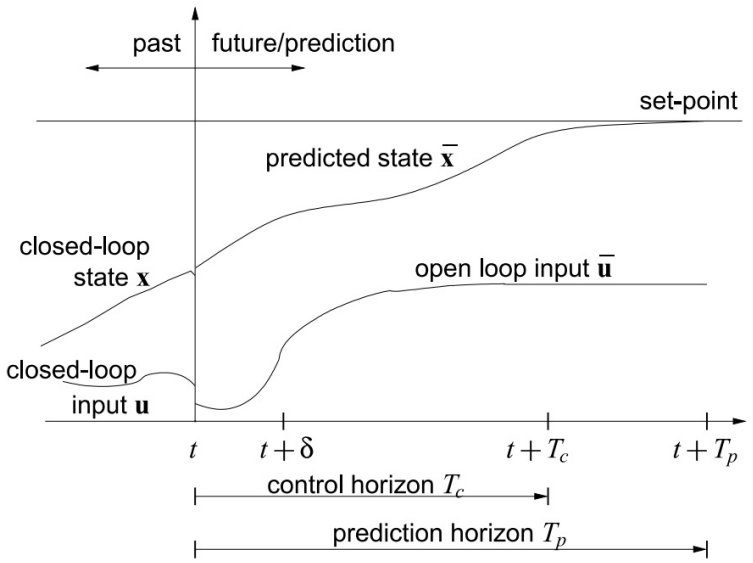

Figure 4.1: Basic scheme Model Predictive Control

The basic principle of MPC is shown in Figure 4.1, which is taken from [79]. At time t, the future states $\overline{x}$ until t+Tp are predicted using the dynamic model of the system. Tp is called the *prediction horizon* of the MPC algorithm and is an important tuning parameter for feasibility and stability, see further. Consequently, the optimal open-loop inputs $\overline{u}$ are calculated until t+Tc, where Tc is called the *control horizon*. For the remainder of the discussion, it will always be assumed that the prediction horizon is equal to the control horizon [79]. These optimal inputs are found in an iterative manner by minimizing a user-defined (often quadratic) cost function, where the number of iterations determine the (sub)optimality of the solution. After these calculations, the open-loop input is implemented until t+δ, with δ being the sampling time. By measuring the states, a new 'initial' state is created. It is at this point that the scheme is shifted from t to t+δ and the whole iteration (prediction and optimisation) starts again [77], [79].

The MPC problem is formulated mathematically as follows (adapted from [79]):

$$\begin{aligned} &\min_{u(\bullet)} \; J(x(t), \overline{u}(\bullet); Tc, Tp) \\ J(x(t), \overline{u}(\bullet); Tp, Tc) &:= \int_t^{t+Tp} F(\overline{x}(\tau), \overline{u}(\tau)) d\tau \end{aligned} \tag{4.1}$$

with

$$\begin{aligned}
&\dot{\overline{x}}(\tau) = f(\overline{x}(\tau), \overline{u}(\tau)),\ \overline{x}(t) = x(t) \\
&\overline{u}(\tau) \in \mathcal{U}, \forall \tau \in [t, t+Tc] \\
&\overline{u}(\tau) = \overline{u}(\tau + Tc), \forall \tau \in [t+Tc, t+Tp] \\
&\overline{x}(\tau) \in \mathcal{X}, \forall \tau \in [t, t+Tp]
\end{aligned} \tag{4.2}$$

In this thesis, box constraints are considered:

$$\begin{aligned}
\mathcal{U} &:= \{u \in \Re^m |\ u_{min} \leq u \leq u_{max}\} \\
\mathcal{X} &:= \{x \in \Re^n |\ x_{min} \leq x \leq x_{max}\}
\end{aligned} \tag{4.3}$$

It is assumed that $\mathcal{U} \subset \Re^m$ is compact, $\mathcal{X} \subseteq \Re^n$ is connected and that the equilibrium point is an element of $\mathcal{X} \times \mathcal{U}$.

The optimal solution (input), which minimises the objective functional in 4.1, can be written as:

$$\begin{aligned}
u^*(\tau) &:= \overline{u}^*(\tau; x(t), Tp, Tc),\ \tau \in [t, t+\delta] \\
V(x; Tp, Tc) &= J(x, \overline{u}^*(\bullet; x(t)); Tp, Tc)
\end{aligned} \tag{4.4}$$

In the paper by Findeisen and Allgöwer, the origin is assumed to be the steady state that needs to be stabilized and all the results are derived using the origin as the equilibrium points. This does not result in a loss of generality as the results do not change under a linear transformation [79]. It is with this argument that it is defended that the results of this paper still hold when realistic equilibrium points for anesthesia are used in this thesis. As this point needs to be feasible, it does have to be in the interior of $\mathcal{X}$ x $\mathcal{U}$.

Note that the values of the variables with bar ($\bar{\bullet}$) represent the variables used internally in the controller and are not the real values of the variables of the real system. This is clear from the fact that at each iteration, the input is recalculated and the internal values are updated [79].

The function F is often referred to as the *stage cost*, often as a quadratic function of the states and the inputs [79]. Here, the inputs will not be included into the stage cost as economising drugs is not the goal at this point. The function F will we written as a quadratic function in the outputs, with the outputs being a nonlinear function of the states.

In 4.4, the value function with as input the optimal input as calculated at time t, can be used as a Lyapunov function. This realisation can be used to great effect when proving the stability of an MPC scheme (see discussion below). Also note that the optimal solution to the optimisation problem is dependent on the value of the states at time t (the 'current' time).

The requirement to have a *connected* set of feasible states originates from the fact that a connected feasible region is necessary to prove asymptotic stability for each point in that feasible region, making it a region of attraction for the equilibrium point [80]. As in this application only box constraints are considered (i.e. inputs and states need to remain within certain bounds) and not nonlinear state constraints for example, it is expected that the region will indeed by connected. This however remains to be proven thoroughly.

4.1.2 Stability and feasibility of QIH-MPC

From an ethical and patient safety point of view, it is essential that the controller is stable during operation to guarantee the well-being of the patient. Furthermore, if the non-linear controller loses feasibility (the ability to find a possible path to the equilibrium point), the controller needs to switch to manual mode where the anesthesiologist will intervene until the controller is once again in a feasible region. It is therefore clear that one needs to have a clear understanding of when the controller is stable and feasible and more importantly, when not. Ideally, this does not depend on the performance parameters in order to make the scheme more robust to inter- and intrapatient variability while maintaining computational feasibility, a considerable issue for nonlinear model predictive control (NMPC) [79].

Changing the terminal state *equality* constraint with a terminal state *inequality* constraint means the calculated state after the prediction horizon does not have to be exactly equal to the equilibrium point but can be within a terminal region Ω around the equilibrium point. The terminal cost then provides an upper bound for the fictitious situation where one starts from $\overline{x}(t+Tp)$ and uses a local linear state feedback until the equilibrium point is reached exactly. The cost function from equation 4.1 is therefore extended with a terminal cost (see equation 4.5), assuming all the costs are quadratic with respective weighting matrices Q, R and P. These weighting matrices will be further discussed in the procedure below. It is important to note that the inputs are only calculated for a finite time, as the infinite "tail" with the state feedback controller is never used in practice [80]. Hence, no switching mechanisms are needed, which is the main difference with the *dual-mode receding horizon control scheme* presented by Michalska and Mayne [81].

$$\begin{aligned} &\min_{u(\bullet)} J(x(t), \overline{u}(\bullet); Tc, Tp) \\ J(x(t), \overline{u}(\bullet); Tp, Tc) &:= \int_t^{t+Tp} \|\overline{x}(\tau)\|_Q^2 + \|\overline{u}(\tau)\|_R^2 \, d\tau + \|\overline{x}(t+T_P)\|_P^2 \end{aligned} \tag{4.5}$$

In the paper by Chen and Allgöwer, a method is proposed to determine off-line a penalty matrix for a quadratic terminal cost as well as an invariant terminal region. This is done by solving the appropriate Lyapunov equation and using the unique, positive-definite and symmetric solution (the penalty matrix) to iteratively construct an invariant region around the equilibrium point. It is further shown that this setup will guarantee asymptotic stability if the Jacobian linearization (evaluated at the equilibrium point) of the (nonlinear) system is stabilizable and the problem is feasible at time t=0. This does not depend on the choice of the performance parameters and is claimed to be more computationally attractive than other MPC schemes that also guarantee asymptotic stability. Furthermore, the globally optimal input profile does not need to be found to have asymptotic stability, only a feasible solution is required. These results hold for both stable and unstable constrained systems [80]. The method of Chen and Allgöwer provides an objective tool for determining the stability of the MPC scheme. Using a patient model, the stability of the given MPC controller can be checked off-line for a database of patients. During operation the anesthesiologist can be kept updated on the stability of the closed-loop using the available patient model. Further research is however required to determine the feasibility regions for the control of depth of anesthesia. This includes the variation of model parameters as well as the influence of disturbances and model/plant mismatches (for instance, intrapatient variability).

The following procedure has been adapted from [80] to determine the terminal penalty matrix and construct the invariant terminal region. This procedure is written using the origin as the equilibrium point. Keep in mind that the states x are thus actually the difference between the "real" states of the system and the "real" equilibrium point. As stated in section 4.1.1, the results do not change under a linear transformation.

1. Calculate the Jacobian linearization at the equilibrium point:

$$\begin{aligned} A &= \frac{\partial f}{\partial x}|_{x_{eq}} \\ B &= \frac{\partial f}{\partial u}|_{x_{eq}} \end{aligned} \tag{4.6}$$

2. Use the Hautus-test for stabilizability [77]. (A,B) is stabilizable if and only if

$$rang[\lambda I - A|B] = n \quad \forall \lambda(A) : Re(\lambda(A)) \geq 0 \tag{4.7}$$

   with $\lambda(A)$ being the eigenvalues of the matrix A and I the unit matrix with the same size as A (equal to n $\times$ n, with n being the number of states).

   If the Jacobian linearization is not stabilizable, the following steps are not applicable as it is an explicit requirement for this procedure to work.

3. Find a linear state feedback matrix K such that A_K is asymptotically stable with:

$$\begin{aligned} u = Kx \in \mathcal{U}\ \forall x \in \mathcal{X} \\ A_K := A + BK \end{aligned} \tag{4.8}$$

4. Solve the following Lyapunov equation and obtain a unique, positive-definite and symmetric solution P. P is the terminal penalty matrix and Q $\in \Re^{n\times n}$, R $\in \Re^{m\times m}$ are chosen positive semidefinite, symmetric weighting matrices.

$$\begin{aligned} Q^* = Q + K^T R K \ \in \ \Re^{nxn} \\ \kappa < \ -\lambda_{max}(A_K),\ \kappa \in \ [0, \infty) \\ (A_K + \kappa I)^T P + P(A_K + \kappa I) = -Q^* \end{aligned} \tag{4.9}$$

5. Using the state feedback matrix K found in step 3, find the largest $\alpha_1 \in (0, \infty)$ such that

$$\begin{aligned} \Omega_{\alpha_1} := \{x \in \Re^n | x^T P x \leq \alpha_1\} \\ Kx \in \mathcal{U}\ \forall x \in \Omega_{\alpha_1} \end{aligned} \tag{4.10}$$

6. Find the largest $\alpha \in (0, \alpha_1]$ such that

$$\begin{aligned} \dot{x} = f(x, Kx) \\ \phi(x) := f(x, Kx) - A_K x \\ L_\phi := sup\{\ \frac{\|\phi(x)\|}{\|x\|}\ |\ x \in \Omega_\alpha,\ x \neq 0\} \\ L_\phi \leq \frac{\kappa\ \lambda_{min}(P)}{\|P\|} \end{aligned} \tag{4.11}$$

   with Ω_α being an invariant terminal region, sup(•) the supremum and $\|\bullet\|$ the Frobenius norm.

Note that the terminal region above is not necessarily unique as it is dependent on the obtained state feedback matrix K and the choice of κ. It is therefore not guaranteed that this region is the largest possible region that can be determined [80]. Obviously, a larger terminal region makes it easier to find a feasible solution, increasing the feasible region. Looking at the Lyapunov-equation in step 4, it is clear that the terminal penalty matrix P will increase when κ does. For the example used in the paper by Chen and Allgöwer, it is noted that the terminal region first rises with κ but shrinks as κ approaches $|\lambda_{max}(A_k)|$. For a value of κ near the absolute value of the largest eigenvalue of A_k, the matrix P will also be large, exemplified by the (Frobenius) norm of the matrix. From the cost function in equation 4.5, it is clear that a large terminal penalty matrix (compared to weighting matrices Q and R) will be detrimental for the performance of the controller. There will therefore be a trade-off between control performance and the size of the terminal region [80]. Further research is required to find the optimal situation, inherently depending on inter- and intrapatient variability.

4.1.3 Robustness of QIH-MPC

So far, only the control problem using the nominal patient model and without disturbances has been discussed. Furthermore, it is assumed that the system states x can either be measured or calculated exactly. In a realistic situation, where model uncertainties and both measured as well as unmeasured disturbances exist, robust stability is not automatically guaranteed. When a non-ideal state estimator (as is always the case in practise) is explicitly or implicitly needed, both asymptotic stability and good closed-loop performance cannot be guaranteed anymore [79]. As this thesis does not considers adaptive control, it is assumed throughout this thesis that no model uncertainties exist. Further, it will still be assumed that all states for prediction are exact because an in-depth comparison and evaluation of state estimators (for instance, extended Kalman filter or moving-horizon estimation) when applied in a QIH-MPC control scheme falls out of the scope of this thesis. Results in literature on chemical reaction networks however suggest that moving-horizon estimation provides more accurate state estimation and greater robustness in return for a lower computational efficiency [82]. As a surgical stimulus as well as the *anesthesiologist in the loop* are considered in this thesis, the robustness of the QIH-MPC control scheme with nominal model and (un)measured disturbances will be discussed below.

The implementation of robust NMPC schemes such as min-max MPC, H_∞-NMPC or optimising the feedback controller during each sampling time is either computationally expensive or so conservative that no feasible solution can be found [79]. Hence, it is of interest to study the inherent robustness properties of the controller designed for the nominal model without disturbances. In the paper by Yu and Allgöwer [83], the inherent robustness properties for QIH-MPC are discussed for persistent but bounded disturbances. As the surgical disturbance is also modelled as a persistent but bounded disturbance, the results in this paper apply to general anesthesia. In [83], an upper bound for the disturbances is constructed that will guarantee robust stability. This upper bound is dependent on the terminal set Ω_α, the prediction horizon T_p, the sampling time δ and the Lipschitz constant v. Equation 4.12 is adapted from [83] and represents the method to determine the upper bound β_0 of the disturbances, using the variables calculated in section 4.1.2. With this method, the maximum disturbance can be found that guarantees the stability of the controller designed for the nominal patient model.

$$\begin{aligned} {d_r}^0(\mathcal{X}_f, \Omega_\alpha) &:= \sqrt{\lambda_{min}(P^{-1})}(\alpha^{1/2} - (e^{-\pi\delta}\alpha)^{1/2}) \\ \beta_0 &:= \frac{v\ {d_r}^0(\mathcal{X}_f, \Omega_\alpha)}{e^{v(Tp+\delta)} - 1} \end{aligned} \tag{4.12}$$

A more pragmatic approach to investigate robust stability for a system with disturbances (but without model uncertainties) is to repeat the proof of stability with the current output (including the disturbance) as the new initial point. As long as this output is within the feasible region, the controller will not lose stability as the (linearized) system is still stabilizable.

4.2 Implementation of predictive control

4.2.1 (Non)linear QIH-MPC scheme

For the implementation of predictive control, the Quasi Infinite-Horizon MPC scheme with guaranteed stability from Allgöwer and Chen [80] has been selected. Because of the inherent nonlinearity of the Hill-curves used in the patient model (and therefore cost function and constraints), a nonlinear MPC scheme was first selected to be used as the controller for the system. Nonlinear MPC is however only introduced in MATLAB and Simulink in the R2018b version [84] and at the time of writing, it is not possible to add terminal weights or constraints to the MATLAB-object or Simulink-block. Therefore, a custom .m-file was written to implement the QIH-MPC scheme, based on examples in the book *Nonlinear Model Predictive Control* written by Grüne and Pannek [85]. In this .m-file, the nonlinear solver *fmincon* is used based on [85] and the fact that it is the default solver for nonlinear MPC in MATLAB [86]. Due to the nonlinearity of the setup, the optimisation problem is now possibly non-convex with multiple local optima. This is not a problem for the QIH-MPC algorithm as convexity is not required, only compactness [79]. However, *fmincon* is a solver of the *Optimization Toolbox*^{TM} in MATLAB and the solvers in this toolbox only find local optima [87]. This means that when the starting point of the solver lies in the basin of attraction of a local optimum outside the feasible region, the solver will converge to that local optimum as it does not search for other local optima (or the global optimum) within the feasible region. Since this can be the case after initialisation as well as during operation (for instance, because of a disturbance), it cannot be guaranteed that the solver converges to a path within the feasible region. As finding at least one feasible solution is a key argument in the proof of stability of QIH-MPC, stability cannot be guaranteed. Moreover, the setpoint will not be reached. Finally, even when all constraints except the equality constraints for the dynamics (i.e. at each timestep the states need to follow the system dynamics) were removed, a feasible could not be found. These constraints can also not be further relaxed as adhering to the system dynamics is a fundamental requirement.

It is clear from the discussion above that a solver must be selected which under any circumstances can find an optimum within the feasible region, assuming of course that there is one. As general anesthesia is a real-life application, a feasible region without a solution means the problem is not well-formulated, so it can always be assumed that there is at least one. Also note that the global

optimum does not have to be within the feasible region to guarantee stability, a feasible local optimum suffices [80]. Due to the time constraints for this thesis, it was not possible to find a solver which can meet the above requirements within a reasonable CPU time (i.e. online feasible) as the convergence for non-convex systems is slow. Rather, it was investigated whether linear MPC with a linear patient model can provide a solution. The objective function to be minimised and the constraints will then both be linear. As the objective function is now a continuous quadratic linear function (with positive semidefinite weighting matrices), its Hessian matrix is positive semidefinite. Hence, the objective function is convex [88]. Because the constraints are linear is the optimisation problem also convex [89]. In this case, *fmincon* is able to find the global optimum and, using the same reasoning as above, it can be assumed that this optimum is within the feasible region.

Simply linearizing the patient model around a certain operating point is an option. The induction phase is well-documented and controllers for this phase can be found in literature. During the maintenance phase, the controller is operating in a small area around the setpoint. Therefore, the Hill-curves can be assumed to be linear in this area. With this method a switching mechanism will have to be provided as different controllers will be used for the induction and maintenance phase. The current states will then provide a new initial point for the controller. As long as this point is in the feasible region for the second controller, this can be used as a new initial point and there will not be any problem for stability. In case this point is outside the feasible region, a predetermined set op inputs needs to be applied until the controller is in a feasible region.

Another option is to use *inverse* Hill-curves to calculate certain states starting from the measured outputs. This is possible as the dynamics of the patient model itself are linear (this fact will also be used to check the stability of the system, see Section 5.6). It are the "outputs" (i.e. effect-site concentrations) of this linear system which then undergo a non-linear transformation to provide the outputs that are measured. If it is possible to calculate the outputs of the linear system by inversing the non-linear transformation, a linearization of the patient model is not required and an exact linear (pharmacokinetic) model can be used in the MPC controller. The inverse non-linear (pharmacodynamic) transformation is applied to the measured outputs of the non-linear system. In practise, the pharmacodynamics and pharmacokinetics are effectively decoupled. A schematic of the full closed-loop control system using this method can be found in Figure 4.2.

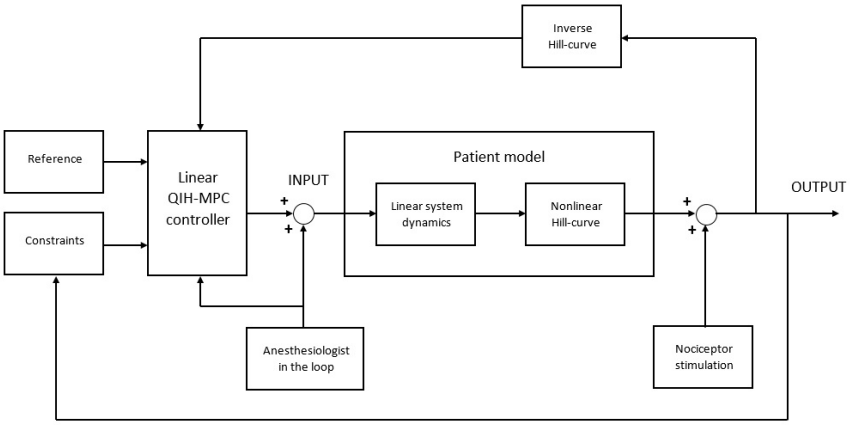

Figure 4.2: Full closed-loop control system for the QIH-MPC scheme

The choice for this scheme also has implications for implementing adaptive control. As assumed in Section 2.2.1 of this thesis, the pharmacokinetics models are accurate and not subject to intrapatient variability. This means the patient model within the MPC controller remains constant during operation and only the non-linear "state observer" needs to be adapted. To then study the robust stability of the system, model uncertainties can be ruled out. However, the robustness against incorrect calculated states needs to be investigated thoroughly, especially considering intrapatient variability. A possible way to do this is to model the deviations as disturbances on the states.

The problem with this method is that the effect-site concentration of Remifentanil has to be known due to its influence on the BIS-surface as well as neuromuscular blockade and mean arterial pressure. The effect-site concentration can be calculated from the measured RASS, but a simple inversion of the RASS transfer function leads to an improper system (the order of the numerator is greater than the order of the denominator). Therefore, the RASS transfer function is simplified (for the calculation) to only its steady-state gain. This is normally only valid during the maintenance phase for the nominal model without disturbances (of RASS), but it will nevertheless be used in this thesis to simplify the problem.

4.2.2 Dynamic state constraints

The box constraints for the states depend on the value of the sensitivity parameter γ. Assuming the exact value of γ is known, the required box constraints can be calculated. Consider the contour plot of the BIS-surface for $\gamma = 1$ in Figure 4.3. During the maintenance phase in general anesthesia, the combined effect of Propofol and Remifentanil is preferably kept between 40% (0.4) and 60% (0.6) with an ideal setpoint of 50% (0.5). To start the calculation one of the borders needs to be chosen (i.e. a degree of freedom). The minimal effect-site concentration of Remifentanil has been chosen in this thesis to be slightly below the required concentration to reach the RASS-setpoint during the maintenance phase (using the gain of the RASS transfer function). The intersections of this fixed concentration with the 0.4 and 0.5 curves in the contour plot then gives the values for the minimal and maximal effect-site concentration of Propofol respectively. The maximum effect-site concentration of Remifentanil can then be calculated by fixing the maximal effect-site concentration of Propofol and finding the intersection with the 0.6 curve. During the induction phase, the minimal concentrations are initially set to zero whereas the maximal concentrations are already set to the values calculated by the procedure above. The minimal concentrations are also set to their calculated values as soon as the measured BIS crosses the 0.4 curve, ensuring the value of BIS stays within the interval 0.4-0.6. Whenever the value of BIS leaves this preferred interval (for instance, due to a disturbance), the constraints are loosened to make sure the controller can find a feasible solution and the BIS value returns to the interval as quickly as possible. The extent to which the constraints are loosened (a fixed number subtracted from the minimal concentration and added to the maximal concentration) is a parameter that can be tuned. The results of this method during simulation are further discussed in Section 5.3.2.

In the case of inter- and intrapatient variability, the constructed box (see Figure 4.3) can be shrunk or expanded depending on the evolution of the sensitivity parameter γ. The contour plots of the nominal BIS-surface for different values of γ can be found in Appendix B.2.1. Should the value of γ be not known, it is recommended to use the box constraints of a conservative (i.e. large) value of γ, but the loosening of a smaller value. It is important to note that the choice for the smaller value of γ is also dependent on the delay to measure the value of BIS. In any case, control performance will be worse depending on the extent to which γ is unknown.

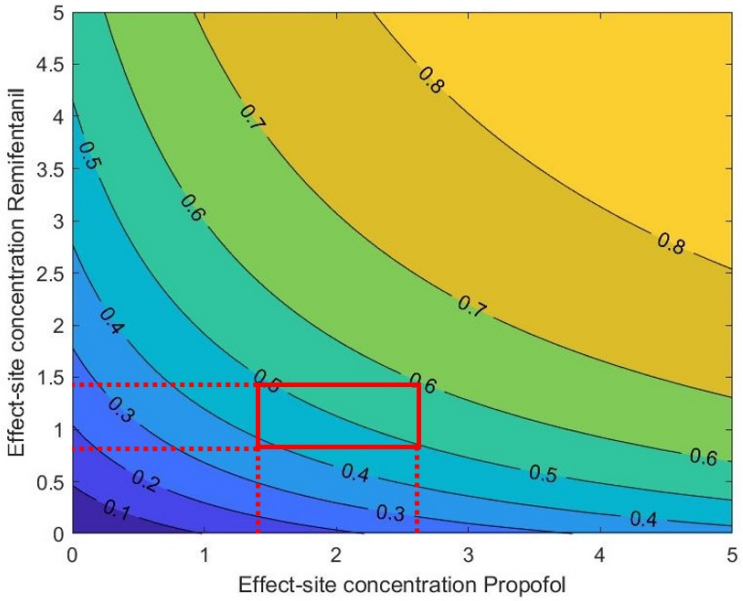

Figure 4.3: Contour plot BIS-surface for $\gamma = 1$

4.2.3 Nociceptor stimulation and anesthesiologist in the loop

The 'Nociceptor stimulation'-block in Figure 4.2 consists of an input from the workspace which is then passed through the nociceptor transfer function of Section 2.2.3. The input from the workspace is an example of a surgical stimulus. For all simulations in Chapter 5, the surgical stimulus from Section 2.4 was used. The output of the block is then added to the BIS-output of the system as an *un*measured output disturbance. Unmeasured because the current state of art does not yet allow a separate measurement of this disturbance.

The anticipatory reaction of the anesthesiologist is realised by the 'Anesthesiologist in the loop'-block (see Figure 4.2), implementing the signal defined in Section 2.4. This signal is modelled to be a measured input disturbance and added to the Propofol input signal calculated by the controller. Although the anesthesiologist manually injects additional Propofol, it is reasonable to assume that this dose can be measured by the device. The case in which this cannot be assumed is further discussed in Section 5.3.2.

Chapter 5

Simulation results and discussion

Note: only the figures relevant for the discussion are included in this chapter. The complete results of the simulations can be found in Appendix B.3.

5.1 Selection of prediction horizon

First of all, the prediction horizon Tp of the mpc controller is tuned depending on the simulated control performance for the nominal model (using the nominal values for the models in Chapter 2 and setting $\gamma = 4$). Although the nominal model is not representative for all patients, it does provide a general indication for the value of the prediction horizon. The sampling time δ for all simulations is chosen to be 1 second as the controller needs to be able to respond quickly to ensure the wellbeing of the patient.

When only hypnosis is controlled, a prediction horizon of 10 seconds is often chosen (for instance, in [90]). Because the hemodynamic models now included in the patient model have larger time constants, the prediction horizon also needs to be larger to guarantee feasibility. In Figures 5.1 to 5.5, the prediction horizon is varied between 10 and 500 seconds. From Figure 5.1 it is clear that the setpoint for BIS will be reached for all values of Tp larger than 10. Only the time in which the setpoint is reached varies, as the controller is tuned more aggressively for smaller values of Tp. Looking however at Figures 5.2 to 5.5, one can conclude that small values of Tp lead to instability of CO and MAP. Furthermore, it is observed that the transition from instability to stability is somewhere between 50 and 100 seconds. The simulation is therefore repeated with prediction horizons between 50 and 100 seconds (see Figures 5.6 and 5.9. From these figures it is evident that the prediction horizon needs to be at least 60 seconds to avoid instability in the induction phase. Note that this is only valid for the nominal model (i.e. $\gamma = 4$) and only gives the border value.

Thus, a more conservative choice of Tp = 150 seconds is chosen for this thesis as Figures 5.2 to 5.5 show that from 150 seconds on the oscillations in CO and MAP are much less profound. Moreover, 150 seconds is approximately the time it takes for the value of BIS to reach its setpoint. Future research into the size of the feasible regions will however allow for a much more precise estimation of the prediction horizon (see Section 6.2).

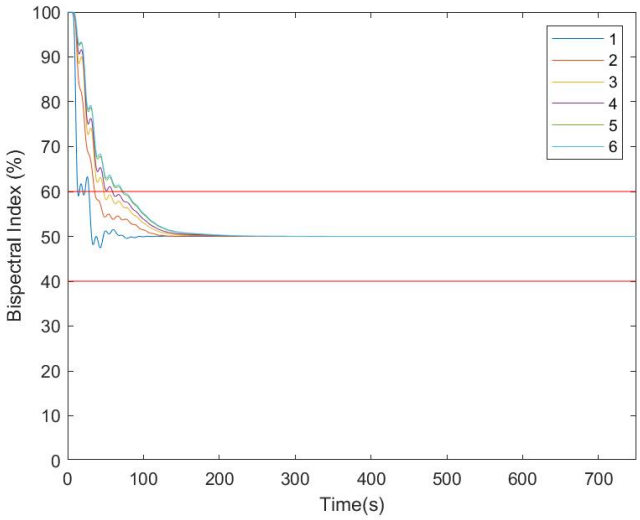

Figure 5.1: BIS output for Tp $\in [10,50,100,150,350,500]$

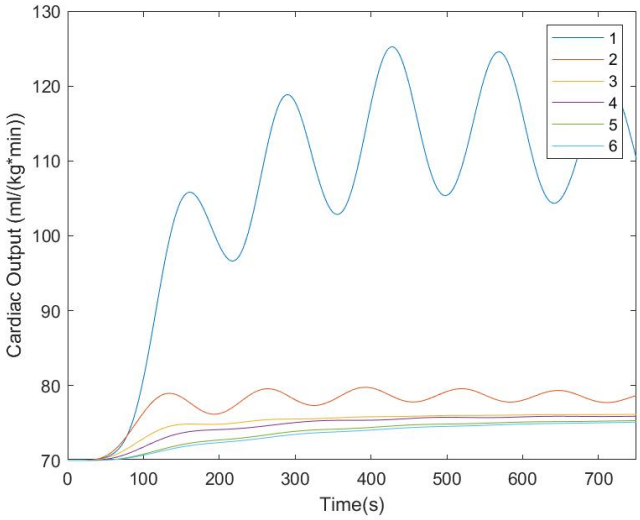

Figure 5.2: CO output for Tp $\in$[10,50,100,150,350,500]

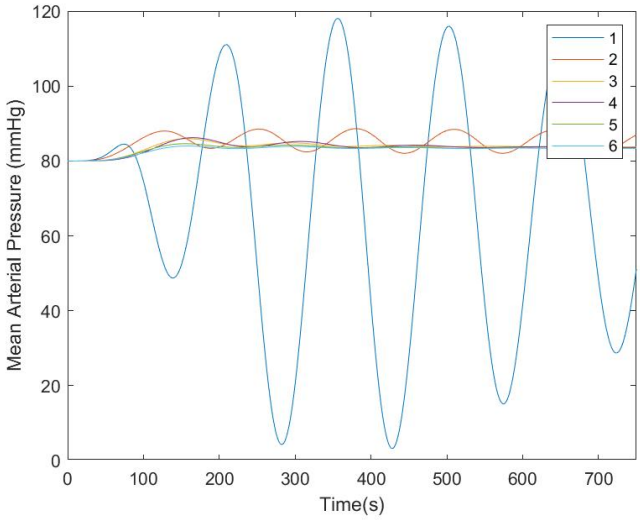

Figure 5.3: MAP output for Tp $\in$[10,50,100,150,350,500]

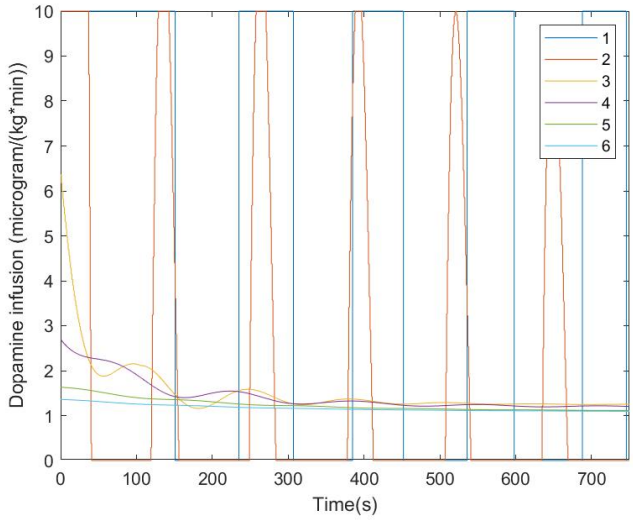

Figure 5.4: Dopamine input for Tp $\in$[10,50,100,150,350,500]

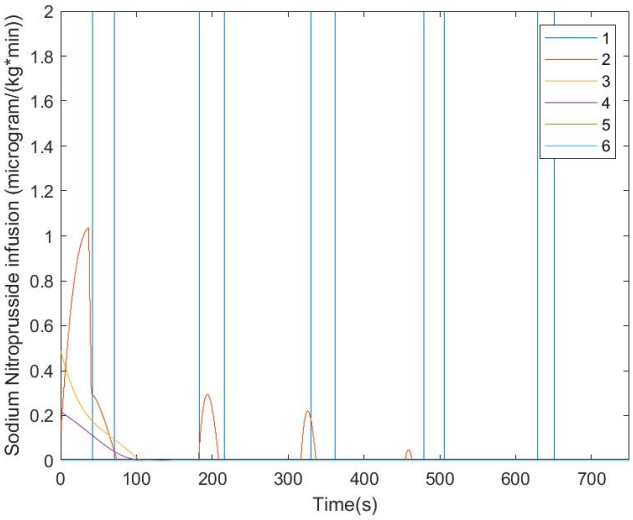

Figure 5.5: Sodium Nitroprusside for Tp $\in$[10,50,100,150,350,500]

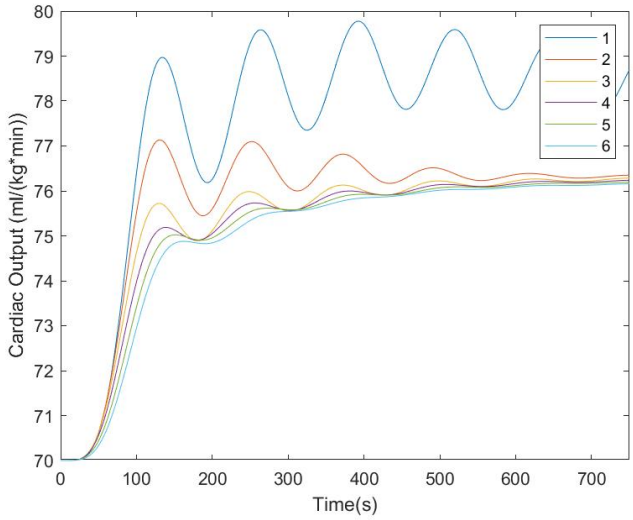

Figure 5.6: CO output for Tp $\in [50,60,70,80,90,100]$

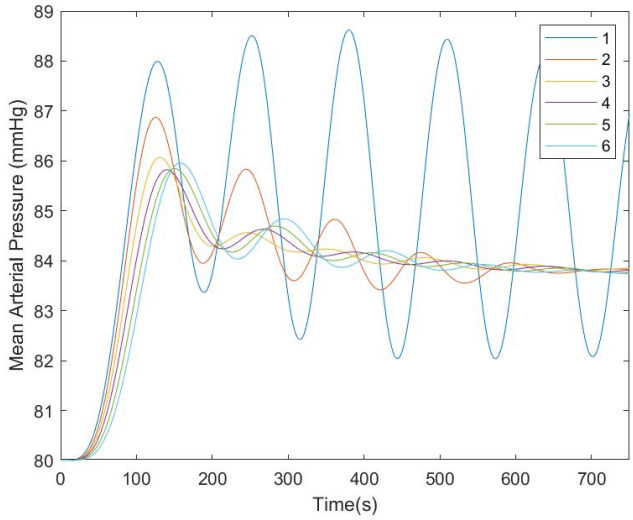

Figure 5.7: MAP output for Tp $\in [50,60,70,80,90,100]$

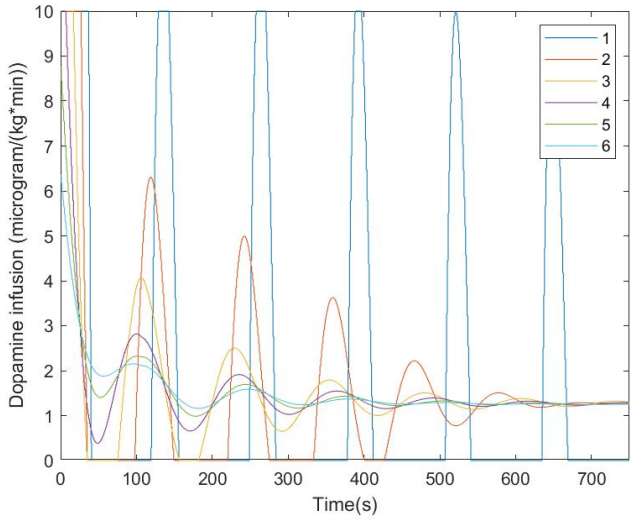

Figure 5.8: Dopamine input for Tp $\in$[50,60,70,80,90,100]

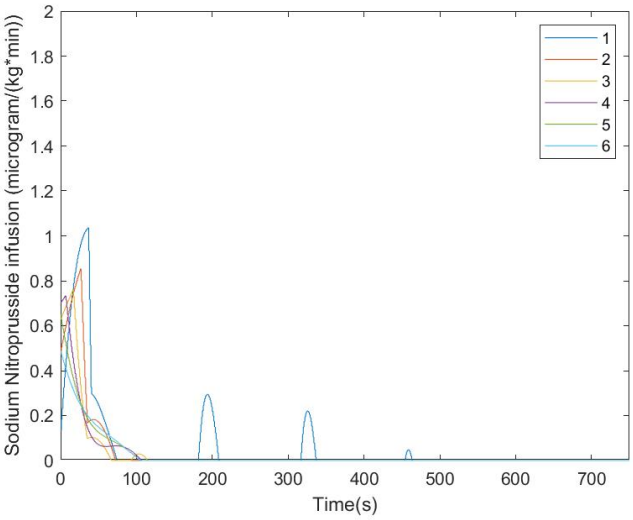

Figure 5.9: Sodium Nitroprusside for Tp $\in$[50,60,70,80,90,100]

5.2 Effect of the delay on a BIS-measurement

Any delay on the measurement of the value of BIS has a negative effect on the performance of the controller. For very large delays, the controller can even lose feasibility (and stability). In reality, there is indeed some delay on the measurement of BIS because of the smoothing algorithms used by the BIS monitor as well as the delay in adaptation of the artifact rejection pre-processing steps [92], [11]. In this section, the effect of this delay on the control performance is investigated. The delay is varied between 0 (no delay) and 100 seconds (Figures 5.10 and 5.11). A larger delay than the latter results in a loss of feasibility for a prediction horizon of 150 seconds. Apart from taking longer to reach the setpoint, the curve is also much less smooth for larger delays. According to [93], the 95% confidence interval for this delay is 12.7-27.6 seconds with a nominal value of 19.7 seconds. This nominal value will be used for the rest of the simulation in this chapter.

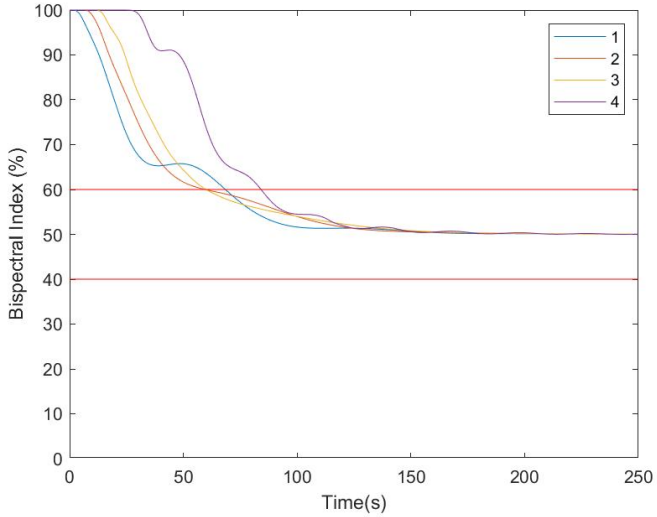

Figure 5.10: BIS output for a delay on the measurement of BIS of 0,5,10,25 seconds

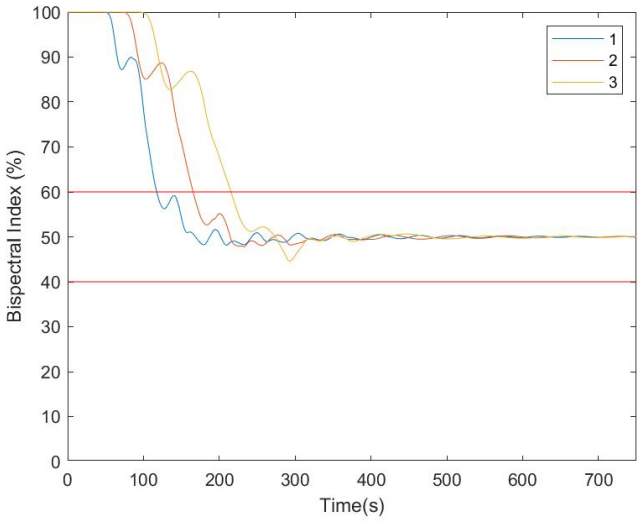

Figure 5.11: BIS output for a delay on the measurement of BIS of 50,75,100 seconds

5.3 Nominal model

The nominal model uses the nominal values for the parameters of the models in Chapter 2. Additional parameters for the controller, setpoints and constraints can be found in Table 5.1 and equation 5.1 (weighting matrices for states and inputs respectively). The performance of this controller is further discussed in Sections 5.3.1 (setpoint following) and 5.3.2 (disturbance rejection).

$$Q = \begin{bmatrix} 50 & 0 & 0 & 0 & 0 \\ 0 & 50 & 0 & 0 & 0 \\ 0 & 0 & 1 & 0 & 0 \\ 0 & 0 & 0 & 1 & 0 \\ 0 & 0 & 0 & 0 & 50 \end{bmatrix} . \beta_{mpc}$$
$$R = \begin{bmatrix} 0 & 0 & 0 & 0 & 0 \\ 0 & 0 & 0 & 0 & 0 \\ 0 & 0 & 0 & 0 & 0 \\ 0 & 0 & 0 & 0 & 0 \end{bmatrix} \tag{5.1}$$

Additional parameters		**Setpoints**	
γ(-)	4	BIS (%)	50
Tp (s)	150	RASS (-)	-1.26
Tc (s)	1	CO ($\frac{ml}{kg*min}$)	75
BIS delay (s)	19.7	MAP (mmHg)	85
β_{mpc} (-)	0.38289	NMB (%)	10
κ (-)	0.0033		

Constraints			
Minima		Maxima	
BIS (%)	40	BIS (%)	60
RASS (-)	-5	RASS (-)	4
CO ($\frac{ml}{kg*min}$)	65	CO ($\frac{ml}{kg*min}$)	110
MAP (mmHg)	65	MAP (mmHg)	110
NMB (%)	0	NMB (%)	100
Propofol infusion ($\frac{\mu g}{kg*min}$)	0	Propofol infusion ($\frac{\mu g}{kg*min}$)	3.5
Remifentanil infusion ($\frac{\mu g}{kg*min}$)	0	Remifentanil infusion ($\frac{\mu g}{kg*min}$)	2.5
Dopamine infusion ($\frac{\mu g}{kg*min}$)	0	Dopamine infusion ($\frac{\mu g}{kg*min}$)	10
SNP infusion ($\frac{\mu g}{kg*min}$)	0	SNP infusion ($\frac{\mu g}{kg*min}$)	10
Atracurium infusion ($\frac{\mu g}{kg*min}$)	0	Atracurium infusion ($\frac{\mu g}{kg*min}$)	15
Propofol concentration ($\frac{\mu g}{ml}$)	1.8655	Propofol concentration ($\frac{\mu g}{ml}$)	1.9737
Remifentanil concentration ($\frac{\mu g}{ml}$)	0.95	Remifentanil concentration ($\frac{\mu g}{ml}$)	1.0430

Table 5.1: Parameters, setpoints and constraints for nominal model

5.3.1 Control performance for the undisturbed nominal model

As can be seen in Figures 5.12 to 5.16, the controller is able to reach all the setpoints of the outputs with acceptable accuracy. There is only a deviation from the setpoint for CO and MAP. As these deviations mirror each other, this is explained by the antagonistic relation between CO and MAP. Furthermore, a damped version of the oscillations present in the MAP output can also be found in the CO output. To have a clearer view on the oscillations of BIS during the induction phase, the same model is simulated for a shorter simulation time (see Figures 5.17). It is evident that the oscillations during the induction phase are caused by the delay on the measurement of BIS (see Figure 5.10).

For NMB, it is clinical practise to administer a bolus of 500 μg kg^{-1} at the beginning of the surgery before the automatic controller is connected. The goal is to achieve a rapid decline in muscle activity [91]. Therefore, it can be assumed that the NMB is at 10% level at the beginning of the induction phase. Although the NMB output of the patient model is initialised to be 10%, the states within the steady-state NMB PK model are not (i.e. according to their internal states, the NMB level is still 100%). This means that it takes some time before the states have catched up. In reality, however, this is not the case. Hence, the oscillation in Figure 5.16 will be much lower. This therefore presents a clear shortcoming of the current simulator, but it can be remedied by initialising the internal states of the steady-state PK model. The values for this initialisation can be found by simulating the PK model separately and finding which state values correspond to a steady-state NMB level of 10%.

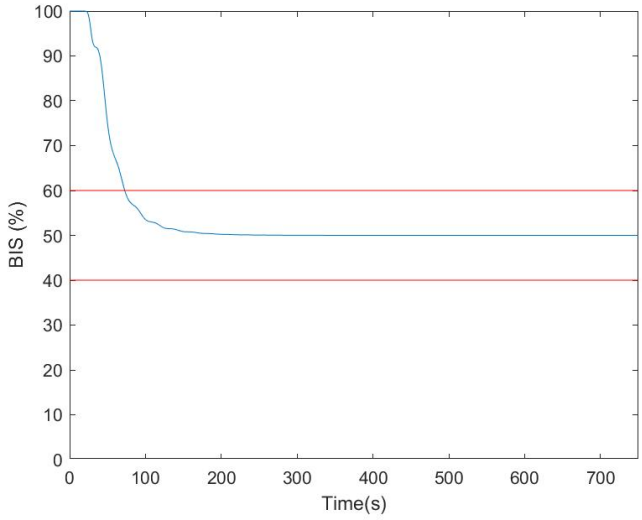

Figure 5.12: BIS output for undisturbed nominal model

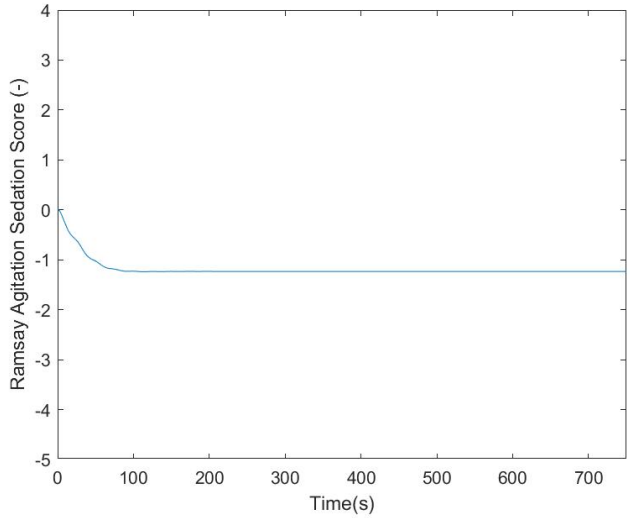

Figure 5.13: RASS output for undisturbed nominal model

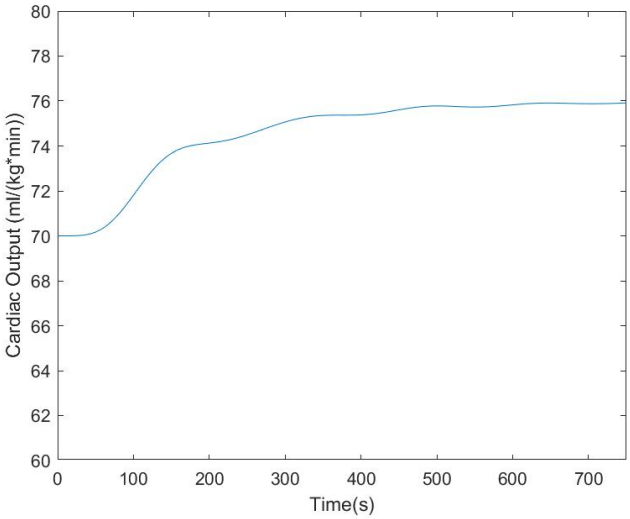

Figure 5.14: CO output for undisturbed nominal model

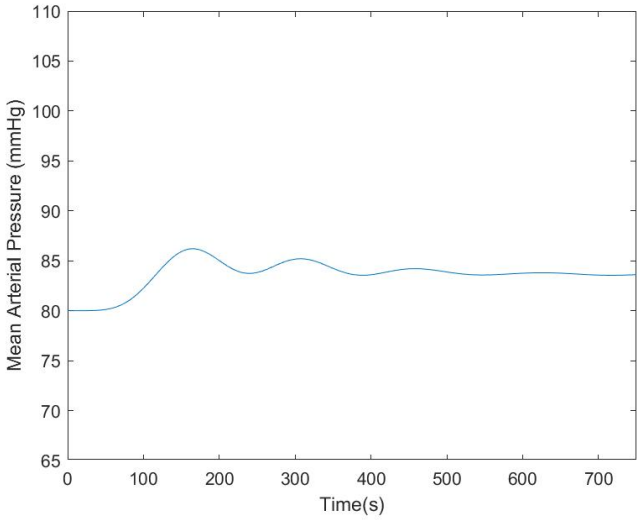

Figure 5.15: MAP output for undisturbed nominal model

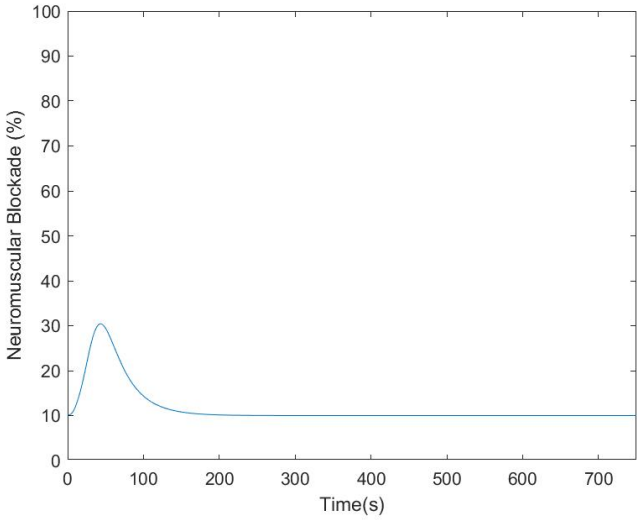

Figure 5.16: NMB output for undisturbed nominal model

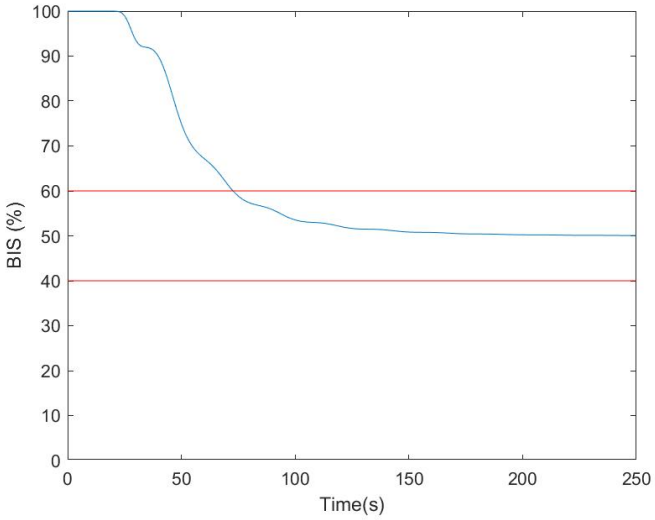

Figure 5.17: BIS output for undisturbed nominal model - zoom

5.3.2 Control performance for the disturbed nominal model

In this section, the nociceptor stimulation and anesthesiologist in the loop from Section 2.4 are added to the same controller and model as simulated in Section 5.3.1. Figure 5.18 shows that the BIS output does leave the preferred interval (indicated by the red lines) because of the disturbance, but not for long (approximately 25 seconds). Because the constraints are loosened as soon as the value of BIS crosses one of the red lines, it is quickly controlled back to the interval. After the BIS output has entered the interval, it is then gradually controlled to the setpoint. Figure 5.19 also clearly demonstrates the advantage of integrating the anesthesiologist in the loop as a measured disturbance. The Propofol infusion calculated by the controller is immediately adapted to the intervention by the anesthesiologist. In case the additional Propofol infusion was only added as an unmeasured disturbance, the controller would adapt more slowly. This would result in a more sluggish response, a larger deviation from the setpoint and longer periods outside the preferred interval. As in Section 5.3.1, the simulation is repeated for a shorter simulation time (see Figures 5.20 and 5.21). These two figures demonstrate that the anticipatory reaction by the anesthesiologist decreases the BIS output and that the reaction on the measured disturbance is indeed instantaneous.

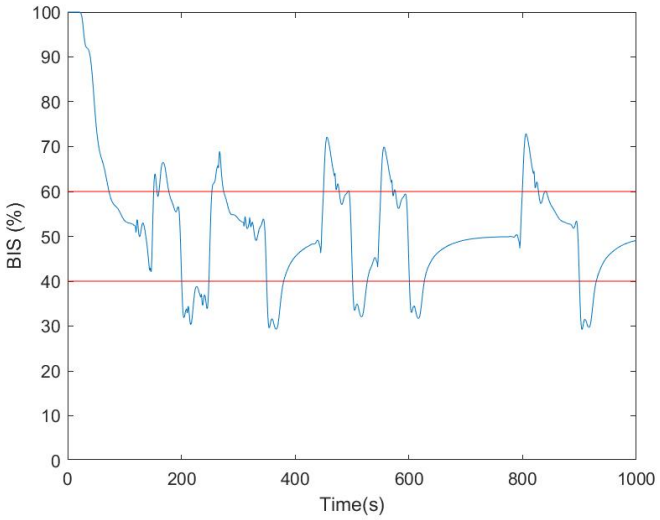

Figure 5.18: BIS output for disturbed nominal model

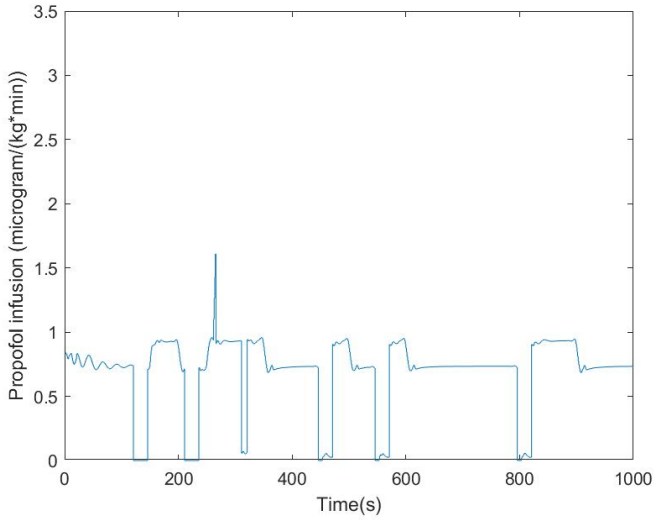

Figure 5.19: Propofol input for disturbed nominal model

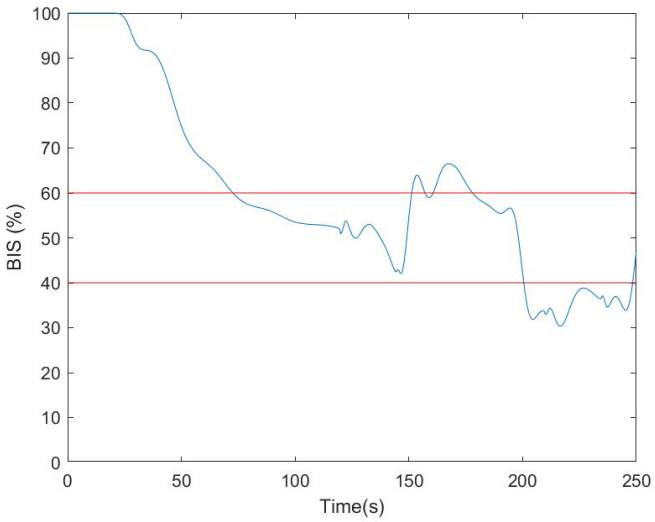

Figure 5.20: BIS output for disturbed nominal model - zoom

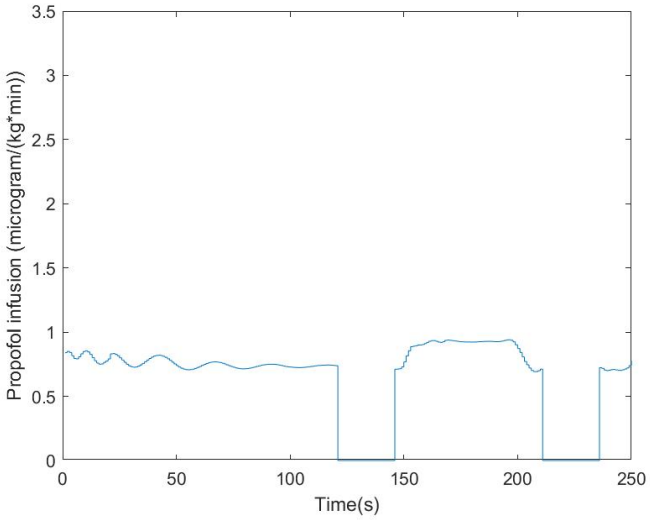

Figure 5.21: Propofol input for disturbed nominal model - zoom

5.4 Interpatient variability

The nominal model of Section 5.3 is now varied by changing γ between 1 and 8. Each new value of gamma is treated as a separate patient for which the simulation is repeated, either with (Section 5.4.2) or without (Section 5.4.1) disturbance. It is assumed that the value of γ is exactly known and the closed-loop controller is adapted according to γ.

5.4.1 Control performance for interpatient variability without disturbances

The controller is able to reach to setpoint for BIS, independent of the value of γ (see Figure 5.22). It can be seen that during the induction phase it takes longer to reach a certain BIS-level for a larger γ. This can be explained by looking at Figure 3.21: for a BIS-level larger than 50%, the required effect-site concentration is higher for a larger value of γ. As the linear patient dynamics are independent of γ, they have not changed. It will therefore take a longer time to reach this higher concentration.

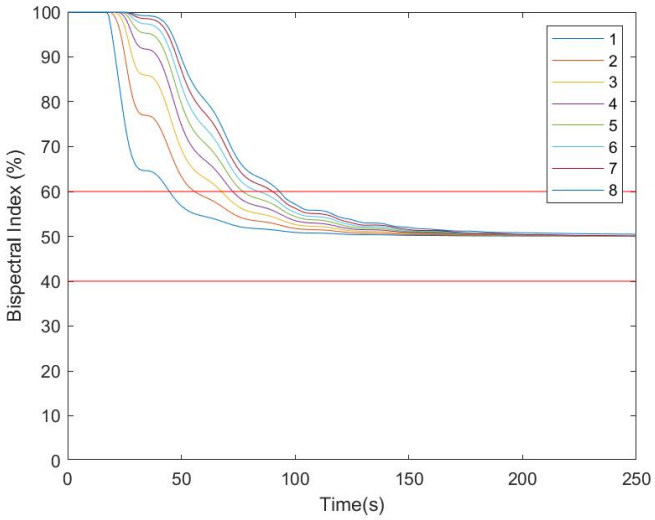

Figure 5.22: BIS output for interpatient variability - undisturbed

5.4.2 Control performance for interpatient variability including disturbances

If the value of γ is exactly known so the controller can be adapted, the control performance is very similar for all values of γ (see Figure 5.23). However, for BIS-levels lower than 50%, patients with smaller values of γ will have a slower decline in BIS-level than patients with larger values of γ. This means that if the bolus injection administered by the anesthesiologist is calculated as is done in this thesis, the BIS-level after the administration will be higher for smaller values of γ. When the same surgical stimulus is then applied to all patients, patients with a lower sensitivity will have a higher resulting BIS-level than patients with a higher sensitivity. Other methods to calculate the bolus injection can be explored, but this is ultimately completely dependent on the anesthesiologist. From Figure 5.24, it is confirmed that the Propofol infusion signal calculated by the controller is different for different values of γ.

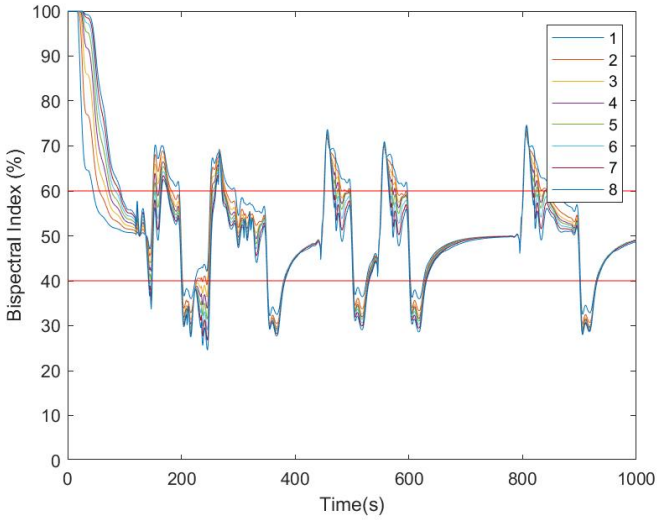

Figure 5.23: BIS output for interpatient variability - disturbed

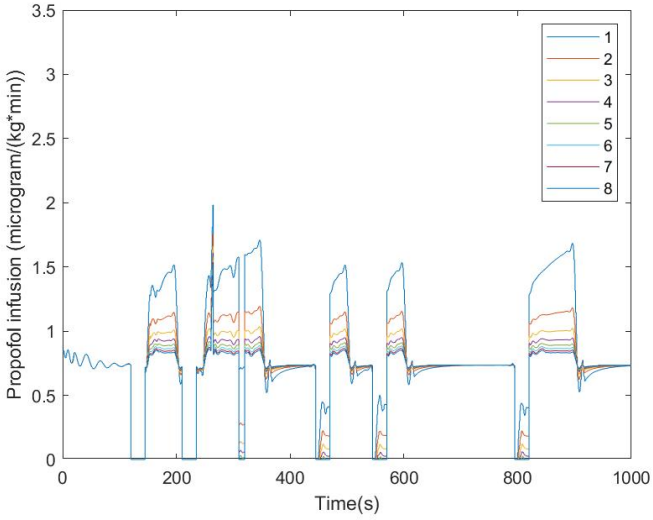

Figure 5.24: Propofol for interpatient variability - disturbed

5.5 Intrapatient variability

In contrast to Section 5.4, the γ-value of one patient changes during the simulation. This will be simulated for a change in γ from 1 to 8, with (Section 5.5.2) or without (Section 5.5.1) disturbance. During the simulation, the change in γ is not gradual but in steps of 1. The steps are equally spaced, i.e. a single value of γ has a period of Tsim/8, with Tsim being the total simulation time. Once again, it is assumed that the value of γ is exactly known at each time instant and that the closed-loop controller is adapted according to γ.

5.5.1 Control performance for intrapatient variability without disturbances

Despite the variation of γ, the setpoint for BIS is reached and maintained (see Figure 5.25). Note that there is now an overshoot of the setpoint during the induction phase. This leads to the conclusion that the induction phase is sensitive to changing values of γ.

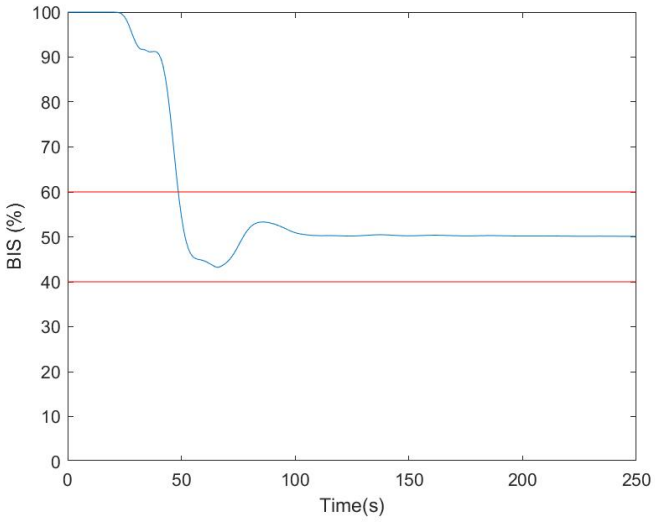

Figure 5.25: BIS output for intrapatient variability - undisturbed

5.5.2 Control performance for intrapatient variability including disturbances

Identical to the previous section, there is an overshoot of the setpoint during the induction phase due to changing γ. These oscillation disappear at the beginning of the maintenance phase but this does confirm the potential issue of changing γ values during the induction phase. Consequently, it has to be made sure that the maintenance phase has certainly begun before any surgical stimulus is applied.

Furthermore, jumps can be clearly seen in Figure 5.26 (see for instance yellow ellips) if the BIS-level is above or below 50% whenever the value of γ changes. When a step to a higher γ value occurs, there is an almost instantaneous jump to higher BIS-levels. The amplitude of these jumps are smaller for BIS-levels closer to 50%. Once again, this can be explained by looking at Figure 3.21. As the effect-site concentrations remain constant, the amplitude of the jump when changing γ increases for BIS-levels higher and lower than 50%, reaches a maximum and becomes zero for BIS-levels close to 100% and 0%. This discussion demonstrates that the current level of BIS determines the effect a change in γ has.

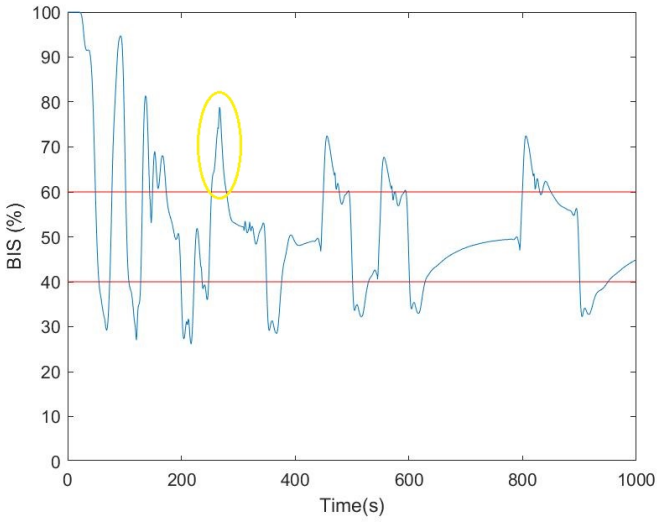

Figure 5.26: BIS output for intrapatient variability - disturbed

5.6 Stability analysis

The stability of the nominal model is checked according the procedure described by Chen and Allgöwer [80], as described in Section 4.1.2. Note that the Jacobian linearization (A,B) of the system is exactly equal to the state and input matrix of the system as the system is linear and time-invariant. It was shown in Section 3.3 that the state matrix for all patients in Table 2.1 is Hurwitz. Hence, the system is asymptotically stable. This should not come as a surprise as it was shown in Chapter 3 that the hemodynamic models are open-loop stable and the pharmacokinetic models open- and closed-loop stable. Following the procedure of Section 4.1.2, the subsequent results for α, K and P were obtained. Due to its size, the matrix P can be found in Appendix B.4. As these results fulfil all requirements described in [80], it is concluded that the resulting closed-loop QIH-MPC controller is asymptotically stable within the feasible region.

$$\alpha = 2.3119 * 10^{20}$$

$$eig(P) \in \left\{ \begin{matrix} 3269.0 & 3184.0 & 2196.0 & 1951.0 & 1889.0 \\ 1729.0 & 1774.0 & 1352.0 & 1291.0 & 1219.0 \\ 740.9 & 706.3 & 564.0 & 572.2 & 436.2 \\ 410.5 & 299.6 & 262.2 & 156.4 & 136.6 \\ 173.1 & 99.0 & 147.5 & 92.42 & 40.03 \\ 76.29 & 64.11 & 52.32 & 35.83 & 0.8651 \\ 1.501 & 3.925 & 17.84 & 6.839 & 14.75 \\ 12.53 & 9.839 & 6.957 & 7.664 & \end{matrix} \right\}$$

$$K^T = \begin{bmatrix}
-0.9022 & 0 & 0 & 0 & 0 & -0.9022 \\
-0.2085 & 0 & 0 & 0 & 0 & -0.2085 \\
-0.1818 & 0 & 0 & 0 & 0 & -0.1818 \\
-2.468 & 0 & 0 & 0 & 0 & -2.468 \\
-0.9815 & 0 & 0 & 0 & 0 & -0.9815 \\
-0.9934 & 0 & 0 & 0 & 0 & -0.9934 \\
-0.6437 & 0 & 0 & 0 & 0 & -0.6437 \\
-0.3646 & 0 & 0 & 0 & 0 & -0.3646 \\
0 & -2.104 & 0 & 0 & 0 & 0 \\
0 & -0.2636 & 0 & 0 & 0 & 0 \\
0 & -0.025 & 0 & 0 & 0 & 0 \\
0 & -8.113 & 0 & 0 & 0 & 0 \\
0 & -3.109 & 0 & 0 & 0 & 0 \\
0 & -3.737 & 0 & 0 & 0 & 0 \\
0 & -3.668 & 0 & 0 & 0 & 0 \\
0 & -6.002 & 0 & 0 & 0 & 0 \\
0 & 0 & -0.7552 & 0 & 0 & 0 \\
0 & 0 & -1.386 & 0 & 0 & 0 \\
0 & 0 & -1.158 & 0 & 0 & 0 \\
0 & 0 & -0.8059 & 0 & 0 & 0 \\
0 & 0 & -0.6601 & 0 & 0 & 0 \\
0 & 0 & -1.007 & 0 & 0 & 0 \\
0 & 0 & -1.574 & 0 & 0 & 0 \\
0 & 0 & -1.691 & 0 & 0 & 0 \\
0 & 0 & -1.449 & 0 & 0 & 0 \\
0 & 0 & -0.8393 & 0 & 0 & 0 \\
0 & 0 & 0 & -1.029 & 0 & 0 \\
0 & 0 & 0 & -1.397 & 0 & 0 \\
0 & 0 & 0 & -1.38 & 0 & 0 \\
0 & 0 & 0 & -1.006 & 0 & 0 \\
0 & 0 & 0 & -0.7331 & 0 & 0 \\
0 & 0 & 0 & -0.5966 & 0 & 0 \\
0 & 0 & 0 & -1.104 & 0 & 0 \\
0 & 0 & 0 & -1.29 & 0 & 0 \\
0 & 0 & 0 & -1.163 & 0 & 0 \\
0 & 0 & 0 & -0.7008 & 0 & 0 \\
0 & 0 & 0 & 0 & -3.494 & 0 \\
0 & 0 & 0 & 0 & -7.563 & 0 \\
0 & 0 & 0 & 0 & -7.069 & 0
\end{bmatrix}$$

Chapter 6

Conclusions

6.1 Concluding remarks

Automated drug delivery minimises the side-effects from over- and underdosing by eliminating human errors and taking advantage of accurate infusion devices. This results in reduced recovery times, more efficient drug usage and in the end, a minimization of the healthcare costs [13]. In this thesis, the models for the multiple effects of general anesthesia are discussed and evaluated in open-loop to gain insight into the full patient model. Further, a Quasi-infinite Horizon MPC algorithm has been devised to control the full patient model. In a last step, this controller was tested in simulation, providing a proof-of-concept for the automated control of general anesthesia.

Quasi-infinite Horizon MPC was chosen as it offers a computationally effective way of controlling general anesthesia. Moreover, it provides a clear path to verify the stability of the controller using the individual model of the patient. The stability of the controller can be checked in simulation studies for a database of patients, something which has already been done in this thesis for a limited set of data. Furthermore, Quasi-infinite Horizon MPC is suited for adaptive control and has inherent robustness against disturbances, eliminating the need for robust MPC schemes. Using dynamical constraints for the effect-site concentrations, setpoints are reached and the control performance is generally as desired, even when considering inter- and intrapatient variability. Further research is however required to investigate the size of the feasible region of the controller as both stability and robustness fundamentally depend on the controller being able to find a feasible solution.

6.2 Suggestions for further research

In this section, some suggestions for further research are given based on the results of this thesis.

1. **Modelling the effect of Dopamine on the effect-site concentration of Propofol and integrating it in the patient model**
   There is one component still missing from the patient model of general anesthesia, namely the effect of Dopamine on the effect-site concentration of Propofol. With Dopamine, the cardiac output is increased, thereby increasing the clearance of the Propofol from the patient's body [40]. Currently, no model for this effect is available [21]. Therefore, this effect still needs to be modelled and integrated in the patient model.

2. **Models based on fractional calculus**
   Current research (for instance [65]) indicates fractional calculus can be used to model effects in anesthesia. New fractional models for the depth of anesthesia can be developed. Afterwards, they can be integrated in the simulation to compare their performance with the traditional models.

3. **Feasible regions**
   As stated above in Section 6.1, both stability and robustness depend on the ability of the controller to find a feasible solution. It is therefore important to be able to determine how large the feasible region is in any given situation and which parameters mostly affect the feasibility of the control problem. This means a formal method to determine the feasible region needs to be derived and a sensitivity analysis needs to be conducted. From the work of Yu and Allgöwer [83], it is already clear that this will certainly depend on the performance parameters of the controller (i.e. prediction horizon, control horizon) as well as the *choice* of the terminal set and terminal penalty function. As described in Section 4.1.2, the terminal region is not unique. It depends on the obtained state feedback matrix K and the *choice* of κ. It is claimed in [80] that it is very difficult or even impossible to find the largest feasible region for a given nonlinear system. For this application, it is however not the goal to find the largest feasible region, but to find a method to predict the size of the feasible region. This way, it can be tuned taking into account the desired control performance.

4. **Robustness properties of QIH-MPC**
   The robustness properties of the QIH-MPC scheme are discussed in Section 4.1.3. Further research is required to determine how robust it is, taking into account the feasible region. Model uncertainties and inaccuracies of the chosen state estimator demand extra attention, especially when implementing adaptive control.

5. **Adaptive control**
   As explained in Chapter 2, a patient gradually changes during operation (i.e. intrapatient variability). This means one cannot hope to attain the desired control performance using a controller with a nominal patient model. Hence, adaptive control is required [21].

6. **Non-convex optimisation within the feasible region**
   In Section 4.2, it is explained that a normal local solver cannot be used for QIH-MPC of a non-convex nonlinear system as the local optimum may be outside the feasible region. Rather, a local solver which uses multiple starting points (ideally in the region of attraction of multiple optima within the feasible region) or a global solver need to be used. Further research has to determine which solver can ideally be used, considering the required computation time for each iteration.

7. **Computational performance (CPU time)**
   So far, no thought has been given to the real-time feasibility of the control scheme. As stated in [79], this is one of the major challenges facing (nonlinear) MPC. Considering the identification algorithms that will be added when implementing adaptive control, the computation time for one iteration will only increase. Therefore, it is good to check the employed algorithms for their computational efficiency. The prediction and control horizon can also be tuned to achieve real-time feasibility. Note that in that case the choice of these two horizons not only affects the real-time feasibility, but also the stability and robustness of the controller.

Bibliography

[1] D. Copot and C. Ionescu, "Models for Nociception Stimulation and Memory Effects in Awake and Aware Healthy Individuals," *IEEE Transactions on Biomedical Engineering*, vol. 66, no. 3, pp. 718-726, March 2019.

[2] R. Hamill-Ruth and M. Marohn, "Evaluation of Pain in the Critically Ill Patient," *Critical Care Clinics*, vol. 15, no. 1, pp. 35-54, 1999.

[3] K. Puntillo, D. Stannard, C. Miaskowski, K. Kehrle and S. Gleeson, "Use of a Pain Assessment and Intervention Notation (P.A.I.N) tool in critical Care Nursing Practice: Nurses' Evaluations," *Heart and Lung: the journal of critical care*, vol. 31, no. 4, pp. 303-314, 2002.

[4] N. Desbiens, A. Wu, S. Broste, N. Wenger, A. Connors, J. Lynn, Y. Yasui, R.S. Philips and W. Fulkerson, "Pain and Satisfaction with Pain Control in seriously ill hospitalized Adults: findings from the SUPPORT research investigations. For the SUPPORT investigators. Study to understand Prognoses and Preferences for Outcomes and Risks of Treatment," *Critical Care Medicine*, vol. 24, no.12, pp. 1956-1961, 1996.

[5] P. McArdle, "Intravenous Analgesia," *Critical Care Clinics*, vol. 15, no. 1, pp. 89-104, 1999.

[6] M. Neckebroek, T. De Smet and M. Struys, "Automated drug delivery in anesthesia," *Curr Anesthesiol Rep*, vol. 3, pp. 18-26, 2013.

[7] T. Schnider, C. Minto, S. Shafer, P. Gampus, C. Andresen, D. Goodale and E. Youngs, "The influence of age on Propofol pharmacodynamics," *Anaesthesiology*, vol. 90, pp. 1502-1516, 1999.

[8] D. Copot, R. De Keyser and C. Ionescu, "Drug Interaction Between Propofol and Remifentanil in Individualised Drug Delivery Systems," *9th IFAC Symposium on Biological and Medical Systems*, The International Federation of Automatic Control, Berlin, Germany, Aug.31 – Sept 2, 2015.

[9] G. Dumont, "Feedback control for clinicians," *Journal of Clinical Monitoring and Computing*, vol. 23, pp. 435-454, 2014.

[10] A. Absalom, R. De Keyser and M. Struys, "Closed loop anaesthesia: are we getting close to finding the holy grail?" *Anesthesia and Analgesia*, vol. 112, pp. 516-518, 2011.

[11] C. Ionescu, J.T. Machado, R. De Keyser, J. Decruyenaere and M.M.R.F. Struys, "Nonlinear dynamics of the patient's response to drug effect during general anesthesia," *Communications in Nonlinear Science and Numerical Simulation*, vol. 20, no. 3, pp. 914-926, 2015.

[12] C. Rocha, T. Mendonca and M. Silva, "Individualizing propofol dosage: a multivariate linear model approach," *Journal of Clinical Monitoring and Computing*, vol. 28, no. 6, pp. 525-536, 2014.

[13] D. Copot and C. Ionescu, "Drug delivery system for general anesthesia: where are we?" *Proceedings of the IEEE International Conference on Systems, Man, and Cybernetics (SMC)*, vol. -, pp. 2452-2457, 2014.

[14] F. Padula, C. Ionescu, N. Latronico, M. Paltenghi, A. Visioli and G. Vivacqua, "Optimized PID control of depth of hypnosis in anesthesia," *Computer Methods and Programs in Biomedicine*, vol. 144, pp. 21-35, 2017.

[15] L. Kovacs, "Linear parameter varying (LPV) based robust control of type I diabetes driven for real patient data," *Knowledge based Systems*, vol. 122, pp. 199-213, 2017.

[16] D. Drexler, L. Kovacs, J. Sapi, I. Harmati and Z. Benyo, "Model-based analysis and synthesis of tumor growth under angiogenic inhibition: a case study," *IFAC Proceedings*, vol. 44, no. 1, pp. 3753-3759, 2011.

[17] B. Kiss, J. Sapi and L. Kovacs, "Imaging method for model-based control of tumor diseases," *Proceedings of the IEEE 11th International Symposium on Intelligent Systems and Informatics (SISY)*, vol. -, pp. 271-275, 2013.

[18] J. K. Popovic, D. Spasic, J. Tovic, J. Kolarovic, R. Malti, I. M. Mitic, S. Pilipovic and T. Atanackovic, "Fractional model for pharmacokinetics of high dose methotrexate in children with acute lymphoblastic leukaemia," *Commun Nonlinear Sci Nummer Simulat*, vol. 22, pp. 451-471, 2015.

[19] A. Churilov, A. Medvedev and A. Shepeljavyi, "Mathematical model of non-basal testosterone regulation in the male by pulse modulated feedback," *Automatica*, vol. 45, pp. 78-85, 2009.

[20] S. Bibian, C.R. Ries, M. Huzmezan and G.A. Dumont, "Introduction to Automated Drug Delivery in Clinical Anesthesia," *European Journal of Control*, vol. 11, pp. 535-557, 2005.

[21] C. M. Ionescu, D. Copot, M. Neckebroek and C. I. Muresan, "Anesthesia regulation: Towards completing the picture," *2018 IEEE International Conference on Automation, Quality and Testing, Robotics (AQTR)*, Cluj-Napoca, 2018, pp. 1-6.

[22] C. Ionescu, I. Nascu and R. De Keyser, "Lessons learned from closed loop control in engineering: towards a multivariable approach regulating depth of anesthesia," *J. Clin Monit and Comp*, vol. 62, pp. 537-546, 2014.

[23] M.R.F. Struys, H. Vereecke, A. Moerman, EW. Jensen, D. Verhaeghen, N. De Neve, F. Dumortier and E. Mortier, "Ability of the bispectral index, autoregressie modelling with exogenous input-derived auditory evoked potentials and predicted propofol concentrations to measure patient responsiveness during anaesthesia," *Anesthesiology*, vol. 99, pp. 802-812, 2003.

[24] N. Liu, T. Chazot, A. Genty, A. Landais, A. Restoux, K. McGee, P.A. Laloe, B. Trillat, L. Barvais and M. Fischler, "Closed-loop coadministration of propofol and remifentanil guided by bispectral index: a randomized multicentre study," *Anesthesia and Analgesia*, vol. 112, no. 3, pp. 546-557, 2011.

[25] G. Dumont, A. Martinez and M. Ansermino, "Robust control of depth of anaesthesia," *International Journal of Adaptive Control Signal Processing*, vol. 23, pp. 435-454, 2009.

[26] M. Denai, D. A. Linkens, A. J. Asbury, A. D. MacLeod and W. M. Gray, "Self-tuning PID control of atracurium-induced muscle relaxation in surgical patients," *IEEE Proceedings*, vol. 137, pp. 261-272, 1990.

[27] T. Mendonça, H. M. Lic, P. Lago and S. Esteves, "Hipocrates: a robust system for the control of neuromuscular blockade," *Journal Clinical Monitoring and Computing*, vol. 18, pp. 265-273, 2004.

[28] C. M. Ionescu , R. D. Keyser, B. C. Torrico, T. D. Smet, M. M. Struys and J. E. Normey-Rico, "Robust Predictive Control Strategy Applied for Propofol Dosing Using BIS as a Controlled Variable During Anesthesia," *IEEE Transactions on Biomedical Engineering*, vol. 55, no. 9, pp. 2161-2170, Sept. 2008.

[29] K. Soltesz, J-O. Hahn, T. Hägglund, G. Dumont and M. Ansermino, "Individualized closed-loop control of propofol anesthesia: a preliminary study," *Biomed Signal Processing Control*, in print 2013.

[30] C.S. Nunes, T. Mendonca, L. Antunes, D.A. Ferreira, F. Lobo and F. Amorim, "Modelling drugs' pharmacodynamic interaction during general anaesthesia: the choice of pharmacokinetic model," *Model Control Biomed Syst*, vol. 6, no. 1, pp. 447-452, 2006.

[31] M. Da Silva, T. Mendonca and T. Wigren, "Nonlinear adaptive control of neuromuscular blockade in anaesthesia," *50th IEEE conference on decision and control, joint with European conference control*, Orlando, FL, 2011, pp. 47-52.

[32] T. De Smet, M.M. Struys, S. Greenwald, E.P. Mortier and S.L. Shafer, "Estimation of optimal modelling weights for a Bayesian-based closed-loop system for propofol administration using the bispectral index as a controlled variable: a simulation study," *Anesth Analg*, vol. 105, no. 6, pp. 1629-38, 2007.

[33] M.M. Struys, T. De Smet, S. Greenwald, A.R. Absalom, S. Bingé and E.P. Mortier, "Performance evaluation of two published closed-loop control systems using bispectral index monitoring: a simulation study," *Anesthesiology*, vol. 100, no. 3, pp. 640-647, 2004.

[34] I. Nascu, C.M. Ionescu and R. De Keyser, "Evaluation of three protocols for automatic DOA regulation using propofol and remifentanil," *The 9th IEEE international conference on control and automation 2011*, Santiago, Chile, 2011.

[35] P. Dua and E. Pistikopoulos, "Modelling and control of drug delivery systems," *Comput Chem Eng* , vol. 29, pp. 2290-6, 2005.

[36] I. Nascu, A. Krieger, C.M. Ionescu and E. Pistikopoulous, "Advanced model-based control studies for the induction and maintenance of intravenous anesthesia," *IEEE Trans. Biomed. Eng.*, vol. 62, pp. 832-841, 2015.

[37] X. Jin, C. Kim and G. Dumont, "A semi-adaptive control approach to closed-loop medication infusion," *Int J Adapt Control and Signal Proce*, vol. 31, pp. 240-354, 2017.

[38] C. Ionescu, D. Copot and R. De Keyser, "Anesthesiologist in the loop and predictive algorithm to maintain hypnosis while mimicking surgical disturbance," *IFAC World Congress*, Toulouse, France, July 2017, pp. 15080-15085, 2017.

[39] A.R. Absalom, v. Mani, T. De Smet and M.M. Struys, "Pharmacokinetic models for propofol – defining and illuminating the devil in the detail," *Br J Anaesth*, vol. 103, pp. 26-37, 2009.

[40] D. Takizawa, K. Nishikawa, E. Sato, H. Hiraoka, K. Yamamoto, S. Saito, R. Horiuchi and F. Goto, "A dopamine infusion decreases propofol concentration during epidural blockade under general anesthesia," *Canadian Anesth J*, vol. 52, pp. 463-466, 2005.

[41] D. Copot, F. Kussé, Ma. Ghita, Mi. Ghita, M. Neckebroek and A. Maxim, "Distributed model predictive control for hypnosis-hemodynamic maintenance during anesthesia," *15th IEEE International Conference on Control & Automation*, 16-19 July, Edinburgh, Scotland, accepted for publication.

[42] C.C. Palerm and B.W. Bequette, "Hemodynamic control using direct model reference adaptive control – experimental results," *European Journal of Control*, vol. 11, no. 6, pp. 558-571, 2005.

[43] B. Geerts, L. Aarts and J. Jansen, "Methods in pharmacology: measurement of cardiac output," *Br J Clin Pharmacol*, vol. 71, no. 3, pp. 316-330, Mar 2011.

[44] W. Bradshaw, "The importance of mean arterial pressure as a patient assessment tool: in haemodialysis and acute care, " *Australian nursing journal*, vol. 20, no. 2, pp. 26-39, 2012.

[45] C. Ionescu, R. Hodrea and R. De Keyser, "Variable time-delay estimation for anesthesia control during intensive care," *IEEE Transactions on biomedical engineering*, vol. 58, no. 2, pp. 363-369, 2011.

[46] Q. Hui, W. Haddad, V. Chellaboina and T. Hayakawa, "Adaptive control of mammillary drug delivery systems with actuator amplitude constraints and system time delays," *European Journal of Control*, vol. 11, pp. 586-600, 2005.

[47] F. Padula, C. Ionescu, N. Latronico, M. Paltenghi, A. Visioli and G. Vivacqua, "Inversion-based propofol dosing for intravenous induction of hypnosis," *Communications in Nonlinear Science and Numerical Simulation*, vol. 39, pp. 481-494, 2016.

[48] D. Copot, A. Chevalier, C. M. Ionescu and R. De Keyser, "A two-compartment fractional derivative model for Propofol diffusion in anesthesia," *2013 IEEE International Conference on Control Applications (CCA)*, Hyderabad, 2013, pp. 264-269.

[49] C. Minto, T. Schnider, T.G. Short, K.M. Gregg, A. Gentilini and S.L. Shafer, "Response surface model for anesthetic drug interactions," *Anesthesiology*, vol. 92, pp. 1603-1616, 2000.

[50] T.W. Schnider, C.F Minto, P.L. Gambus, C. Andresen, D.B. Goodale, S.L. Shafer and E.J. Youngs, "The Influence of Method of Administration and Covariates on the Pharmacokinetics of Propofol in Adult Volunteers," *Anesthesiology*, vol. 88, no. 5, pp. 1170-1182, 1998.

[51] C.F. Minto, T.W. Schnider, T.D. Egan, E. Youngs, H.J.M. Lemmens, P. L. Gambus, V. Billard, J. F. Hoke, K.H.P. More, D. J. Hermann, K.T. Muir, J.W. Mandema and S.L. Shafer, "Influence of Age and Gender on the Pharmacokinetics and Pharmacodynamics of Remifentanil: I. Model Development," *Anesthesiology*, vol. 86, no. 1, pp. 10-23, 1997.

[52] C.F. Minto, M. White, N. Morton and G.N. Kenny, "Pharmacokinetics and pharmacodynamics of remifentanil, II model application," *Anesthesiology*, vol. 86, pp. 24-33, 1997.

[53] E. Gepts, K. Jonckheer, V. Maes, W. Sonck and F. Camu, "Disposition kinetics of propofol during alfentanil anesthesia," *Anaesthesia*, vol. 43, pp. 8-13.

[54] S. Shafer and J. Varvel, "Pharmacokinetics, pharmacodynamics and rational opioid selection," *Anesthesiology*, vol. 74, pp. 53-63.

[55] T. Kirkpatrick, I. Cockshott, E. Douglas and W. Nimmo, "Pharmacokinetics of propofol (diprivan) in elderly patients," *Anesthesia*, vol. 60, pp. 146-150.

[56] C. Rocha, T. Mendonça and M.E Silva, "Modelling neuromuscular blockade: a stochastic approach based on clinical data," *Mathematical and Computer Modelling of Dynamical Systems*, vol. 19, no. 6, pp. 540-556, 2013.

[57] K. Leslie and T.G. Short, "Low bispectral index values and death: the unresolved causality dilemma," *Anesth. Analg*, vol. 113, pp. 660-663, 2011.

[58] C.M. Ionescu, "Modelling Drug Effect Using Fractional Calculus," *Fractional Calculus*, Ed. Roy Abi Zeid Daou & Xavier Moreau, Nova Science Publishers, 2015, pp. 243-258. Print.

[59] C.M. Ionescu, D. Copot and R. De Keyser, "Three compartmental models for propofol diffusion during general anesthesia," *Discontinuity, Nonlinearity and Complexity*, vol. 2, no. 4, pp. 357-368, 2013.

[60] J.J. Trujillo, "Fractional models: sub and super-diffusives, and undifferentiable solutions," *Innovation in Engineering Computational Technology*, pp. 371-401, 2006.

[61] I. Petras and R. L. Magin, "Simulation of drug uptake in a two compartmental fractional model for a biological system," *J. Commun Nonlinear Sci Nummer Simulat*, vol. 16, pp. 4588-4595, 2011.

[62] M. Weiss, "Comparison of distributed and compartmental models of drug disposition: assessment of tissue uptake kinetics," *Journal of Pharmacokinetics and Pharmacodynamics*, vol. 43, pp. 505-512, 2016.

[63] R. De Keyser, C. Ionescu, C. Festila, "A one-step procedure for frequency response estimation based on switch-mode transfer function analyser," *Proc. IEEE-CDC Conf on Decision and Control joint with ECC - European Control Conference*, December 12-15, Orlando, Florida, pp. 1189-1194.

[64] S. Milne, G. Kenny and S. Schraag, "Propofol sparing effect of remifentanil using closed loop anaesthesia," *British Journal of Anaesthesia*, vol. 90, no. 5, pp. 623-629, 2003.

[65] D. Copot and C. M. Ionescu, "A fractional order impedance individualised model of nociceptor stimulation," *9th IFAC Symposium on Robust Control Design ROCOND*, Florianópolis, 2018, pp. 416-421.

[66] J.C. Scott and D.R. Stanski, "Decreased fentanyl and alfentanil dose requirements with age. A simultaneous pharmacokinetic and pharmacodynamic evaluation," *J. Pharmacol Exp Ther*, vol. 240, pp. 159-166, 1987.

[67] N. Yang, M.Z. Zuo, Y. Yue, Y. Wang, Y. Shi and X.N. Zhang, “Comparison of C50 for Propofol-Remifentanil Target Controlled Infusion and Bispectral Index at Loss of Consciousness and Response to painful Stimulus in Elderly and Young Patients," *Chinese Medical Journal*, vol. 128, pp. 1994-1999, 2015.

[68] T.W. Bouillon, J. Bruhn, L. Radulescu, C. Andresen, T.J. Shafer, C. Cohane and S.L Shafer, “Pharmacodynamic interaction between Propofol and Remifentanil regarding hypnosis, tolerance of laryngoscopy, bispectral index, and electroencephalographic approximate entropy," *Anesthesiology*, vol. 100, no. 6, pp. 1353-1372, 2004.

[69] M.M. Silva, T. Wigren and T. Mendonça, “Nonlinear identification of a minimal neuromuscular blockade model in anesthesia," *IEEE Trans Control System Technologies*, vol. 20, pp. 181-188, 2012.

[70] H. Alonso, T. Mendonça and P. Rocha, “A hybrid method for parameter estimation and its application to biomedical systems," *Computer Methods and Programs in Biomedicine*, vol. 89, pp. 112-122, 2008.

[71] C.N. Sessler, M.S. Gosnell, M.J. Grap, G.M. Brophy, P.V. O'Neal, K.A. Keane, E.P. Tesore and R.K. Elswick, "The Richmond Agitation-Sedation Scale: validity and reliability in adult intensive care unit patients ," *Am J Respir Crit Care Med*, vol. 166, pp. 1338-1344, 2002.

[72] Zh. Zhusubaliyev, A. Medvedev and M. Silva, “Bifurcation Analysis of PID Controlled Neuromuscular Blockade in Closed-loop Anesthesia," *Journal of Process Control*, Vol. 25, pp. 152-163, 2015.

[73] J.F. Standing, G.B. Hammer, W.J. Sam and D.R. Drover, “Pharmacokinetic-pharmacodynamic modelling of the hypotensive effect of Remifentanil in infants undergoing cranioplasty," *Pediatric Anesthesia*, vol. 20, no. 1, pp. 7-18, 2010.

[74] A.M. Kirit and S. Rajaguru, "Adopting pade approximation for first order plus dead time models for blending process," *International Journal of Engineering & Technology*, vol. 7, pp. 2800-2805, 2018.

[75] C. Yu, R. J. Roy, H. Kaufman and B. W. Bequette, "Multiple-model adaptive predictive control of mean arterial pressure and cardiac output," *IEEE Transactions on Biomedical Engineering*, vol. 39, no. 8, pp. 765-778, 1992.

[76] S. H. Lehnigk, "On the Hurwitz Matrix, " *Zeitschrift für Angewandte Mathematik und Physik*, vol. 21, no. 3, pp. 498-500, 1970.

[77] J.B. Rawlings and D.Q Mayne, *Model predictive control: Theory and design*, Madison, Wisconsin: Nob Hill Pub. 2009.

[78] F. Allgöwer, R. Findeisen and Z.K. Nagy, "Nonlinear model predictive control: From theory to application," *J. Chin. Inst. Chem. Engrs.*, vol. 35, pp. 299-315, 2004.

[79] R. Findeisen and F. Allgöwer. "An introduction to nonlinear model predictive control," *21st Benelux Meeting on Systems and Control*, 2002, pp. 1-23.

[80] H. Chen and F. Allgöwer. "A quasi-infinite horizon nonlinear model predictive control scheme with guaranteed stability," *Automatica*, vol. 34, no. 10, pp. 1205-1218, 1998.

[81] H. Michalska and D. Q. Mayne, "Robust receding horizon control of constrained nonlinear systems," *IEEE Transactions on Automatic Control*, vol. 38, no. 11, pp. 1623-1633, Nov. 1993.

[82] E.J. Haseltine and J.B. Rawlings , "Critical Evaluation of Extended Kalman Filtering and Moving-Horizon Estimation," *Ind. Eng. Chem. Res.*, vol. 44, no. 8, pp. 2451-2460, 2005.

[83] S. Yu, M. Reble, H. Chen and F. Allgöwer, "Inherent robustness properties of quasi-infinite horizon nonlinear model predictive control," *Automatica*, vol. 50, no. 9, pp. 2269-2280, 2014.

[84] "nlmpcmove," https://nl.mathworks.com/help/mpc/ref/nlmpc.nlmpcmove.html. Accessed: 11-05-2019.

[85] L. Grüne and J. Pannek, *Nonlinear Model Predictive Control*. Springer, Cham, 2017.

[86] "Configure Optimization Solver for Nonlinear MPC," https://nl.mathworks.com/help/mpc/ug/configure-optimization-solver-for-nonlinear-mpc.html. Accessed: 11-05-2019.

[87] "Local vs. Global Optima," https://nl.mathworks.com/help/optim/ug/local-vs-global-optima.html. Accessed: 11-05-2019.

[88] G.V. Reklaitis, A. Ravindran and K.M. Ragsdell, *Engineering optimization: Methods and applications*, New York: Wiley, 1983.

[89] S.J. Wright, "Efficient convex optimization for linear MPC," in *Handbook of Model Predictive Control*. Birkhäuser, Cham, pp. 287-303, 2019.

[90] M. Neckebroek, C.-M. Ionescu, K. van Amsterdam, T. De Smet, P. De Baets, J. Decruyenaere, R. De Keyser and M. Struys. "A comparison of propofol-to-BIS post-operative intensive care sedation by means of target controlled infusion, Bayesian-based and predictive control methods: an observational, open-label pilot study," *Journal of Clinical Monitoring and Computing*, 2019.

[91] T. Mendonça, J. M. Lemos, H. Magalhaes, P. Rocha and S. Esteves, "Drug Delivery for Neuromuscular Blockade With Supervised Multimodel Adaptive Control," *IEEE Transactions on Control Systems Technology*, vol. 17, no. 6, pp. 1237-1244, Nov. 2009.

[92] M.M. Struys, M.J. Coppens, N. De Neve, E.P. Mortier, A.G. Doufas, J.F. Van Bocxlaer and S.L. Shafer, "Influence of administration rate on propofol plasma-effect site equilibration," *Anesthesiology*, vol. 107, pp. 386-96, 2007.

[93] K. Masui, M. Kira, T. Kazama, S. Hagihira, E.P. Mortier and M.M.R.F. Struys, "Early phase pharmacokinetics but not pharmacodynamics are influenced by propofol infusion rate," *Anesthesiology*, vol. 111, pp. 805-817, 2001.

Appendix A

User manual for the Simulink model

A.1 Introduction

The goal of this appendix is to provide an overview and explanation of all functions blocks in the patient model for general anesthesia. To start, please make sure you have the following files in your folder: 'Initialisation_main.m', 'hypnosis_model.m', 'hemodyn_model.m', 'dist_model.m', 'BISsurface.m', 'General_Anesthesia_Patient_Model.mdl'. In case some of these files are missing or have been renamed, please refer to your mentor or predecessor for more info. A detailed description of the purpose of each file is given below.

A.2 Initialisation

Before the first simulation, run 'Initialisation_main.m'. This will initialise all constants as well as the state space models used in the Simulink model. More specifically, it initialises the controller sampling time, simulation time and certain parameters necessary for the calculation of the surface (more information can be found in the section on the calculation of this surface). Finally, it performs the constant declaration for all the anesthetic, hemodynamic and disturbance models implemented in 'hypnosis_model.m', 'hemodyn_model.m' and 'dist_model.m', which are run subsequently. If a set of patients needs to be simulated, it suffices to alter the constants in this file. They do not have to be changed by 'hand' in the files with the models itself. Currently, the values of the variables are taken from literature and corresponds to the population mean. Adaptation schemes and parameter intervals are available in literature and can be found in chapter 2 of this thesis.

In case of errors such as 'The expression x has a syntax error' or 'Undefined

function or variable y', the initialisation has been forgotten. To remedy this, simply run 'Initialisation_main.m'.

A.2.1 Hypnosis_model.m

This .m-file initialises all the transfer functions and state space models necessary for the modelling of the three parts of anesthesia: hypnosis, analgesia and neuromuscular blockade (in that order). Every line in the MATLAB-file is commented in order to be clear as to what each line does.

The only exception is the transfer function from the Remifentanil effect-site concentration to the RASS sedation score. There is a concentration-dependent gain which is implemented directly in Simulink. To alter this gain, the MATLAB-function in the subsystem 'RASS PK model' needs to be adapted.

A.2.2 Hemodyn_model.m

This .m-file initialises all the transfer functions for the Cardiac Output (CO) and Mean Arterial Pressure (MAP).

The transfer function from the Remifentanil effect-site concentration to MAP also has a concentration-dependent gain. Once again, this is implemented directly in Simulink, in the subsystem 'MAP PK model'.

A.2.3 Distmodel.m

This last .m-file provides all the transfer functions for the modelling of disturbances. A signal is created, which is filtered both in the forward and reverse direction, to be passed through the nociceptor pathway model (also provided). Finally, there is the option of an additional bolus signal , which could be a bolus administered by the anesthesiologist before a surgical stimulus. At present, the code for this bolus is added as a comment in the bottom of the file.

A.3 Inputs

There are six inputs in the Simulink-model: stimulation (nociception), Propofol, Remifentanil, Dopamine, Sodium Nitroprusside and Atracurium.

A.3.1 Stimulation (Nociception)

The input disturbance (see Figure A.1) is fed through the nociceptor pathway model, which was initialised in the previous section.

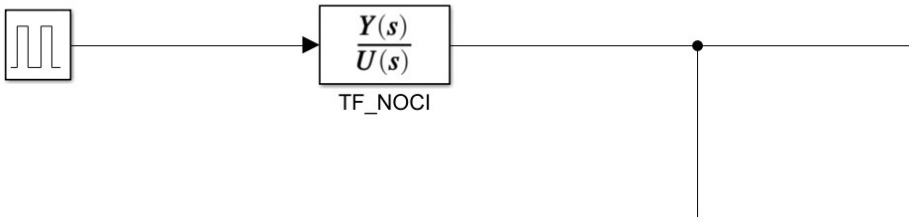

Figure A.1: Stimulation input

A.3.2 Propofol

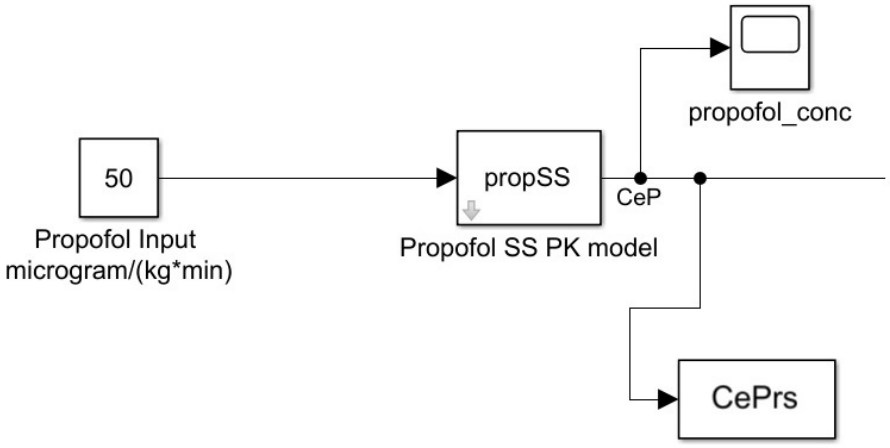

Figure A.2: Propofol input

The Propofol input (see Figure A.2) is passed through the state space PK-model defined in the previous section. The 'To Workspace' block 'CePrs' exports the

evolution of the Propofol-concentration in the blood to the MATLAB-workspace after the simulation is complete.

A.3.3 Remifentanil

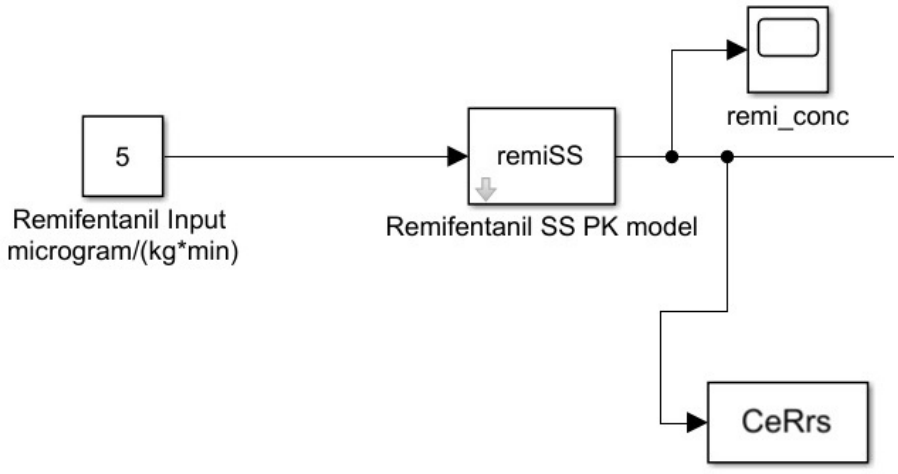

Figure A.3: Remifentanil input

The implementation of Remifentanil is exactly the same as for Propofol (see Figure A.3). The Simulink model also has PK-models from Remifentanil to RASS and MAP. Once again, these models were defined in the previous section.

A.3.4 Dopamine and Sodium Nitroprusside

As the Cardiac Output in a normal patient is different from zero, the cardiac output is initialised at a constant value (70 ml/(kg*min)). The same is true for the Mean Arterial Pressure (80 mmHg). The Dopamine and Sodium Nitroprusside inputs are passed through the transfer functions gij, with i = 1,2 and j = 1,2 (see Figure A.4).

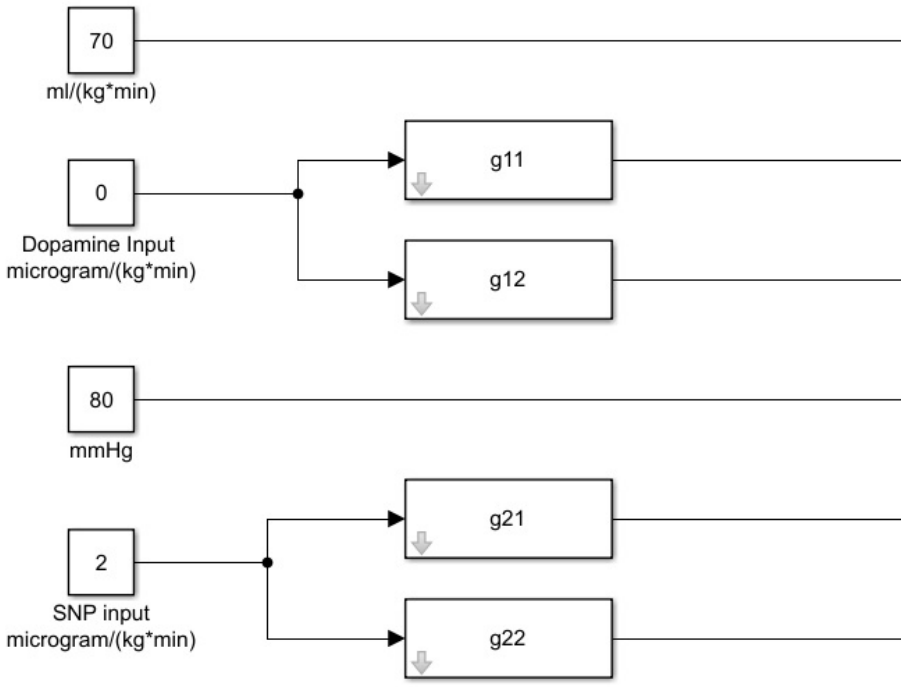

Figure A.4: Dopamine and Sodium Nitroprusside inputs

A.3.5 Atracurium

Just as for Propofol and Remifentanil, Atracurium is passed through a PK-model initialised in the previous section (see Figure A.5).

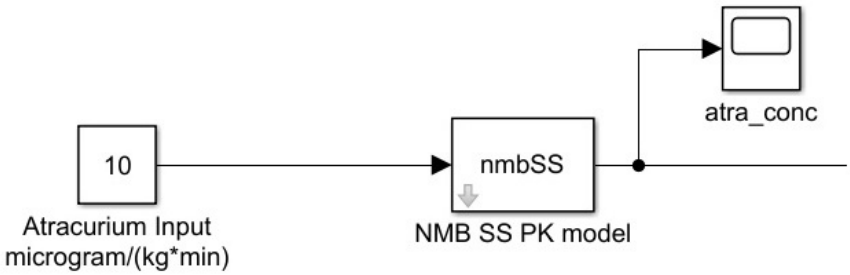

Figure A.5: Atracurium

A.4 Hill functions

All the Hill functions in the model (Propofol, Remifentanil, Remifentanil to MAP, Remifentanil to NMB, Atracurium) are Fcn-blocks. The expression is hard-coded in the block itself, the values for the variables were set during initialisation. Together with the concentration-dependent gain in the second section are these the only models that are just implemented in the Simulink-model itself.

A.5 Outputs

The system has seven outputs, i.e. 'Nociception output', 'Bispectral index', 'RASS', 'Cardiac Output', 'MAP', 'NMB' and the 'Surface Plots'. The calculation of these outputs is done in a straightforward way, summing the appropriate output signals of the corresponding Hill functions. This is done in the two user-defined MATLAB-functions. All the outputs are visualised using Scope-blocks (except the 'Surface plots' which are terminated, more information about their calculation and plotting below).

A.6 Surface Calculation

The surface is calculated using the same model for the interaction between Propofol and Remifentanil as in Section 2.2.2. The calculation is done in a subsystem block to keep the overview. The range for which the surface is calculated depends on the maximum concentration of the past time steps. This means that at each time step, it needs to be checked whether there is a new maximum and if so, it needs to be stored. Note that the output port for the 3D plot is being plotted at runtime and the values of the corresponding matrix are exported to the workspace at the end of the simulation. To change the parameters of this 3D Hill curve, one can easily change the constants initialised in section 2.

A.6.1 Subsystem 'Surface calculation'

Open the subsystem. The system itself has two inputs (the effect-site concentrations of Propofol CeP and Remifentanil CeR) and two outputs (Bispectral index BIS and 3D Plot). Here, CeP, CeR and BIS are signals versus time whereas 3D Plot is a 3D-matrix (i.e. the requested surface). In the middle, there is a MATLAB-function which will update the maximum concentrations if necessary as well as calculate the new surface.

At each time step, the current values of CeP and CeR, the known values for the maximum concentrations CePmax and CeRmax (remember that they were initialised in 'Initialisation_main.m'), the current simulation time and the necessary constants are used as an input for the MATLAB-function. For computational efficiency, the surface is only recalculated at certain timesteps. It has a default value of 1 (i.e. no timesteps are skipped).

Using the constants as an explicit input is unavoidable as a user-defined MATLAB-function in Simulink cannot read them directly from the workspace. The only constants still hard-coded in the MATLAB-function itself are the sampling time, simulation time and the step size needed for computational efficiency. The reason being that they determine the size of the 3D-matrix, which is required to be known for plotting.

The MATLAB-function outputs the (new) values of CePmax and CeRmax as well as the current value of the BIS-signal (using only the current values of CeP and CeR) and the 'surface'. Using 'To Workspace' blocks, these signals are exported as timeseries to the MATLAB-workspace after the simulation so that they can be used for debugging or comparison.

It is however crucial to note that Date Store Read/Write/Memory blocks are used for the online transmission of the values of CePmax and CeRmax. This is necessary as Simulink does not allow workspace-variables to change during simulation and a simple feedback loop results in an error. These blocks are therefore to the author's knowledge the only ones that can be used to update the parameters while the simulation is ongoing.

A.6.2 MATLAB-function '3D-calculations'

Open the MATLAB-function within the subsystem. The code for the MATLAB-function is divided into four sections: 'adaptation of maxima', 'constant declaration', '2D calculations' and '3D calculations'. The first section determines whether the maxima need to change. In the second section, the constants for the models as in Section 2.2.2 are initialised. The third section calculates the current value of the BIS-signal (note: this is a single value). Finally, the fourth section determines the 3D-matrix which gives the surface when plotted.

The first three sections do not involve real calculations, but this is different for the fourth section. In the fourth section, there are two row vectors created (CePr and CeRr), corresponding with the possible values of CeP and CeR respectively. The resolution of these two vectors depends on both the simulation time and the sampling time. Using the model from Section 2.2.2 and a for-loop, the resulting BIS-values are calculated for every combination within CePr and CeRr. This result is then concatenated with the corresponding values within CePr and CeRr to create the 3D-object that is the surface.

To confirm that the surface is being calculated correctly and that it indeed corresponds with those found in literature, a real-time visualisation should be used. Alternatively, a Stop Callback-function could be used to call upon an external MATLAB .m-file (i.e. 'BISsurface.m' see section 1) to calculate the surface after the simulation and this is also implemented, but that surface is not online available. There is however a problem when trying to implement a real-time 3D visualisation as Simulink does not support the necessary plotting capabilities from MATLAB. This results in the following error: 'The function X is not supported for standalone code generation'.

In order to circumvent this problem, one needs to understand how the Simulink coder works at runtime. When compiling, the Simulink model is converted into C/C++ code. The real problem is that the Simulink coder does not generate code for functions from the MATLAB engine. Therefore, if these functions could be neglected during code generation, there wouldn't be an error. This is done by declaring the plotting function (for example 'surf') as an extrinsic function (for more info about extrinsic functions, please refer to https://nl.mathworks.com/help/simulink/ug/calling-matlab-functions.html) with the command *coder.extrinsic('function X')*. Now, the function will not result in code generation and the MATLAB engine will instead execute the call, resulting in a real-time 3D visualisation.

Appendix B

Complete results simulation study

In this appendix the full results of all the simulations discussed in the different chapters of this thesis are included for future reference.

B.1 Chapter 3

B.1.1 Dynamics of pharmacokinetic models

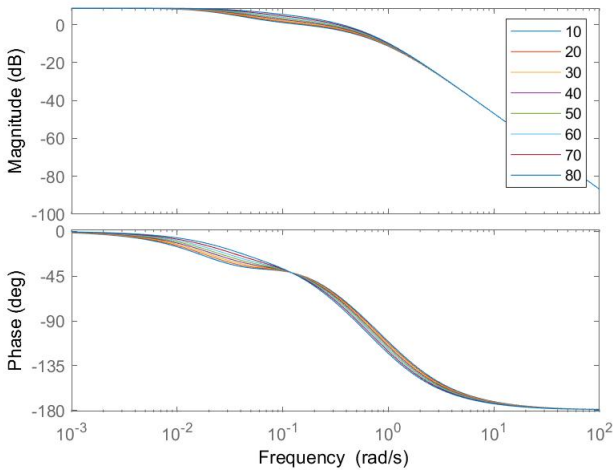

Figure B.1: Bode plot Propofol Male Age

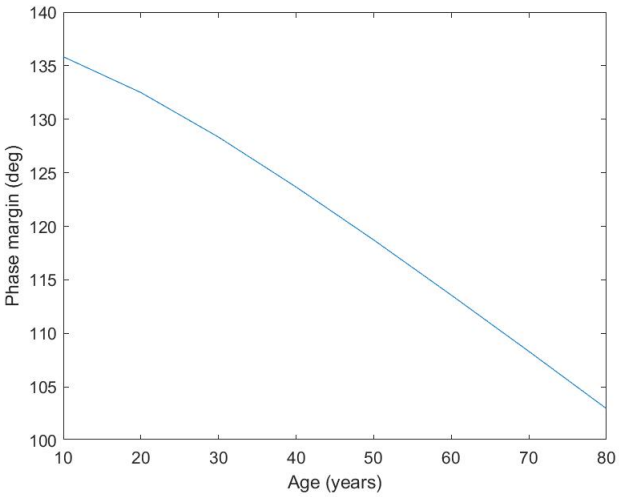

Figure B.2: Phase margin Propofol Male Age

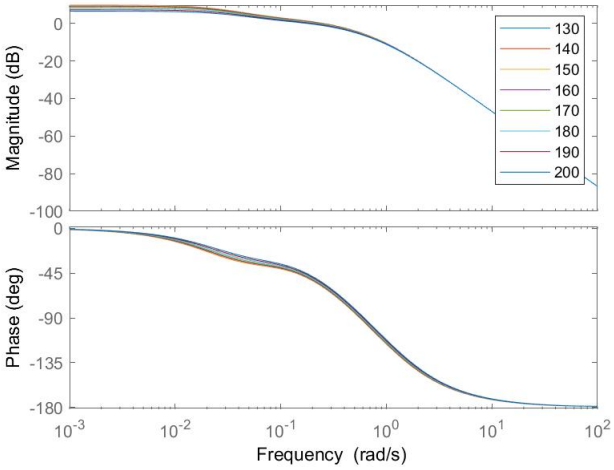

Figure B.3: Bode plot Propofol Male Height

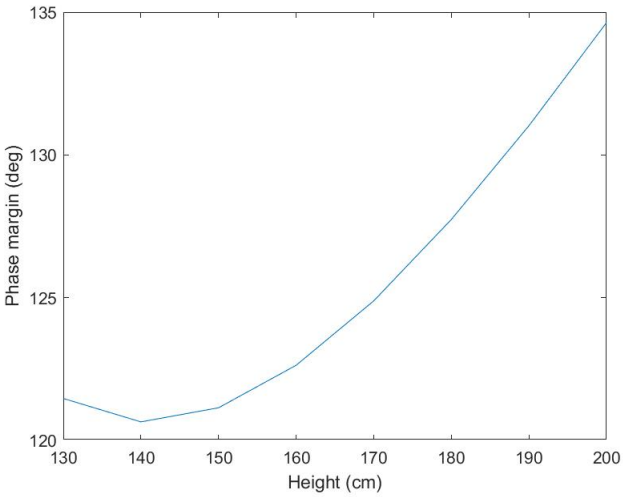

Figure B.4: Phase margin Propofol Male Height

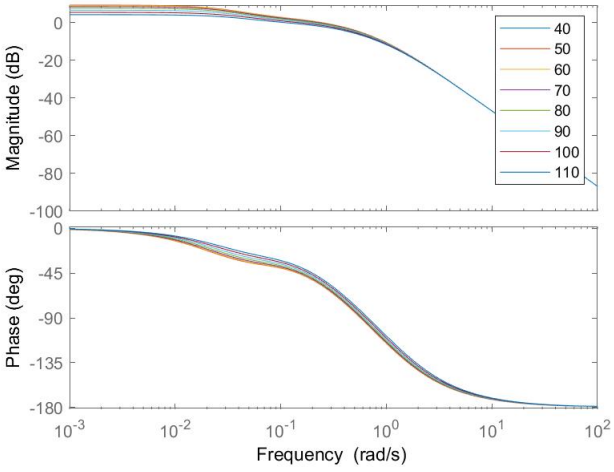

Figure B.5: Bode plot Propofol Male Weight

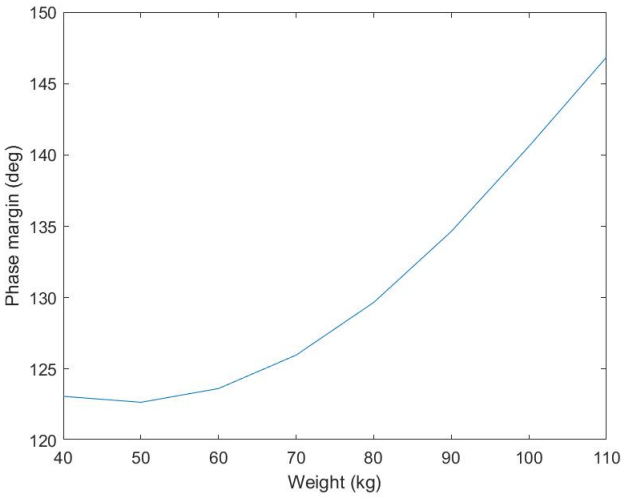

Figure B.6: Phase margin Propofol Male Weight

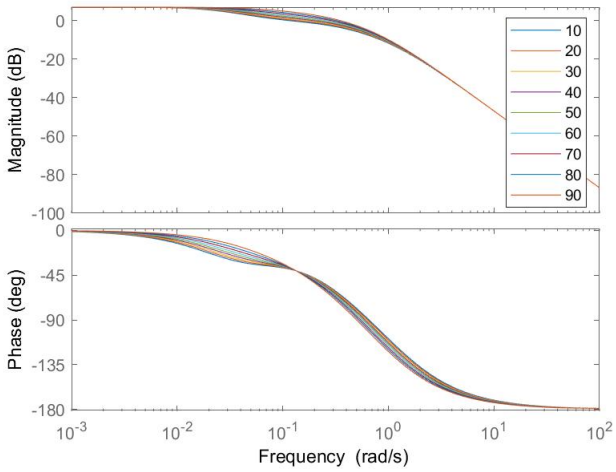

Figure B.7: Bode plot Propofol Female Age

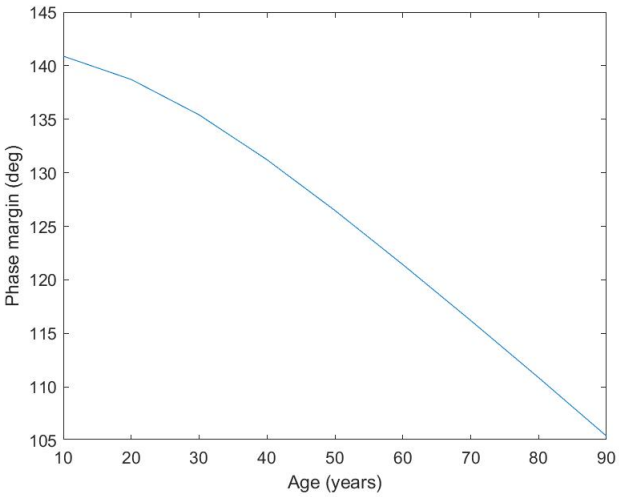

Figure B.8: Phase margin Propofol Female Age

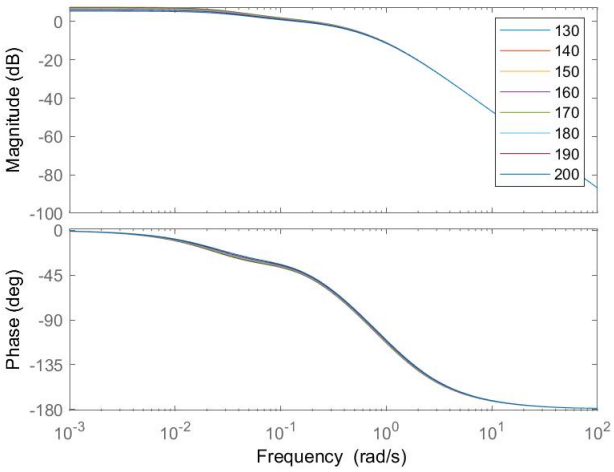

Figure B.9: Bode plot Propofol Female Height

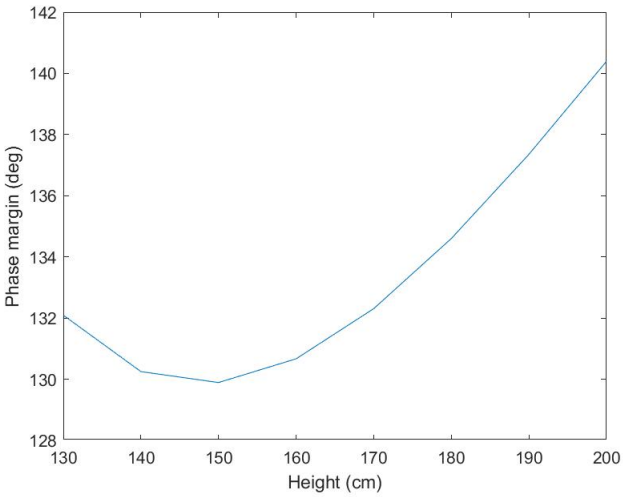

Figure B.10: Phase margin Propofol Female Height

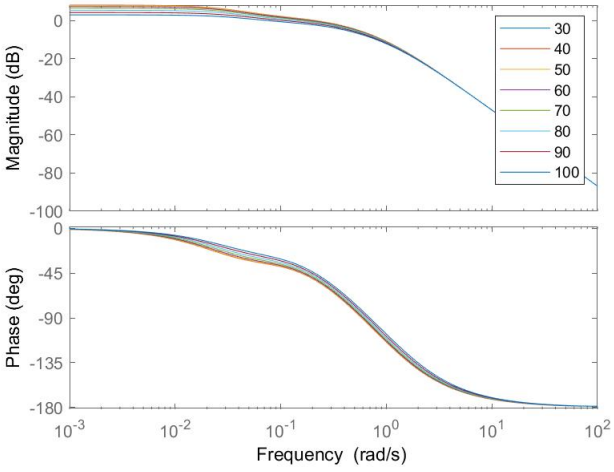

Figure B.11: Bode plot Propofol Female Weight

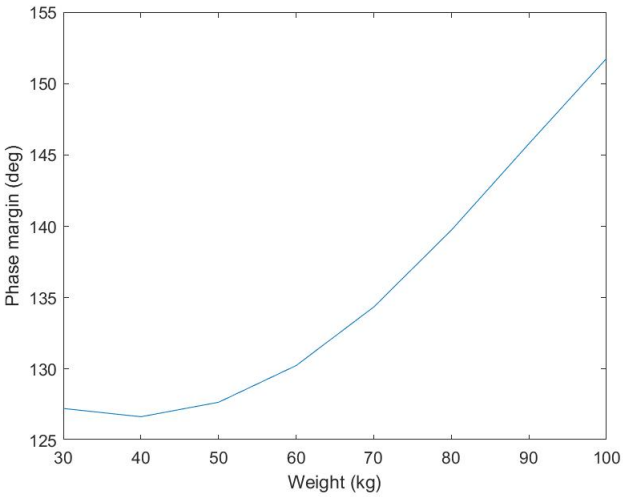

Figure B.12: Phase margin Propofol Female Weight

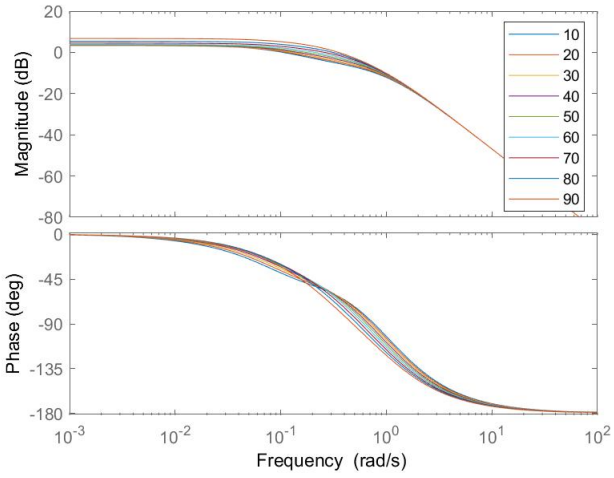

Figure B.13: Bode plot Remifentanil Male Age

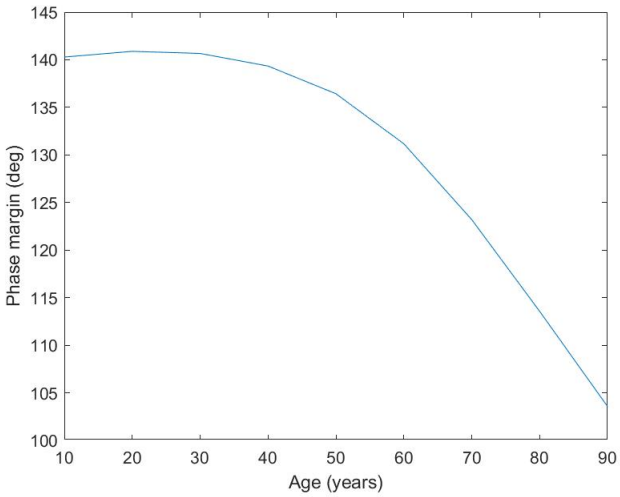

Figure B.14: Phase margin Remifentanil Male Age

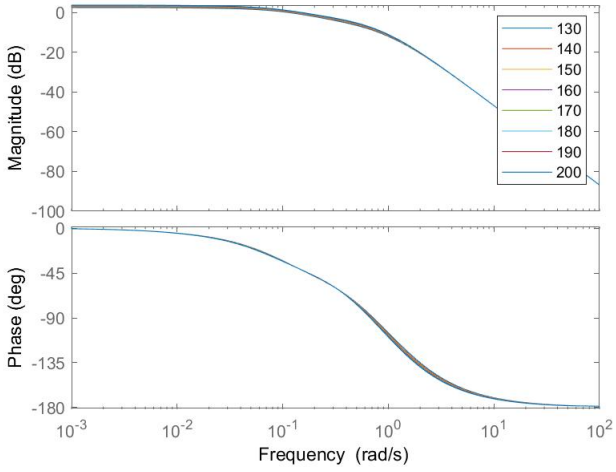

Figure B.15: Bode plot Remifentanil Male Height

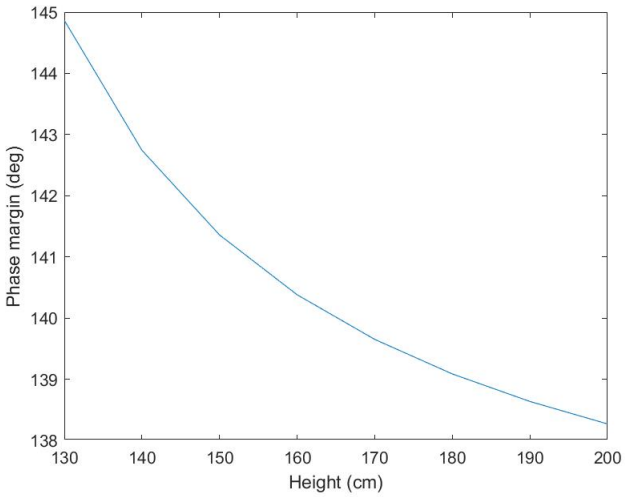

Figure B.16: Phase margin Remifentanil Male Height

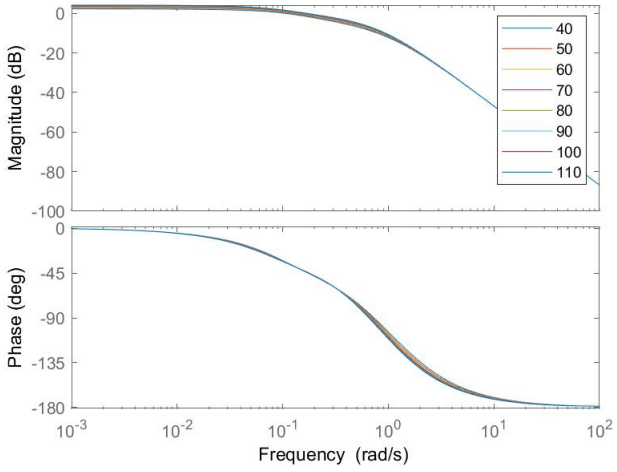

Figure B.17: Bode plot Remifentanil Male Weight

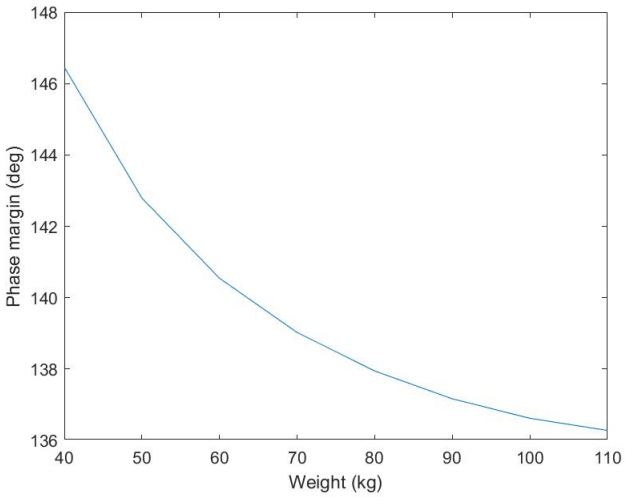

Figure B.18: Phase margin Remifentanil Male Weight

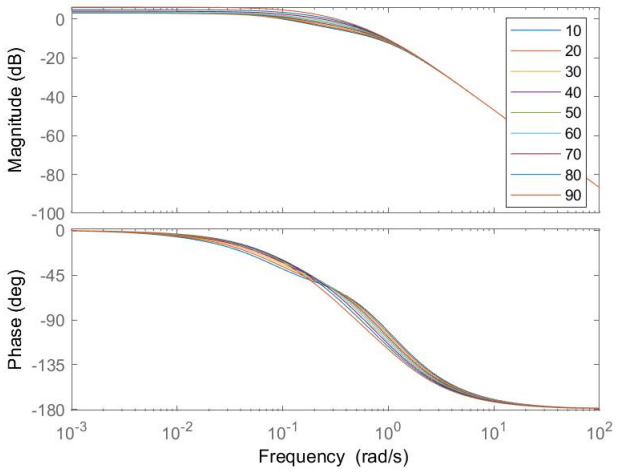

Figure B.19: Bode plot Remifentanil Female Age

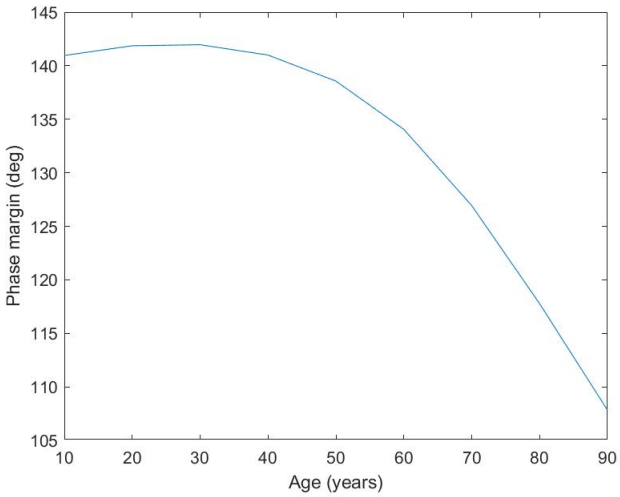

Figure B.20: Phase margin Remifentanil Female Age

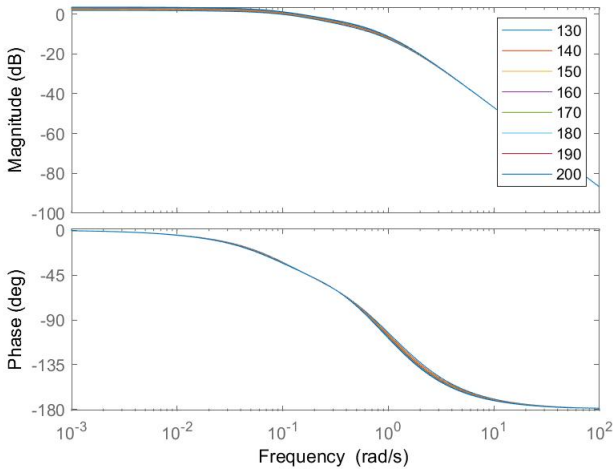

Figure B.21: Bode plot Remifentanil Female Height

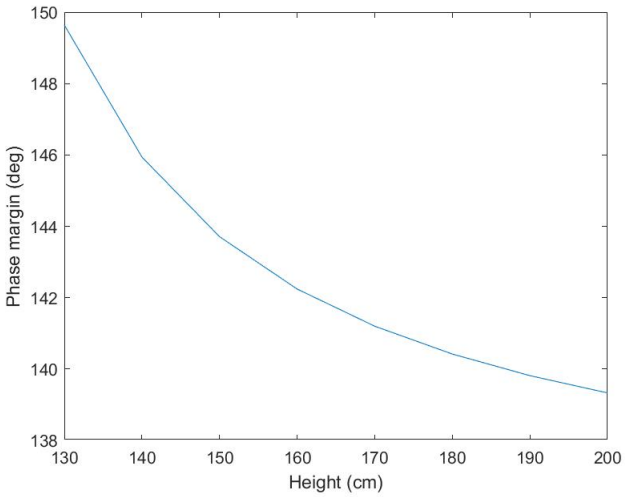

Figure B.22: Phase margin Remifentanil Female Height

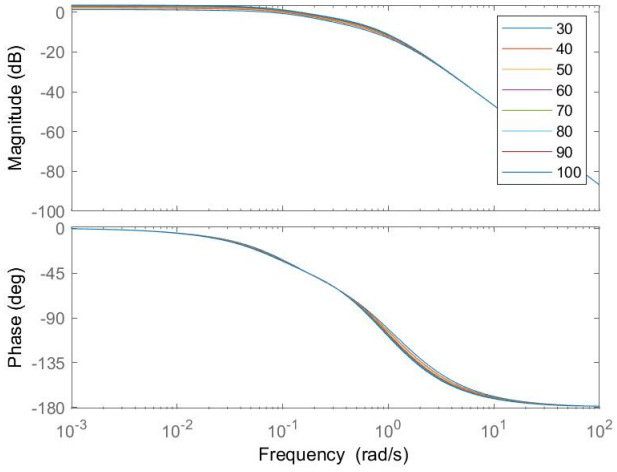

Figure B.23: Bode plot Remifentanil Female Weight

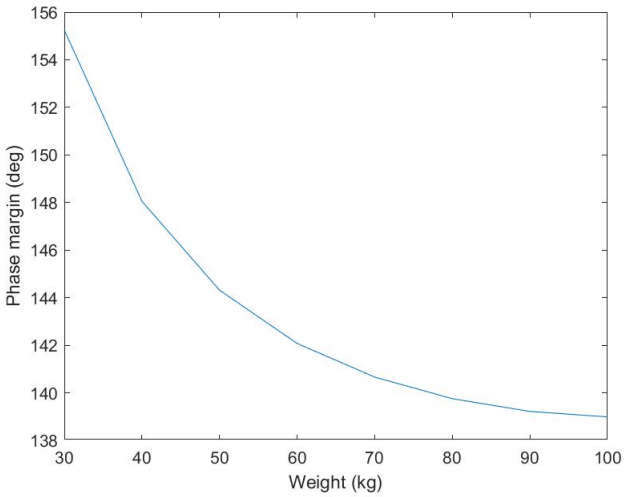

Figure B.24: Phase margin Remifentanil Female Weight

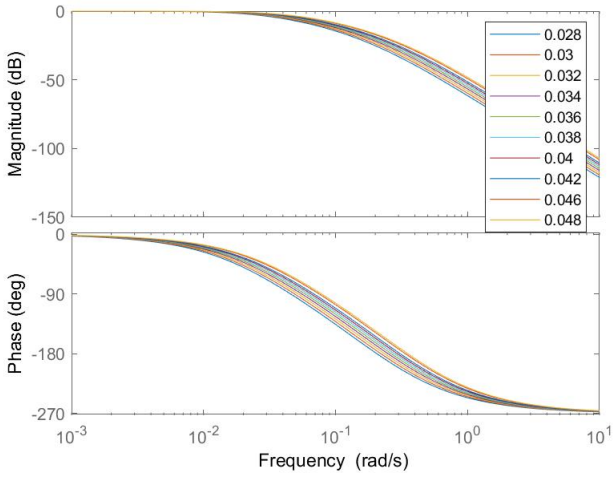

Figure B.25: NMB SS PK model alpha

B.1.2 Dynamics of hemodynamic models

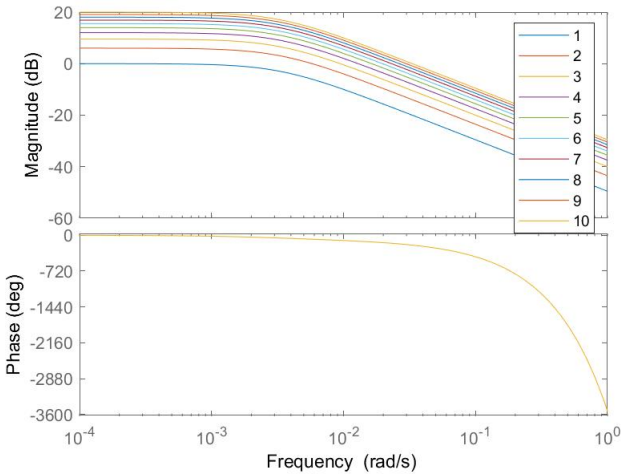

Figure B.26: Bode plot g11 K11

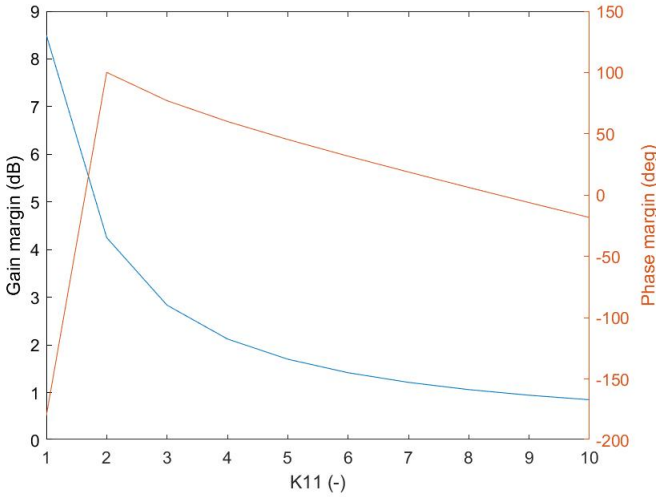

Figure B.27: Gain and phase margin g11 K11

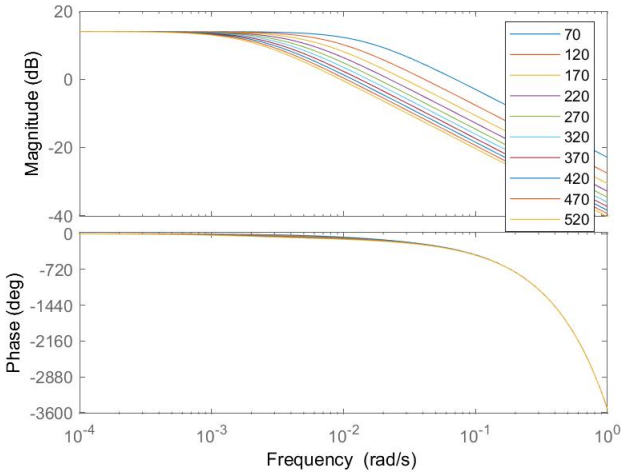

Figure B.28: Bode plot g11 τ11

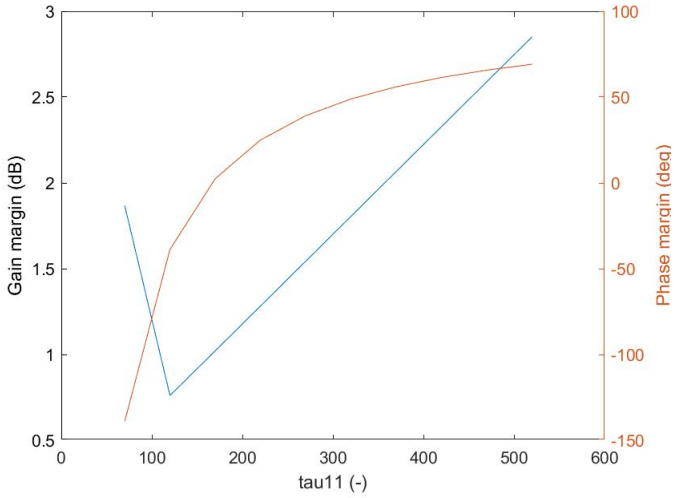

Figure B.29: Gain and phase margin g11 τ11

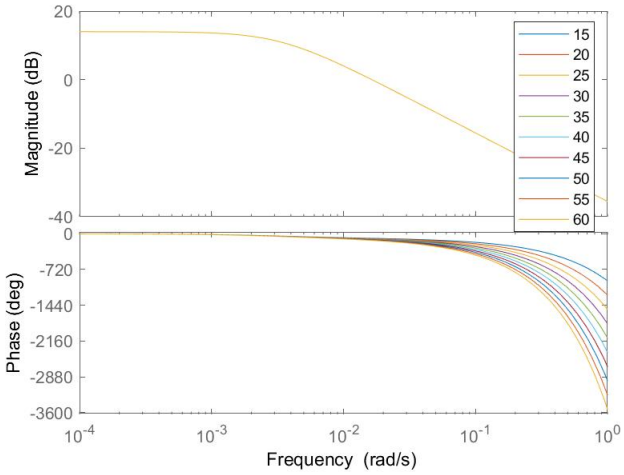

Figure B.30: Bode plot g11 T11

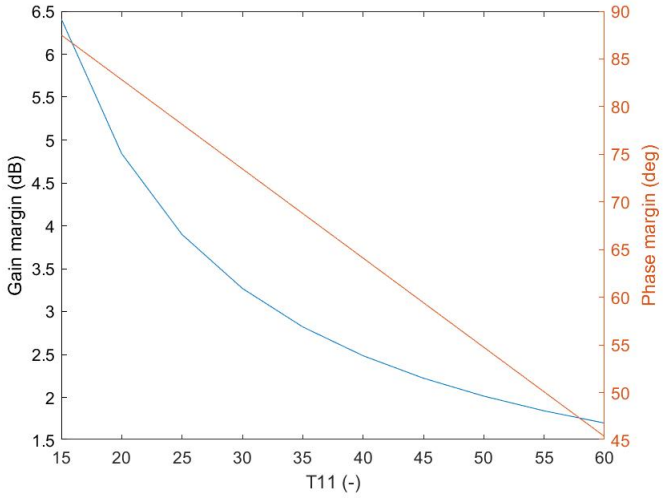

Figure B.31: Gain and phase margin g11 T11

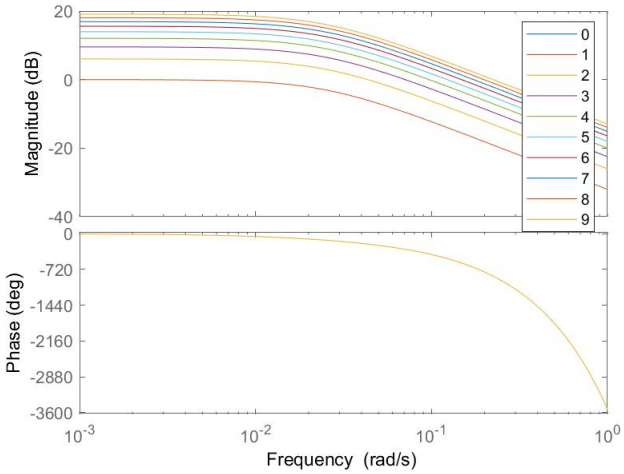

Figure B.32: Bode plot g12 K12

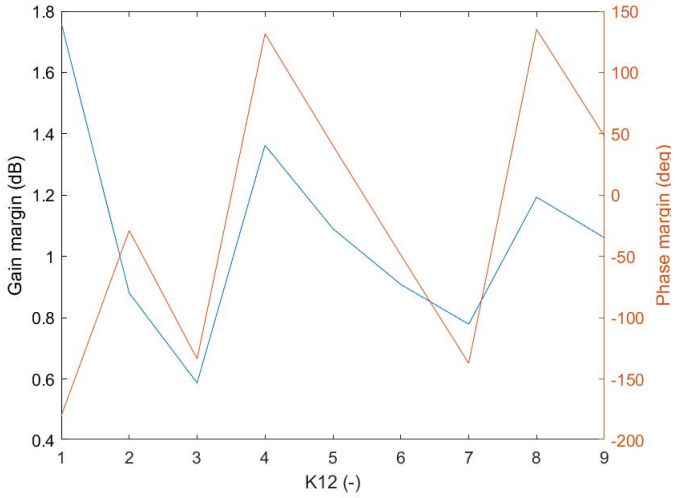

Figure B.33: Gain and phase margin g12 K12

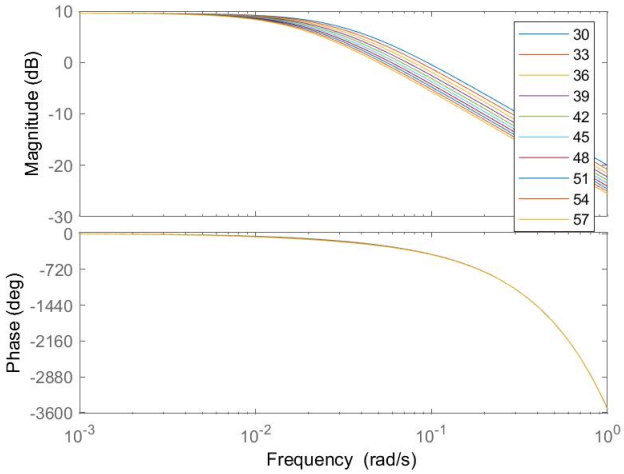

Figure B.34: Bode plot g12 τ12

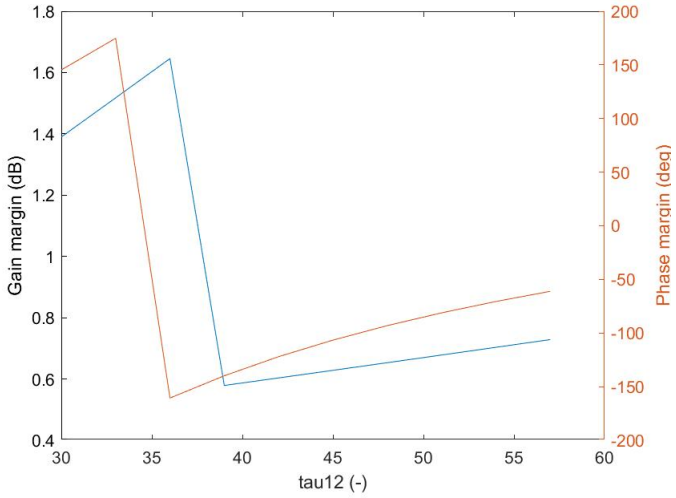

Figure B.35: Gain and phase margin g12 τ12

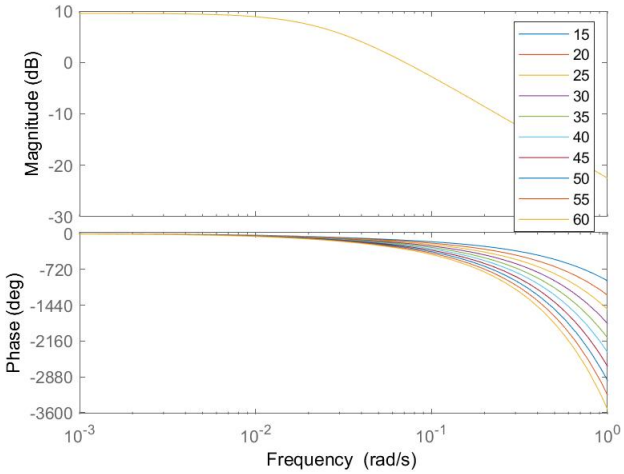

Figure B.36: Bode plot g12 T12

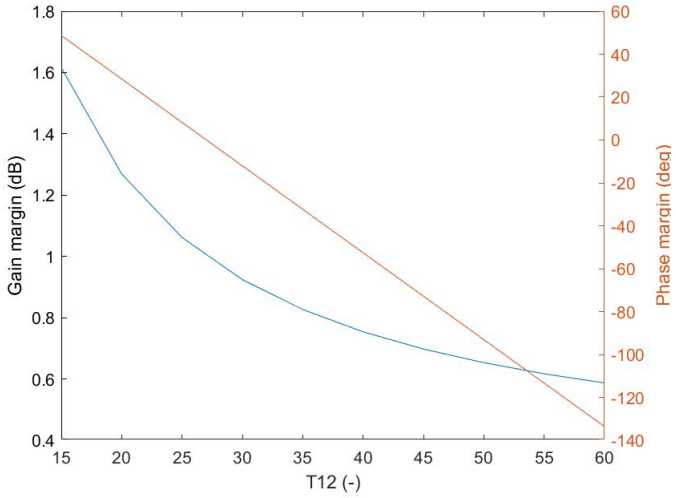

Figure B.37: Gain and phase margin g12 T12

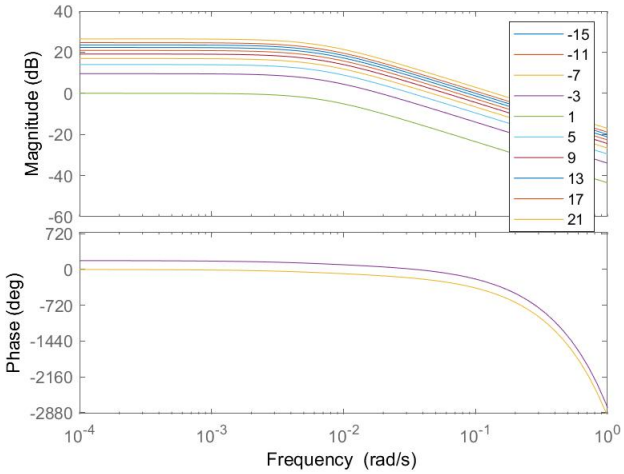

Figure B.38: Bode plot g21 K21

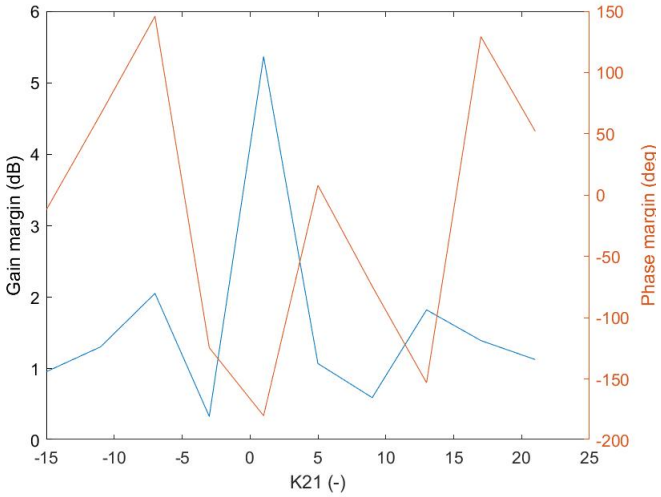

Figure B.39: Gain and phase margin g21 K21

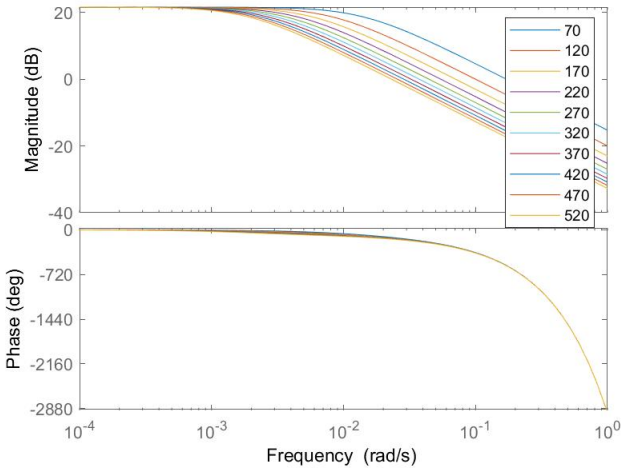

Figure B.40: Bode plot g21 τ21

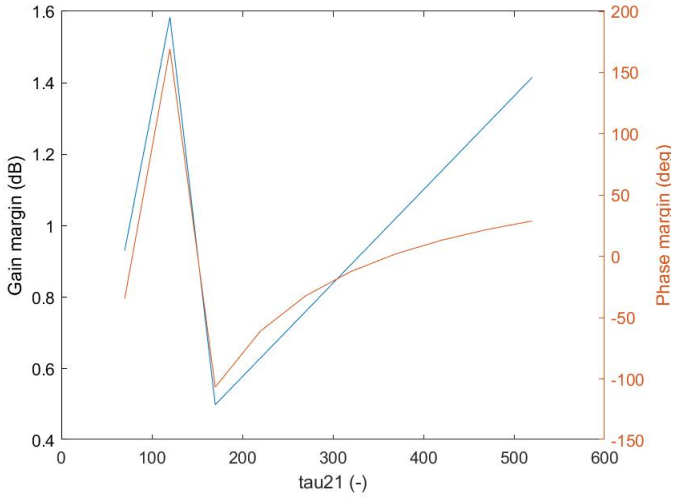

Figure B.41: Gain and phase margin g21 τ21

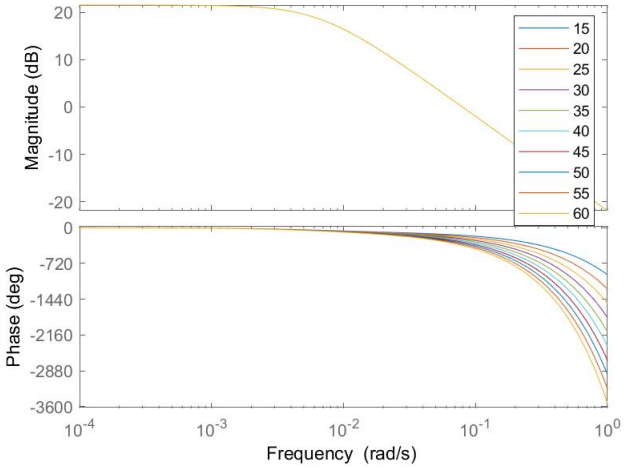

Figure B.42: Bode plot g21 T21

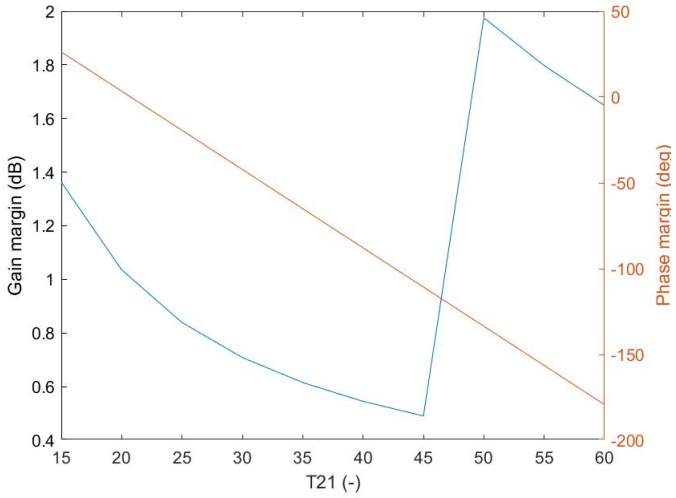

Figure B.43: Gain and phase margin g21 T21

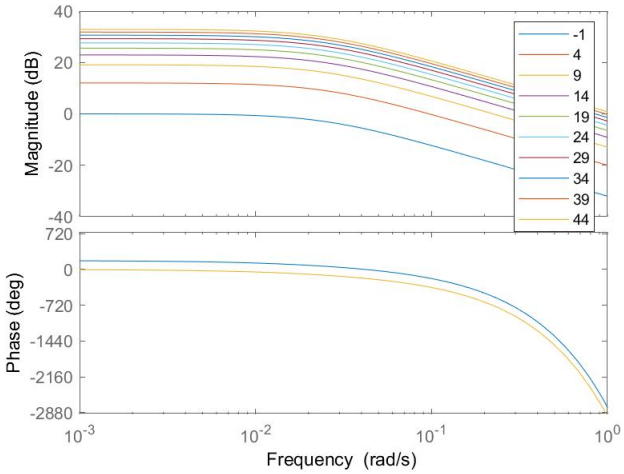

Figure B.44: Bode plot g22 K22

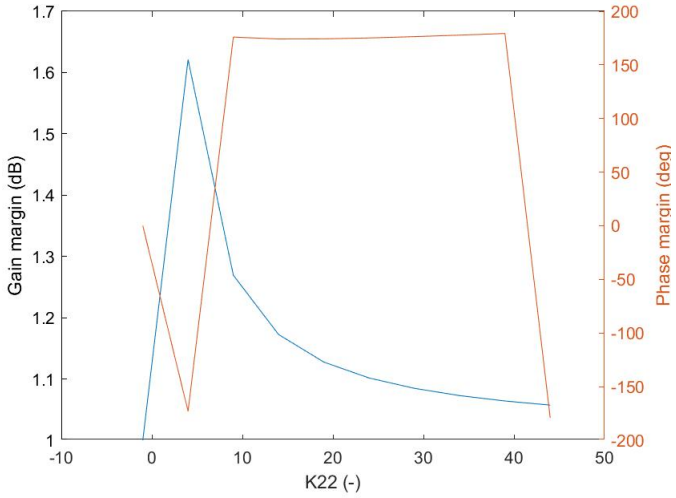

Figure B.45: Gain and phase margin g22 K22

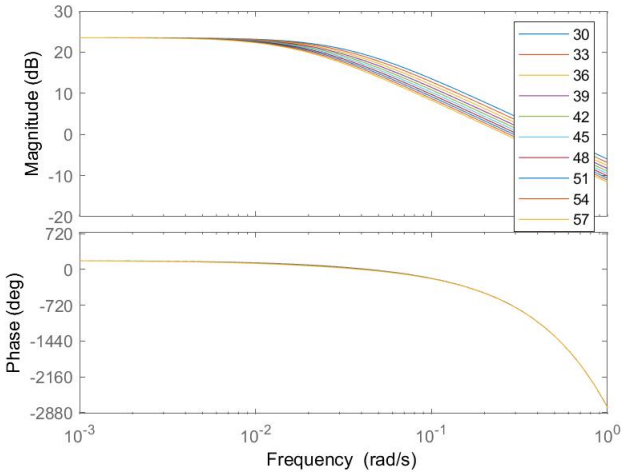

Figure B.46: Bode plot g22 τ22

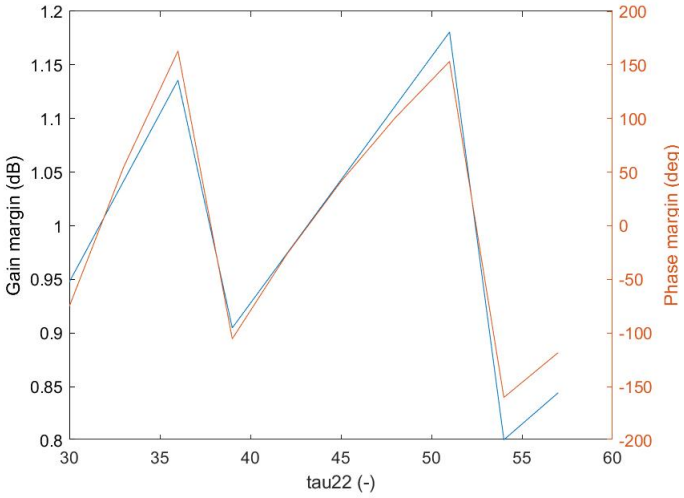

Figure B.47: Gain and phase margin g22 τ22

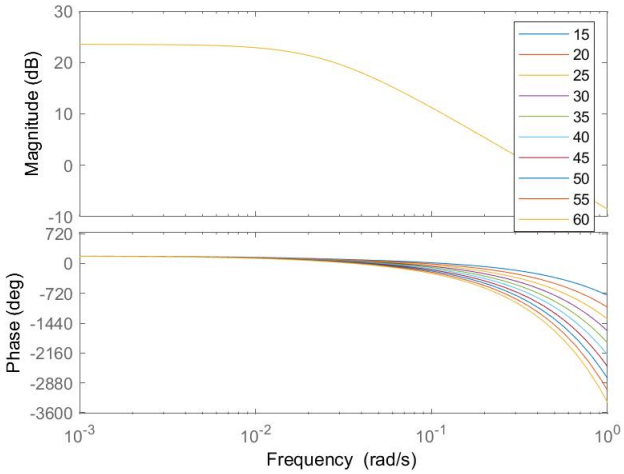

Figure B.48: Bode plot g22 T22

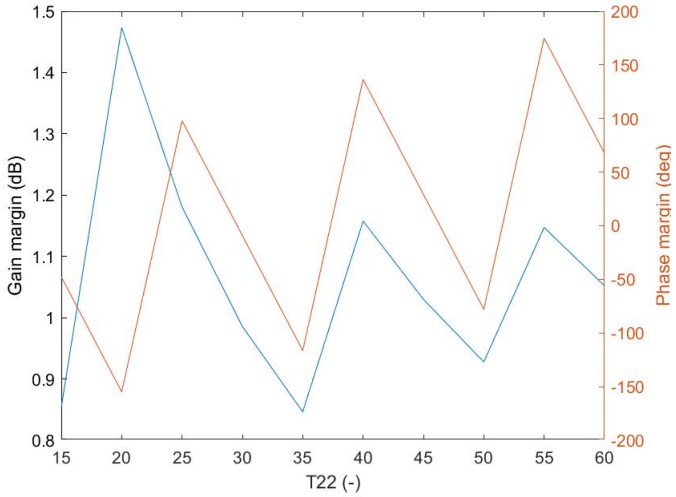

Figure B.49: Gain and phase margin g22 T22

B.1.3 Hill-curve variation

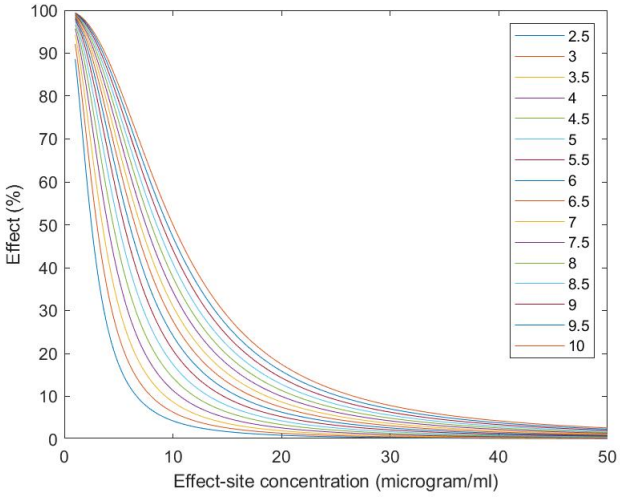

Figure B.50: Hill-curve C_{50} variation

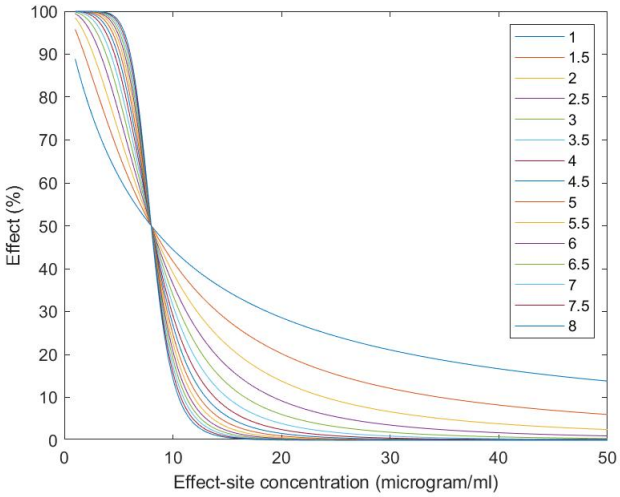

Figure B.51: Hill-curve γ variation

B.2 Chapter 4

B.2.1 Contour plots BIS-surface

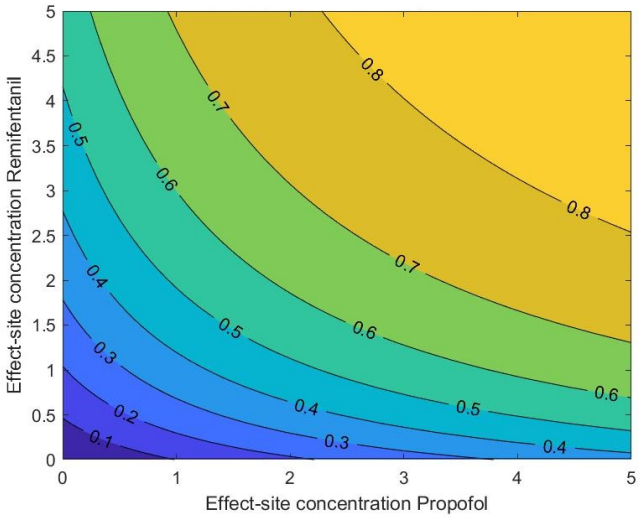

Figure B.52: Contour plot BIS-surface for $\gamma = 1$

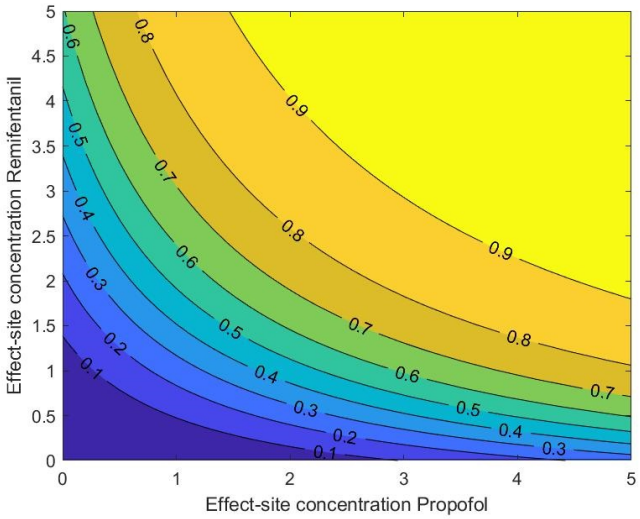

Figure B.53: Contour plot BIS-surface for $\gamma = 2$

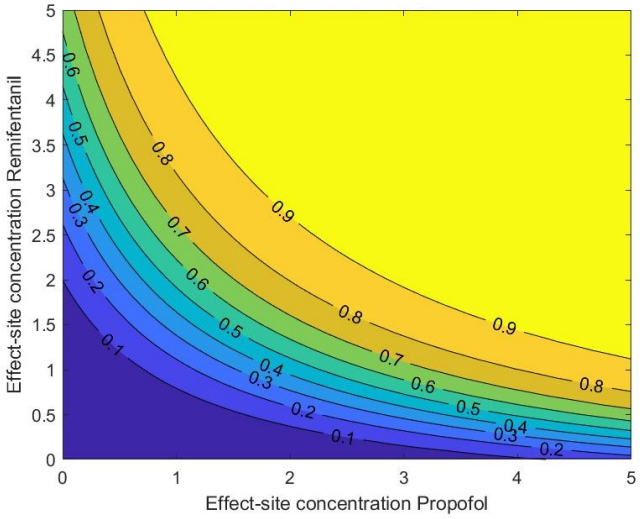

Figure B.54: Contour plot BIS-surface for $\gamma = 3$

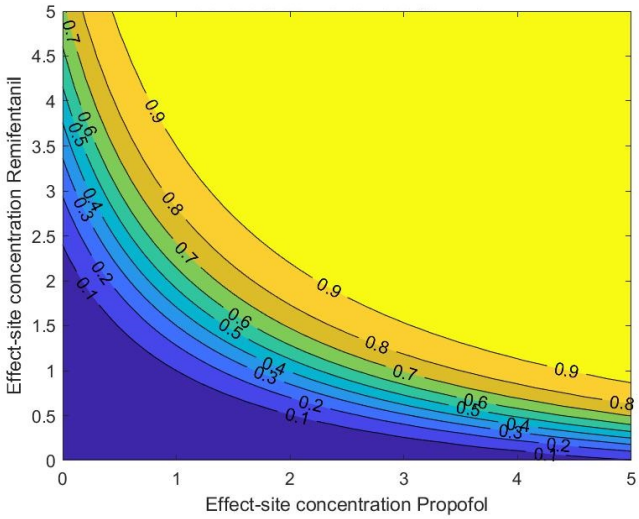

Figure B.55: Contour plot BIS-surface for $\gamma = 4$

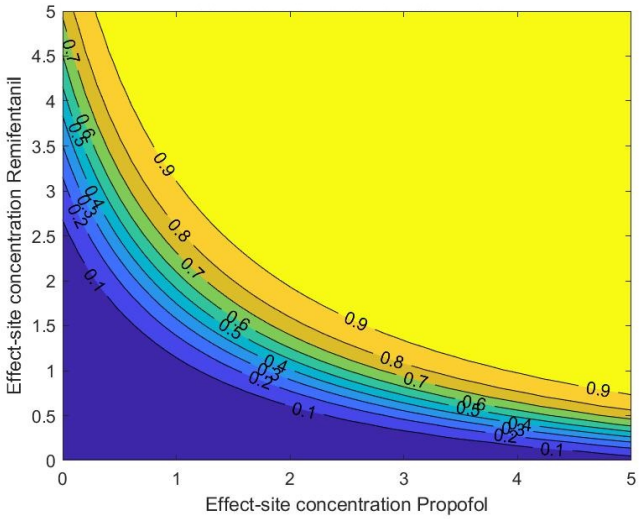

Figure B.56: Contour plot BIS-surface for $\gamma = 5$

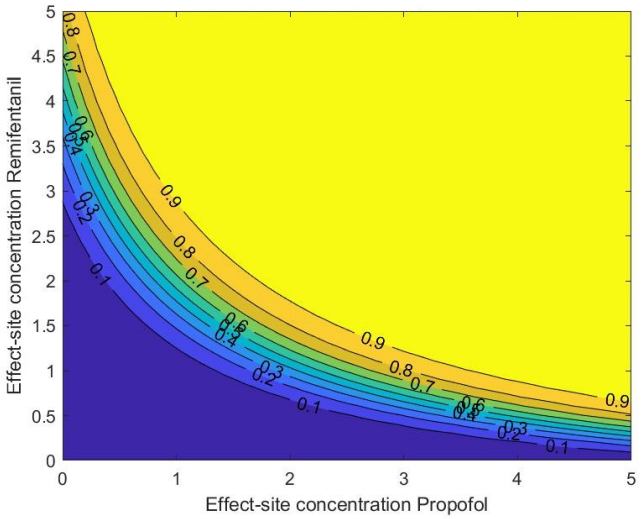

Figure B.57: Contour plot BIS-surface for $\gamma = 6$

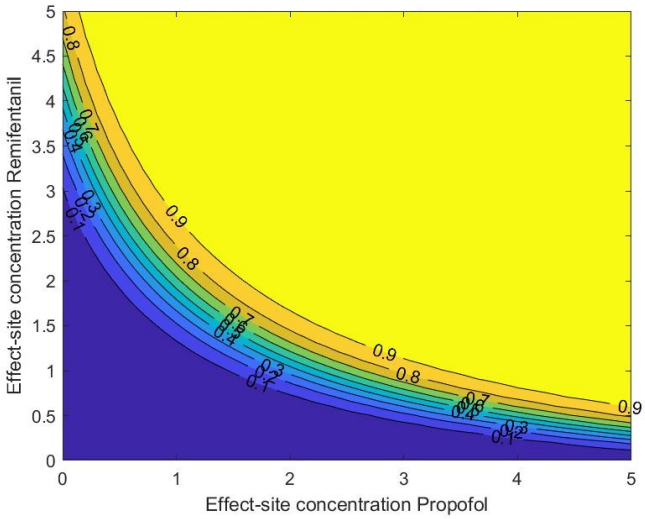

Figure B.58: Contour plot BIS-surface for $\gamma = 7$

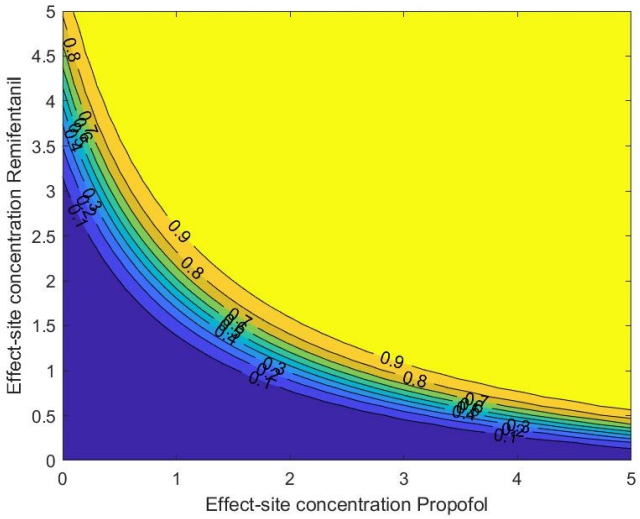

Figure B.59: Contour plot BIS-surface for $\gamma = 8$

B.3 Chapter 5

B.3.1 Selection of prediction horizon

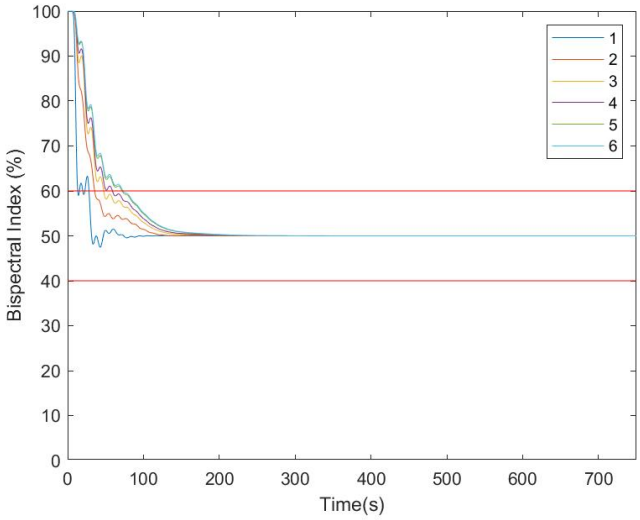

Figure B.60: BIS output for Tp $\in$[10,50,100,150,350,500]

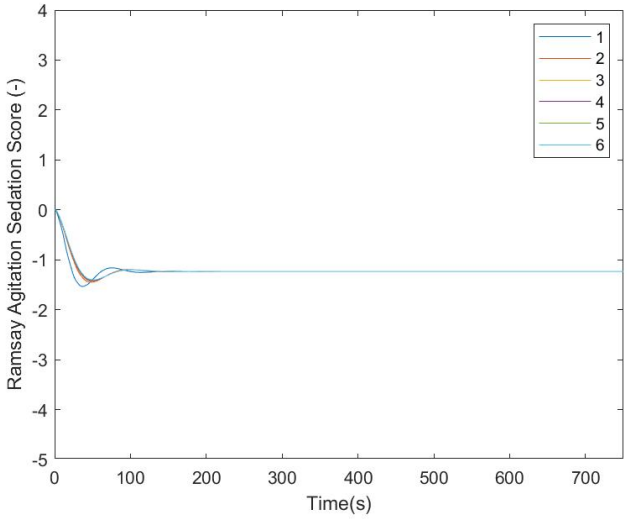

Figure B.61: RASS output for Tp $\in$[10,50,100,150,350,500]

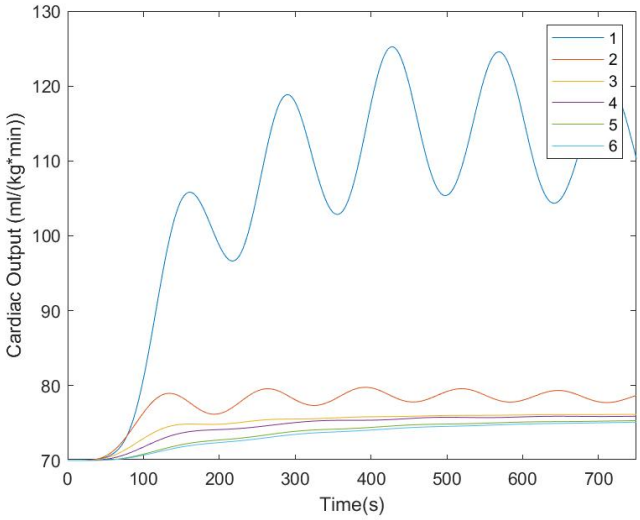

Figure B.62: CO output for Tp $\in$[10,50,100,150,350,500]

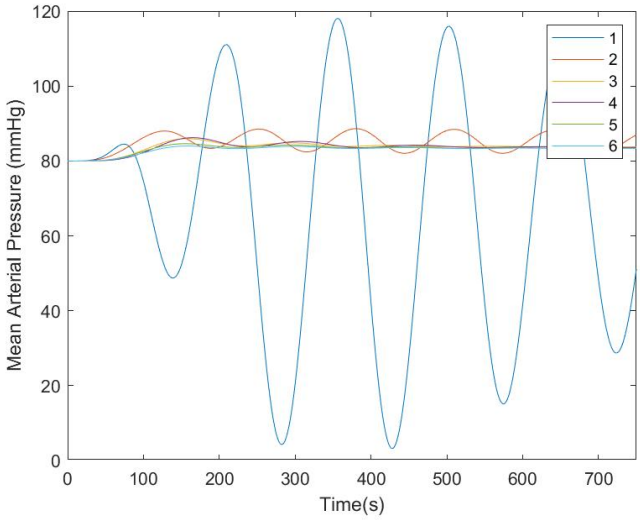

Figure B.63: MAP output for Tp $\in$[10,50,100,150,350,500]

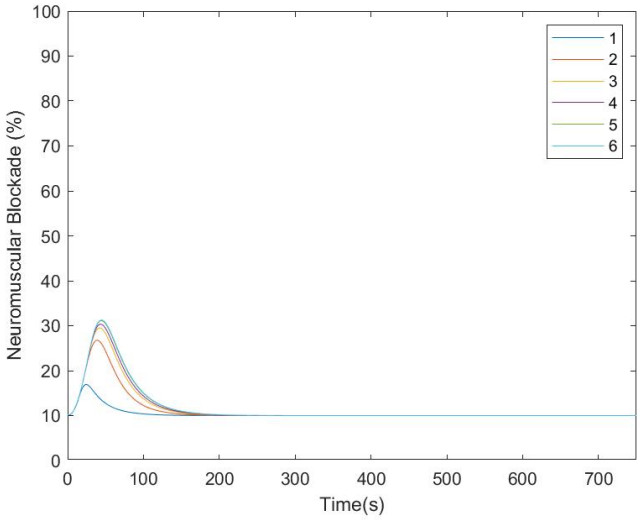

Figure B.64: NMB output for Tp $\in$[10,50,100,150,350,500]

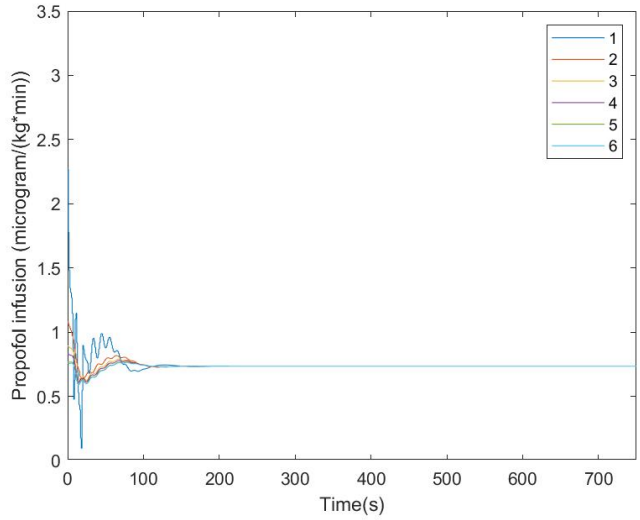

Figure B.65: Propofol input for Tp $\in$[10,50,100,150,350,500]

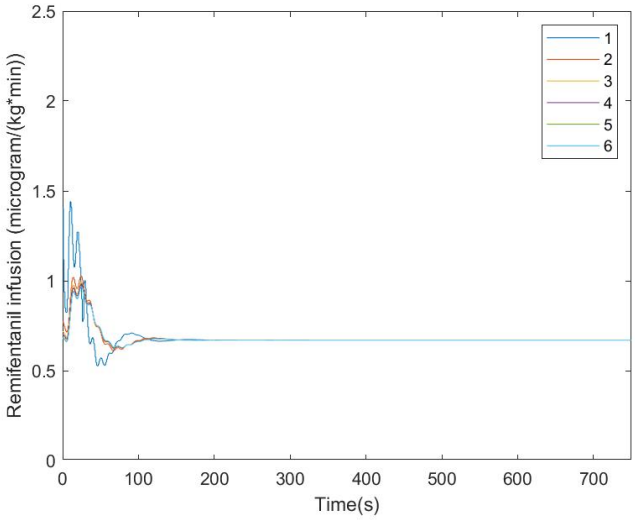

Figure B.66: Remifentanil input for Tp $\in$[10,50,100,150,350,500]

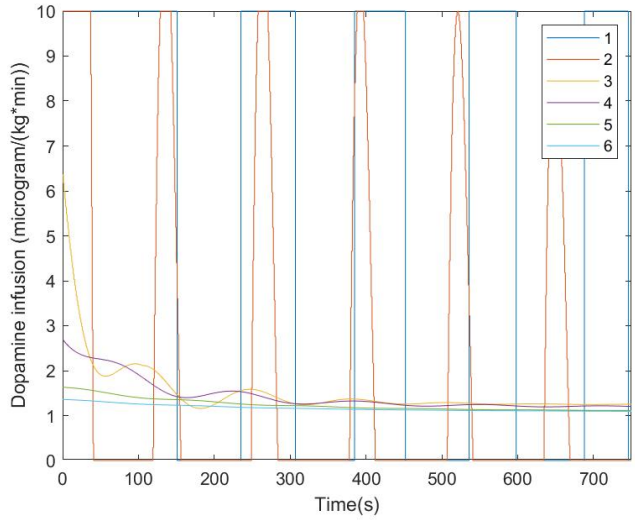

Figure B.67: Dopamine input for Tp $\in$[10,50,100,150,350,500]

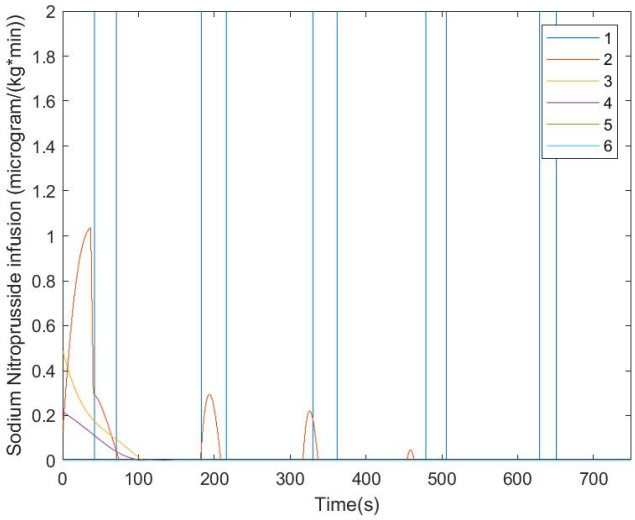

Figure B.68: Sodium Nitroprusside input for Tp $\in$[10,50,100,150,350,500]

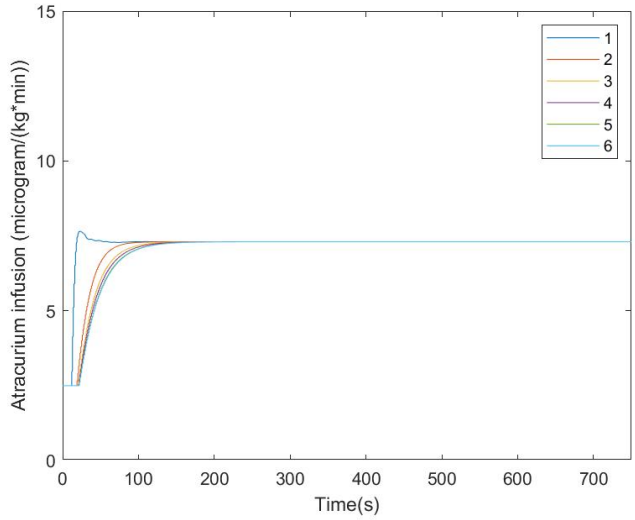

Figure B.69: Atracurium input for Tp $\in$[10,50,100,150,350,500]

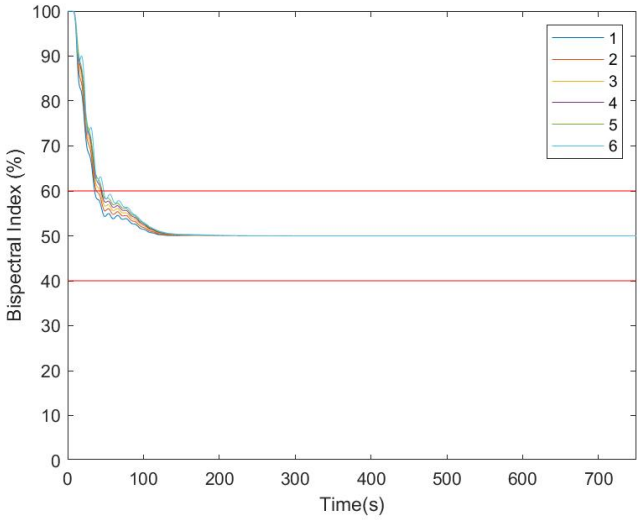

Figure B.70: BIS output for Tp $\in$[50,60,70,80,90,100]

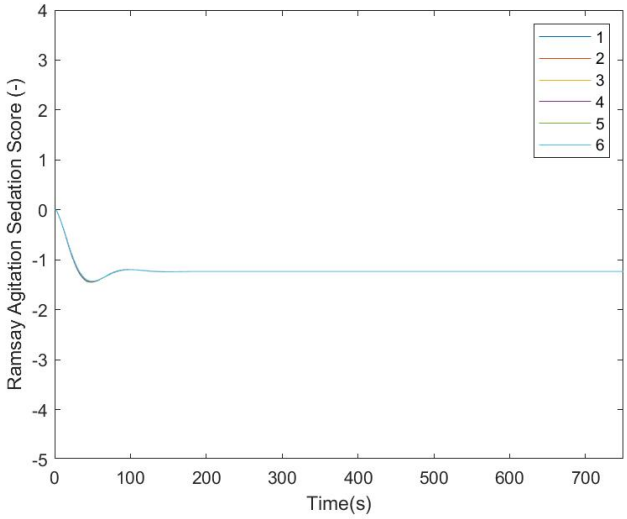

Figure B.71: RASS output for Tp $\in$[50,60,70,80,90,100]

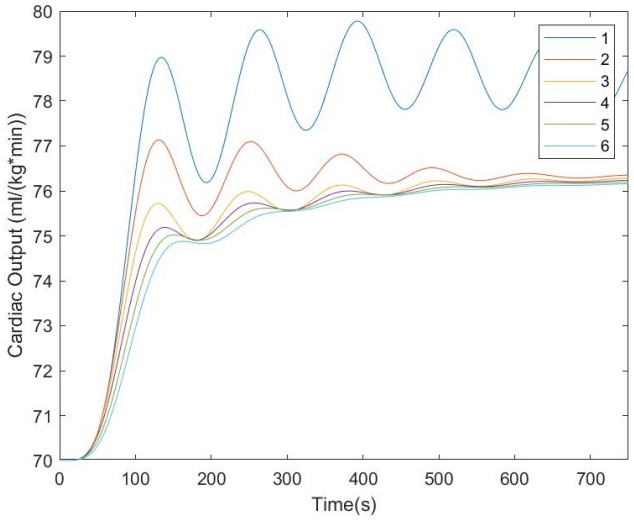

Figure B.72: CO output for Tp $\in$[50,60,70,80,90,100]

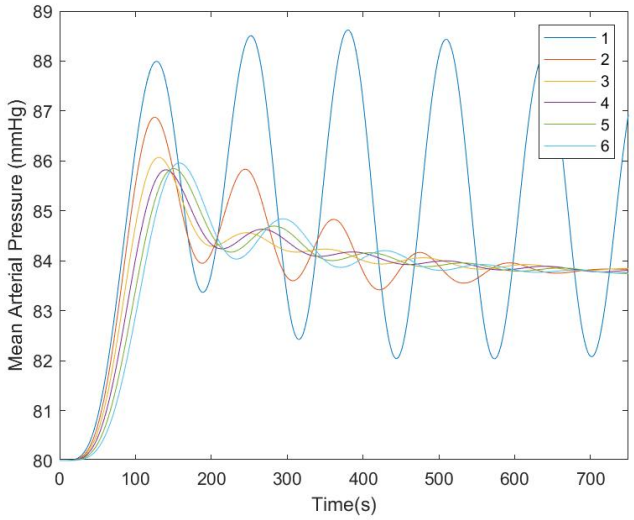

Figure B.73: MAP output for Tp $\in$[50,60,70,80,90,100]

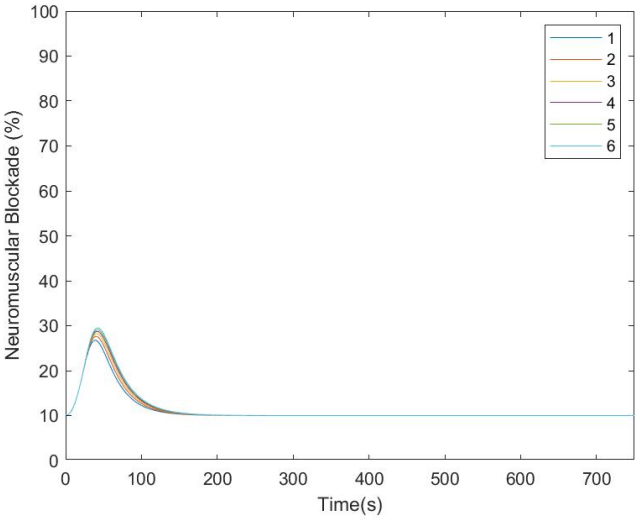

Figure B.74: NMB output for Tp $\in$[50,60,70,80,90,100]

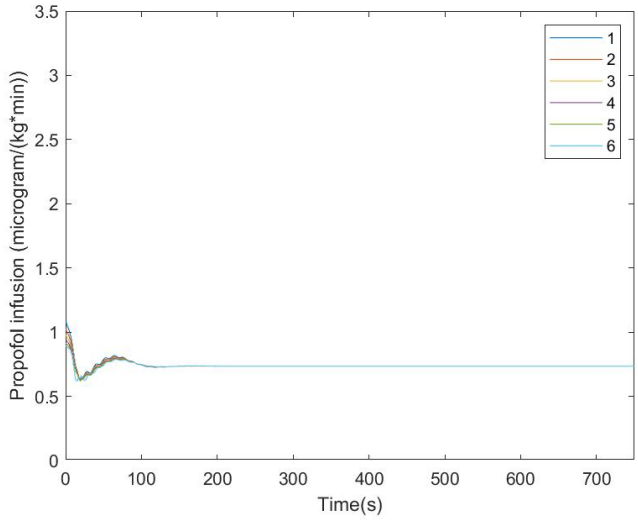

Figure B.75: Propofol input for Tp $\in$[50,60,70,80,90,100]

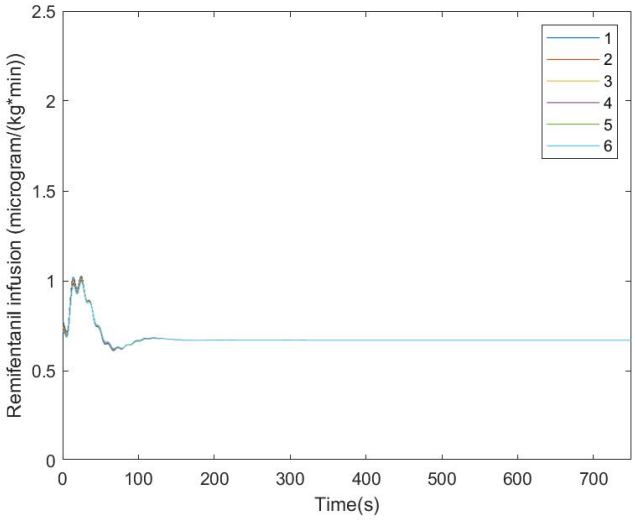

Figure B.76: Remifentanil input for Tp $\in$[50,60,70,80,90,100]

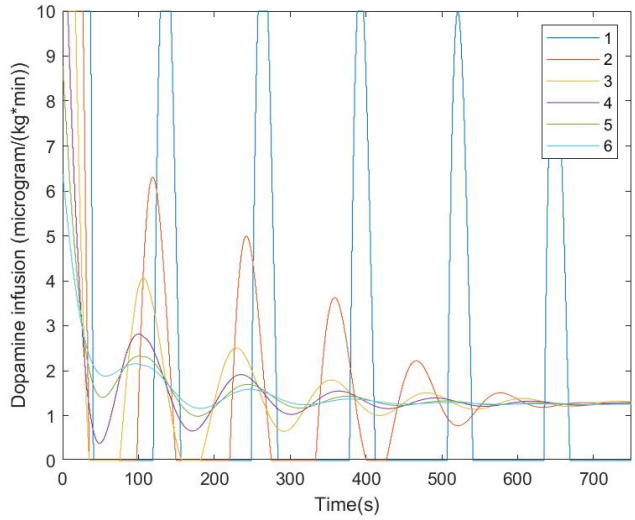

Figure B.77: Dopamine input for Tp $\in$[50,60,70,80,90,100]

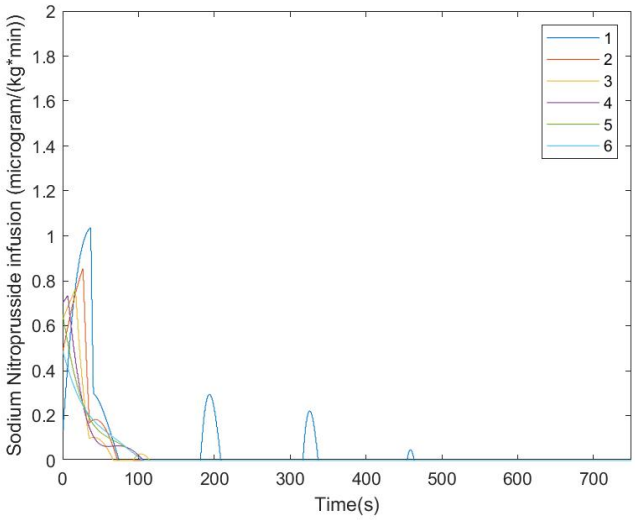

Figure B.78: Sodium Nitroprusside input for Tp $\in$[50,60,70,80,90,100]

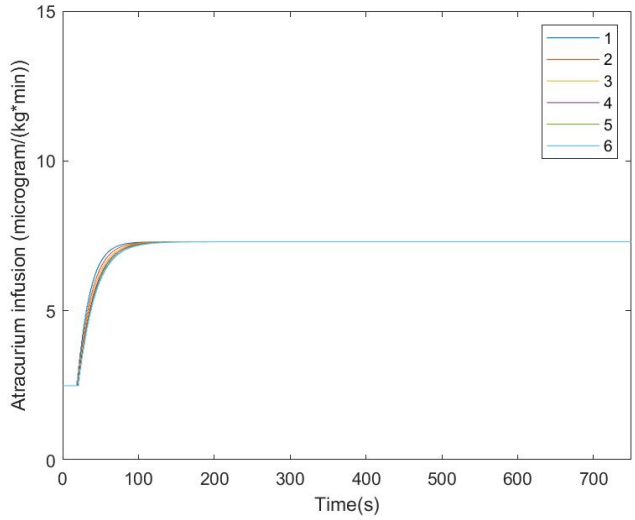

Figure B.79: Atracurium input for Tp $\in$[50,60,70,80,90,100]

B.3.2 Effect delay BIS-measurement

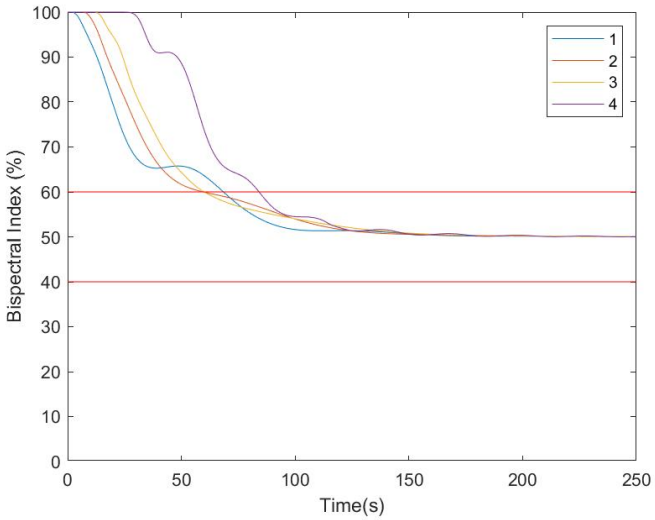

Figure B.80: BIS output for a delay on the measurement of BIS of 0,5,10,25 seconds

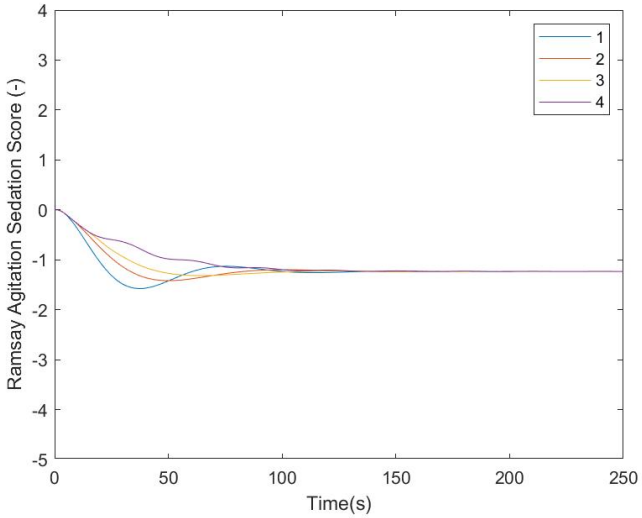

Figure B.81: RASS output for a delay on the measurement of BIS of 0,5,10,25 seconds

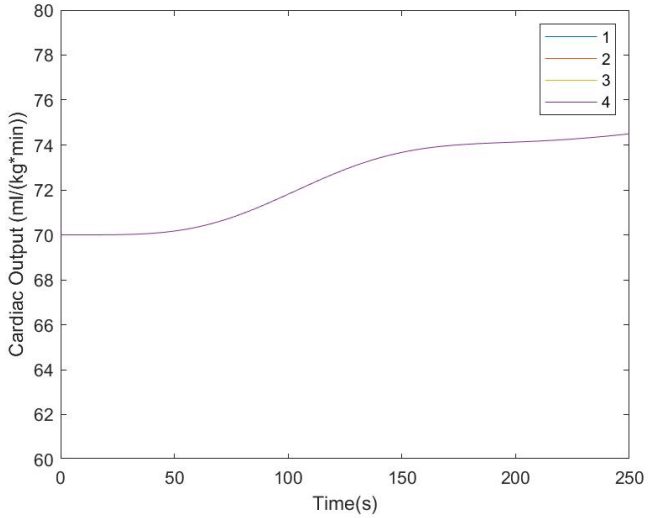

Figure B.82: CO output for a delay on the measurement of BIS of 0,5,10,25 seconds

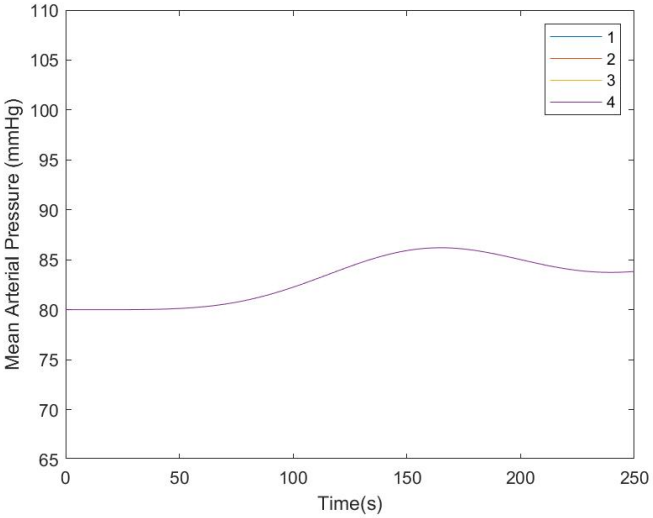

Figure B.83: MAP output for a delay on the measurement of BIS of 0,5,10,25 seconds

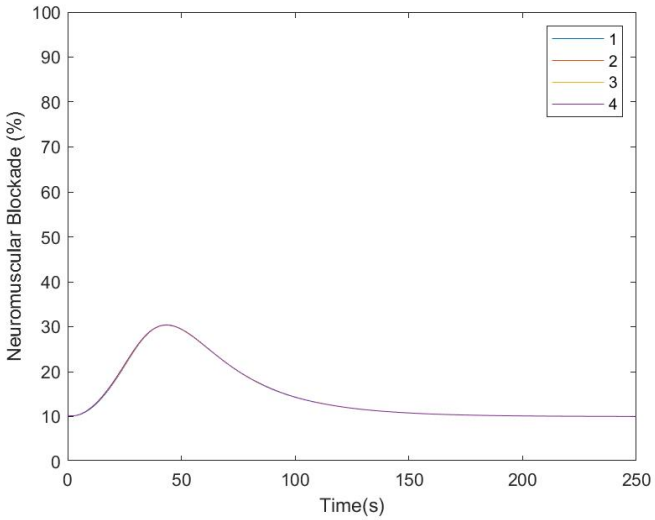

Figure B.84: NMB output for a delay on the measurement of BIS of 0,5,10,25 seconds

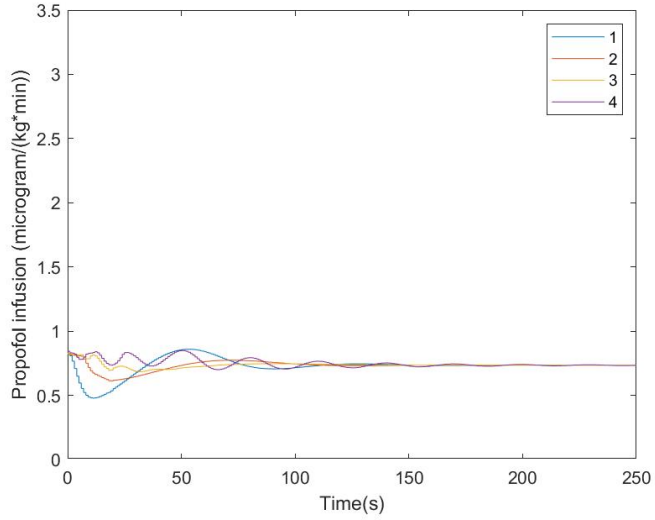

Figure B.85: Propofol input for a delay on the measurement of BIS of 0,5,10,25 seconds

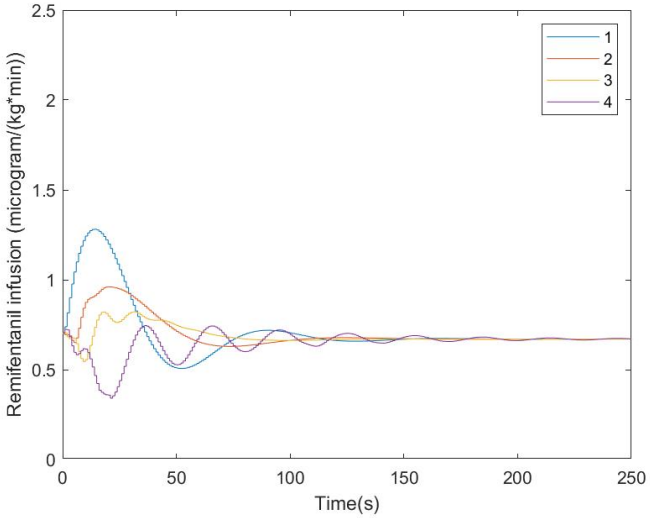

Figure B.86: Remifentanil input for a delay on the measurement of BIS of 0,5,10,25 seconds

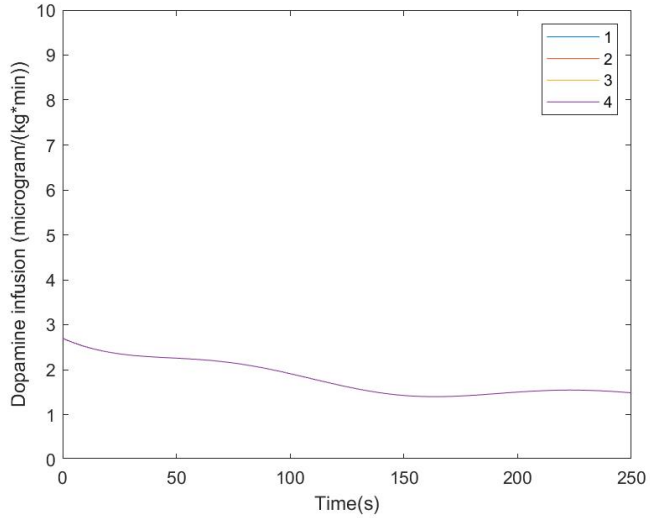

Figure B.87: Dopamine input for a delay on the measurement of BIS of 0,5,10,25 seconds

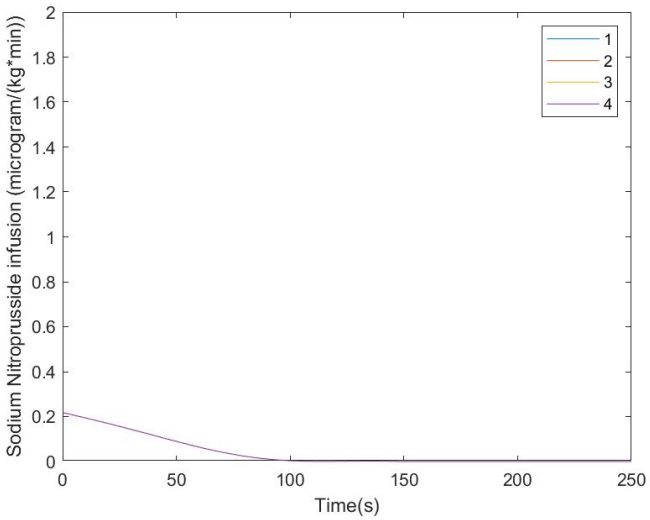

Figure B.88: Sodium Nitroprusside input for a delay on the measurement of BIS of 0,5,10,25 seconds

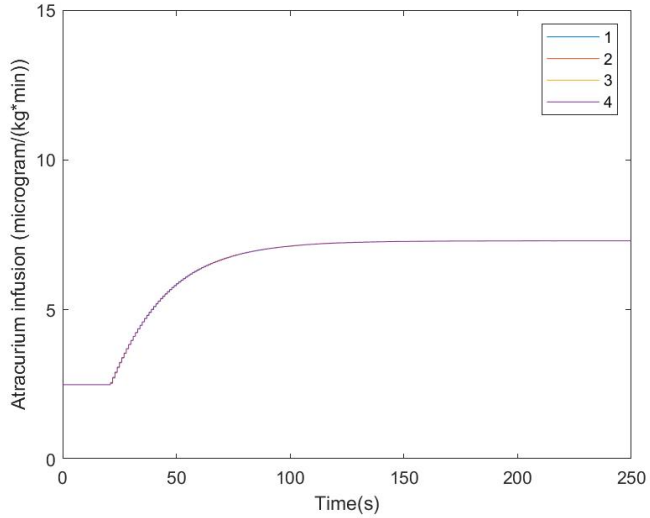

Figure B.89: Atracurium input for a delay on the measurement of BIS of 0,5,10,25 seconds

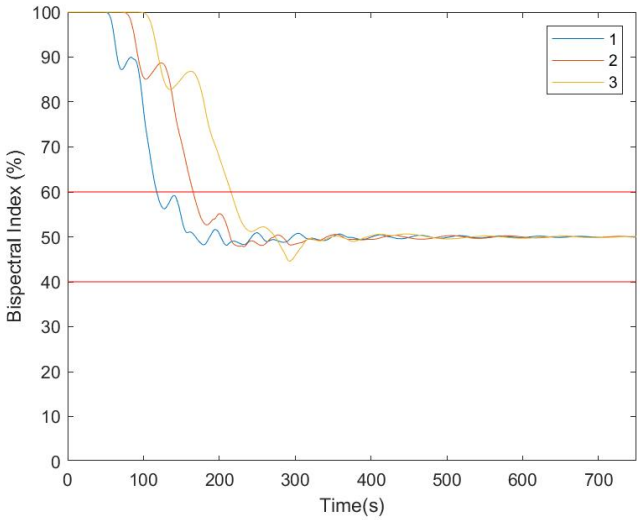

Figure B.90: BIS output for a delay on the measurement of BIS of 50,75,100 seconds

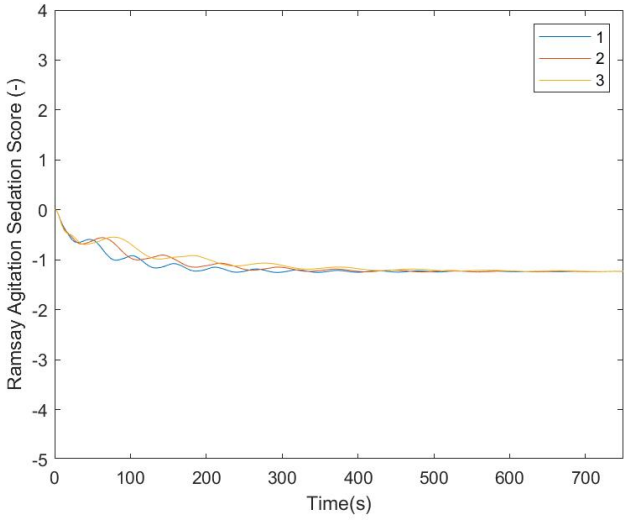

Figure B.91: RASS output for a delay on the measurement of BIS of 50,75,100 seconds

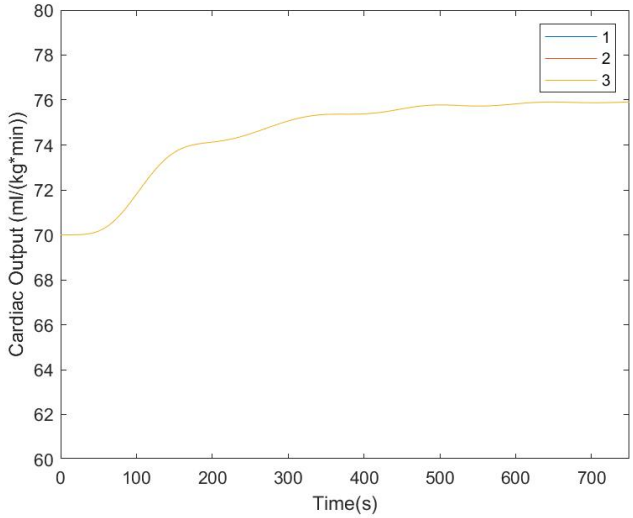

Figure B.92: CO output for a delay on the measurement of BIS of 50,75,100 seconds

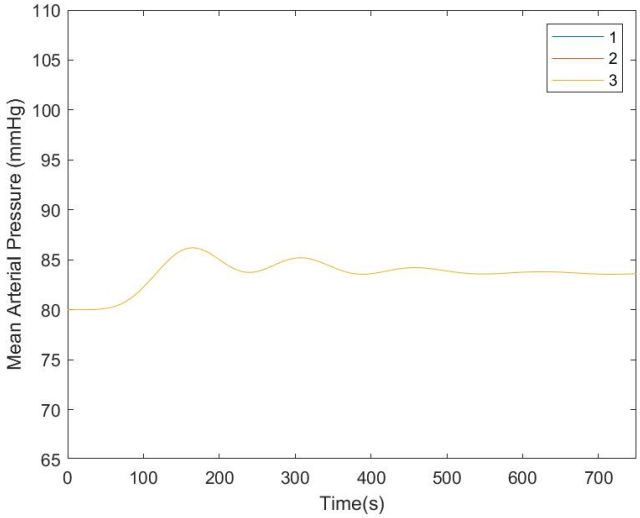

Figure B.93: MAP output for a delay on the measurement of BIS of 50,75,100 seconds

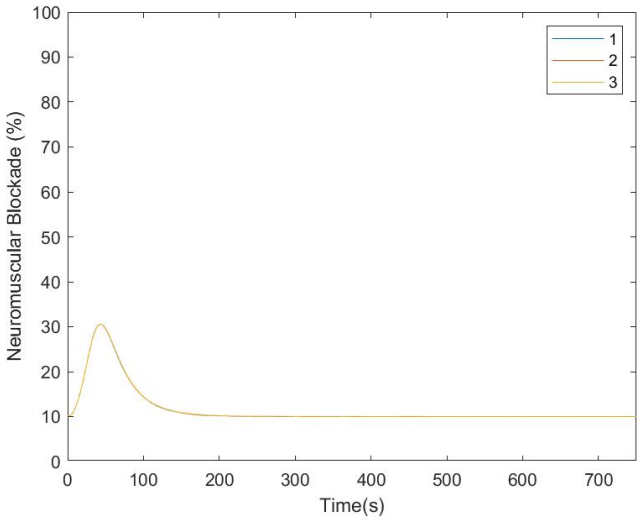

Figure B.94: NMB output for a delay on the measurement of BIS of 50,75,100 seconds

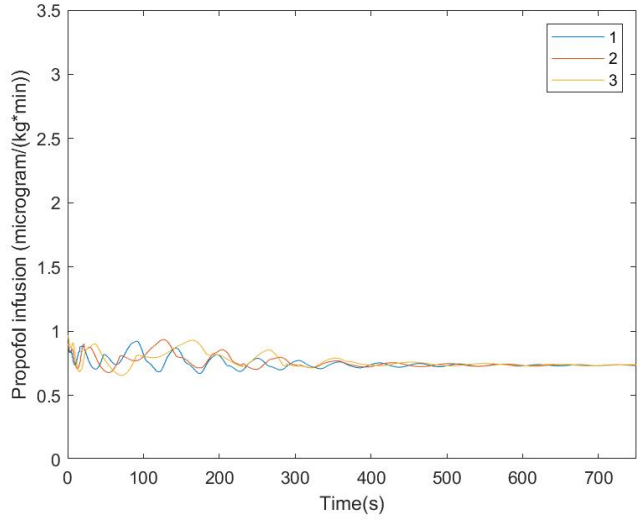

Figure B.95: Propofol input for a delay on the measurement of BIS of 50,75,100 seconds

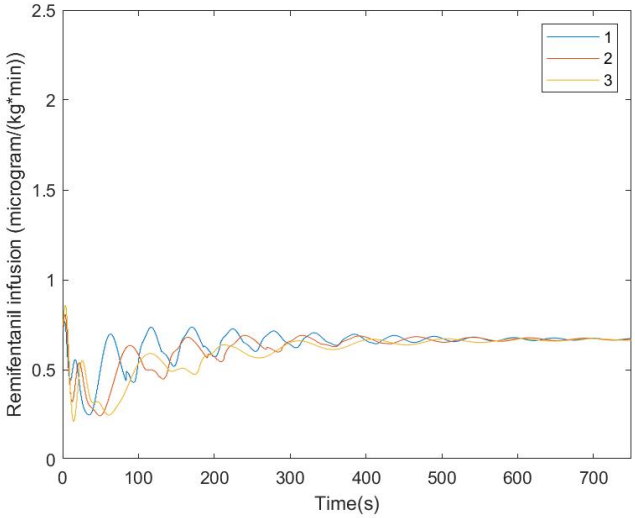

Figure B.96: Remifentanil input for a delay on the measurement of BIS of 50,75,100 seconds

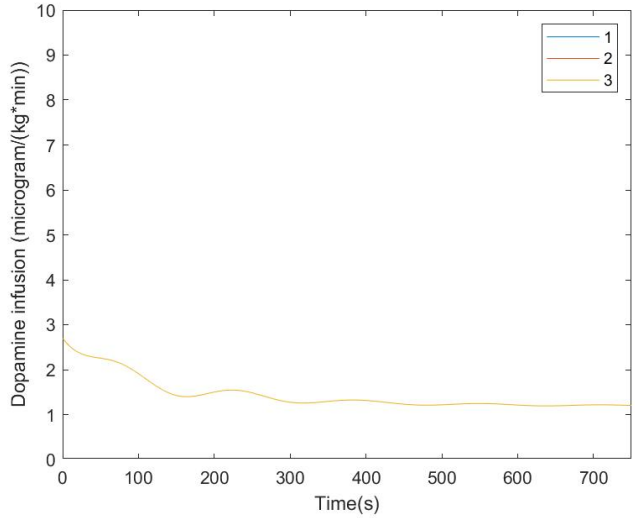

Figure B.97: Dopamine input for a delay on the measurement of BIS of 50,75,100 seconds

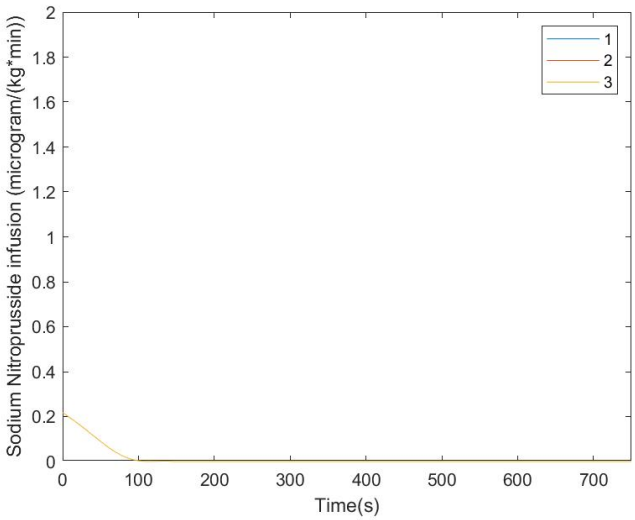

Figure B.98: Sodium Nitroprusside input for a delay on the measurement of BIS of 50,75,100 seconds

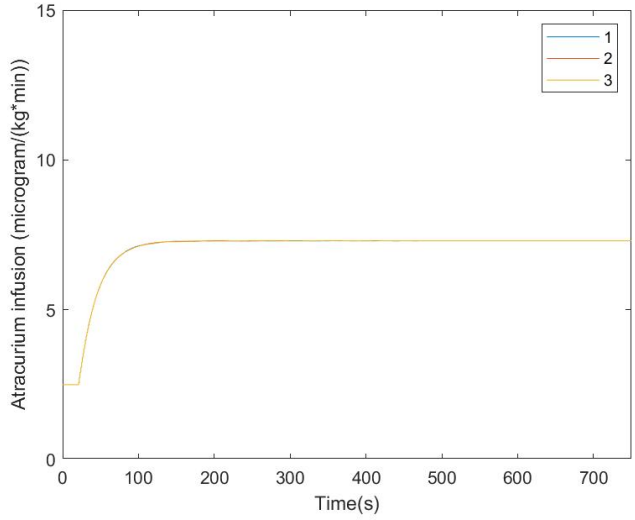

Figure B.99: Atracurium input for a delay on the measurement of BIS of 50,75,100 seconds

B.3.3 Undisturbed nominal model

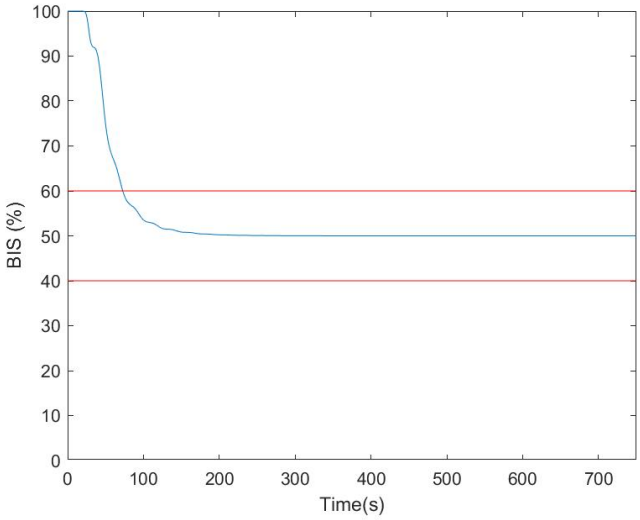

Figure B.100: BIS output for undisturbed nominal model

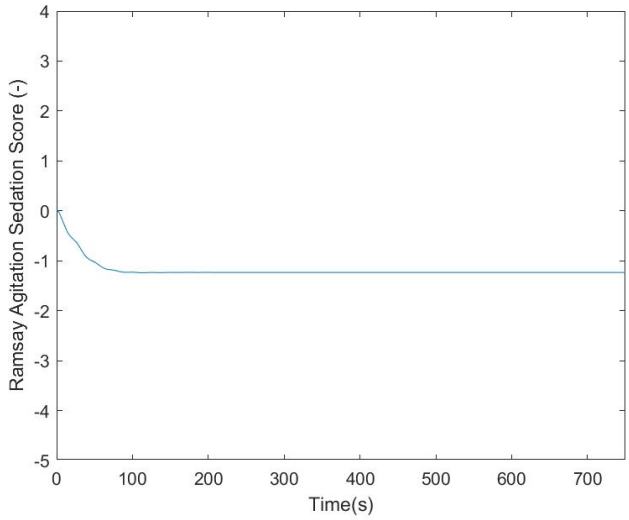

Figure B.101: RASS output for undisturbed nominal model

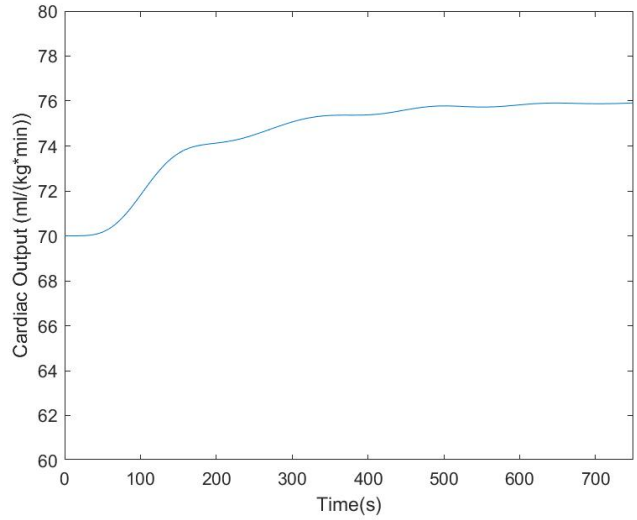

Figure B.102: CO output for undisturbed nominal model

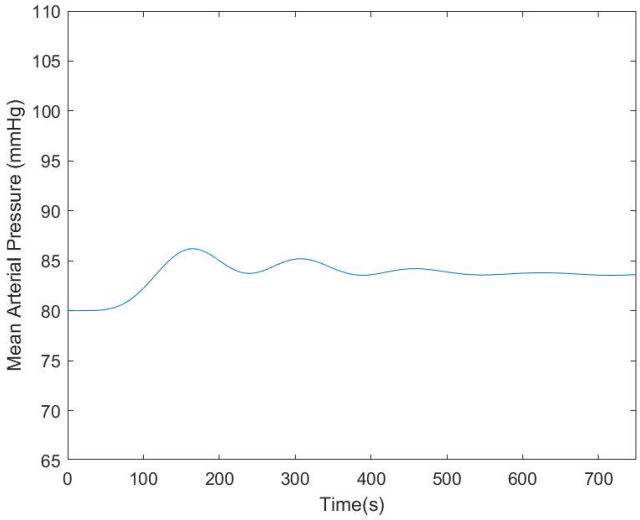

Figure B.103: MAP output for undisturbed nominal model

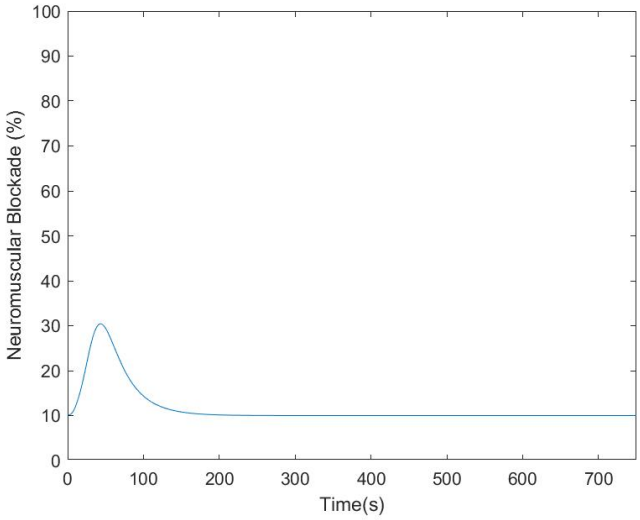

Figure B.104: NMB output for undisturbed nominal model

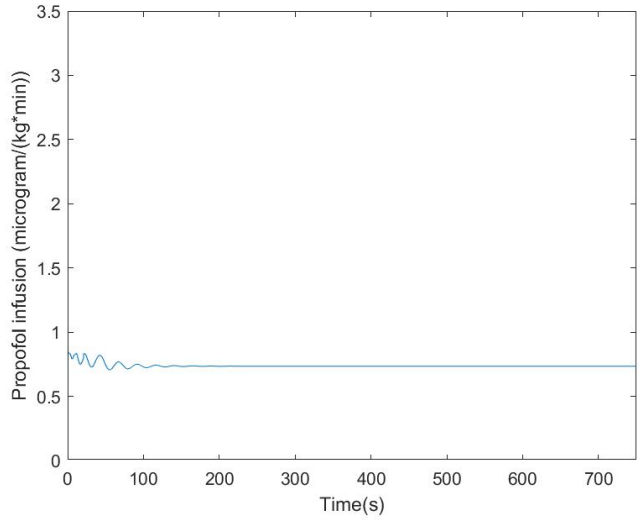

Figure B.105: Propofol input for undisturbed nominal model

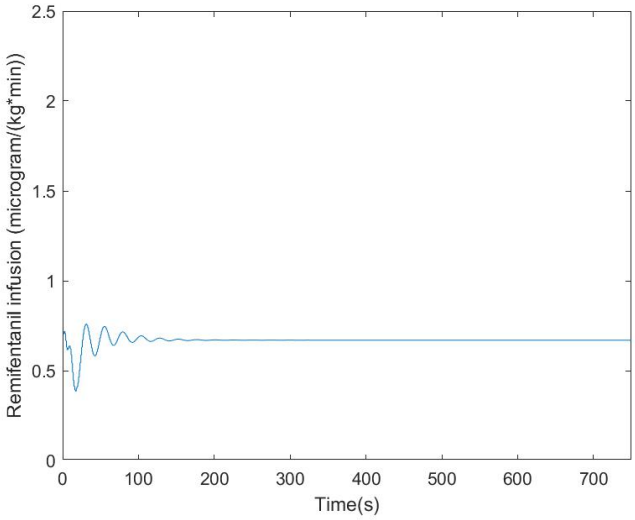

Figure B.106: Remifentanil input for undisturbed nominal model

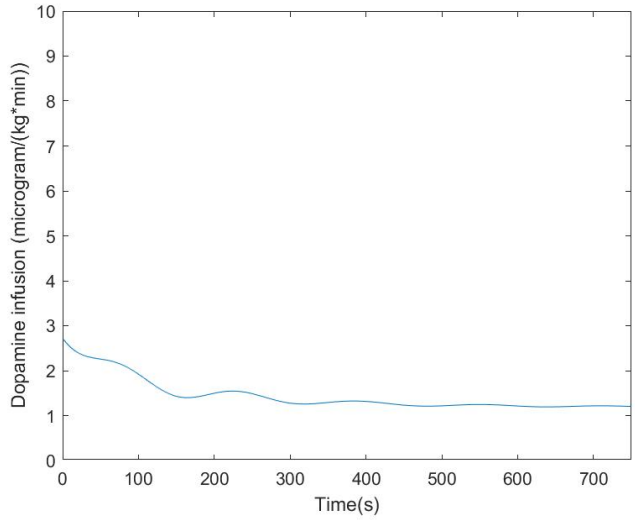

Figure B.107: Dopamine input for undisturbed nominal model

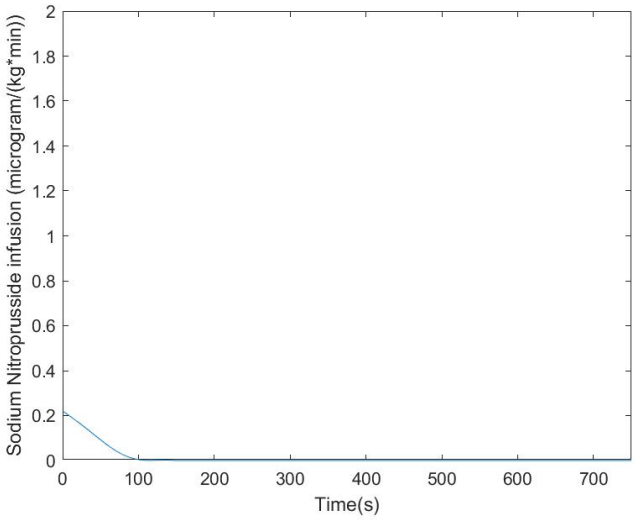

Figure B.108: Sodium Nitroprusside input for undisturbed nominal model

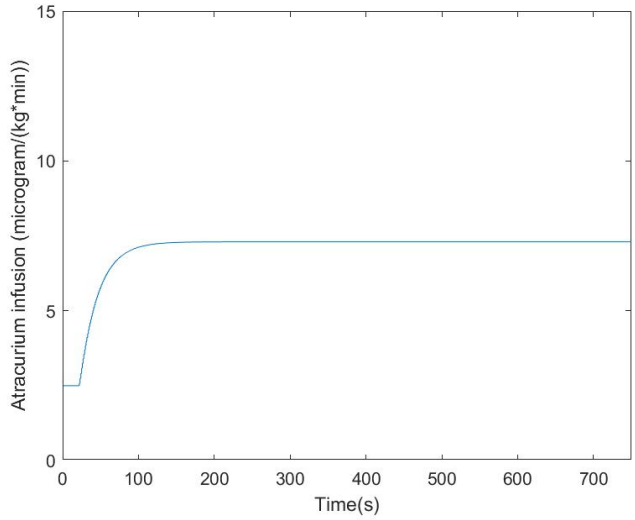

Figure B.109: Atracurium input for undisturbed nominal model

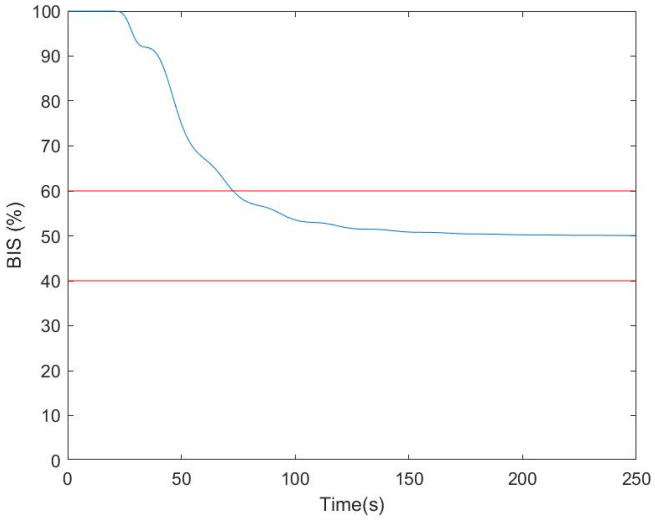

Figure B.110: BIS output for undisturbed nominal model - zoom

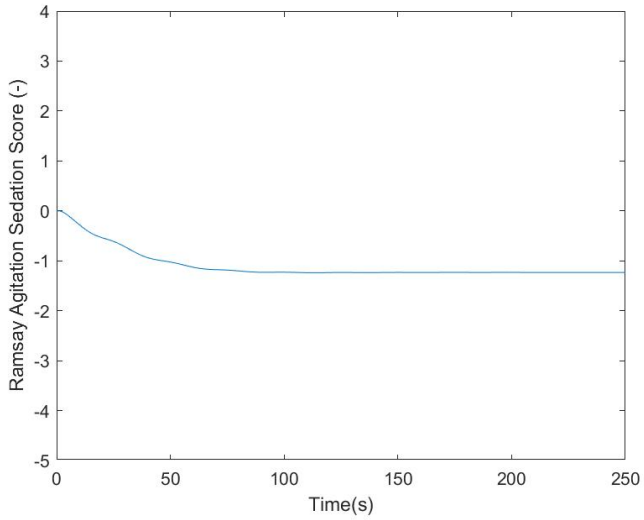

Figure B.111: RASS output for undisturbed nominal model - zoom

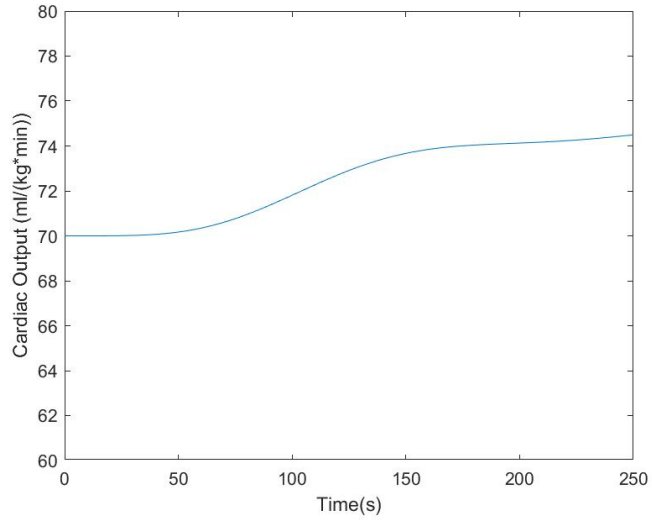

Figure B.112: CO output for undisturbed nominal model - zoom

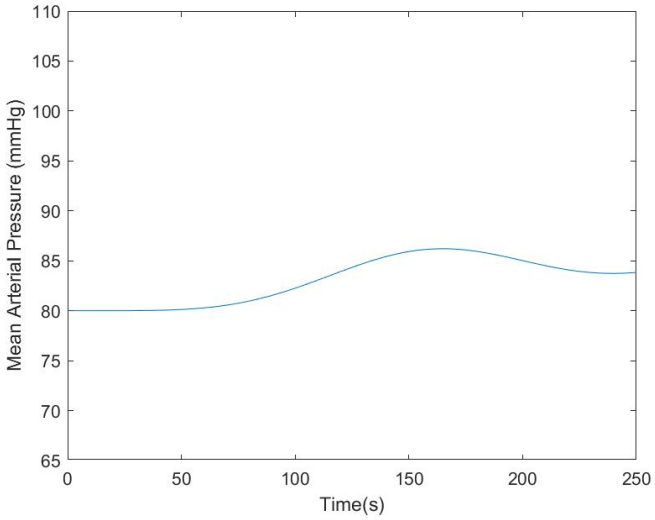

Figure B.113: MAP output for undisturbed nominal model - zoom

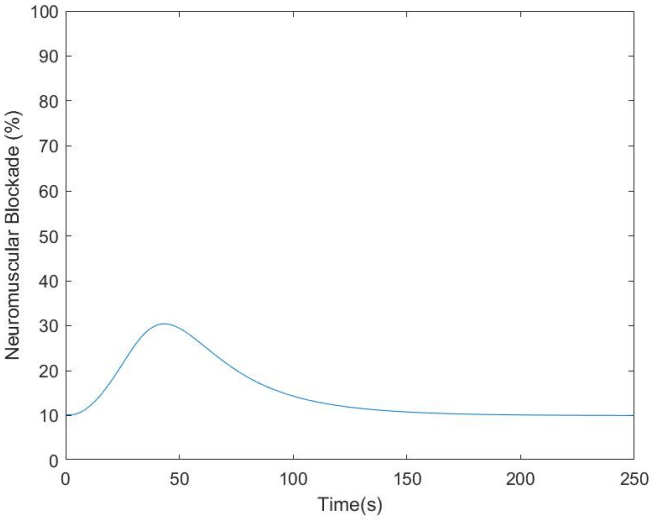

Figure B.114: NMB output for undisturbed nominal model - zoom

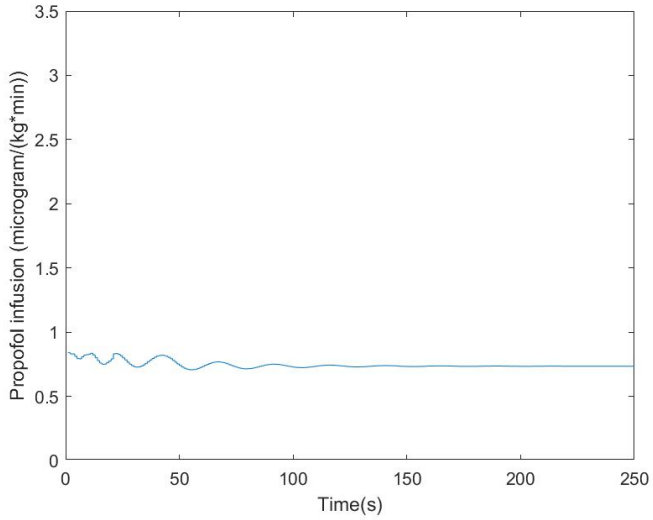

Figure B.115: Propofol input for undisturbed nominal model - zoom

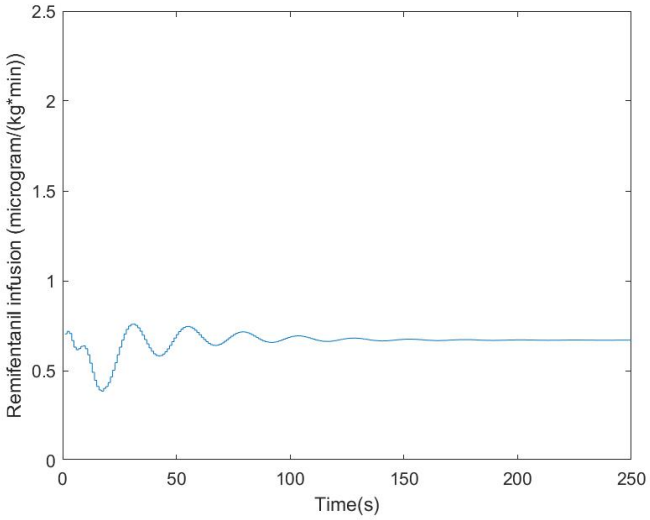

Figure B.116: Remifentanil input for undisturbed nominal model - zoom

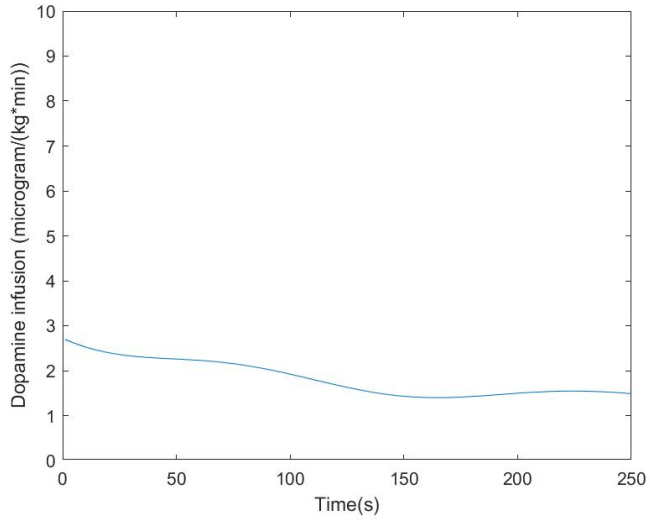

Figure B.117: Dopamine input for undisturbed nominal model - zoom

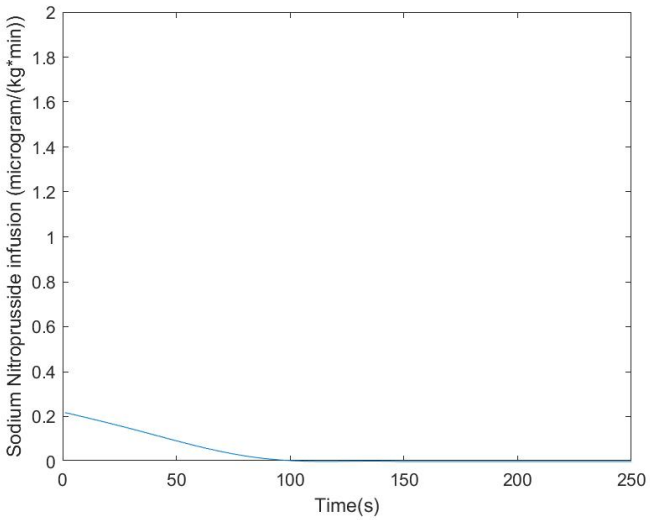

Figure B.118: Sodium Nitroprusside input for undisturbed nominal model - zoom

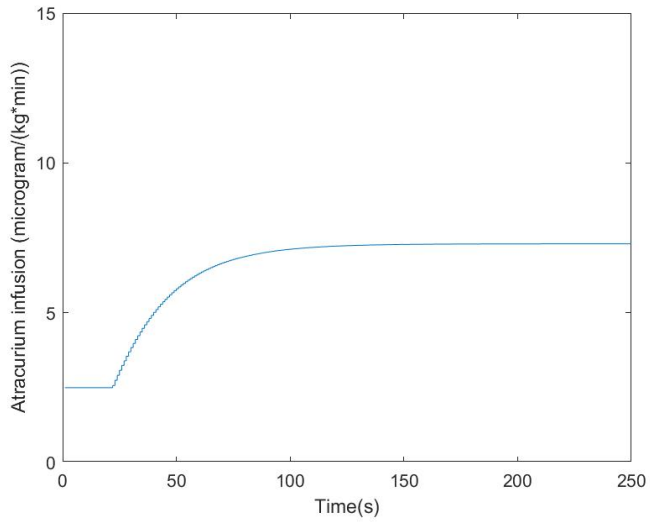

Figure B.119: Atracurium input for undisturbed nominal model - zoom

B.3.4 Disturbed nominal model

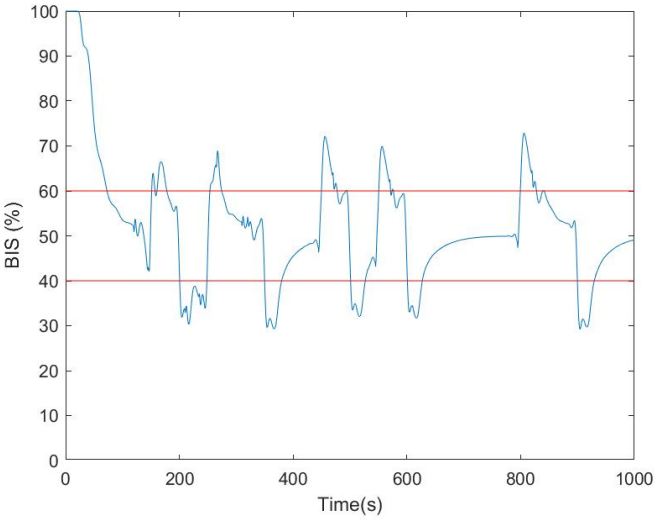

Figure B.120: BIS output for disturbed nominal model

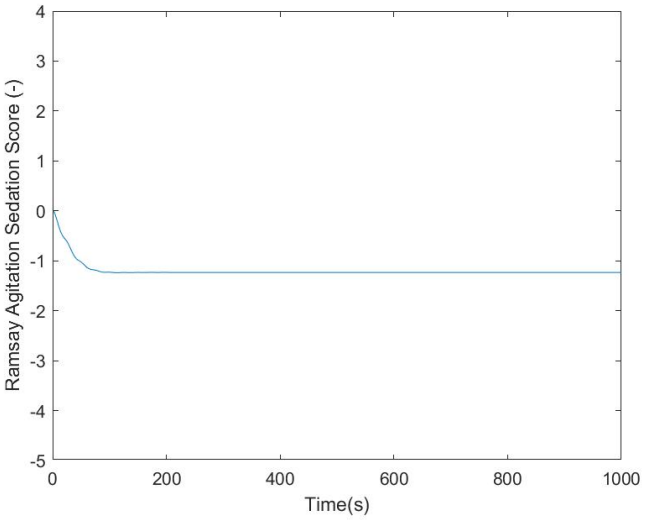

Figure B.121: RASS output for disturbed nominal model

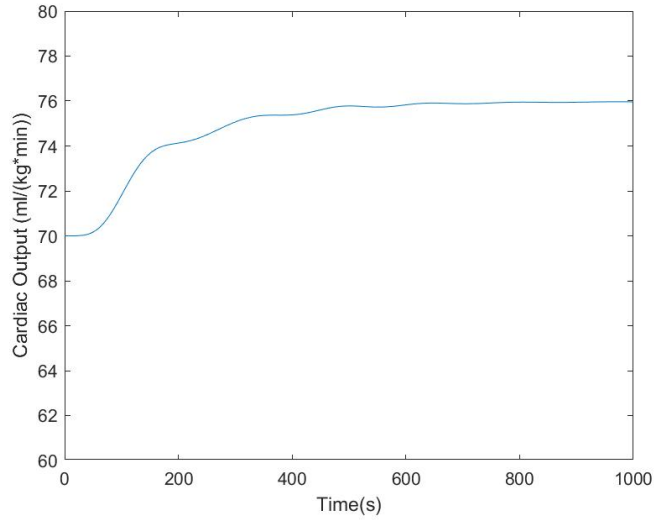

Figure B.122: CO output for disturbed nominal model

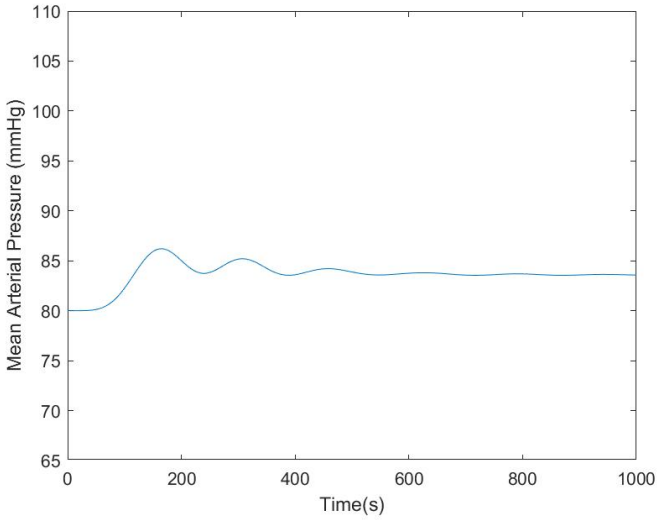

Figure B.123: MAP output for disturbed nominal model

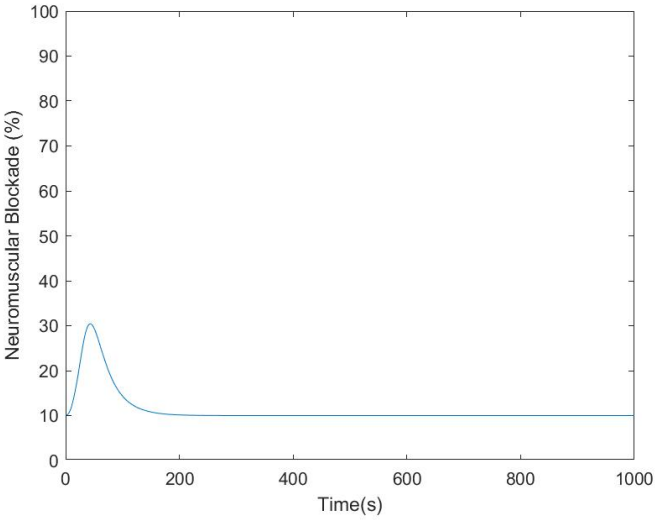

Figure B.124: NMB output for disturbed nominal model

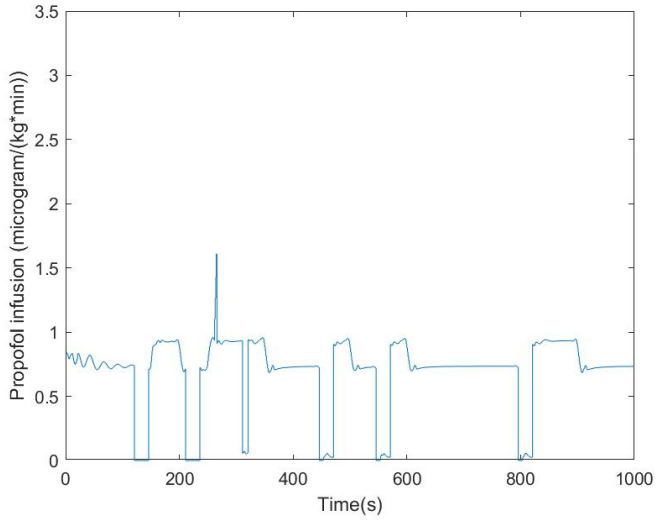

Figure B.125: Propofol input for disturbed nominal model

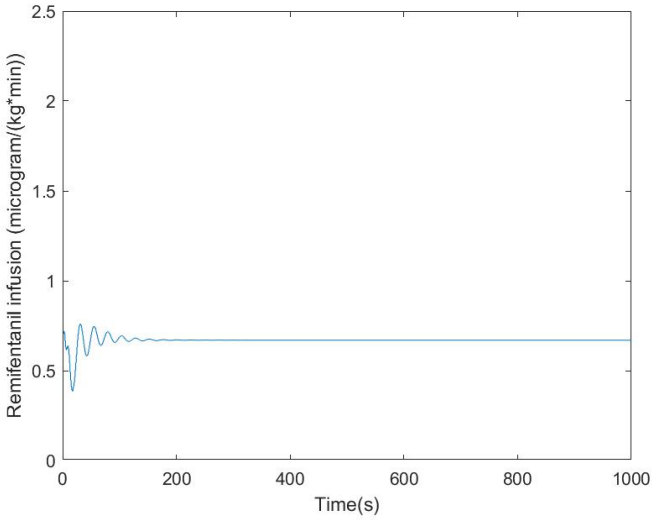

Figure B.126: Remifentanil input for disturbed nominal model

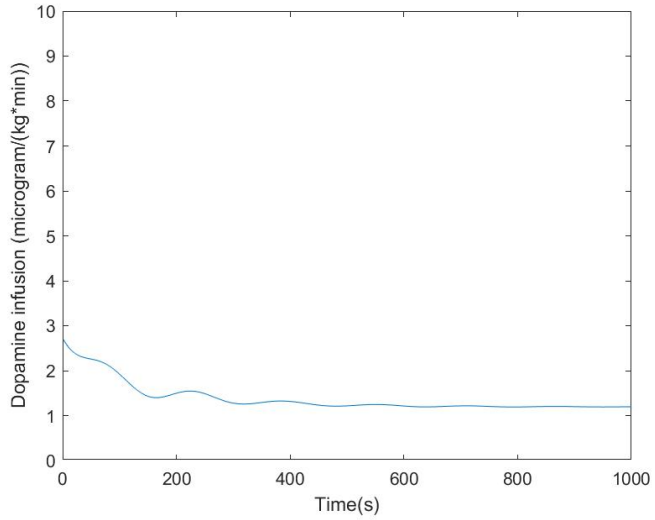

Figure B.127: Dopamine input for disturbed nominal model

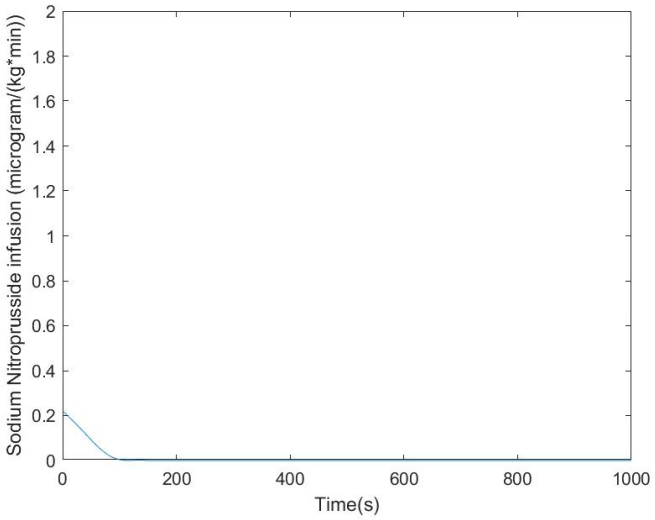

Figure B.128: Sodium Nitroprusside input for disturbed nominal model

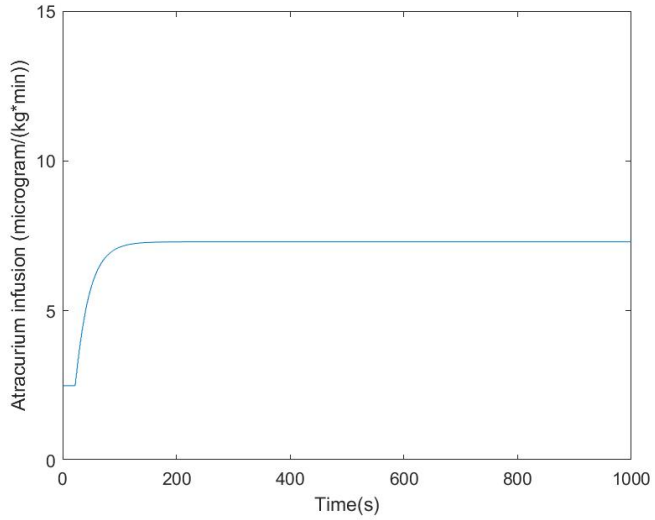

Figure B.129: Atracurium input for disturbed nominal model

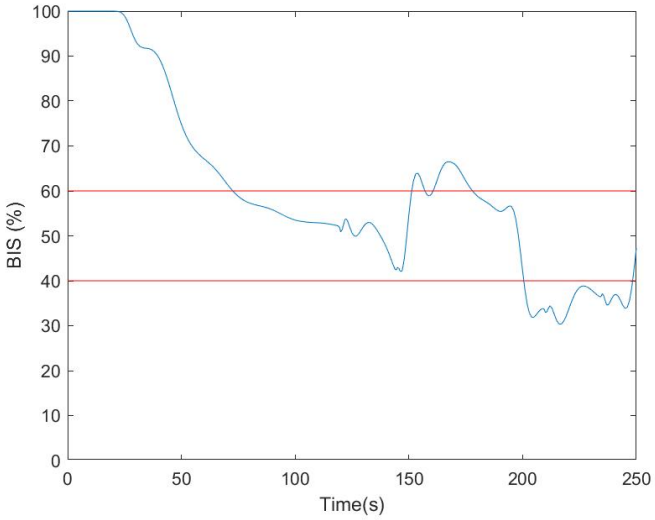

Figure B.130: BIS output for disturbed nominal model - zoom

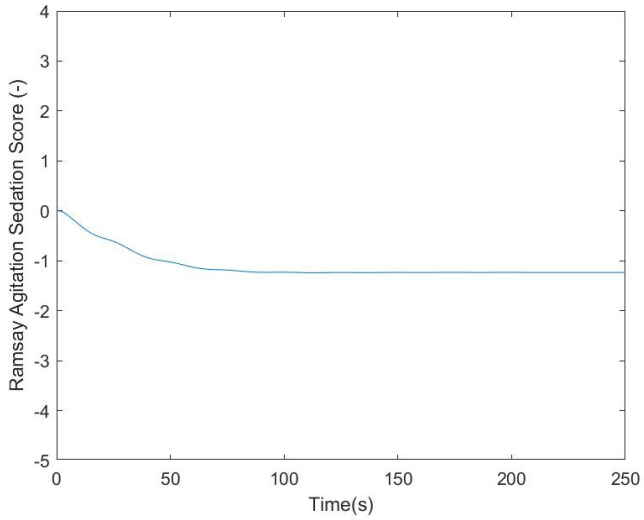

Figure B.131: RASS output for disturbed nominal model - zoom

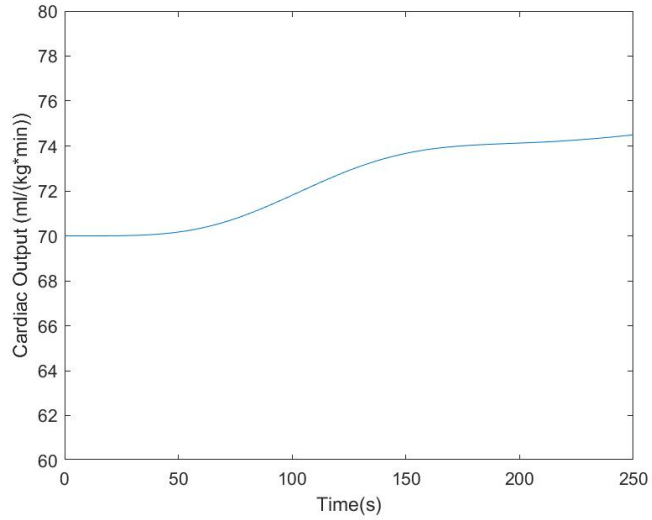

Figure B.132: CO output for disturbed nominal model - zoom

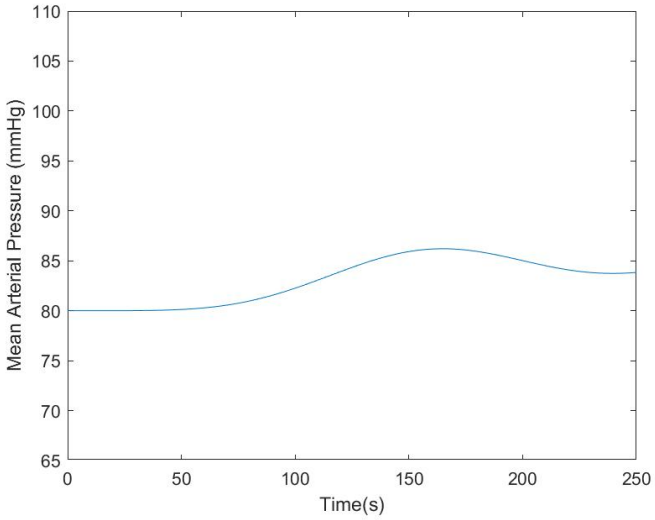

Figure B.133: MAP output for disturbed nominal model - zoom

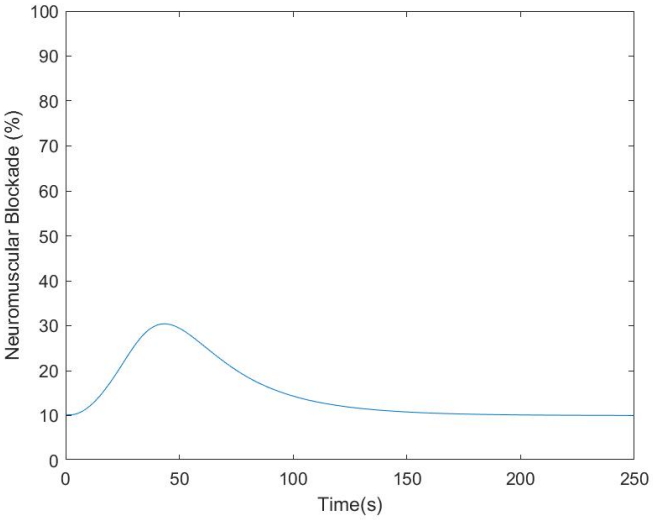

Figure B.134: NMB output for disturbed nominal model - zoom

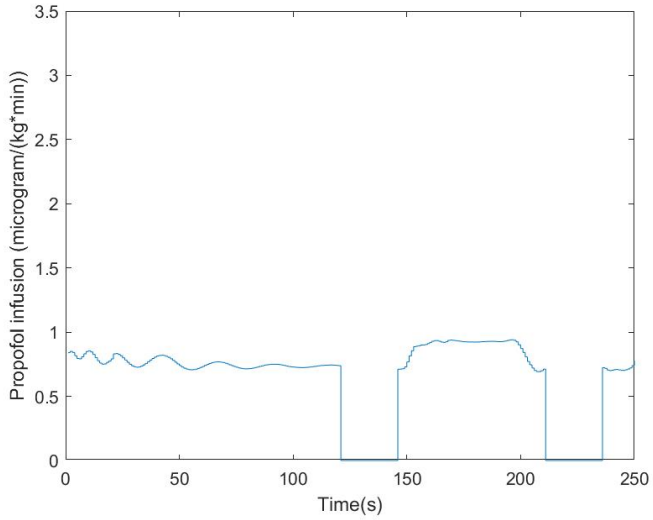

Figure B.135: Propofol input for disturbed nominal model - zoom

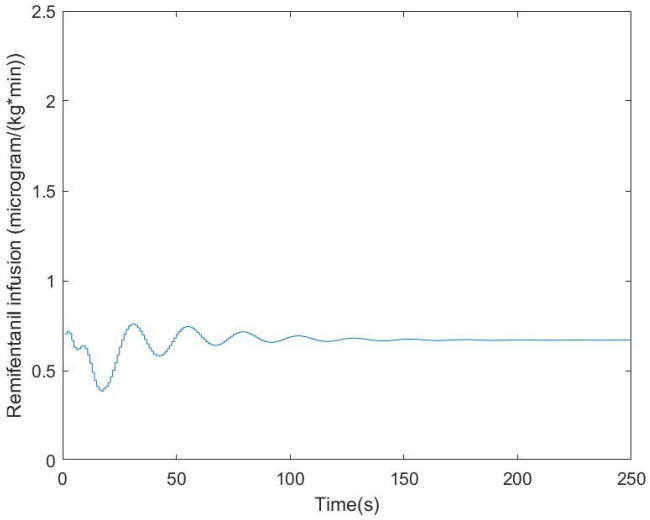

Figure B.136: Remifentanil input for disturbed nominal model - zoom

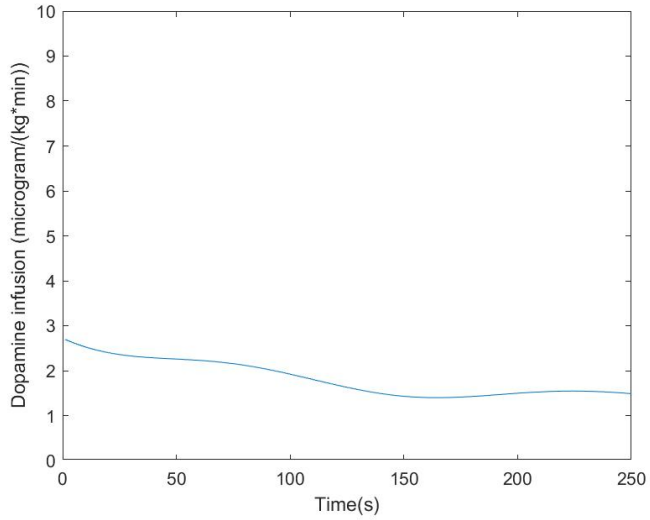

Figure B.137: Dopamine input for disturbed nominal model - zoom

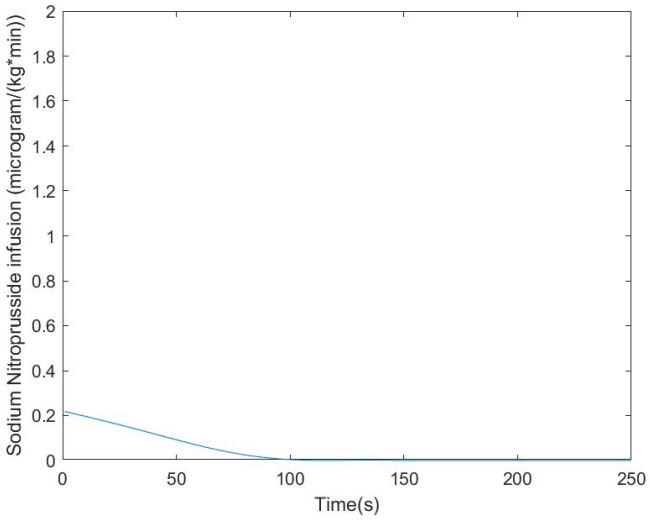

Figure B.138: Sodium Nitroprusside input for disturbed nominal model - zoom

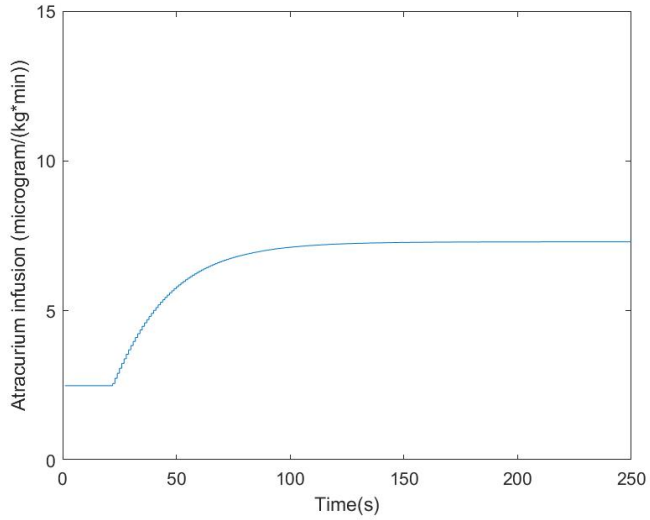

Figure B.139: Atracurium input for disturbed nominal model - zoom

B.3.5 Interpatient variability without disturbance

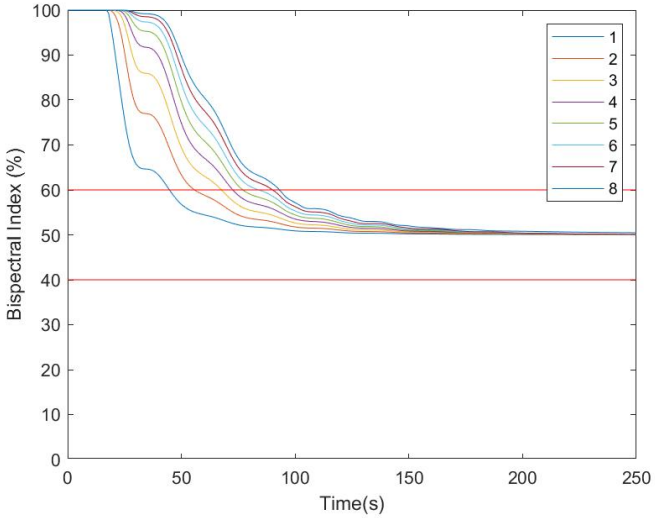

Figure B.140: BIS output for interpatient variability - undisturbed

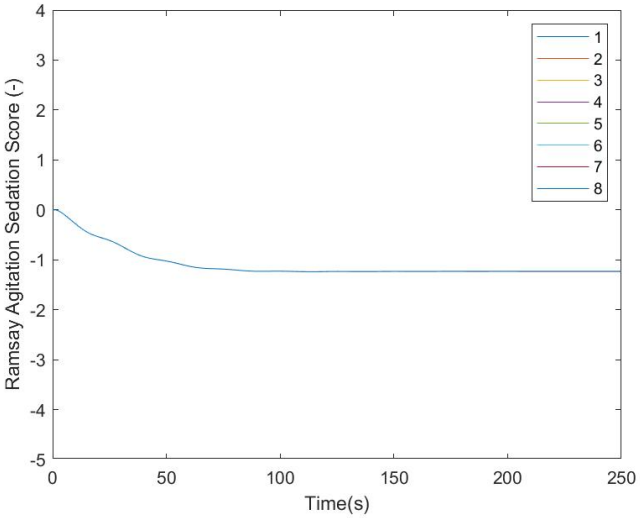

Figure B.141: RASS output for interpatient variability - undisturbed

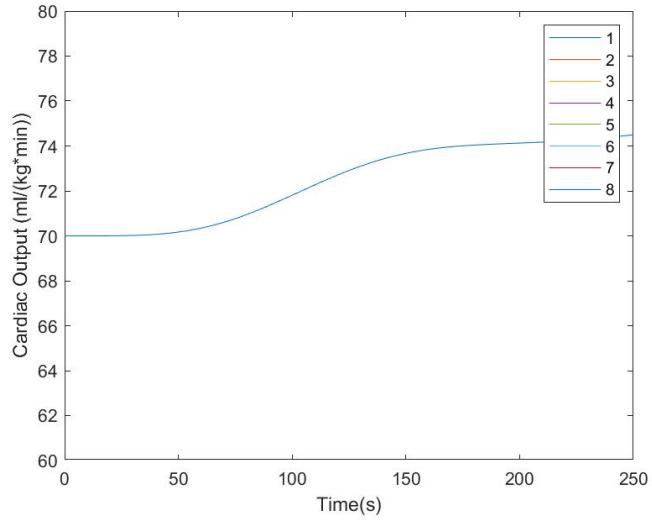

Figure B.142: CO output for interpatient variability - undisturbed

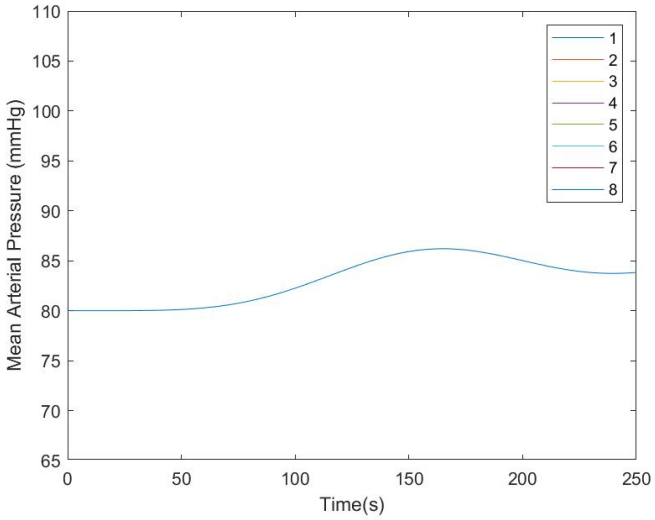

Figure B.143: MAP output for interpatient variability - undisturbed

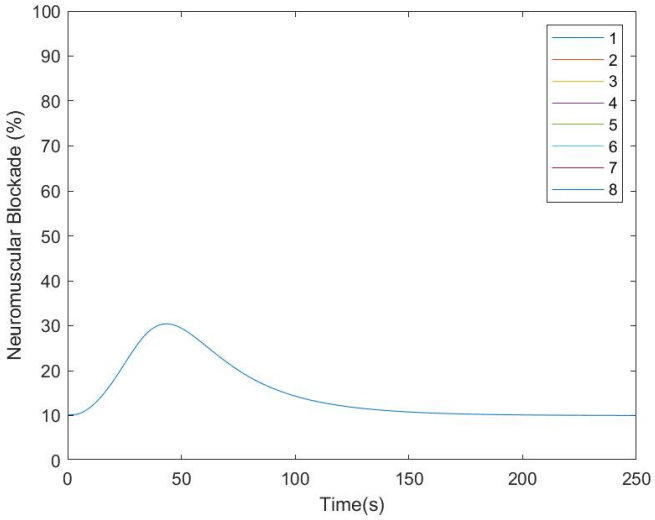

Figure B.144: NMB output for interpatient variability - undisturbed

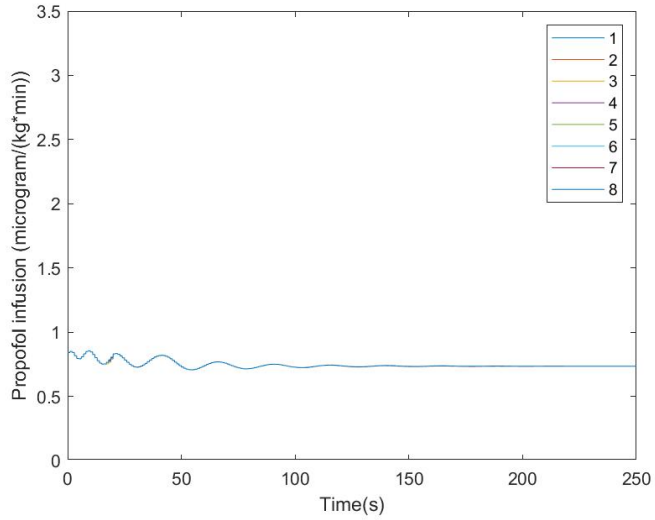

Figure B.145: Propofol input for interpatient variability - undisturbed

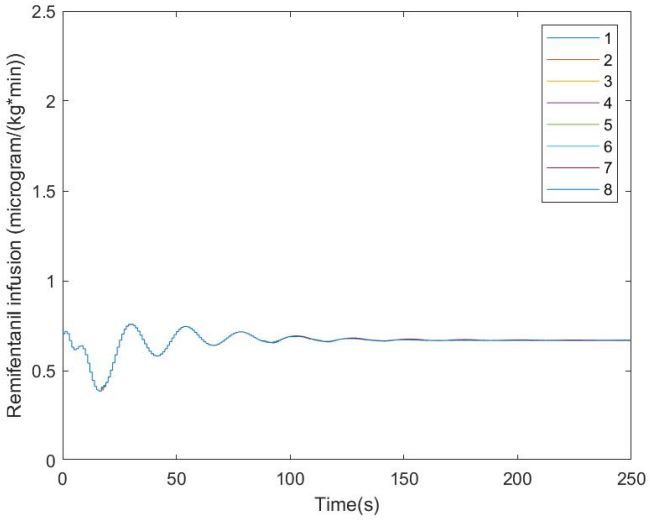

Figure B.146: Remifentanil input for interpatient variability - undisturbed

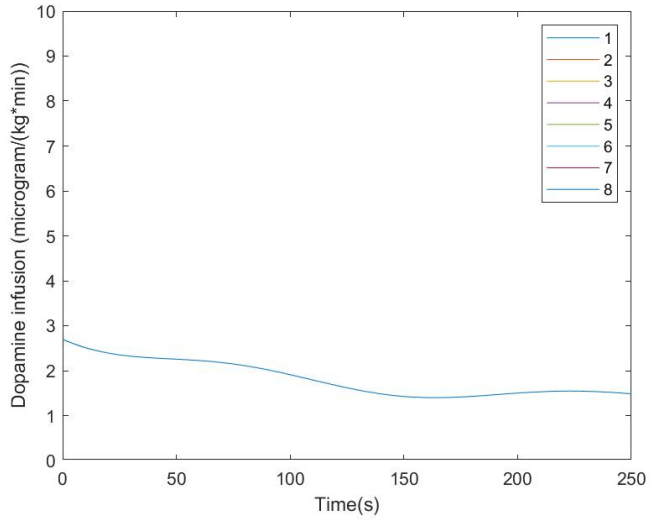

Figure B.147: Dopamine input for interpatient variability - undisturbed

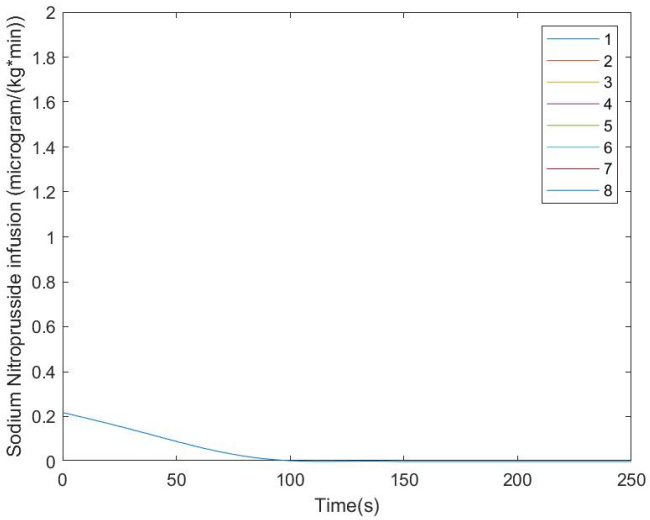

Figure B.148: Sodium Nitroprusside input for interpatient variability - undisturbed

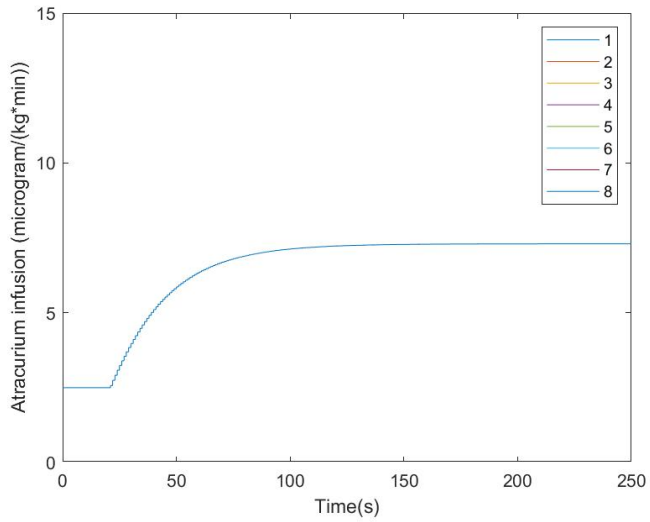

Figure B.149: Atracurium input for interpatient variability - undisturbed

B.3.6 Interpatient variability with disturbances

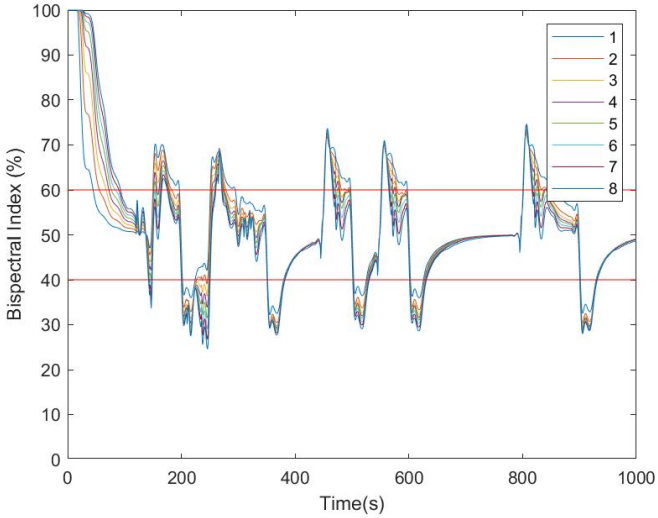

Figure B.150: BIS output for interpatient variability - disturbed

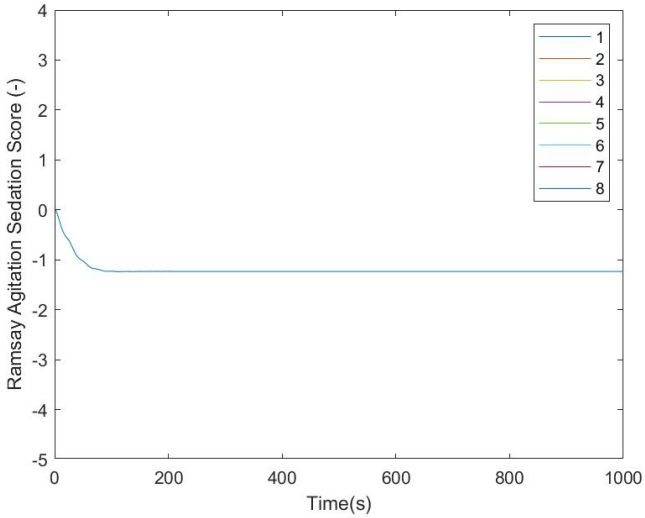

Figure B.151: RASS output for interpatient variability - disturbed

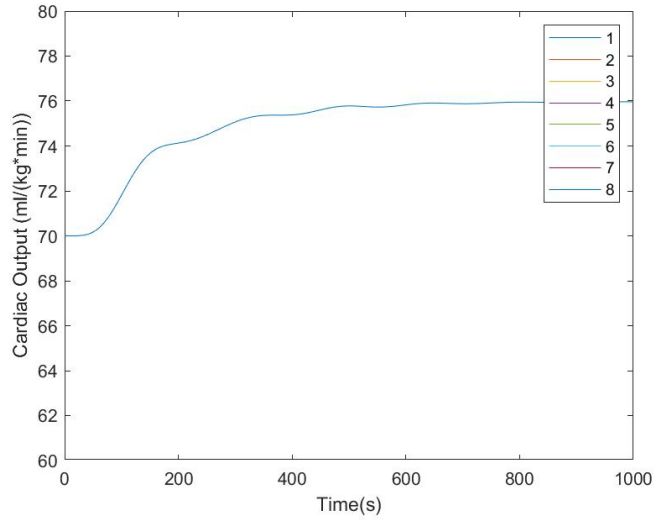

Figure B.152: CO output for interpatient variability - disturbed

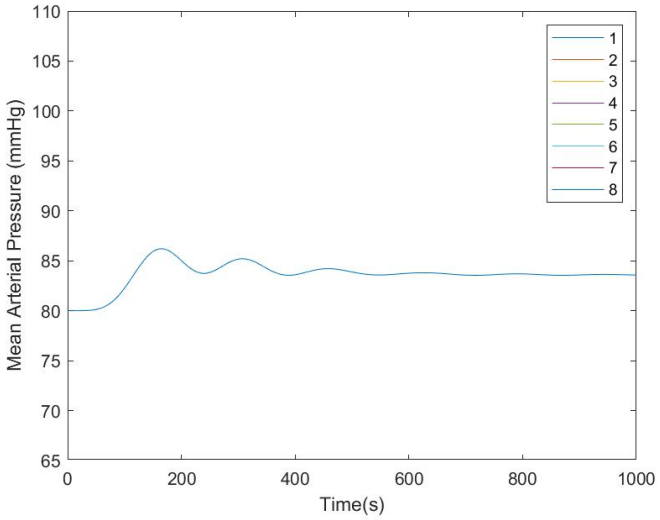

Figure B.153: MAP output for interpatient variability - disturbed

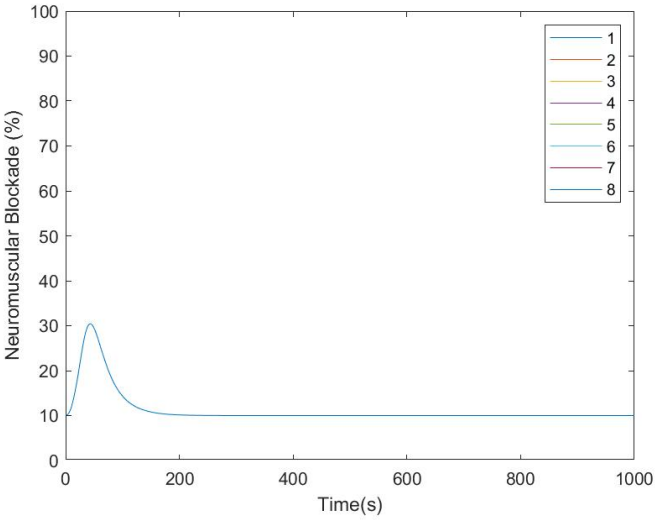

Figure B.154: NMB output for interpatient variability - disturbed

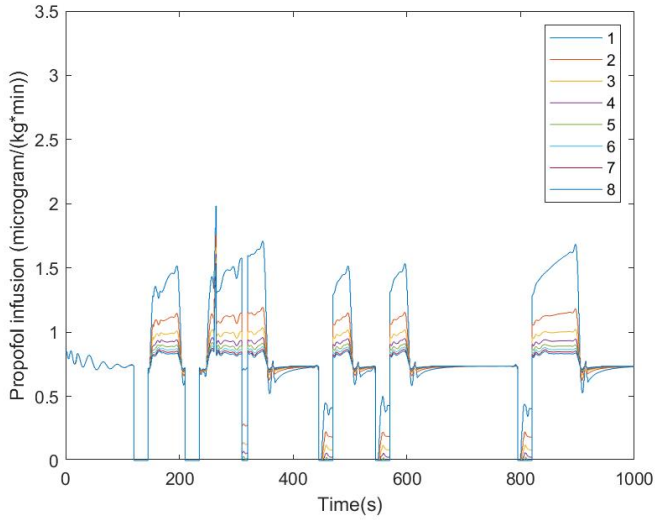

Figure B.155: Propofol input for interpatient variability - disturbed

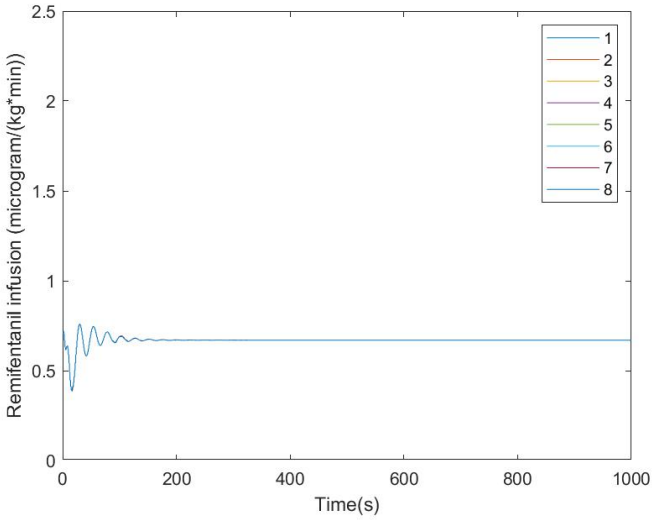

Figure B.156: Remifentanil input for interpatient variability - disturbed

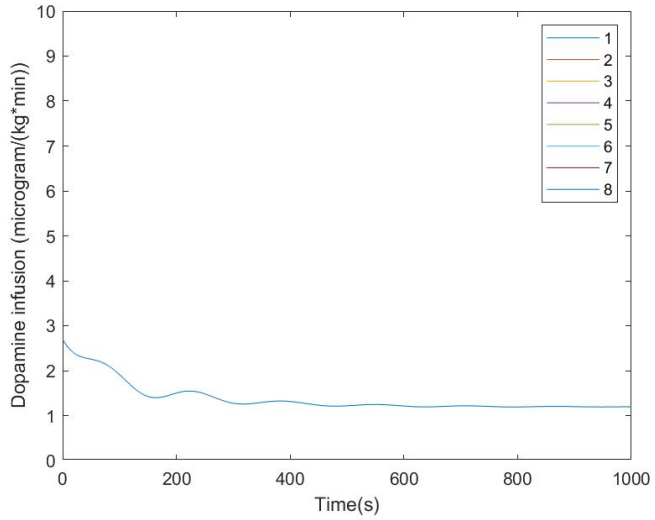

Figure B.157: Dopamine input for interpatient variability - disturbed

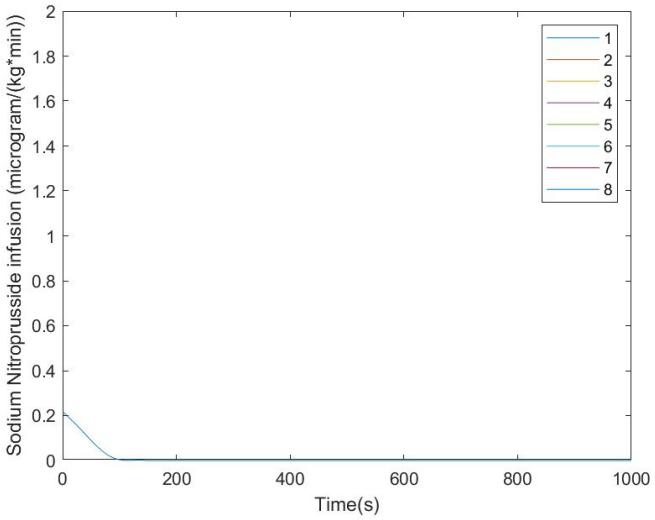

Figure B.158: Sodium Nitroprusside input for interpatient variability - disturbed

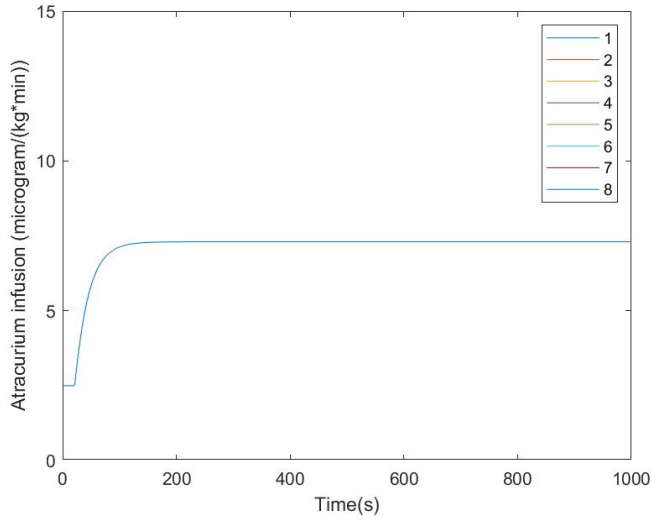

Figure B.159: Atracurium input for interpatient variability - disturbed

B.3.7 Intrapatient variability without disturbance

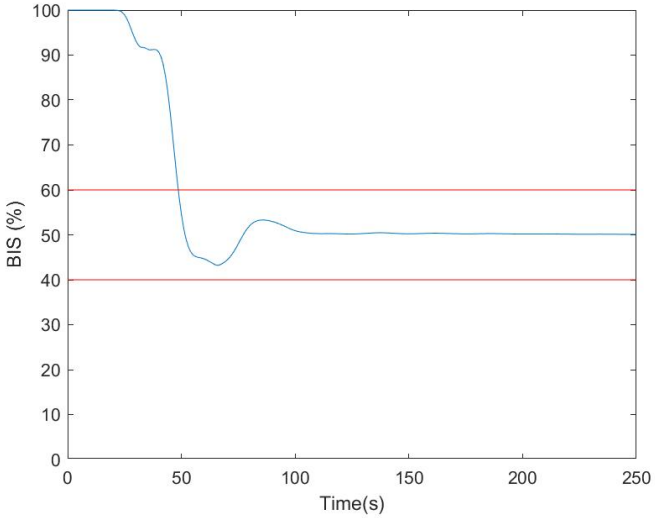

Figure B.160: BIS output for intrapatient variability - undisturbed

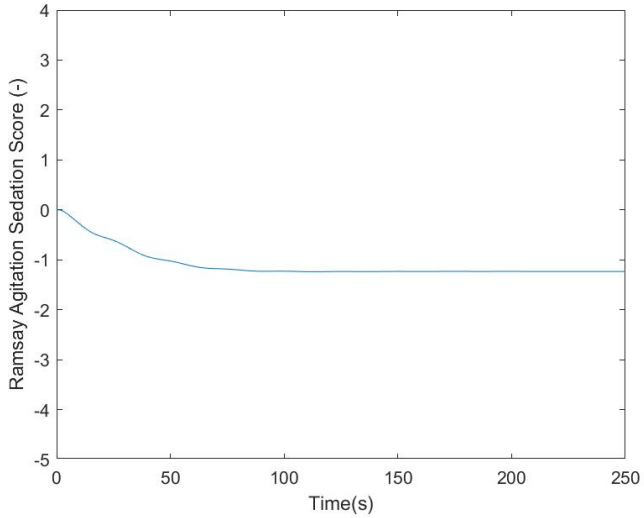

Figure B.161: RASS output for intrapatient variability - undisturbed

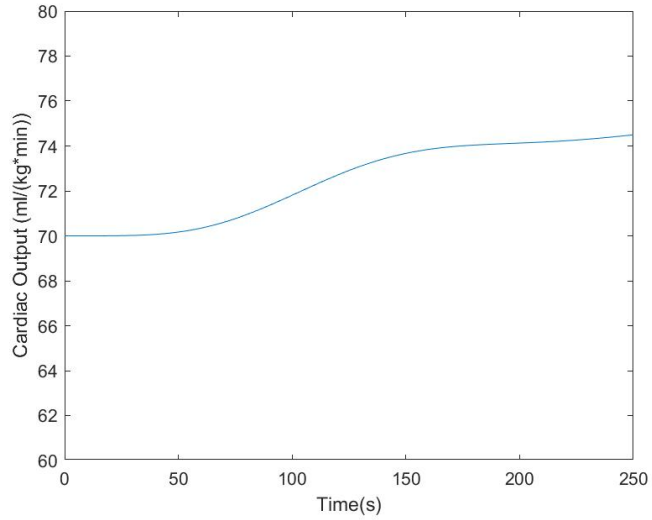

Figure B.162: CO output for intrapatient variability - undisturbed

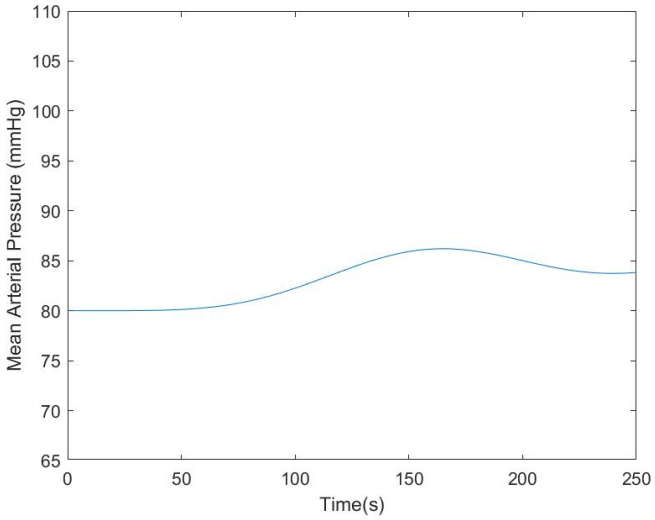

Figure B.163: MAP output for intrapatient variability - undisturbed

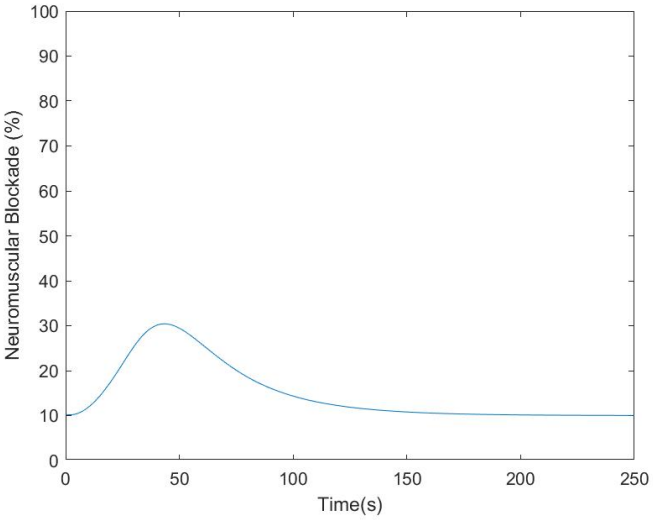

Figure B.164: NMB output for intrapatient variability - undisturbed

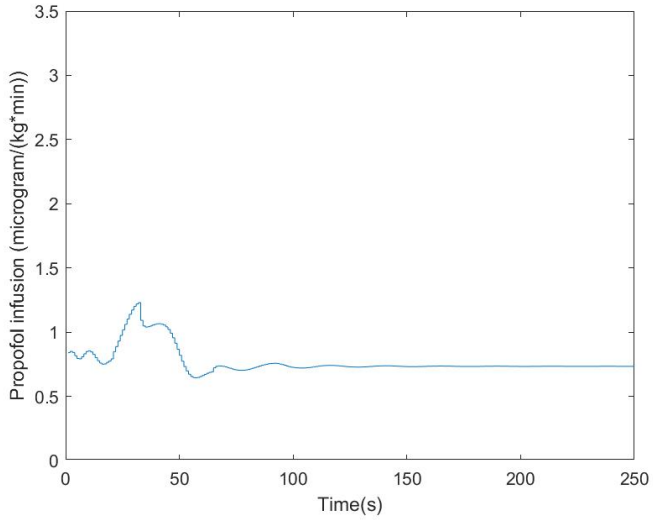

Figure B.165: Propofol input for intrapatient variability - undisturbed

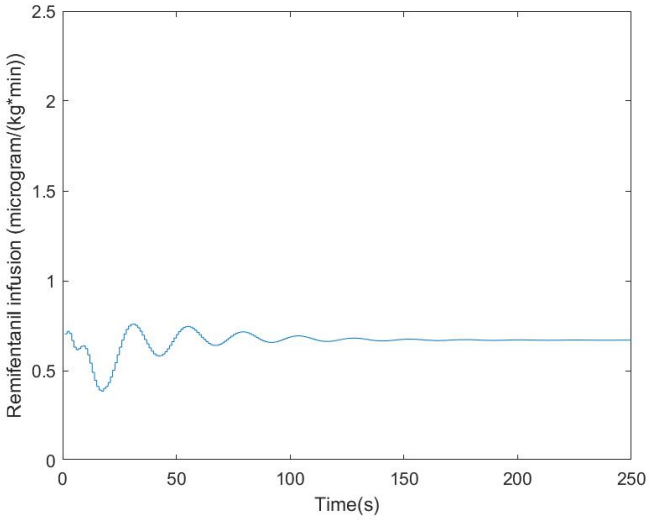

Figure B.166: Remifentanil input for intrapatient variability - undisturbed

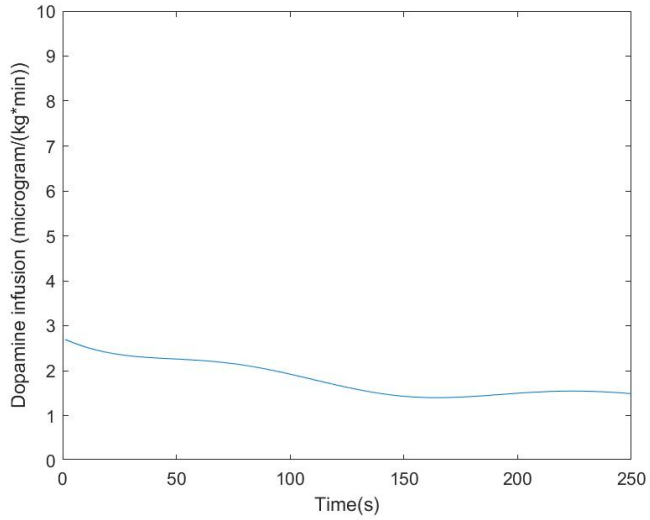

Figure B.167: Dopamine input for intrapatient variability - undisturbed

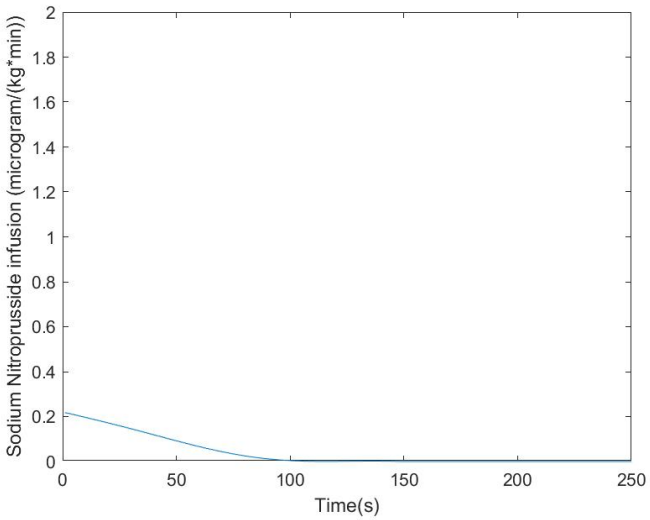

Figure B.168: Sodium Nitroprusside input for intrapatient variability - undisturbed

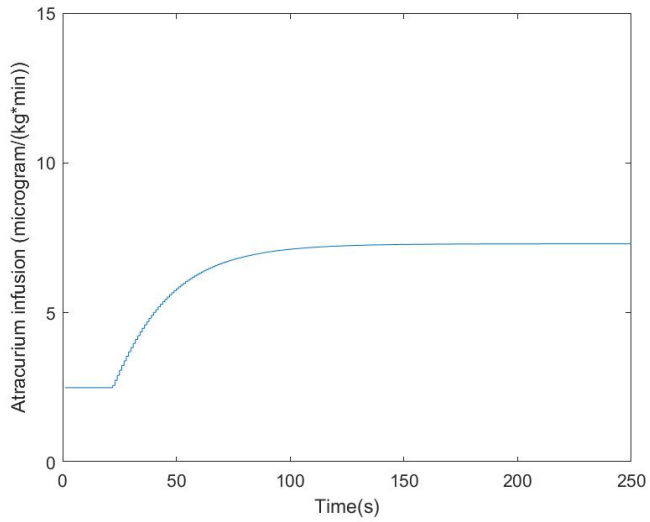

Figure B.169: Atracurium input for intrapatient variability - undisturbed

B.3.8 Intrapatient variability with disturbances

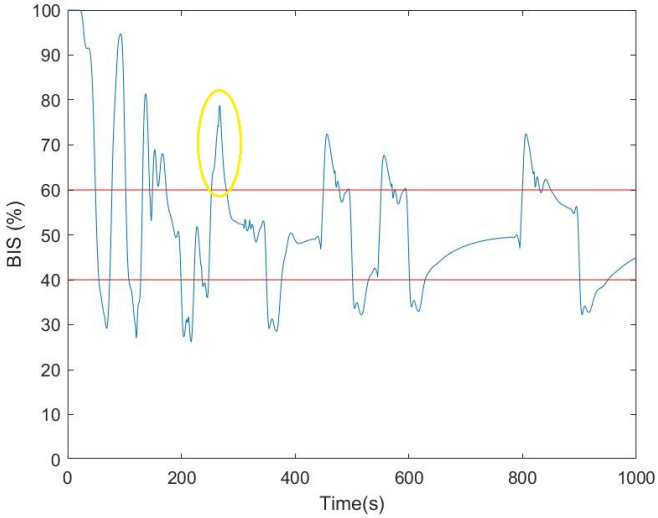

Figure B.170: BIS output for intrapatient variability - disturbed

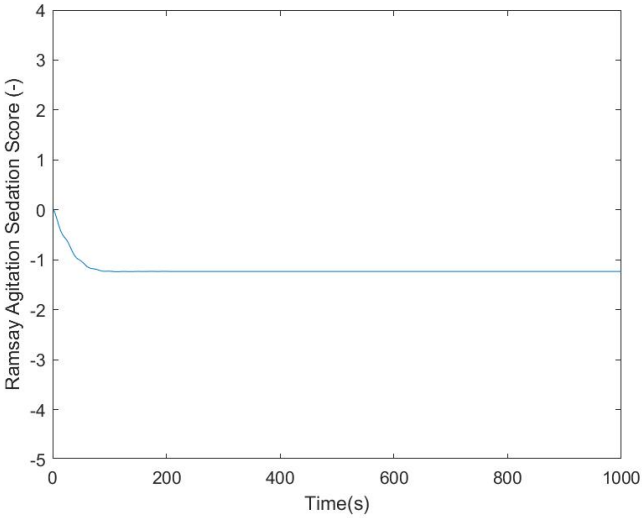

Figure B.171: RASS output for intrapatient variability - disturbed

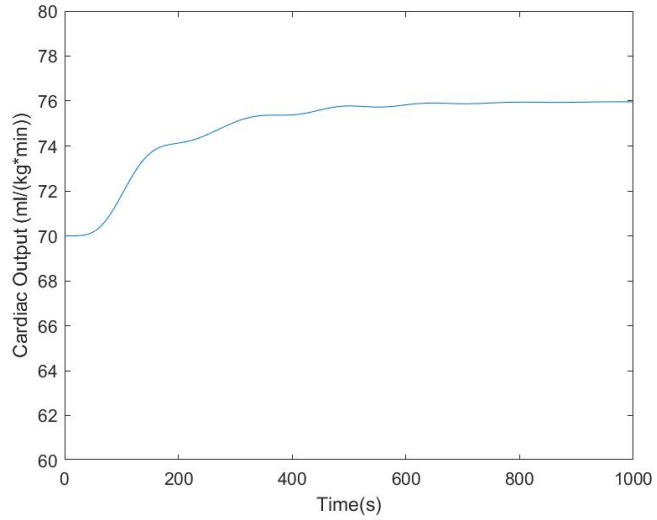

Figure B.172: CO output for intrapatient variability - disturbed

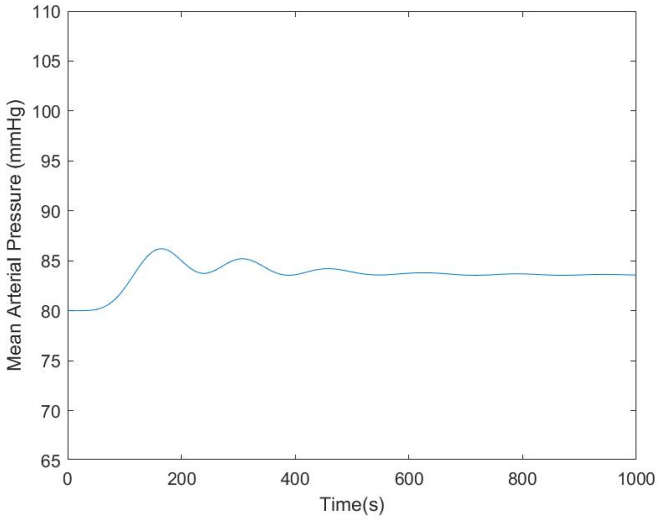

Figure B.173: MAP output for intrapatient variability - disturbed

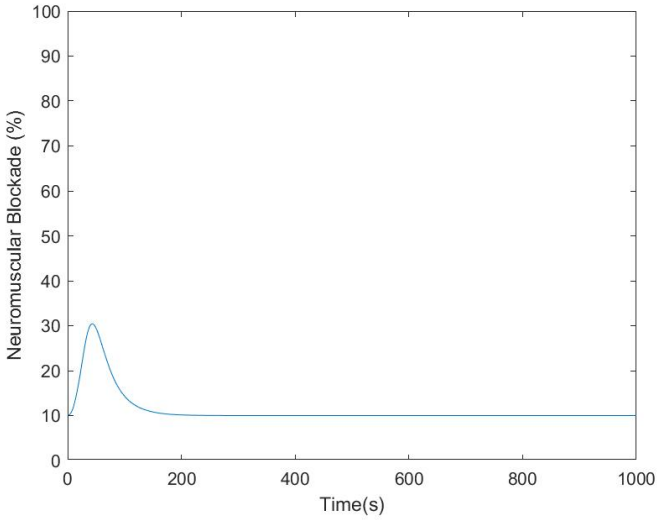

Figure B.174: NMB output for intrapatient variability - disturbed

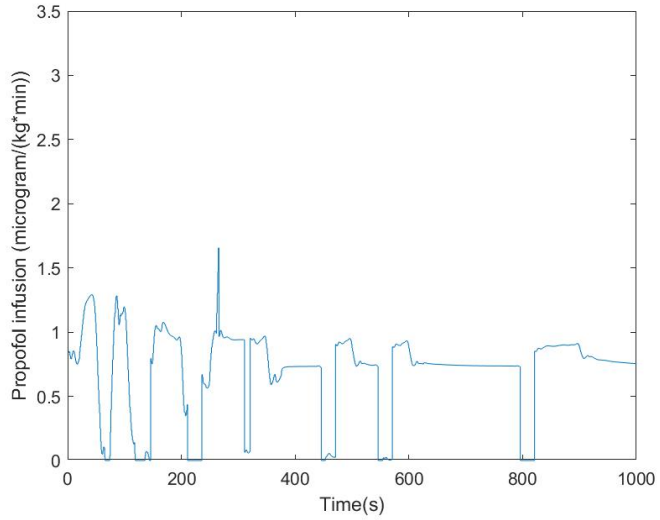

Figure B.175: Propofol input for intrapatient variability - disturbed

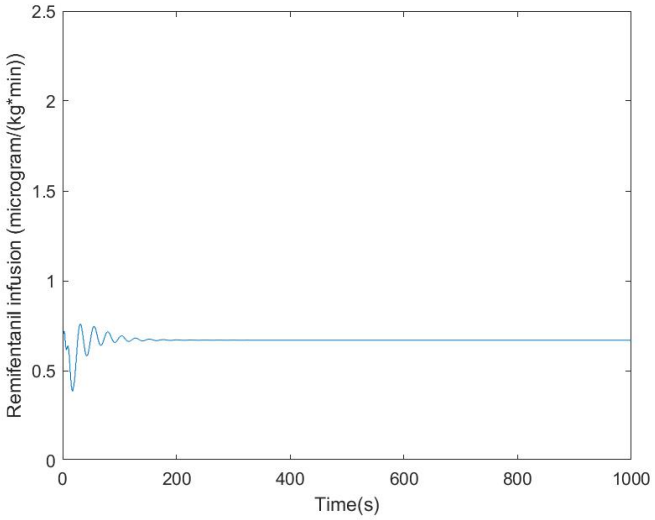

Figure B.176: Remifentanil input for intrapatient variability - disturbed

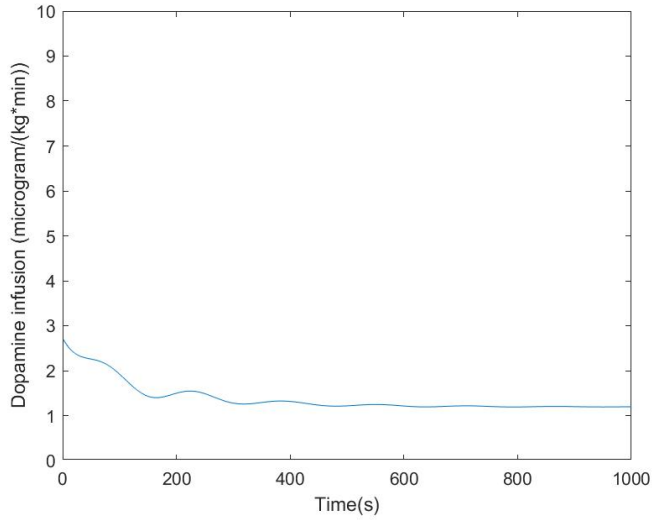

Figure B.177: Dopamine input for intrapatient variability - disturbed

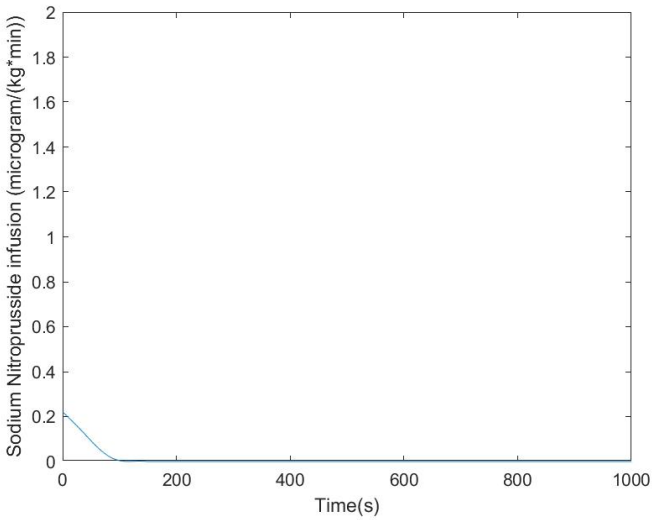

Figure B.178: Sodium Nitroprusside input for intrapatient variability - disturbed

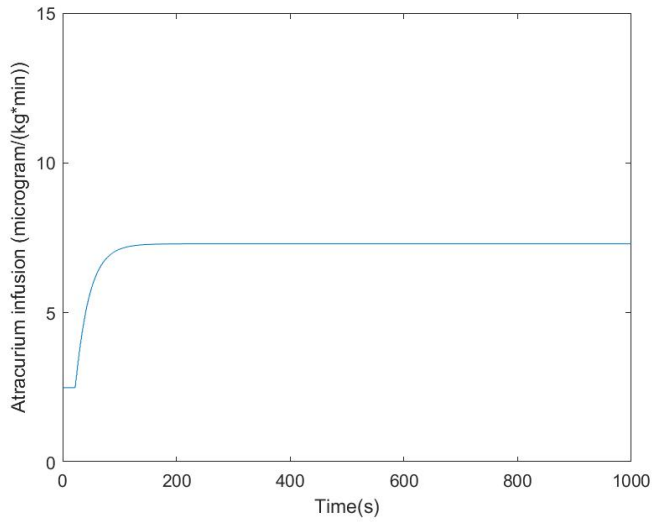

Figure B.179: Atracurium input for intrapatient variability - disturbed

B.4 Stability analysis

$$
P(:,1:7) = \begin{bmatrix}
55.26 & 7.634 & 4.844 & -6.004 & -17.31 & -41.08 & -10.37 \\
7.634 & 55.17 & 8.37 & 4.245 & 15.69 & 3.789 & -30.76 \\
4.844 & 8.37 & 4.258 & 2.412 & 5.797 & -5.469 & -13.15 \\
-6.004 & 4.245 & 2.412 & 8.514 & 11.85 & -4.409 & -8.362 \\
-17.31 & 15.69 & 5.797 & 11.85 & 34.14 & -1.735 & -38.9 \\
-41.08 & 3.789 & -5.469 & -4.409 & -1.735 & 75.28 & -2.594 \\
-10.37 & -30.76 & -13.15 & -8.362 & -38.9 & -2.594 & 115.9 \\
1.151 & -54.11 & -3.73 & 2.847 & -0.2034 & -29.82 & -7.616 \\
0 & 0 & 0 & 0 & 0 & 0 & 0 \\
0 & 0 & 0 & 0 & 0 & 0 & 0 \\
0 & 0 & 0 & 0 & 0 & 0 & 0 \\
0 & 0 & 0 & 0 & 0 & 0 & 0 \\
0 & 0 & 0 & 0 & 0 & 0 & 0 \\
0 & 0 & 0 & 0 & 0 & 0 & 0 \\
0 & 0 & 0 & 0 & 0 & 0 & 0 \\
0 & 0 & 0 & 0 & 0 & 0 & 0 \\
0 & 0 & 0 & 0 & 0 & 0 & 0 \\
0 & 0 & 0 & 0 & 0 & 0 & 0 \\
0 & 0 & 0 & 0 & 0 & 0 & 0 \\
0 & 0 & 0 & 0 & 0 & 0 & 0 \\
0 & 0 & 0 & 0 & 0 & 0 & 0 \\
0 & 0 & 0 & 0 & 0 & 0 & 0 \\
0 & 0 & 0 & 0 & 0 & 0 & 0 \\
0 & 0 & 0 & 0 & 0 & 0 & 0 \\
0 & 0 & 0 & 0 & 0 & 0 & 0 \\
0 & 0 & 0 & 0 & 0 & 0 & 0 \\
0 & 0 & 0 & 0 & 0 & 0 & 0 \\
0 & 0 & 0 & 0 & 0 & 0 & 0 \\
0 & 0 & 0 & 0 & 0 & 0 & 0 \\
0 & 0 & 0 & 0 & 0 & 0 & 0 \\
0 & 0 & 0 & 0 & 0 & 0 & 0 \\
0 & 0 & 0 & 0 & 0 & 0 & 0 \\
0 & 0 & 0 & 0 & 0 & 0 & 0 \\
0 & 0 & 0 & 0 & 0 & 0 & 0 \\
0 & 0 & 0 & 0 & 0 & 0 & 0 \\
0 & 0 & 0 & 0 & 0 & 0 & 0 \\
0 & 0 & 0 & 0 & 0 & 0 & 0 \\
0 & 0 & 0 & 0 & 0 & 0 & 0 \\
0 & 0 & 0 & 0 & 0 & 0 & 0
\end{bmatrix}
$$

$$P(:,8:14) = \begin{bmatrix}
1.151 & 0 & 0 & 0 & 0 & 0 & 0 \\
-54.11 & 0 & 0 & 0 & 0 & 0 & 0 \\
-3.73 & 0 & 0 & 0 & 0 & 0 & 0 \\
2.847 & 0 & 0 & 0 & 0 & 0 & 0 \\
-0.2034 & 0 & 0 & 0 & 0 & 0 & 0 \\
-29.82 & 0 & 0 & 0 & 0 & 0 & 0 \\
-7.616 & 0 & 0 & 0 & 0 & 0 & 0 \\
96.68 & 0 & 0 & 0 & 0 & 0 & 0 \\
0 & 1181.0 & 254.7 & 6.752 & 33.11 & -62.79 & -507.7 \\
0 & 254.7 & 517.2 & 31.24 & 160.3 & 266.8 & 158.9 \\
0 & 6.752 & 31.24 & 55.2 & 6.231 & 8.595 & 9.131 \\
0 & 33.11 & 160.3 & 6.231 & 120.5 & 185.3 & -26.37 \\
0 & -62.79 & 266.8 & 8.595 & 185.3 & 517.7 & -11.59 \\
0 & -507.7 & 158.9 & 9.131 & -26.37 & -11.59 & 1244.0 \\
0 & -266.8 & -186.7 & 16.58 & -174.4 & -635.4 & -25.7 \\
0 & -144.4 & -393.9 & -29.12 & -64.69 & -16.15 & -465.0 \\
0 & 0 & 0 & 0 & 0 & 0 & 0 \\
0 & 0 & 0 & 0 & 0 & 0 & 0 \\
0 & 0 & 0 & 0 & 0 & 0 & 0 \\
0 & 0 & 0 & 0 & 0 & 0 & 0 \\
0 & 0 & 0 & 0 & 0 & 0 & 0 \\
0 & 0 & 0 & 0 & 0 & 0 & 0 \\
0 & 0 & 0 & 0 & 0 & 0 & 0 \\
0 & 0 & 0 & 0 & 0 & 0 & 0 \\
0 & 0 & 0 & 0 & 0 & 0 & 0 \\
0 & 0 & 0 & 0 & 0 & 0 & 0 \\
0 & 0 & 0 & 0 & 0 & 0 & 0 \\
0 & 0 & 0 & 0 & 0 & 0 & 0 \\
0 & 0 & 0 & 0 & 0 & 0 & 0 \\
0 & 0 & 0 & 0 & 0 & 0 & 0 \\
0 & 0 & 0 & 0 & 0 & 0 & 0 \\
0 & 0 & 0 & 0 & 0 & 0 & 0 \\
0 & 0 & 0 & 0 & 0 & 0 & 0 \\
0 & 0 & 0 & 0 & 0 & 0 & 0 \\
0 & 0 & 0 & 0 & 0 & 0 & 0 \\
0 & 0 & 0 & 0 & 0 & 0 & 0 \\
0 & 0 & 0 & 0 & 0 & 0 & 0 \\
0 & 0 & 0 & 0 & 0 & 0 & 0 \\
0 & 0 & 0 & 0 & 0 & 0 & 0
\end{bmatrix}$$

$$P(:, 15:21) = \begin{bmatrix}
0 & 0 & 0 & 0 & 0 & 0 & 0 \\
0 & 0 & 0 & 0 & 0 & 0 & 0 \\
0 & 0 & 0 & 0 & 0 & 0 & 0 \\
0 & 0 & 0 & 0 & 0 & 0 & 0 \\
0 & 0 & 0 & 0 & 0 & 0 & 0 \\
0 & 0 & 0 & 0 & 0 & 0 & 0 \\
0 & 0 & 0 & 0 & 0 & 0 & 0 \\
0 & 0 & 0 & 0 & 0 & 0 & 0 \\
-266.8 & -144.4 & 0 & 0 & 0 & 0 & 0 \\
-186.7 & -393.9 & 0 & 0 & 0 & 0 & 0 \\
16.58 & -29.12 & 0 & 0 & 0 & 0 & 0 \\
-174.4 & -64.69 & 0 & 0 & 0 & 0 & 0 \\
-635.4 & -16.15 & 0 & 0 & 0 & 0 & 0 \\
-25.7 & -465.0 & 0 & 0 & 0 & 0 & 0 \\
1703.0 & -362.1 & 0 & 0 & 0 & 0 & 0 \\
-362.1 & 680.0 & 0 & 0 & 0 & 0 & 0 \\
0 & 0 & 632.3 & -71.1 & -916.4 & 149.6 & 104.5 \\
0 & 0 & -71.1 & 903.9 & -124.8 & -995.2 & 49.52 \\
0 & 0 & -916.4 & -124.8 & 2008.0 & -225.3 & -318.0 \\
0 & 0 & 149.6 & -995.2 & -225.3 & 1884.0 & -804.7 \\
0 & 0 & 104.5 & 49.52 & -318.0 & -804.7 & 1688.0 \\
0 & 0 & 120.9 & 44.53 & 123.9 & -107.2 & -28.22 \\
0 & 0 & -91.27 & -309.7 & 308.9 & 374.9 & -66.72 \\
0 & 0 & 298.5 & -249.8 & -856.5 & 298.6 & 109.3 \\
0 & 0 & 47.74 & 426.4 & -237.1 & -467.8 & -108.6 \\
0 & 0 & -128.1 & 27.16 & 156.9 & 262.1 & -137.2 \\
0 & 0 & 0 & 0 & 0 & 0 & 0 \\
0 & 0 & 0 & 0 & 0 & 0 & 0 \\
0 & 0 & 0 & 0 & 0 & 0 & 0 \\
0 & 0 & 0 & 0 & 0 & 0 & 0 \\
0 & 0 & 0 & 0 & 0 & 0 & 0 \\
0 & 0 & 0 & 0 & 0 & 0 & 0 \\
0 & 0 & 0 & 0 & 0 & 0 & 0 \\
0 & 0 & 0 & 0 & 0 & 0 & 0 \\
0 & 0 & 0 & 0 & 0 & 0 & 0 \\
0 & 0 & 0 & 0 & 0 & 0 & 0 \\
0 & 0 & 0 & 0 & 0 & 0 & 0 \\
0 & 0 & 0 & 0 & 0 & 0 & 0
\end{bmatrix}$$

$$P(:, 22:28) = \begin{bmatrix}
0 & 0 & 0 & 0 & 0 & 0 & 0 \\
0 & 0 & 0 & 0 & 0 & 0 & 0 \\
0 & 0 & 0 & 0 & 0 & 0 & 0 \\
0 & 0 & 0 & 0 & 0 & 0 & 0 \\
0 & 0 & 0 & 0 & 0 & 0 & 0 \\
0 & 0 & 0 & 0 & 0 & 0 & 0 \\
0 & 0 & 0 & 0 & 0 & 0 & 0 \\
0 & 0 & 0 & 0 & 0 & 0 & 0 \\
0 & 0 & 0 & 0 & 0 & 0 & 0 \\
0 & 0 & 0 & 0 & 0 & 0 & 0 \\
0 & 0 & 0 & 0 & 0 & 0 & 0 \\
0 & 0 & 0 & 0 & 0 & 0 & 0 \\
0 & 0 & 0 & 0 & 0 & 0 & 0 \\
0 & 0 & 0 & 0 & 0 & 0 & 0 \\
0 & 0 & 0 & 0 & 0 & 0 & 0 \\
120.9 & -91.27 & 298.5 & 47.74 & -128.1 & 0 & 0 \\
44.53 & -309.7 & -249.8 & 426.4 & 27.16 & 0 & 0 \\
123.9 & 308.9 & -856.5 & -237.1 & 156.9 & 0 & 0 \\
-107.2 & 374.9 & 298.6 & -467.8 & 262.1 & 0 & 0 \\
-28.22 & -66.72 & 109.3 & -108.6 & -137.2 & 0 & 0 \\
252.1 & -30.39 & -328.7 & 36.84 & 61.44 & 0 & 0 \\
-30.39 & 624.6 & -92.45 & -605.5 & 69.7 & 0 & 0 \\
-328.7 & -92.45 & 1166.0 & -158.4 & -500.2 & 0 & 0 \\
36.84 & -605.5 & -158.4 & 1030.0 & -255.2 & 0 & 0 \\
61.44 & 69.7 & -500.2 & -255.2 & 950.2 & 0 & 0 \\
0 & 0 & 0 & 0 & 0 & 209.2 & -26.79 \\
0 & 0 & 0 & 0 & 0 & -26.79 & 567.4 \\
0 & 0 & 0 & 0 & 0 & -295.4 & -70.02 \\
0 & 0 & 0 & 0 & 0 & 30.09 & -451.5 \\
0 & 0 & 0 & 0 & 0 & 19.14 & 16.72 \\
0 & 0 & 0 & 0 & 0 & 59.45 & 58.52 \\
0 & 0 & 0 & 0 & 0 & -52.54 & -346.9 \\
0 & 0 & 0 & 0 & 0 & 166.8 & -146.0 \\
0 & 0 & 0 & 0 & 0 & 7.755 & 298.0 \\
0 & 0 & 0 & 0 & 0 & -44.84 & -4.383 \\
0 & 0 & 0 & 0 & 0 & 0 & 0 \\
0 & 0 & 0 & 0 & 0 & 0 & 0 \\
0 & 0 & 0 & 0 & 0 & 0 & 0
\end{bmatrix}$$

$$P(:,29:35) = \begin{bmatrix}
0 & 0 & 0 & 0 & 0 & 0 & 0 \\
0 & 0 & 0 & 0 & 0 & 0 & 0 \\
0 & 0 & 0 & 0 & 0 & 0 & 0 \\
0 & 0 & 0 & 0 & 0 & 0 & 0 \\
0 & 0 & 0 & 0 & 0 & 0 & 0 \\
0 & 0 & 0 & 0 & 0 & 0 & 0 \\
0 & 0 & 0 & 0 & 0 & 0 & 0 \\
0 & 0 & 0 & 0 & 0 & 0 & 0 \\
0 & 0 & 0 & 0 & 0 & 0 & 0 \\
0 & 0 & 0 & 0 & 0 & 0 & 0 \\
0 & 0 & 0 & 0 & 0 & 0 & 0 \\
0 & 0 & 0 & 0 & 0 & 0 & 0 \\
0 & 0 & 0 & 0 & 0 & 0 & 0 \\
0 & 0 & 0 & 0 & 0 & 0 & 0 \\
0 & 0 & 0 & 0 & 0 & 0 & 0 \\
0 & 0 & 0 & 0 & 0 & 0 & 0 \\
0 & 0 & 0 & 0 & 0 & 0 & 0 \\
0 & 0 & 0 & 0 & 0 & 0 & 0 \\
0 & 0 & 0 & 0 & 0 & 0 & 0 \\
0 & 0 & 0 & 0 & 0 & 0 & 0 \\
0 & 0 & 0 & 0 & 0 & 0 & 0 \\
0 & 0 & 0 & 0 & 0 & 0 & 0 \\
0 & 0 & 0 & 0 & 0 & 0 & 0 \\
0 & 0 & 0 & 0 & 0 & 0 & 0 \\
0 & 0 & 0 & 0 & 0 & 0 & 0 \\
0 & 0 & 0 & 0 & 0 & 0 & 0 \\
-295.4 & 30.09 & 19.14 & 59.45 & -52.54 & 166.8 & 7.755 \\
-70.02 & -451.5 & 16.72 & 58.52 & -346.9 & -146.0 & 298.0 \\
886.0 & -130.5 & -157.1 & 151.5 & 184.3 & -633.0 & -67.55 \\
-130.5 & 931.0 & -469.7 & -70.22 & 288.9 & 64.92 & -165.0 \\
-157.1 & -469.7 & 879.1 & -23.06 & -27.78 & 42.94 & -137.3 \\
151.5 & -70.22 & -23.06 & 247.8 & -28.88 & -385.8 & 42.35 \\
184.3 & 288.9 & -27.78 & -28.88 & 757.6 & -83.52 & -601.3 \\
-633.0 & 64.92 & 42.94 & -385.8 & -83.52 & 1178.0 & -111.9 \\
-67.55 & -165.0 & -137.3 & 42.35 & -601.3 & -111.9 & 703.0 \\
54.89 & 23.76 & 219.0 & 66.32 & 50.24 & -347.8 & -140.7 \\
0 & 0 & 0 & 0 & 0 & 0 & 0 \\
0 & 0 & 0 & 0 & 0 & 0 & 0 \\
0 & 0 & 0 & 0 & 0 & 0 & 0
\end{bmatrix}$$

$$P(:,36:39)=\begin{bmatrix}
0 & 0 & 0 & 0\\
0 & 0 & 0 & 0\\
0 & 0 & 0 & 0\\
0 & 0 & 0 & 0\\
0 & 0 & 0 & 0\\
0 & 0 & 0 & 0\\
0 & 0 & 0 & 0\\
0 & 0 & 0 & 0\\
0 & 0 & 0 & 0\\
0 & 0 & 0 & 0\\
0 & 0 & 0 & 0\\
0 & 0 & 0 & 0\\
0 & 0 & 0 & 0\\
0 & 0 & 0 & 0\\
0 & 0 & 0 & 0\\
0 & 0 & 0 & 0\\
0 & 0 & 0 & 0\\
0 & 0 & 0 & 0\\
0 & 0 & 0 & 0\\
0 & 0 & 0 & 0\\
0 & 0 & 0 & 0\\
0 & 0 & 0 & 0\\
0 & 0 & 0 & 0\\
0 & 0 & 0 & 0\\
0 & 0 & 0 & 0\\
0 & 0 & 0 & 0\\
-44.84 & 0 & 0 & 0\\
-4.383 & 0 & 0 & 0\\
54.89 & 0 & 0 & 0\\
23.76 & 0 & 0 & 0\\
219.0 & 0 & 0 & 0\\
66.32 & 0 & 0 & 0\\
50.24 & 0 & 0 & 0\\
-347.8 & 0 & 0 & 0\\
-140.7 & 0 & 0 & 0\\
440.5 & 0 & 0 & 0\\
0 & 343.2 & -29.46 & -163.9\\
0 & -29.46 & 110.7 & -50.47\\
0 & -163.9 & -50.47 & 147.7
\end{bmatrix}$$